HF RADAR OCEANOGRAPHY

A thesis

presented for the degree

of

Doctor of Philosophy in Physics

in the

University of Canterbury

Christchurch,New Zealand

by

J.A. McGregor

University of Canterbury

1985

ABSTRACT

The development of a 26MHz pulsed Doppler radar system for remote sensing of ocean surface conditions is described. This radar obtains Doppler spectra of echoes from ocean waves within the range 10-40 km from the shore. From these Doppler spectra it is possible to estimate oceanographic parameters such as sea state, wind speed, wind direction, radial components of current velocities and properties of swell.

The work concentrates on the radar design principles and includes a detailed study of the effect of ground wave propagation conditions on the performance of radar systems of this type. Results obtained with the radar are discussed from the points of view of both the performance of the system and the oceanographic information contained in the Doppler spectra.

CONTENTS

CONTENTS, cont.

LIST OF FIGURES

CHAPTER 1:

INTRODUCTION

1.1 RADAR REMOTE SENSING OF OCEAN SURFACE CONDITIONS

Over the past decade radar has emerged as a powerful tool for remote sensing of ocean surface conditions. In contrast to traditional techniques which monitor only one point on the ocean surface (e.g. buoys and ship observations) radar measurements can obtain data simultaneously from a large number of points over a large area of the ocean surface. Additionally, radar has the potential to measure oceanographic quantities that are difficult or impossible to measure by conventional means. Examples of these quantities are wave direction, variation of current velocity with depth and measurements of wave components travelling in oposition to the wind. The major disadvantages with radar are the large and cumbersome antennas required by some techniques, mutual interference between radar and other users of the electromagnetic spectrum and the fact that radar oceanographic information is not obtained in a direct form as with conventional techniques. Data of interest to oceanographers is only obtained after proper interpretation, and sometimes very complicated analyses of, the radar data. Radar oceanographic techniques can be classified into two groups on the basis of the regions of the electromagnetic spectrum that they use: hf techniques (3-30MHz) and microwave techniques (0.3-300GHz).

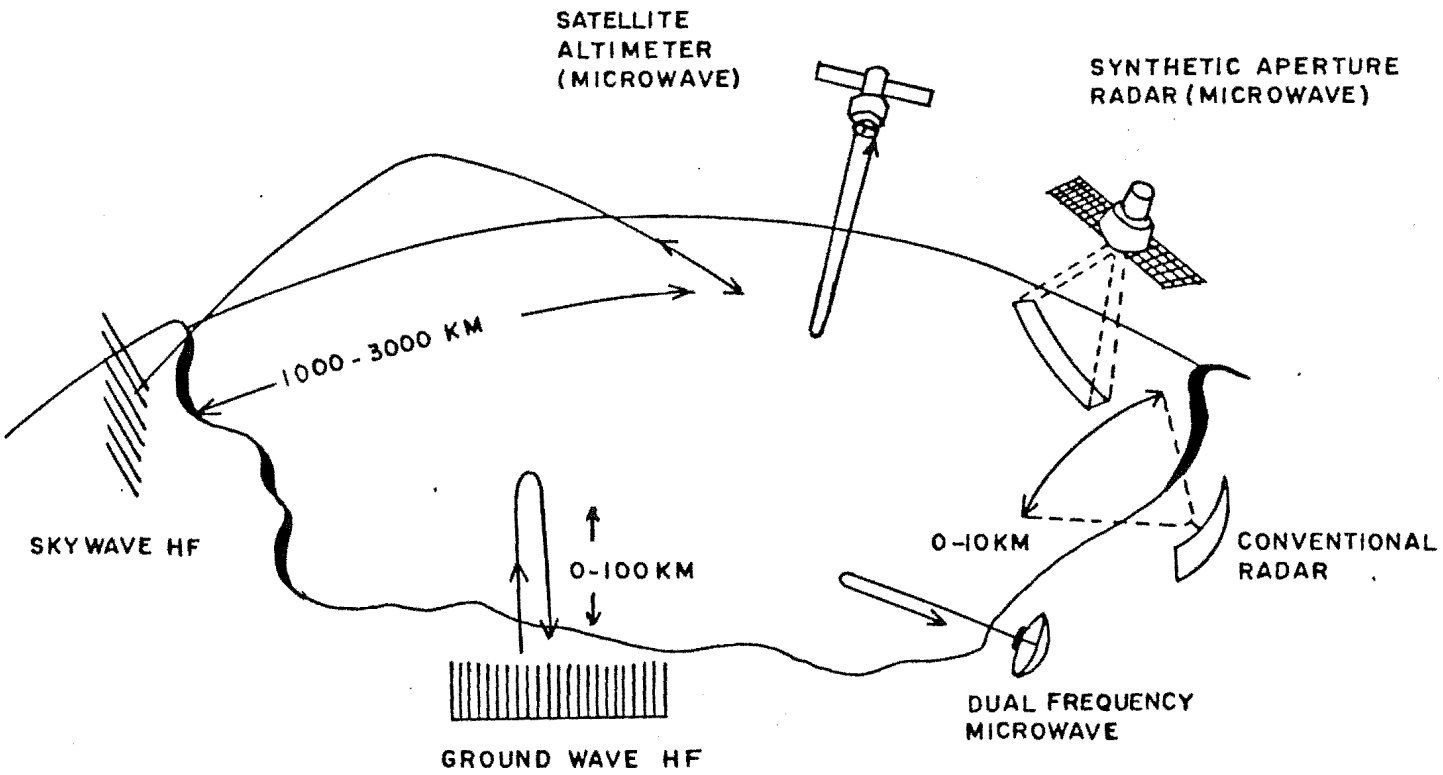

FIG. 1.1 RADAR OCEANOGRAPHY TECHNIQUES.

(1) hf techniques. Conventional radar systems transmit a beam of elecromagnetic energy which is specularly reflected at perpendicular incidence from the surface of a target. This target is usually relatively small. In contrast hf radar oceanography uses a transmitted beam which "grazes" the ocean surface at a very shallow angle. Energy is scattered back to the reciever by means of an interaction between the radar wave and the ocean waves over a relatively large area of the sea surface. Radar data are thus averages over this area and extreme events, such as the maximum height of an individual wave, cannot be measured.

The interaction mechanism responsible for scattering the transmitted energy back to the receiver was discovered in a pioneering experiment by a New Zealand researcher (CROMBIE, 1955). The mechanism is Bragg scatter, analogous to the Bragg scattering of X-rays by crystal structures. Out of the entire spectrum of waves present on the ocean surface the radar energy reflects most strongly from those waves with half the wavelength of the radar. A simple explanation of this process is that under these conditions the radar reflections from successive crests of the ocean wave differ in phase by exactly one wavelength and therefore reinforce. CROMBIE'S (1955) discovery of this Bragg scattering mechanism provided the basis for hf radar oceanography and many of the techniques

in microwave radar oceanography.

hf radar techniques fall into two classes depending on the mode of propagation of the radar energy between the radar and the ocean surface. In the ground wave mode energy propagates as a combination of a direct line of sight wave, a wave reflected from the earth's surface and a surface wave. The surface wave, which predominates for over-the-horizon distances and antennas at ground level, is a guided wave trapped by the interface between the conducting sea water and the air. This wave can therefore propagate beyond the line of sight horizon resulting in maximum radar ranges of up to 300km at 1-2MHz and up to 100km at frequencies around 30MHz. Ranges substantially greater than these can be obtained by using the skywave mode. In this propagation mode the radar beam propagates into the upper atmosphere where it is reflected back down to the sea surface by an ionised layer. The echo from the sea surface returns by the same path (fig. 1.1). At the typical frequencies used (around 30MHz) the reflection is from the F region of the ionosphere at a height of about 300km. Maximum ranges with this technique are about 3000km. Ionospheric reflection geometry, however, imposes a minimum range of 1000km. Data obtained by the skywave technique are not as accurate as those obtained by ground wave propagation as movement of the ionospheric layer can contaminate the echo. In addition, as ionospheric

conditions are highly variable, it may not always be possible to obtain a stable propagation path to the point of interest on the sea surface.

With either of these techniques the motion of the Bragg scattering waves on the ocean surface causes the frequency of the received echo to be Doppler shifted from the transmitted frequency. The raw data obtained from hf radar is a Doppler spectrum giving the echo power as a function of Doppler shift from the transmitted carrier. Oceanographic data are obtained by interpreting this Doppler spectrum. Data that have been obtained with hf radar include directional and non-directional ocean waveheight spectra, significant wave height, wind speed and direction, the period and direction of arrival of swell and surface current velocities. The most successful and widely established measurements are the measurement of wind speeds and directions at long ranges using skywave radar (STEWART and BARNUM 1975) and the measurement of surface current vectors using groundwave radar (BARRICK et. al., 1977; LIPA and BARRICK, 1983).

(2) Microwave techniques. These techniques make use of both specular reflection from the ocean surface, as in a traditional radar, and Bragg scattering. At microwave frequencies Bragg scattering occurs from short capillary waves, with wavelengths of the order of centimetres,

rather than the longer gravity waves detected by hf radar. Information on these longer gravity waves is obtained through their modulating effects on the capillary waves. The simplest microwave technique is a conventional radar (i.e. with a rotating beam and plan position indicator display) set up on the coast or on a ship at sea. Radar echoes from ocean waves are often visible as "sea clutter" on the displays of such systems. Under certain conditions images of long period ocean wave trains may be present and from these it is possible to estimate the period and direction of arrival of the waves.

Sea surface roughness (i.e. waveheight) may be measured with a satellite mounted radar altimeter. This radar transmits a narrow pulse directly downward towards the earth. From the time taken for the echo from the earth to be received back at the satellite the altitude of the satellite may be determined. Alternatively, if the orbit of the satellite is accurately known the topography of the earth's surface may be accurately measured. If a radar altimeter with a sufficiently narrow pulse is used over the ocean the received echo will be broadened by an amount which is a function of the ocean waveheight. The waveheight can thus be determined from the echo pulse width once this pulse width has been calibrated against conventional waveheight measurements. A similar technique uses a beam transmitted obliquely towards the earth (as

opposed to vertical incidence). If the sea surface is perfectly smooth a specular reflection will not be observed back at the satellite. Deviations from a smooth surface caused by ocean waves, however, will scatter some energy back to the satellite. A scatterometer measures this backscattered energy and determines the ocean waveheight from it.

A satellite or aircraft mounted radar may be used to form an image of the wave pattern on the ocean surface by means of the synthetic aperture technique. In this technique the motion of the satellite is used to synthesize a radar antenna much larger than the physical antenna. Due to its size this synthesized antenna has a resolution high enough to detect individual waves. Synthetic aperture radar images can be subject to a two dimensional Fourier transform in order to obtain directional ocean waveheight spectra.

An interesting ground based microwave technique makes use of the Bragg scatter of microwaves from capillary waves mentioned previously. If two closely spaced microwave frequencies are transmitted towards the sea surface an echo is obtained which appears to be due to Bragg scatter of a wave with a frequency equal to the difference between the transmitted frequencies. This effect is due to modulation of the capillary waves (which

Bragg scatter the individual frequencies) by longer ocean waves (which would Bragg scatter the difference frequency - if this frequency had been transmitted directly). By varying the difference between the transmitted frequencies over a suitable range it is thus possible to measure the ocean waveheight spectrum (PLANT, 1977; BARRICK, 1972b).

An excellent review of the entire field of radar oceanography has been given by SHEARMAN (1983). A more detailed review of hf ground wave techniques may be found in BARRICK and LIPA (1979b). One fact that emerges in consideration of the various systems is that rather than any technique being superior to any other the techniques are complementary in their advantages and disadvantages. Satellite techniques, for instance, can give intermittent coverage over almost the entire ocean area of the earth. In contrast ground based techniques give continuous coverage of a more limited area. Similarly skywave hf radar provides long range data which is subject to ionospheric contamination. On the other hand ground wave hf radar, while limited in range, is free of this contamination and can obtain data from close ranges that are inaccessible to skywave systems. The antennas used for microwave systems are compact and relatively portable whereas those used at hf are often large and expensive. In contrast ground based microwave radars are limited to line of sight operation whereas almost all current hf systems

can obtain data from beyond the line of sight horizon. The vhf region of the spectrum (30-300MHz) is presently unexplored for the purposes of radar oceanography. We suggest in this work (chapter 8) that a system operating at these frequencies may be able to combine the advantages of compact antennas with microwave systems and over-the-horizon coverage with hf systems.

In conclusion the choice of a particular radar oceanographic system (or whether to use radar at all) will be dictated by the nature of the oceanographic problem for which data is required. For example coastal erosion studies would use microwave or hf groundwave systems. Global monitoring of surface wind speeds would require satellite techniques while continuous monitoring of sea states in, for example, the Tasman sea could best be done by the skywave hf technique.

1.2 AIMS AND SCOPE OF THIS WORK

Two factors influenced the descision to undertake this work. Firstly very little radar oceanography has been done in New Zealand since CROMBIE'S (1955) pioneering work. This is in spite of the fact that there are many potential uses for radar oceanographic information in New Zealand. As examples coastal erosion studies need sea state and wave direction information while Meteorologists are interested in routine monitoring of coastal sea states. In addition weather forcasting in New Zealand is made difficult by the lack of wind speed and direction information from the vast areas of ocean surrounding the country. Skywave hf radars have a proven ability to obtain this information.

Secondly, hf oceanographic radars have close similarities to hf radars developed for ionospheric observation. If these ionospheric radars are situated near a coast echoes from ocean waves are often obtained as a byproduct of the ionospheric observation (DOWDEN, 1957). It is not surprising, therefore, that much current radar oceanographic research is carried out by previous ionospheric researchers or at ionospheric installations (e.g. Shearman's group (SHEARMAN, 1983) and the groups at Adelaide and Townsville, Australia). The Physics Department at the University of Canterbury has a strong

tradition of ionospheric and atmospheric research. This research is carried out at a field station at Birdlings Flat, a coastal site. As a result echoes from ocean waves have often been observed (FRASER and VINCENT, 1970).

On the basis of these two factors a trial investigation of radar oceanography was proposed. The hf groundwave technique was chosen as:

(a) higher quality spectra are obtained than with the skywave technique,

(b) a wide variety of useful information can be exracted from these spectra,

(c) The equipment is compatable with equipment existing at Birdlings Flat,

(d) the antenna systems are simpler and cheaper than those for skywave systems,

(e) the knowledge gained in the construction of this system can be directly applied to more elaborate systems (e.g. skywave or direction finding systems) in the future. All of these features of the hf groundwave system are

consistent with the requirements of an initial investigation.

The design of a new system at any research establishment always has features and problems unique to that establishment (Murphy's law!). As a result the emphasis in this work is on the problems inherent in the design, construction and operation of the radar and on the steps leading up to the production of Doppler spectra of sea echo. The radar design information developed during this work is not readily available in the literature and will therefore be of interest to other researchers wishing to develop their own radar systems. In contrast the subsequent analysis of the sea echo Doppler spectra to obtain oceanographic information has been extensively treated in the literature (e.g. BARRICK, 1977 a,b; LIPA and BARRICK, 1980; FORGET et.al., 1981) and is a relatively straight-forward data analysis problem not subject to the unique difficulties of experimental research.

An important part of this work has been the investigation and understanding of the role played by groundwave propagation conditions in determining the performance of the radar system. This work is described in chapter 6. Due to the interdisciplinary nature of radar oceanography it was realised that some readers may be

oceanographers not acquainted with radar theory or, alternatively, radar experts not acquainted with oceanography. For this reason a review of the basic principles of oceanography is given in chapter 2 and a review of the theory of pulsed Doppler radars is given in chapter 3. In chapter 3 we also apply the theory of pulsed Doppler radars to the specific case of hf oceanographic radars and determine design rules for the basic radar and data analysis parameters. This work lays the foundations for the groundwave propagation and radar performance analysis work in chapter 6. Chapter 4 combines oceanographic and radar theory to outline the characteristics of the sea echo Doppler spectrum. The previously mentioned work on obtaining oceanographic information from this spectrum is reviewed. The system hardware and software for data collection and processing are described in chapters 5 and 7.

CHAPTER 2:

BASIC OCEANOGRAPHY

2.1 WAVE MOTION IN THE OCEAN

Wave motion can occur in any physical system in which a restoring force acts to return some system variable to an equilibrium value. The ocean is no exception to this rule. A large number of restoring forces gives rise to an equally large variety of wave motions within the ocean and on its surface. Following MEI (1983) we can classify these waves according to their restoring force, their typical period and the region of the ocean in which they are found.

The shortest period waves are sound waves. These are the result of the restoring force provided by the slight compressibility of sea water and have typical periods ranging from 10^{-2} to 10^{-5} seconds.

Next come capillary waves with periods of the order of 0.1 seconds. As surface tension provides the restoring force for these waves they exist only at the interface between two different media e.g. air and water.

Gravity waves, as their name suggests, arise because of a restoring force equal to the difference between the gravitational and bouyant forces on a particle. Due to their large range of periods (seconds to days) gravity

3

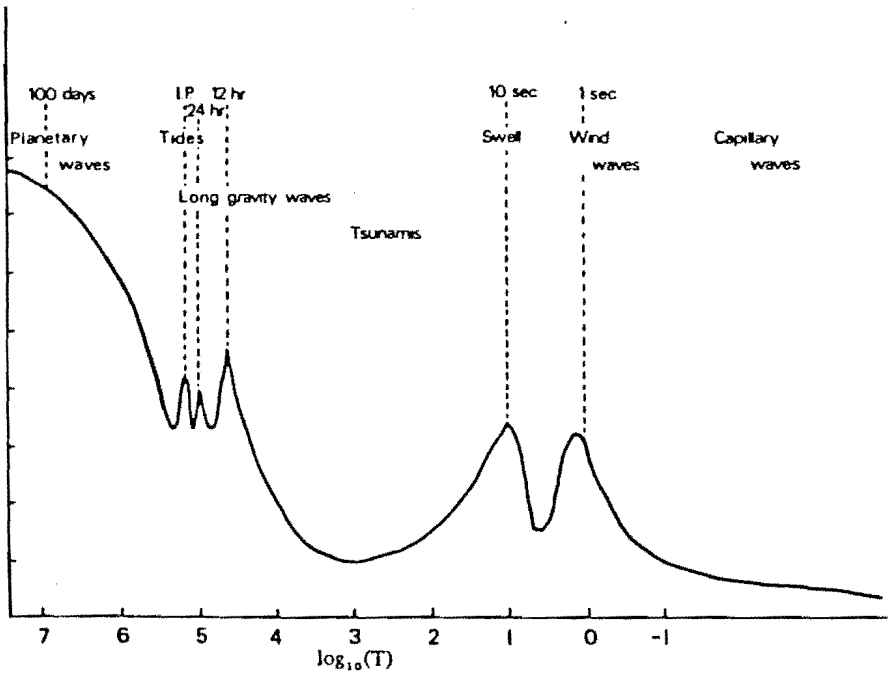

Fig. 2.1. Schematic energy spectrum of oceanic variability, showing the different types of waves occurring in the ocean. I.P. denotes the inertial period and is defined as $\pi/\Omega|\sin\phi|$, where Ω = magnitude of the Earth's rotation vector and ϕ is the geographic latitude (Section 3). In this picture I.P. = 35 hours, corresponding to a latitude of ± 20°. The relative amplitudes of the various parts of the spectrum do not necessarily reflect actual conditions.

(From LeBLOND and MYSAK, 1978)

waves are further subdivided on the basis of their generation mechanism. The shortest period gravity waves are generated by the action of wind on the ocean surface and have typical periods ranging from 1 second to 20 seconds. Earthquakes and landslides on the ocean floor generate tsunamis, which are gravity waves with periods ranging from ten minutes to over an hour. The final example of surface gravity waves are tides. These are gravity waves with periods of 12 to 24 hours. The driving force for these waves is the gradient of the gravitational attraction of the moon and the sun.

Gravity waves are not restricted to the ocean surface. Variaitons in water density within the ocean (e.g. due to temperature or salinity changes) can provide the bouyant part of the restoring force neccessary for gravity waves to exist. These waves are an important class of waves known as internal waves. Their periods range from a few minutes to half a day.

Coriolis force, due to the earth's rotation, begins to have an important effect as we move towards very long period gravity waves. The effect of Coriolis force is noticeable in tide sand storm surges, which are gravity waves generated by atmospheric pressure fluctuations. In the extreme case of oceanic planetary waves, which have periods of the order of 100 days, the variation of

Coriolis force with latitude actually supplies the restoring force for the wave motion.

Fig. 2.1 (from LeBLOND and MYSAK 1978) is a purely schematic energy spectrum showing the various types of waves that exist on the ocean surface. In this work we will be almost exclusively concerned with wind generated surface gravity waves.

The basic properties of surface gravity waves are given by the first order, linear solution to the equation for irrotational, incompressible fluid motion with gravity and pressure gradient forces acting as the only force terms. Detailed mathematical treatments are given by PHILLIPS (1966), MEI (1983) and LeBLOND and MYSAK (1978). The account given by KINSMAN (1965) is very detailed and gives a great deal of insight into the physical meaning of the mathematics.

The basic gravity wave solutions are sine waves with wavelength, λ , and period, T, related by the dispesion relation:

$$\omega^2 = g\kappa \tanh(\kappa d_{max}) \qquad 2.1$$

where

$$\omega = 2\pi/T$$

and

$$\kappa = 2\pi/\lambda$$

d_{max} is the water depth.

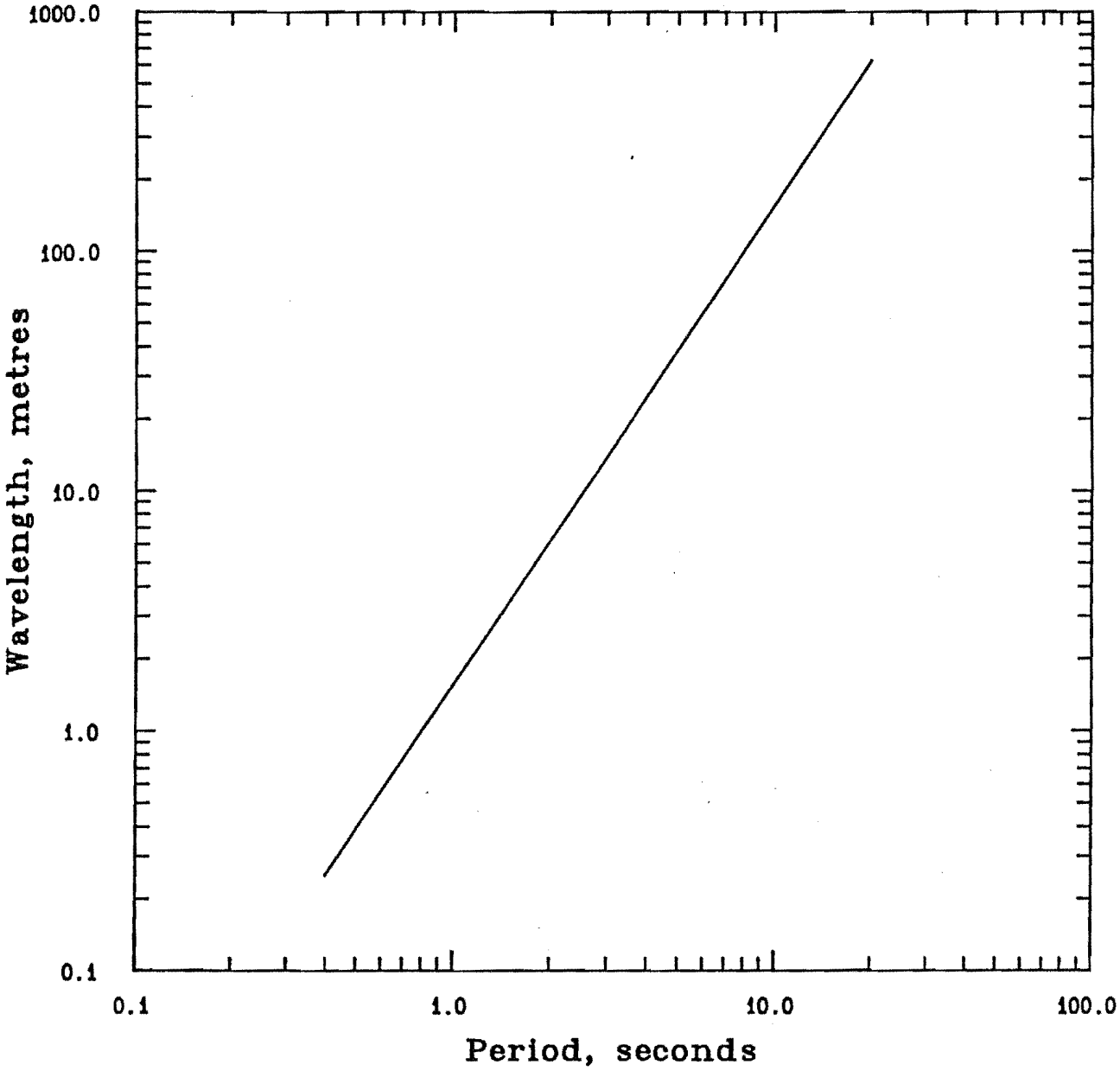

Fig. 2.2 Gravity wave dispersion relation.

The phase velocity of the wave, v_ϕ , is therefore given by:

$$v_\phi^2 = \left(\frac{\omega}{\kappa}\right)^2 = \frac{g}{\kappa} \tanh\ (\kappa d_{max}) \qquad 2.2$$

Two approximations to the hyperbolic tangent function are possible: When κd_{max} is small (< 0.33) we have $\tanh(\kappa d_{max}) \approx \kappa d_{max}$ and when κd_{max} is large we have $d_{max} \approx 1$. The phase velocity for these two cases becomes:

$$\begin{aligned} v_\phi^2 &= g d_{max} \qquad \kappa d_{max} \text{ small} \\ v_\phi^2 &= g/\kappa \qquad \kappa d_{max} \text{ large} \end{aligned} \qquad 2.3$$

Physically, the condition that κd_{max} is small corresponds to water that is shallow compared to the wavelength i.e. $\lambda > 20 d_{max}$. In this case the phase velocity of the wave is determined entirely by the water depth. Interesting examples of shallow water gravity waves are tsunamis and tides, which, because of their long wavelength, are shallow water waves even in the open ocean. From the phase speeds of tsunamis (approximately 200 m/s) a value for the average depth of the ocean can be found (approximately 4000m).

The condition that κd_{max} is large physicaly corresponds to the condition that the water is deep compared to the wavelength i.e. $\lambda < 4\, d_{max}$. The velocity of these waves is dependant upon their period. i.e.

$$v_\phi = \frac{g}{2\pi} T \approx (1.5)\ T\ ms^{-1}$$

and 2.4

$$\lambda = \frac{g}{2\pi} T^2 \approx (1.5)\ T^2\ m\ .$$

Hence deep water waves are dispersive with longer waves travelling faster than shorter waves. A plot of the gravity wave dispersion relation is given in fig. 2.2. The basic properties of deep water waves are illustrated in fig. 2.3. The water particles move in circular orbits. This fact can be easily seen if an object floating in swell is observed. The radius, r, of the circular orbit is equal to the wave amplitude, a, at the surface and decreases exponentially with depth. i.e.

$$r = ae^{-\kappa d} \qquad 2.5$$

The fact that the rate of decay is greater for shorter waves indicates that a low pass filtering effect takes place as one goes deeper beneath the surface. As we will see in section 2.5 this has important consequences for some types of wave recorders.

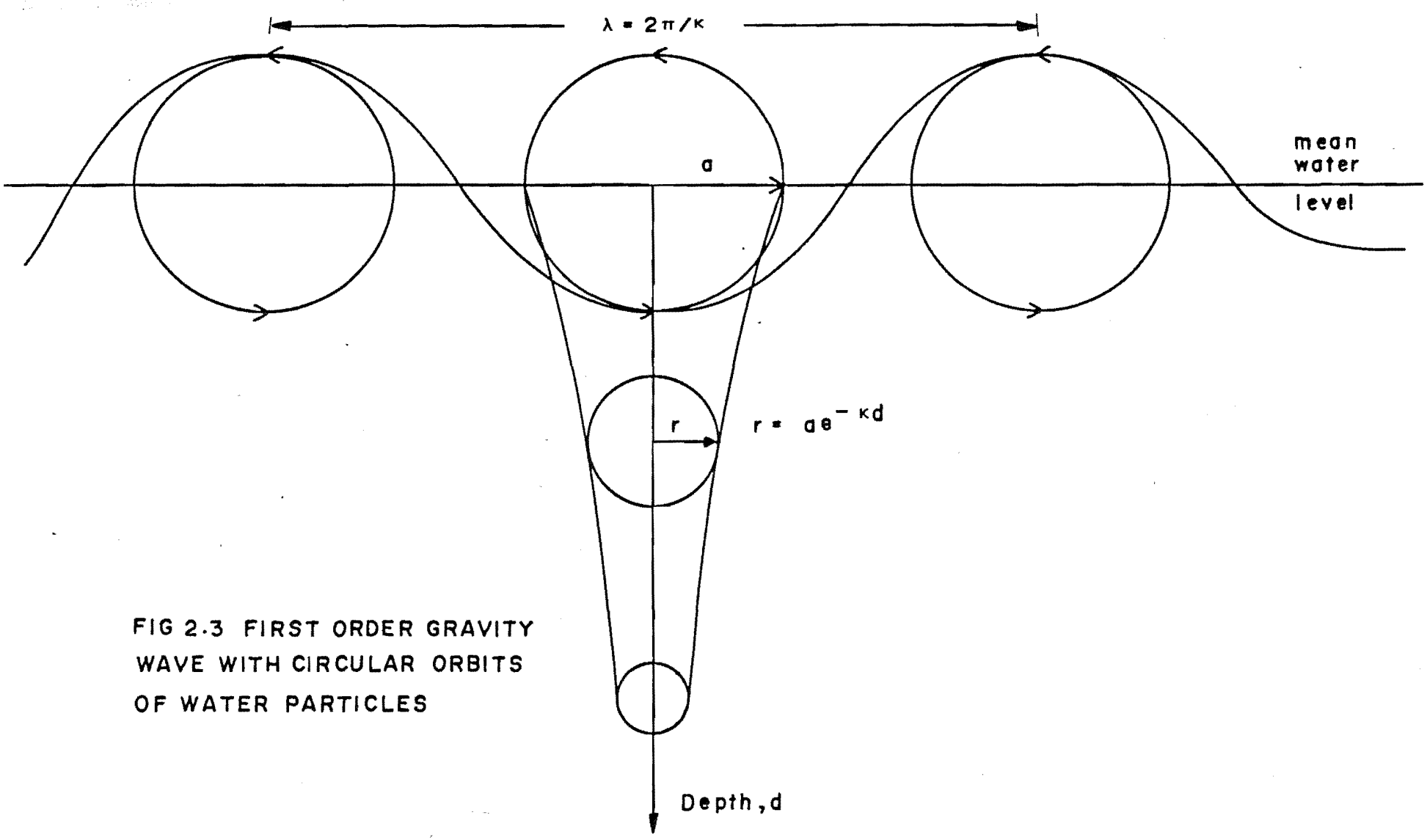

FIG 2.3 FIRST ORDER GRAVITY WAVE WITH CIRCULAR ORBITS OF WATER PARTICLES

Water waves in shallow water waves move in elliptical orbits with semi-major axis, A, and semi-minor axis, B, given by:

$$A = \frac{a}{\kappa d_{max}} \qquad B = a\,\frac{d_{max}+d}{d_{max}} \qquad 2.6$$

Thus the semi-major axis, which is horizontal, stays constant with depth while the vertical semi-minor axis decreases linearly with depth and becomes zero on the ocean floor.

Wave motion usually transports energy from one point to another. In the case of ocean surface waves this energy transport is considerable. MEI (1983) and KINSMAN (1965) show that the energy per unit surface area, E, in a monochromatic surface wave is:

$$E = \tfrac{1}{2}\rho g a^2 \qquad 2.7$$

This energy is equally partitioned between kinetic and potential energy. Multiplication of this quantity by the wave group velocity, $\frac{1}{2}v_\phi$, gives the energy flux per unit

length of wave crest:

$$F = \tfrac{1}{4}\, g a^2 v_\phi = \frac{\rho g^2 a^2 T}{8\pi} \qquad 2.8$$

As a typical example consider a wave with amplitude a = 1m and period T = 10s. The surface energy density is 5000 Jm^{-2} and the energy flux is 39kW/m. These figures make the current interest in tapping this energy source understandable (SHAW 1982).

These expressions apply to a single, sinusoidal gravity wave. In order to apply them to an actual wave field they require some generalization. This generalization to ocean waveheight spectra will be provided in the next section.

2.2 THE OCEAN WAVEHEIGHT SPECTRUM

It is only under very special conditions that the real sea surface approximates the simple sinusoidal form of the first order gravity wave solution. Usualy, in a storm driven sea, the height of the ocean surface above its mean level, η ,is a highly irregular, random function of position and time, $\eta(x, y, t)$. KINSMAN (1965) gives several excellent photographs showing this random character of the sea surface. In order to represent the sea surface mathematically we consider it to be an interference pattern resulting from the superposition of sinusoidal plane waves of all wavelengths, λ , frequencies, $f = 2\pi/T$, and directions of propagation, θ . Thus we can describe the sea surface as a power spectrum giving the energy in a narrow band of wave components as a function of the wavelengths and frequencies of the components. This spectrum is defined as the Fourier transform of the autocorrelation function of surface waveheight:

$$S(\underline{\kappa},\omega) = \frac{1}{(2\pi)^3} \iiint < \eta(x,y,t)\, \eta\,(x+\Delta x, y+\Delta y, t+\Delta t) > e^{-i\kappa_x \Delta x - i\kappa_y \Delta y + i\omega\Delta t}\, d\Delta x d\Delta y d\Delta t \qquad 2.9$$

Where $\underline{\kappa} = (\kappa_x, \kappa_y)$ is the wavevector of the ocean wave component propagating in the direction $\theta = \tan^{-1}(\kappa_y/\kappa_x)$.

This spectrum is completely general and can be applied to any time varying rough surface. In particular, the component waves of the spectrum are not restricted to first order gravity waves but can be waves resulting from second or higher order hydrodynamic processes. The spectrum is also multi-dimensional, being a function of the two components of spatial wavevector and temporal frequency. Thus numerous forms of ocean waveheight spectra are quoted in the literature (e.g. JOHNSTONE 1975 Ph.D. thesis) corresponding to the many possible ways of reducing the number of dimensions in the spectrum.

If we restrict our attention to first order wave components the dispersion relation (eqn. 2.1) can be used to eliminate one variable from the spectrum to give what is known as the directional ocean waveheight spectrum $S(\kappa_x, \kappa_y)$ i.e. :

$$S(\kappa_x, \kappa_y, \omega) = S(\kappa_x, \kappa_y)\ \delta\ (\omega - \sqrt{g\kappa})$$

with 2.10

$$\kappa = \sqrt{\kappa_x^2 + \kappa_y^2}$$

The Cartesian form, $S(\kappa_x, \kappa_y)$ is used mainly in electromagnetic scattering theories (chapter 4). For practical work it is more convenient to use a polar form of the spectrum. The transformation between the two uses

the normalization condition that both forms, when integrated, must give the same total energy for the ocean surface (JOHNSTONE 1975 Ph.D. thesis). Hence:

$$S(\kappa_x, \kappa_y) = \frac{g}{2[g\kappa]^{3/2}} S(\kappa, \theta) \qquad 2.11$$

with

$$\underline{\kappa} = (\kappa_x, \kappa_y) = (\kappa, \theta)$$

$$\tan\theta = \kappa_y / \kappa_x$$

We can use the first order dispersion relation once again to substitute ω for κ giving the temporal directional ocean waveheight spectrum $S(\omega, \theta)$. . The sea surface is now represented by a superposition of many first order waves with frequencies, ω , $\kappa = \omega^2/g$ and propagation directions, θ .

The next step in the simplification of these spectra is to integrate out the directional dependance, θ , to give non-directional ocean waveheight spectra:

$$S(\kappa) = \int_0^{2\pi} S(\kappa, \theta)\, d\theta$$

$$S(\omega) = \int_0^{2\pi} S(\omega, \theta)\, d\theta \qquad 2.12$$

These are the forms of the ocean waveheight spectrum that are most commonly found in texts on oceanography. This partly reflects the relative ease of obtaining non-directional versus directional ocean wave information

(section 2.5). For instance $S(\omega)$ is the spectrum that would result from spectral analysis of a record of surface height at some point versus time.

Finally, the non-directional spectra can be integrated to give a single parameter characterising the roughness of the surface. This is the rms waveheight, h:

$$h^2 = \int_0^\infty S(\omega)\, d\omega \qquad 2.13$$

Several other sea state parameters can be related to the rms waveheight. The significant wave height, $H_{1/3}$, defined as the average height of the largest 1/3 of the waves is given by:

$$H_{1/3} = 4h \qquad 2.14$$

Where it is assumed that the distribution of surface heights is the Rayleigh distribution. Note that here we are measuring height from trough to crest rather than from mean water level to the surface as previously. To avoid confusion we will use an upper case H to distinguish this type of measurement. Now-a-days it is usual to define

significant wave height by eqn. 2.14. This significant waveheight is usually denoted Hs.

The mean waveheight, $\bar{H}$, and the average height of the largest 1/10 of the waves are two other commonly used parameters. They are given by (BLACK and HEALY 1981):

$$\bar{H} = 0.626\ H_S$$

and

$$H_{1/10} = 1.271\ H_S \qquad 2.15$$

The non-directional ocean waveheight spectrum has units of $m^2 s$ and gives the variance, h^2 , of the surface in a narrow band of frequencies. We can convert this variance to energy density by multiplying by the appropriate constants. Hence:

$$E(\omega) = \rho\ g\ S\ (\omega) \qquad 2.16$$

is the ocean wave energy spectrum with units $Jm^{-2}s$ and the total energy density of the ocean surface, in Jm^{-2} , is found by integrating over frequency:

$$E = \rho g \int_0^\infty S(\omega)\ d\omega = \rho\ g\ h^2 \qquad 2.17$$

Compare this with eqn. 2.8 for the case of a single sinusoidal component.

Most of the tabulated information on ocean waves is in the form of one or the other of these sea state parameters. Again, this reflects the fact that it is much easier to measure and store one parameter than a complete ocean wave spectrum. Additionally, parameters such as significant wave height can be estimated form visual observation on board a ship or a lighthouse. The term "sea state" refers to a scale of numbers, from one to eight, traditionaly used by mariners to describe the visual appearance of the ocean surface. This sea state scale has been found to correlate quite well with other measures, such as significant wave height

2.3 GENERATION OF OCEAN WAVES BY THE WIND

The most common gravity waves on the ocean's surface are generated by the action of wind. The exact mechanism for this process is, at present, uncertain although some basic details are understod. A simple physical description of the generation of ocean waves by the wind may be found in SHEARMAN (1983) while more detailed accounts are given by KINSMAN (1965) and LeBLOND and MYSAK (1978).

If a wind starts blowing over a completely smooth ocean surface, turbulence and pressure irregularities in the wind will cause small capillary waves to form on the surface. These capillary waves roughen the surface thereby increasing the friction between the surface and the wind. This allows more momentum to be transferred from the wind to longer gravity wave components. Eventually, for a given steady windspeed, an equilibrium condition will be reached in which the energy input to any given component of the ocean waveheight spectrum will equal the energy loss from this component and no further development of the spectrum will occur. Wave components that have reached this equilibrium condition are said to be saturated. The resulting ocean waveheight spectrum is said to be fully developed.

An equation for the energy balance of an ocean wave component can be written by considering that the rate of change of surface energy density of the component is due to the nett input of energy from sources and sinks, $W(\underline{\kappa})$, and the advection of energy away from the area under consideration. Hence:

$$\frac{\partial E(\underline{\kappa})}{t} + \nabla .\{(v_c+v_g)E(\underline{\kappa})\} = W(\kappa) \qquad 2.18$$

We have allowed for the possibility that energy may be carried from the region by a current, with velocity v_c, as well as by natural propagation of energy at the group velocity, $v_g = \frac{1}{2}v_\phi$, of the component. The equilibrium condition will be reached when

$$\frac{\partial E(\underline{\kappa})}{\partial t} = 0 \qquad 2.19$$

for all wave components, $\underline{\kappa}$.

The energy sources in the term $W(\underline{\kappa})$ are the wind and energy transfer from shorter waves by non_linear hydrodynamic interactions between these waves. The energy sinks are breaking of the wave, viscous damping and transfer of energy to longer components by non-linear interactions. Breaking is by far the most important of

these loss terms. Breaking occurs when the amplitude of the wave becomes so large that the maximum downward acceleration of a particle at the water surface becomes equal to the gravitational acceleration. Any further increase in amplitude will then result in water becoming detached from the surface as foam. The resulting energy loss from breaking thus sets an upper limit to the amplitude of the wave component. PHILLIPS (1958) showed by means of a dimensional argument that this equilibrium, or saturated, amplitude depended only on the wave frequency and not on the wind speed. This equilibrium amplitude is of the form:

$$S(\omega) \propto \omega^{-5} \qquad 2.20$$

The wind speed, however, determines a low frequency cutoff point for this relationship as we do not expect much transfer of energy from the wind to wave components travelling faster than the wind to occur.

On the basis of these arguments PHILLIPS (1958) proposed the first mathematical expression for the spectrum of a fully developed sea:

$$S(\omega) = \begin{cases} \beta_e g^2/\omega^5 & \omega \geq g/u \\ 0 & \omega < g/u \end{cases} \qquad 2.21$$

Where u is the wind speed (m/s) and the Phillips saturation constant, β_e , has been found from comparison with observed spectra to lie in the range $5x10^{-3}$ - $1.48x10^{-2}$. A plot of the Phillips spectrum with $\beta_e = 5x10^{-3}$ and with cutoffs corresponding to different wind speeds is given in fig. 2.4.

Two mechanisms have been proposed for the transfer of energy from the wind to the waves. In the resonant interaction mechanism, energy is fed directly from random fluctuations in air pressure to ocean wave components with the same spatial scale. When the ocean waves become sufficiently developed energy may be transferred by induced interactions in which the waves perturb the flow of air above them to produce pressure variations that are coupled to the wave.

Non-linear interactions between wave components are of two types depending on the relative frequencies of the interacting waves. If the components have widely differing frequencies the long wave component appears to the short wave component as an oscillating current which periodically modulates the short wave. For components with nearby frequencies the non-linear interaction arises from second and higher order terms in the hydrodynamic equations for fluid motion. The result of these non-linear interactions is a "cascade of energy" form short waves to

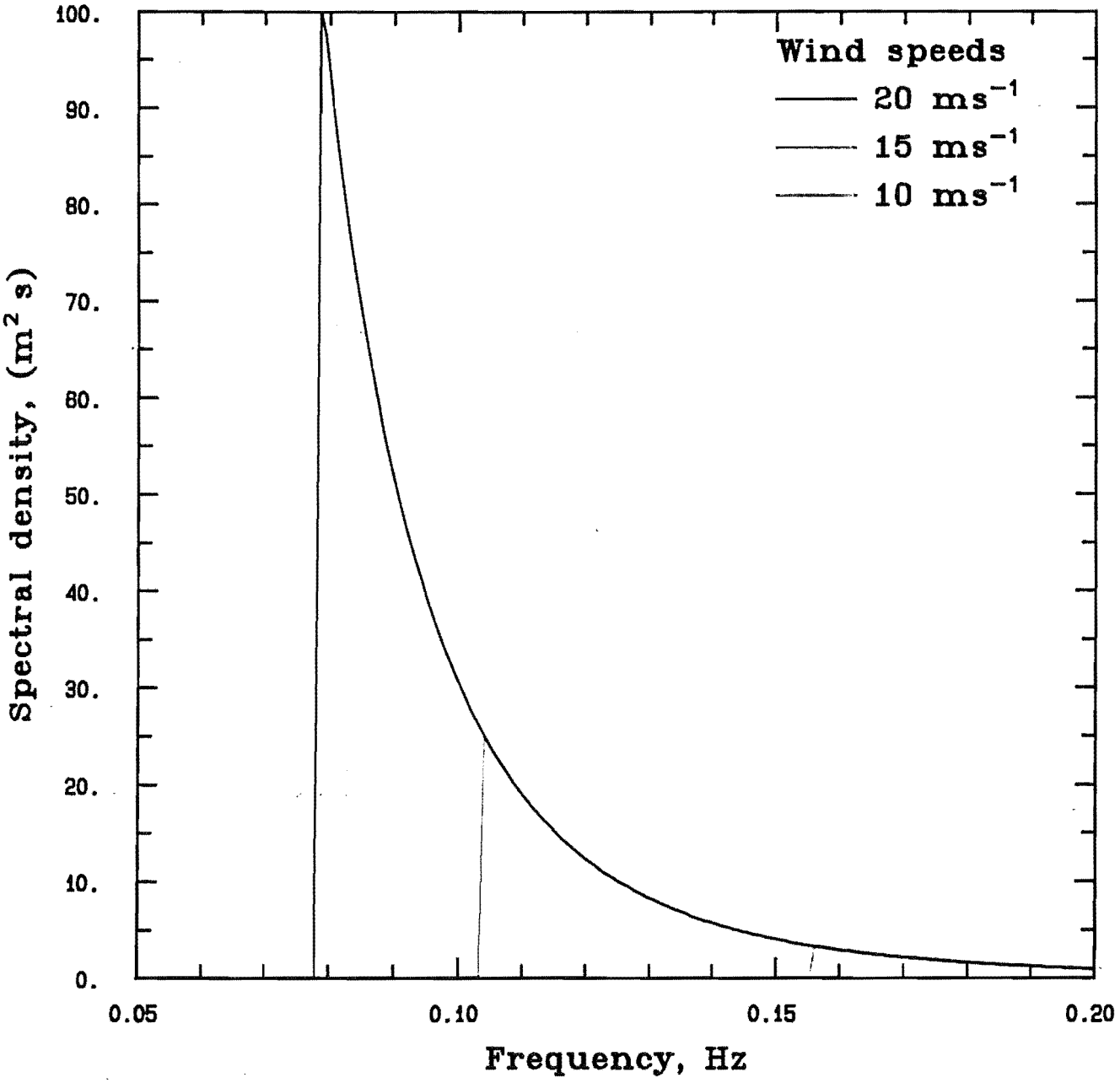

Fig. 2.4 The Phillips spectrum.

longer waves and a concentration of energy in the peak of the spectrum near the cutoff frequency $\omega = g/u$. This process has been compared to maser action (KRAUS, 1972).

When compared to observed ocean waveheight spectra the Phillips spectrum, eqn. 2.21, is found to have a number of deficiencies. The most important of these is that it applies only to a fully developed sea in which every component has reached its equilibrium amplitude. However considerable time is required for the longer wave components to reach their equilibrium amplitude, and, during this time, these waves will propagate for a large distance because of their high velocities. Therefore the wind must be of sufficient duration and must exist over a sufficient extent of ocean, known as the fetch, in order for the spectrum to become fully developed. Spectra for which these conditions are not met are said to be duration limited or fetch limited respectively.

Secondly, observed spectra do not have a cutoff at $\omega = g/u$ that is as sharp as that implied by the Phillips spectrum. Although very little energy can be transferred directly from the wind to components with greater phase velocities the non-linear processes discussed previously can generate these longer components. As a result the cutoff at $\omega = g/u$ is much more gradual than that given by the Phillips spectrum.

Finally, the Phillips spectrum is a model for the non-directional ocean waveheight spectrum and takes no account of the observed directional properties of ocean wave spectra.

Many model spectra have been proposed to take account of these difficulties. Most of these spectra were the result of studies in which many observations of actual ocean waveheight spectra were made and a mathematical form developed to provide a good fit to the measured data. BLACK and HEALY (1981) and KINSMAN (1965) provide good accounts of these model spectra and the history of their development. The model spectra can be roughly classified according to which of the three previously mentioned difficulties they attempt to solve.

The problem of non-linear transfer affecting the low frequency cutoff is dealt with by using an exponential function to provide a smoother cutoff. Hence these spectra have the general form:

$$S(\omega) = \frac{A}{\omega^5} \exp\left(\frac{B}{\omega^4}\right) \qquad 2.22$$

Where A and B are functions of wind speed. At high frequencies they retain the ω^{-5} tail of the Phillips spectrum. A good example of this class of spectra is the Pierson Moskowitz spectrum (PIERSON and MOSKOWITZ 1964):

$$S(\omega) = \frac{\beta_e g^2}{\omega^5} \exp\left[-\nu\left(\frac{\omega_c}{\omega}\right)^4\right] \qquad 2.23$$

Where $\omega_c = g/u$ is the cutoff frequency and the constant, ν, is empirically found to be $\nu = 0.74$. A plot of this spectrum for several windspeeds is given in fig. 2.5.

The directional properties of spectra are usualy considered by writing the directional ocean waveheight spectrum as the product of a non-directional spectrum and a directional function, $G(\theta)$ i.e.

$$S(\omega,\theta) = S(\omega)\, G(\theta) \qquad 2.24$$

Where $\theta = 0$ is the wind direction and $G(\theta)$ is normalised so that integration of $S(\omega, \theta)$ over angle yields the non-directional spectrum $S(\omega)$ (Eqn. 2.12) i.e.

$$\int_{-\pi}^{+\pi} G(\theta)\, d\theta = 1 \qquad 2.25$$

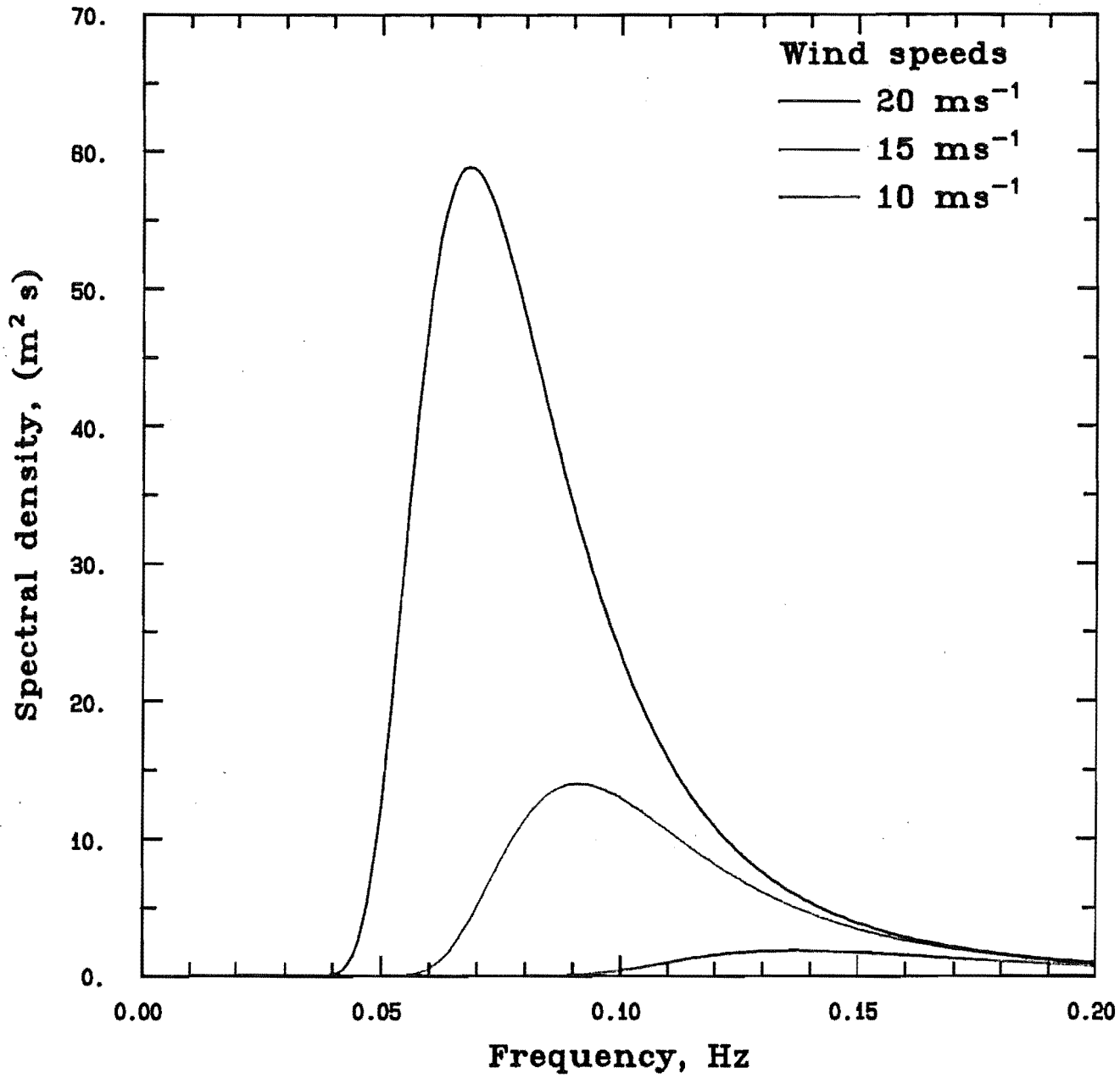

Fig. 2.5 The Pierson–Moskowitz spectrum.

The simplest direcitonal function is the semi-isotropic form:

$$G(\theta) = \begin{cases} \frac{1}{\pi} & -\frac{\pi}{2} \leqslant \theta \leqslant +\frac{\pi}{2} \\ \\ \theta & \text{otherwise} \end{cases} \qquad 2.26$$

Which describes a wave component having a constant amplitude for all directions within 90 degrees of the wind direction and zero amplitude in directions with a component opposed to the wind direction.

A more gradual decrease of amplitude with direction is provided by an important class of functions with the general form:

$$G(\theta) = \frac{\cos^{s}(a\theta)}{N} \qquad 2.27$$

Where N is a normalisation constant chosen so that eqn. 2.25 applies. An example is the cardioid distribution which has s = 2 and a = 0.5 giving N = $1/\pi$. i.e.

$$G(\theta) = \frac{1}{\pi} \cos^{2}\left(\frac{\theta}{2}\right) \qquad 2.28$$

This function allows for propagation in all directions except that directly opposing the wind direction, $\theta = \pi$.

Munk (TYLER et.al. 1974) has generalised this form of the directional dependence to allow the possibility of a different spread of energy with different frequencies. This is done by wrriting s as a function of frequency:

$$G(\theta) = \frac{\cos^{s(\theta)}(\theta/2)}{N(s)} \qquad 2.29$$

The spreading is usualy greater for shorter high frequency waves than for the longer components.

The directional distributions considered so far do not allow any wave propagation directly against the wind ($\theta = \pi$). However there is much evidence from radar studies, including this work, that some energy propagates in the direction $\theta = \pi$ even under strong wind conditions (CROMBIE et.al., 1978; STEWART and TEAGUE, 1980). Munk has allowed for this by further generalising eqn. 2.27 to:

$$G(\theta) = \varepsilon + (1-\varepsilon) \cos^{s(\omega)}(\theta/2) \qquad 2.30$$

Where a typical value for ε is 0.05 (SHEARMAN 1981).Model directional spectra are formed by multiplying these directional distributions with any of the non-directional spectra.

All of the spectra we have been considering so far apply to fully developed seas for which the wind has been blowing long enough, and over a sufficient fetch, that each wave component has developed to its equilibrium amplitude. Several models have been proposed that describe the sea under conditions of limited fetch and wind duration. The first of these to come into general use was a wave forecasting system developed by Sverdrup, Munk and Bretschneider (KINSMAN 1965). This system predicted the mean height, H, and mean period of the ocean waves from the wind speed, the wind fetch and the water depth. The duration of the wind was assumed to be infinite.

The most recent fetch limited model spectrum is a result of the Joint North Sea Wave Project (JONSWAP):

$$S(\omega) = \frac{\alpha g^2}{(2\pi)^4 \omega^5} \exp\left[-\frac{5}{4}\left(\frac{\omega_m}{\omega}\right)^4\right]\gamma^q \qquad 2.31$$

This spectrum is an extension of the Pierson Moskowitz spectrum (eqn. 2.23), the main differences being the peak

enhancement factor γ^q and the fact that the parameters specifying this spectrum are functions of fetch. q is given by:

$$q = \exp\left[-(\omega-\omega_m)^2/2\sigma^2\right] \qquad 2.32$$

With

$$\sigma = \begin{cases} \sigma_a & \omega \leqslant \omega_m \\ b & \omega > \omega_m \end{cases}$$

The JONSWAP spectrum is thus specified by the five parameters ω_m , α , γ , σ_a , σ_b . If we define non-dimensional frequency and fetch by:

$$\begin{aligned} \bar{\omega}_m &= \omega_m u_{10} \\ \bar{x} &= xg/u_{10}^2 \end{aligned} \qquad 2.33$$

(where u is the wind speed measured 10m above the surface) the parameters can be given in terms of the fetch by:

$$\begin{aligned} \omega_m &= 3.5\ \bar{x}^{(-0.33)} \\ \alpha &= 0.076\ (2\pi)^5 \bar{x}^{(-0.22)} \\ \gamma &= 0.33 \\ \sigma_a &= 0.07 \\ \sigma_b &= 0.09 \end{aligned} \qquad 2.34$$

We have considered the generation of ocean waves by the wind. We now consider what happens to the waves when the wind dies out. As the energy losses from gravity waves are relatively small (below saturation amplitude and particularly at long wavelengths) waves can propagate to very large distances from the storm that generated them. However because gravity waves obey the dispersion relation (eqn. 2.1) longer waves will travel faster than the shorter waves so that the spectrum will become separated out into its component waves. As the spread factor, s, in the directional distribution (eqn. 2.29) decreases with increasing wavelength the long waves at the front of this dispersed wave train will approximate to plane waves. An observer at a distant point in the upwind direction from the storm will see nearly sinusoid waves with long crests and steadily decreasing period. This condition, known as swell, is one of the few instances when the sea surface takes on a regular form.

If the storm occurs at a time t_o a distance x from the observer the time at which waves of frequency ω will be observed is given by:

$$\frac{x}{t - t_o} = v_g \qquad 2.35$$

Since $v_g = g/2\omega$ we can rearrange this expression as:

$$\omega = \frac{g(t - t_o)}{2x} \qquad 2.36$$

Showing that the time and distance to a storm can be found from the intercept and slope of a graph of swell frequency versus time. MUNK et. al. (1963), BARBER and URSEL (1948) and BARBER (1954) describe a study in which waves originating from a storm near New Zealand were identified from wave records made in California by using this technique. Since swell is nearly monochromatic the direction of the storm could be estimated from the difference in phase of the waves between two observation points. SNODGRASS et. al. (1966) describe a similar study conducted in Honolulu.

2.4 METHODS OF WAVE OBSERVATION

The earliest wave observations came from visual observations from observers on either a ship or the coast. These observations were of single parameters such as sea state, average wave period or some measure of wave height (H, $H_{1/3}$, etc.). The measurement of non-directional ocean waveheight spectrum, $S(\omega)$ requires a time series of surface height relative to the mean sea level at a point (i.e. $\eta(x,y,t)$). The measurement of $S(\omega)$ will similarly require a spatial series of height measurements at a fixed point in time. The directional ocean waveheight spectra, $S(\kappa, \theta)$ and $S(\omega, \theta)$ will generaly require measurements to be made at many points over an area of the ocean surface.

A good summary of the various techniques for wave measurement is provided by STEWART (1980). The simplest methods for measuring surface height at a point use a vertical pole attached to the sea floor and protruding through the surface. The changes in water level relative to this pole are transduced into an electrical signal by means of the changes in resistance or capacitance of electrodes attached to the pole and partly immersed in the water. This technique relies on the fact that the pole is attached to the ocean floor to provide a reference level for the height measurement. The technique is, therefore,

suitable for use only in shallow water.

Deep water measurements can be made by using the same transducing systems attached to a vertical, floating spar buoy. This technique uses the fact that wave motion dies out exponentially with depth in deep water. (eqn. 2.5). If the buoy is long and thin then most of its buoyancy will come from those portions of it deep down in the ocean where motion due to the shorter wavelengths is small. It will therefore tend to remain at a constant height with respect to the mean water level. Sometimes a large horizontal disc is attached to the bottom of these buoys to provide additional damping of vertical motion.

If a sinusoidal gravity wave with amplitude, a, is present on the ocean surface pressure fluctuations, with amplitude, Δp, will occur beneath the surface:

$$\Delta p = \rho g a \frac{\cosh[\kappa(d+d_{max})]}{\cosh(\kappa d_{max})} \qquad 2.37$$

A pressure measuring device mounted on the ocean floor can therefore measure the amplitude of wave components on the surface and hence measure ocean wave spectra. Considerable care, however, is required in the interpretation of these measurements. If we consider shallow and deep water

approximations to eqn. 2.37 :

$$\Delta p_{deep} \approx \rho g a e^{-\kappa d}$$
$$\Delta p_{shallow} \approx \rho g a \qquad 2.38$$

We see that in deep water a low pass filtering effect takes place due to the shorter waves being more rapidly attenuated with depth than the longer waves. In the shallow water case the large horizontal water movements induced by the wave (section 2.2) can cause erroneous measurements due to the Bernoulli effect. STEWART (1980) discusses the conditions under which this effect will be important.

An important class of wave measurement techniques uses measurements of the acceleration of an object floating in the sea. The height of the surface is obtained by integrating the acceleration record twice with respect to time. Since the mean sea level has zero vertical acceleration this technique avoids the problem of providing a reference level and may therefore be used in deep water. A common example of this technique consists of a buoy fitted with either a pendulum or a gyroscope in order to maintain a vertical reference direction. An accelerometer attached to the pendulum or gyroscope will then measure the vertical component of the surface

acceleration. Rather than integrate this acceleration directly the spectrum of the acceleration, $\phi(\omega)$, is calculated. From the standard properties of Fourier transforms it is then easy to show that the non-directional ocean waveheight spectrum is given by:

$$S(\omega) = \frac{\phi \omega}{\omega^4} \qquad 2.39$$

In another implementation of the acceleration measurement technique accelerometers are mounted on a ship and measure the response of the ship to the waves. The ocean wave spectrum can then be found from calibrations of the ship response against an accelerometer buoy.

Measurements of the directional spectrum are much more difficult to make due to the need to make many simultaneous measurements over an extent of the surface. The most popular technique for direcitonal spectrum measurements is the pitch and roll buoy. This is an extension of the accelerometer buoy technique mentioned previously. As well as measuring vertical acceleration the pitch and roll buoy measures the slope of the surface by measuring the two components of the tilt of the buoy with respect to the vertical reference provided by the

pendulum. By fitting these measurements to a Taylor series expansion for the water surface the coefficients of the first five terms in a Fourier series expansion for the directional distribution of the ocean waveheight spectrum may be found. If we write the directional spectrum as

$$S(\kappa,\theta) = G(\kappa,\theta)\ S(\kappa) \qquad 2.40$$

Then the buoy data provides coefficients $a_i(\kappa)$, $b_i(\kappa)$ such that

$$G(\kappa,\theta) = a_o(\kappa) + a_1(\kappa)\cos\theta + b_1(\kappa)\sin\theta + a_2(\kappa)\cos^2\theta + b_2(\kappa)\sin^2(\theta) \qquad 2.41$$

It is interesting to note here that BARRICK and LIPA (1979a) have developed an hf radar technique that obtains these same five coefficients from inversion of the second order component of sea echo Doppler spectra (chapter 3).

The directional ocean wave spectrum may also be measured by means of an array of any of the sensors considered in the discussion of non-directional spectrum measurements. The problems here are analogous to similar problems in radio astronomy and seismology where the direction of arrival of a wave train is deduced from the variation in phase between individual wave sensors in an

array. Generally the accuracy of this technique is quite good provided that only one or two monochromatic waves are present. Otherwise the accuracy in the determination of the direction of arrival of the components falls off unless the array is made large compared to the wavelength of the waves being studied.

In addition to these wave observation techniques a number of exotic techniques have been used on odd occasions (STEWART 1980). An interesting example is the Stereo Wave Observation Project (SWOP) (KINSMAN 1967). The directional ocean waveheight spectrum was measured in this project by taking stereo pairs of photographs of the ocean surface from an aircraft. The heights of the surface at a grid of points covering the area of the photograph were found by using standard techniques of photogrammetry. The spectrum could then be calculated from a two dimensional Fourier transform of this array of heights.

None of these traditional means for measuring ocean waveheight spectra is entirely satisfactory. A single piece of apparatus can obtain measurements from only one point or, at most, a limited area of the ocean surface. The equipment is also directly exposed to the harsh marine environment and is liable to damage as a result. In heavy seas wave buoys can be pushed directly beneath the surface or overturned. Marine growths and organisms can interfere

with the operation of pole-type recorders and bottom mounted pressure transducers. Expensive underwater cables are sometimes required to connect pressure transducer recorders to the shore. As the size of most devices is much smaller than the wavelength of the waves being measured it is difficult for such devices to have a narrow beam directional response. Directional information is, therefore, limited to uncertainties of the order of ± 45 degrees. Arrays using interferometric, rather than beamforming, techniques have much smaller uncertainties but are limited in the number of directional components they can resolve. Additionally, the interpretation of data from conventional recorders requires care in order to avoid the systematic errors that can occur. KINSMAN (1967) gives an excellent dscussion of these sources of error.

The hf radar technique has the potential to overcome many of these disadvantages. A single set of equipment can provide simultaneous measurements at a large number of points covering a large area of the ocean surface. The equipment is usualy housed in a shore based installation and is therefore protected from damage by the marine environment.

From a single radar experiment several ocean surface parameters can be simultaneously measured. Examples are

sea state parameters, ocean waveheight spectra, wind speeds and directions, radial components of current velocities and peak frequencies and directions of arrival of swell. The particular parameter measured depends on the way the radar output data is analysed and does not depend much on the configuration of the hardware. Thus records collected to study one particular parameter, e.g. significant wave height, can often be re-analysed at a later date to extract some other unrelated quantity, e.g. current velocity. With conventional equipment seperate experiments would be needed to measure each of the above quantities.

Radar can also obtain accurate ($\sim \pm 10$ degrees) directional information for both wind driven seas and swell conditions. Under some conditions, however, the directional information may contain ambiguities that would require a second radar or beam direction to resolve. A good example of the use of radar to perform an oceanographic experiment that would otherwise have been difficult or impossible is the work of STEWART and TEAGUE (1980) on wave growth and decay.

The hf radar technique is not without some disadvantages. Perhaps the most serious of these is that the frequency range used (approximately 1 to 30MHz) is heavily used by commercial interests. The problem of

mutual interference between radar and other users thus appears.

Another problem is that antenna arrays in the hf band are often large and expensive, particularly if narrow beams are required. This problem provided some of the motivation for the study of the second order part of the sea echo Doppler spectrum and the work by BARRICK and LIPA (1979a) on compact direction finding antenna systems.

The processing and interpretation of sea echo Doppler spectra can also be difficult. Generally, single parameters are fairly easy to obtain. The extraction of current velocities, wind speeds and wind directions has been particularly successful. Ocean waveheight spectra, however, have to be extracted from the second order part of the Doppler spectrum by using complicated inversion techniques.

CHAPTER 3:

PULSED DOPPLER RADAR

THEORY

3.1 DOPPLER RADARS

Radar is a technique for measuring properties of a distant object by transmitting electromagnetic energy towards the object and studying the energy that is reflected or scattered by the object. In conventional radar the time delay between transmission and reception of a pulse of energy is used to find the distance, r, to the scattering object. In addition we can get some information on the size and scattering properties of the object from the amplitude of the received echo. The basic principle of Doppler radar is illustrated by the block diagram in fig. 3.1. Here we use the variation in phase of the echo from the object to measure the radial component of the object's velocity. $v = dr/dt$.

If the transmitter transmits a continuous wave with frequency, ω_o, and wavenumber, $\kappa_o=\omega_o/c$, (where c is the speed of light), the complex echo voltage at the receiver input will be of the form:

$$V = Ae^{-i(\omega_o t - 2\kappa_o r)} \qquad 3.1$$

We can write this in terms of the phase, $\phi=\omega_o t - 2\kappa_o r$, of the wave as

$$V = Ae^{-i\phi} \qquad 3.2$$

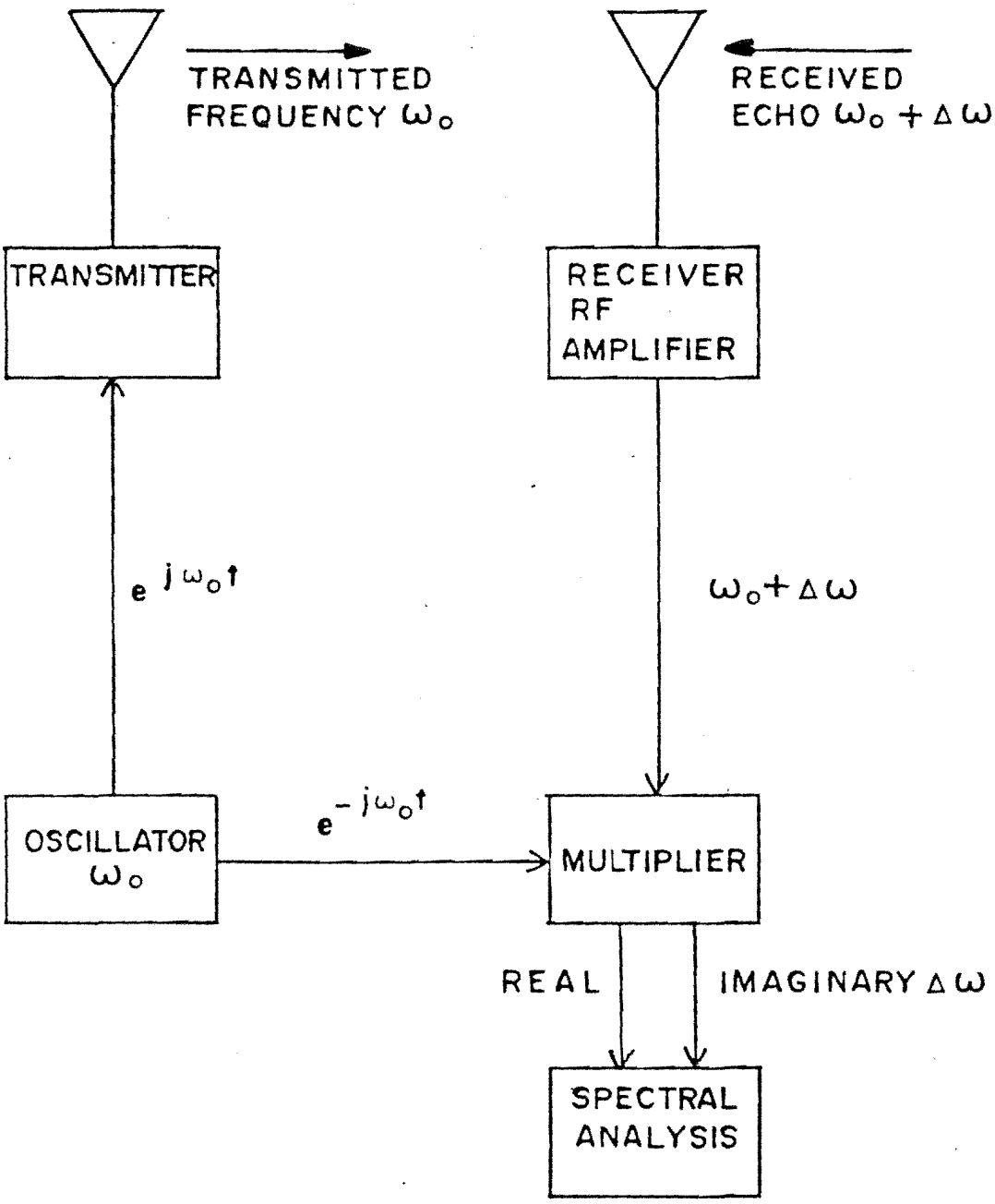

FIG 3.1 C ω DOPPLER RADAR

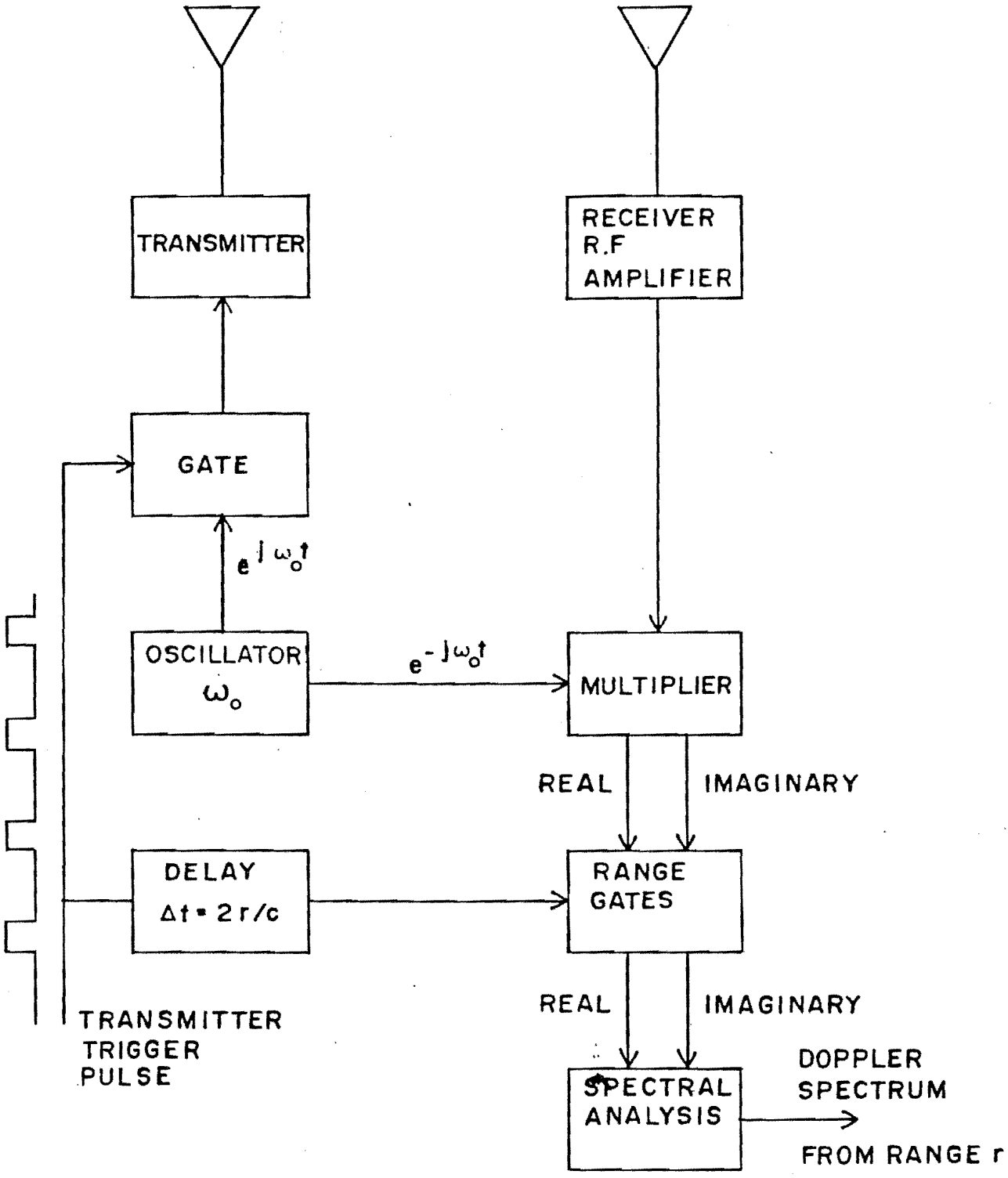

FIG. 3.2 PULSED DOPPLER RADAR

To a first order approximation the received frequency, ω', is given by the rate of change of phase with time

$$\omega' = \omega_o - 2\kappa_o \frac{dr}{dt} \qquad 3.3$$

Thus the received echo has a Doppler shift, $\omega' = \omega_o + \Delta\omega$, from the original carrier frequency which is related to the radial component of the object's velocity by:

$$\Delta\omega = -2\kappa_o v \qquad 3.4$$

This form of the derivation of the Doppler shift equation stresses the important point that Doppler velocity information is contained in the phase of the received signal.

We have considered the case of a single moving target at range, r. In Geophysics we are normally interested in radar scattering from a continuum, such the atmosphere or ocean, from which reflections are produced by many targets with different ranges and velocities. As a first step in the treatment of this problem we consider the case of multiple targets with different velocities but all at the same range from the radar. Each target will contribute a different Doppler shift to the echo so that, in the limit

of a large number of scatterers, the echo will consist of a continuous spectrum of frequencies, $P_{ex}(\omega)$, known as the Doppler spectrum.

This Doppler spectrum will consist of a narrow band of frequencies clustered around the transmitted frequency. These Doppler shifts are extreemly small when compared to the transmitted frequency. For the example of hf radar oceanography the Doppler shifts are of the order of 1 Hz with transmitted frequencies of the order of megahertz. The direct measurement of such a spectrum is clearly impractical. (In addition the A/D convertors required to digitise the received signal are limited in frequency response to approximately 1MHz.)

We can solve this problem by using the baseband mixing technique (KRENEK 1977 Ph.D. thesis). The received echo voltage, $v_{RX}(t)$, is multiplied by the original carrier signal at frequency ω_o :

$$v(t) = v_{RX}(t)e^{i\omega_o t} \qquad 3.5$$

By using the shifting property of Fourier transforms (BURDIC 1968) we see that this multiplication shifts the power spectrum of the received echo down in frequency by an amount ω_o. The carrier frequency will now appear at 0Hz and Doppler shifts $\Delta\omega$ on either side of this

carrier will appear as easily measurable frequencies, $\Delta\omega$:

$$P(\Delta\omega) = P_{RX}\ (\omega_o + \Delta\omega) \qquad 3.6$$

Physically, this corresponds to forming a beat frequency between the Doppler shifted echo and the carrier frequency.

The echo Doppler spectrum is obtained by performing spectral analysis on the time series of mixer output voltage. The spectral analysis techniques used are the subject of section 3.3. In general the Doppler spectrum will be asymmetrical about 0Hz and will therefore require the full complex nature of the echo signal to be preserved.

We have considered the case of multiple targets at the same range, r. We now generalise to the problem of targets at many different ranges from the radar. In conventional radar the problem of seperating echoes from different ranges is solved by transmitting short pulses of energy rather than a continuous wave. Echoes from different ranges will then be received at different times after the transmitted pulse. If we sample the received voltage a time, t, after the transmitted pulse the sample will be the echo from range r = ct/2 from the radar. The

receiver output voltage at any time, $v_{out}(t)$, is a convolution of the envelope of the transmitted pulse, $v_{TX}(t)$, with a function, $f(r)$, describing the scattering properties of the continuum being observed:

$$v_{out}(t) = \int_{-\infty}^{\infty} v_{TX}(\tau) f\left[\frac{c}{2}(t-\tau)\right] d\tau \qquad 3.7$$

In the frequency domain we have:

$$P_{out}(\omega) = P_{TX}(\omega) \mid F(\omega) \mid^2 \qquad 3.8$$

where $|F(\omega)|^2$ is the power spectrum of the scattering function. In order to seperate echoes from ranges spaced apart by some small amount Δr the receiver output spectrum must preserve frequency components of the scattering function within a bandwidth of the order of $c/2\Delta r$. . Thus the condition we must meet in order to seperate echoes in range with a resolution Δr is that the envelope of the transmitted signal must have a bandwidth of at least:

$$B_{TX} = \frac{c}{2\Delta r} \qquad 3.9$$

In the time domain we can acheive this by transmitting a short pulse of duration τ_{TX} given by:

$$\tau_{TX} \quad \frac{1}{B_{TX}} = \frac{2\Delta r}{c} \qquad 3.10$$

Transmission of a short pulse is only one of several techniques for generating a wide bandwidth transmitted spectrum. Pulse compression radars (KRENEK, 1979 Ph.D. thesis; BARTON, 1977) achieve very high resolutions with relatively long pulses by using some form of frequency modulation to increase the signal bandwidth.

If we transmit a square pulse of width τ_{TX} and assume, without loss of generality, that the surface scattering function has a flat power spectrum then the receiver output spectrum will have a sin(x)/x form with the bandwidth of the main lobe being $1/\tau_{TX}$. In the case of a single transmitted pulse this spectrum will be a continuous spectrum with all frequencies present. Any Doppler shifts of this spectrum due to target movement will clearly be masked as they are very much smaller than the bandwidth of the spectrum ($\sim 1H_z$ $V_s \sim 100KH_z$).

A possible solution is to transmit a train of pulses evenly spaced in time by some amount t_{pr} , the pulse repetition time. Since the received echo will now be periodic in time the receiver output spectrum will consist

of discrete lines spaced apart in frequency by $f_{pr} = 1/t_{pr}$ (fig 3.3c). Doppler shifts due to the medium being observed will cause the received echo spectrum to have a copy of a Doppler spectrum at the position of each of these discrete lines. Each Doppler spectrum will be an average over range, the information on the variation in the Doppler spectra with range is contained in the overall envelope. Provided that the spacing of the lines, f_{pr}, is greater than twice the bandwidth of the Doppler spectra no overlap of the spectra will occur and our aim of preserving both range and Doppler information will be achieved. The condition that the pulse repetition frequency f_{pr} be greater than twice the Doppler spectrum bandwidth is the Nyquist criterion of signal processing theory (BURDIC 1968).

One practical difficulty remains. In a conventional radar transmitter pulses are formed by turning the carrier frequency oscillator on and off. No attempt is made to control the phase of the oscillator at each pulse. If this phase varies randomly from pulse to pulse the pulse train will not be periodic and its spectrum will be a continuous spectrum such as fig 3.3a. The random variation in phase from pulse to pulse destroys the Doppler information, which is contained in the phase of the echo. A truly periodic spectrum, in which the starting phase of each pulse is constant, has the disadvantage of not producing a discrete line at the carrier frequency unless the carrier frequency and pulse

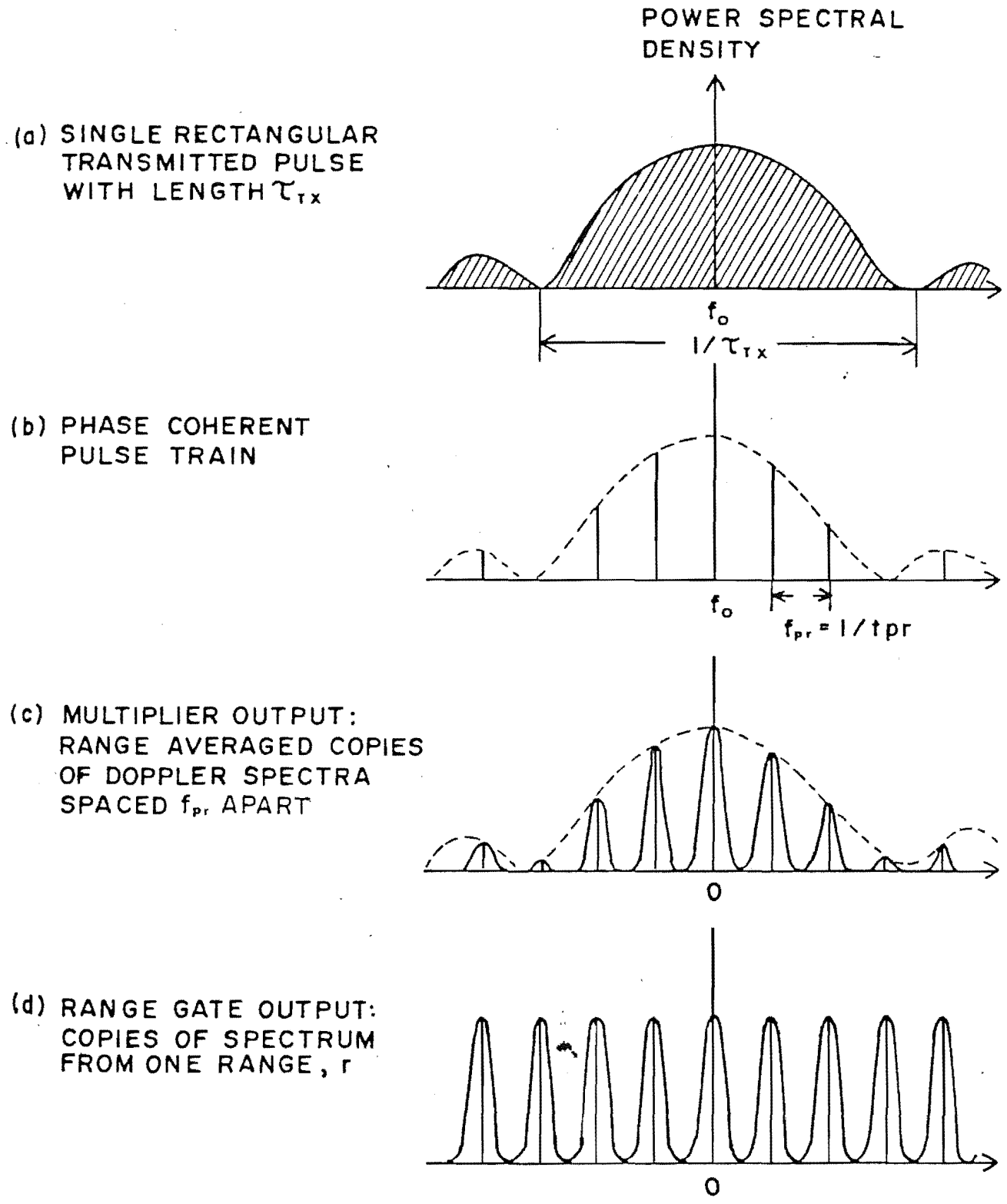

FIG. 3.3 SPECTRA OF PULSED DOPPLER RADAR SIGNALS

repetition frequency are harmonically related (BURDIC 1968). Thus, when the echo spectrum is shifted down to 0 Hz the lowest frequency copy of the Doppler spectrum may be offset from zero by some amount. As a result the subsequent spectral analysis process will have to have a larger bandwidth than would be the case if the Doppler spectrum were centered about zero frequency. We overcome this difficulty by transmitting a phase coherent pulse train in which the pulses are formed by switching, or gating, the signal from a continuously running oscillator into the transmitter power amplifier. There will thus be a linear progression in carrier phase from one pulse to the next. As BURDIC (1968) shows, the spectrum of a phase coherent pulse train will consist of a series of discrete lines spaced f_{pr} apart and with a line at the carrier frequency, f_o. The continuously running oscillator from which this pulse train is derived can also supply the reference signal for the receiver multiplier, thus ensuring that the echo spectrum is shifted down in frequency by exactly the carrier frequency. The effect of the stability of this oscillator on system performance will be discussed further in chapter 5.

In order to obtain the Doppler spectrum from range, r, the received echoes from this coherent pulse train are sampled at a time t = 2r/c after each transmitted pulse. Traditionally this sampling was performed by a range gate triggered by the transmitted pulse through a time delay, t. Nowadays the signal is sampled by a track and hold

circuit and the sample converted into a binary number by an analogue to digital (A-D) convertor. The sample is then in a suitable format for processing by a computer. The range gate and the A-D track and hold circuit perform essentially equivalent functions. The range gate output will consist of a series of samples of the power reflected only from range r. As illustrated by fig 3.3 the spectrum of this sampled signal is a series of copies of the Doppler spectrum from range r at frequencies spaced apart by f_{pr} . The spectrum is, in fact, the spectrum of a sampled version of the continuous signal that would have been obtained from a CW Doppler radar if scatterers only existed at the range r (fig 3.1). Spectral analysis of this sampled signal thus yields an estimate of the Doppler spectrum of the echo from just this range.

More than one range sample may be taken after each transmitted pulse, allowing simultaneous measurements of the Doppler spectrum at a number of ranges from the radar. The smallest range spacing from which independant Doppler spectra may be obtained is the range resolution of the radar, Δr , which is determined by the transmitter pulse length via eqn 3.10. The echo from range r is an average over this range interval, Δr . The maximum range, r_{max} , from which echoes can be obtained will be determined by transmitter power and receiver noise level considerations to be discussed in following sections.

In order that echoes from one transmitted pulse do not overlap with subsequent transmitted pulses or their echoes the transmitted pulses must be spaced apart by at least a time $2r_{max}/c$, This condition places an upper limit on the pulse repetition frequency:

$$f_{pr_{max}} = \frac{c}{2r_{max}} \qquad 3.11$$

We have seen that the Nyquist criterion places a lower limit on f_{pr} of twice the Doppler spectrum bandwidth. In some situations we can have $f_{pr_{min}} = f_{pr_{max}}$ making unambiguous determination of range and Doppler shift impossible. Fortunately this conflict does not arise in radar oceanography using ground-wave propagation. Typically, maximum ranges are of the order of 70km and Doppler spectrum bandwidths are no greater than 2Hz (See e.g. BARRICK et. al. 1977). Thus we have

$$\begin{aligned} f_{pr_{max}} &\approx 2000\text{Hz} \\ f_{pr_{min}} &\approx 4\text{Hz} \end{aligned} \qquad 3.12$$

We shall show in the following sections that there is considerable advantage in sampling at as high a rate as possible (i.e. close to $f_{pr_{max}}$) in order to reduce the level of background noise in the spectrum.

3.2 THE RADAR RANGE EQUATION

The power density produced at range, r, from a radar transmitter is given by:

$$P = \frac{P_{TX}G_{TX}}{4\pi r^2} \qquad 3.13$$

Where P_T is the power fed into the antenna input terminals averaged over the transmitter pulse width and G_{TX} is the gain of the transmitting antenna. G_{TX} is the product of a geometrical factor, known as the directivity, and an efficiency factor which takes into account resistive losses in the antenna. The quantity $P_{TX}G_{TX}$ is known as the equivalent isotropic radiated power (EIRP). In other words it is the power, radiated isotropically, that would produce the same power density at range r.

An object at range r will scatter some of this power back in the direction of the radar. The equivalent isotropic power scattered by the target is given by the scattering cross-section, σ, of the target. This is the area of a perfect reflector that scatters the same power as the target. i.e.

$$P_{Target} = \sigma P = \frac{P_{TX}G_{TX}}{4\pi r^2} \qquad 3.14$$

Since, from the definition of σ , this power radiates isotropically the power density received back at the radar is:

$$P_{RX} = \frac{P_{Target}}{4\pi r^2} = \frac{P_{TX}G_{TX}\sigma}{(4\pi)^2 r4} \qquad 3.15$$

To find the received power we multiply the received power density by the effective cross-section area of the receiving antenna, A_{RX} . The antenna cross-section is given in terms of the antenna gain, G_{RX} , by (JASIK, 1961):

$$A_{RX} = \frac{G_{RX}\lambda^2}{4\pi} \qquad 3.16$$

This antenna cross-section is defined in such a way that the resulting received power is the power dissipated in a matched load resistor connected across the antenna terminals. Thus the 50% power loss in the transfer of power from the antenna to a receiver with matched input impedance is accounted for. If either the transmitter or receiver is not properly matched to its respective antenna then an additional loss factor must be included to take this into account. We now have, for the echo power dissipated in the (matched) receiver input impedance:

$$P_{RX} = P_{RX} A_{RX} = \frac{P_{TX}G_{TX}G_{RX}\lambda^2\sigma}{} \qquad 3.17$$

When the scattering is produced by a continuum, such as the atmosphere or ocean, the echo power from range r will be an integral over some finite area (ocean) or volume (atmosphere) known as the radar resolution cell. This is illustrated for the oceanographic case in fig 3.4. The width of this cell is determined by the radar beamwidth, θ , and the length of the cell by the transmitter pulse width, τ_{TX} , as discussed in the previous section. The area of the radar resolution cell is therefore:

$$A = r\,\theta\,\frac{c\tau_{TX}}{2} \qquad 3.18$$

and will increase with range from the radar. For this case we redefine the radar cross-section, σ , as the radar cross-section per unit area of surface so that the received power becomes:

$$P_{RX} = \frac{P_{TX}G_{TX}G_{RX}\lambda^2\sigma A}{(4\pi)^3\, r^4} \qquad 3.19$$

showing that σ can be thought of as that fraction of the surface area, A, that acts as a perfect reflector for the incident energy.

In pulsed Doppler radar our aim is to measure the

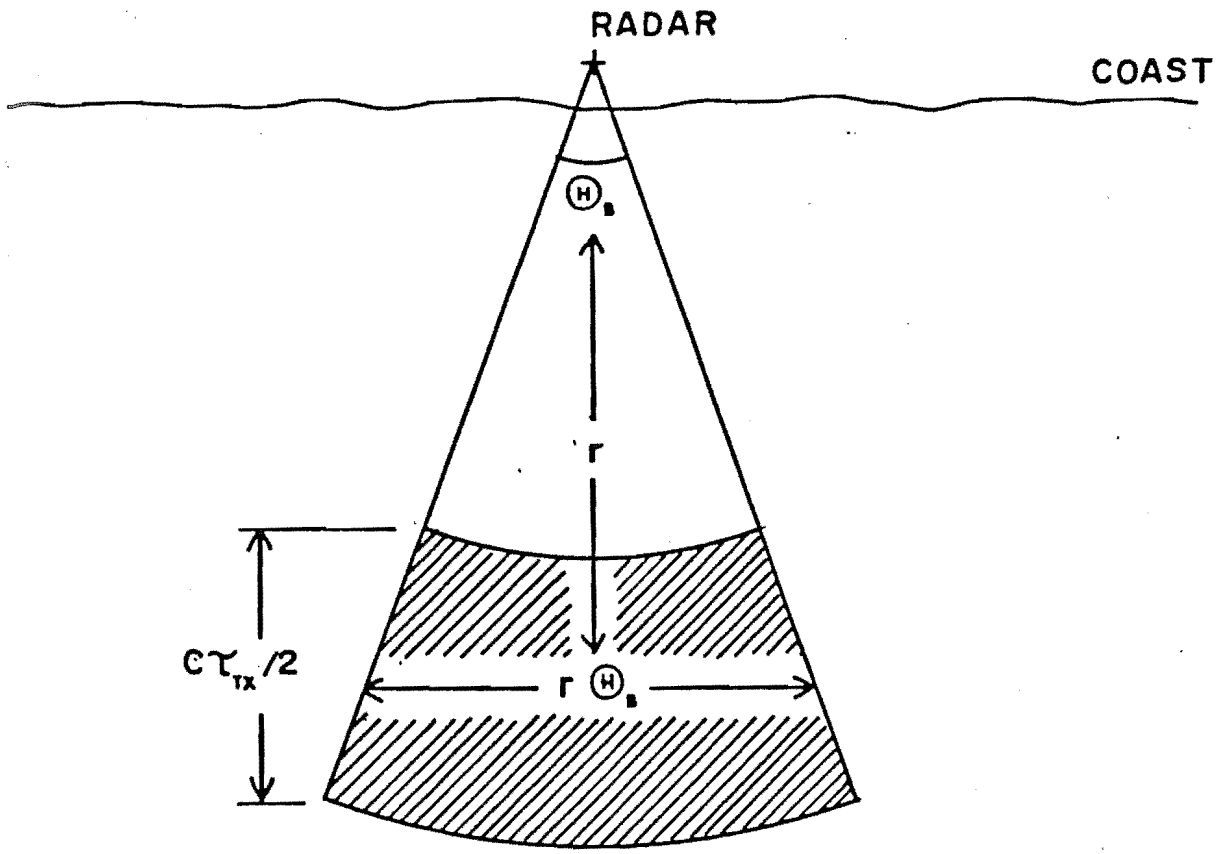

FIG. 3.4 RADAR RESOLUTION CELL DEFINED BY PULSEWIDTH AND BEAMWIDTH.

Doppler spectrum of the echo from range r. The total power is the integral of the Doppler spectrum of the received signal over frequency

$$P_{RX} = \int_{-B/2}^{+B/2} P_{RX}(\omega)\, d\omega \qquad 3.20$$

where B is the bandwidth of the Doppler spectrum. We therefore define the frequency dependent cross-section, $\tau(\omega)$, as that fraction of the sea surface that acts as a perfect reflector for frequencies in the range ω to $\omega + d\omega$. The Doppler spectrum of the echo from range r is thus given by:

$$P_{RX}(\omega) = \frac{P_{TX} G_{TX} G_{RX} \lambda^2 \sigma(\omega) A}{(4\pi)^3 r^4} \qquad 3.21$$

The output from a radar receiver will be the sum of the echo power given by eqn and power due to noise. This noise arises from sources both internal and external to the radar receiver. External noise sources usually dominate at frequencies below about 100 MHz with internally generated noise becoming increasingly more important above this frequency.

Any resistor with a temperature above absolute zero

will generate thermal noise. This noise has a flat spectrum with power spectral density, N, given by:

$$N = k\,T \qquad 3.22$$

where k is Boltzmann's constant, $1.38\times10^{-23} JK^{-1}$, and T is the absolute temperature of the resistor. Even though noise generated by the resistances in a receiver is typically small compared to noise from other sources thermal noise provides a useful model for other types of noise. If a noise source generates a power, P_n , at the receiver input and this noise has a power spectrum which is flat over the bandwidth, B_{RX} , of the receiver then we can assign an effective "temperature", T, to the noise such that:

$$P_n = k\,T\,B_{RX} \qquad 3.23$$

The temperatures of various noise sources can be added together at a particular point in the circuit to yield an overall noise temperature at that point (FLOCK 1979). In this work we will generally assume that the flat spectrum model for noise applies. It should be noted, however, that there are instances when this model fails and the concept of noise temperature is invalid. Examples of this

are some types of man-made interference and internally generated receiver noise (See e.g. HOROWITZ and HILL 1980).

Apart from man-made interference external noise arises from three sources; Atmospheric noise, caused by ligthning flashes, cosmic noise caused by the sun and various interstellar sources and thermal noise caused by black body radiation from objects in the receiving antenna beam. Atmospheric noise tends to dominate below 20MHz, cosmic noise from 20-300MHz while thermal noise from the earth and atmosphere is important above 300MHz.

Internal noise is sometimes expressed in terms of a noise factor, F_n ,. This is the ratio of noise power output by the receiver, W, to the noise power that would have been present if no noise had been added by the receiver:

$$F_n = \frac{W}{GkTB} \qquad 3.24$$

Where G is the receiver power gain.

The relation between noise factor and the receiver noise temperature, T_{RX} , is readily deduced (e.g. FLOCK 1979):

The relative importance of these various types of noise is summarised in fig. 3.5 (from ITT CORP., 1968). We see that noise in an hf radar system will be largely of external origin in contrast to a microwave radar where receiver noise is dominant. Therefore we conclude that at hf we do not need to place as much emphasis on designing receivers with low internal noise levels as we do with more conventional microwave radars. Once the receiver's internal noise temperature is below the external noise temperature no further gain can be achieved by going to a lower noise design.

The presence of noise in the receiver output sets an ultimate limit to the range of the radar. As the range, r, is increased the echo power will decrease according to eqn. 3.19. Eventually a point will be reached where the statistical fluctuations due to noise will be comparable to the echo voltage and the descision as to whether a pulse is a noise fluctuation or a genuine echo will become uncertain. The minimum echo power required for reliable detection is usually specified in terms of the probability that a noise fluctuation will exceed this value and thus be falsely detected as an echo. (e.g. HALL 1956). The magnitude of the noise fluctuation is measured by the noise variance, σ^2 , and, in the case of noise with a zero mean value this is equal to the noise power, P_n . From eqn. 3.23 we see that the variance will depend on the overall system bandwidth. This includes not only the receiver bandwidth but also the effect of any averaging,

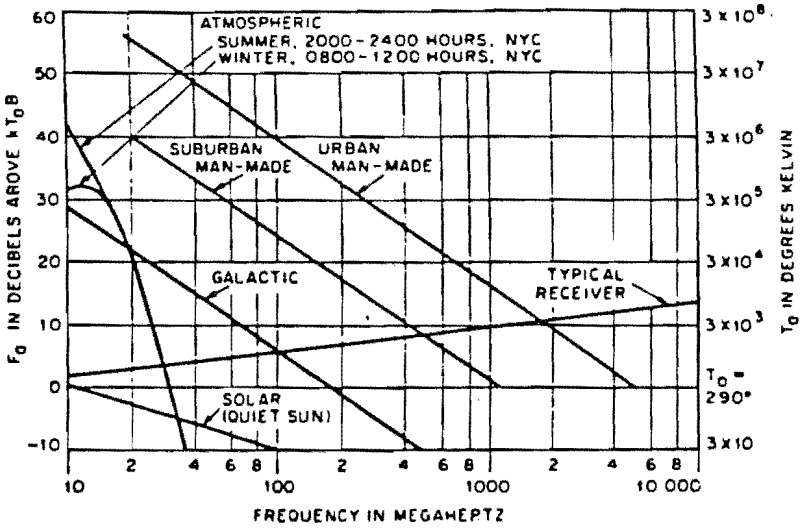

Fig. 3.5 Background radio noise. (From ITT Corp., 1968).

or filtering, performed by the detection device attatched to the receiver output. In conventional radar the "detector" is often a human operator viewing the output on a CRT screen. The human eye averages over a time of the order of 1/20s and, as a first approximation, can just detect echo powers equal to the noise variance at the receiver output. The maximum range of this type of radar can therefore be found by equating the received echo power eqn. 3.19 to the noise power eqn. 3.23 giving:

$$r_{max} = \left[\frac{P_{TX} G_{TX} G_{RX} \lambda^2 \sigma A}{(4\pi)^3 k\ T\ B} \right]^{\frac{1}{4}} \qquad 3.26$$

This equation is known as the radar range equation and serves as the usual starting point for more detailed analyses of radar performance (BARTON 1977). In pulsed Doppler radar spectral analysis forms a major part of the echo detection processing following the receiver. The large amount of averaging of signal and noise performed by spectral analysis enables echoes to be detected from far greater ranges than can be detected visually on a CRT screen. The effect of spectral analysis on the performance of a pulsed Doppler radar will be discussed in detail in the next section.

The radar equation we have developed assumes free space propagation. In other words the power density decreases with distance from the transmitter as $1/r^2$.

The radar system described in this work uses ground-wave propagation in which the radiated energy travels as a surface wave on the interface between the air and the curved surface of the earth. We account for this by using the free space propagation result (eqn 3.19) and including an attenuation factor, F, which is the ratio of power density received over the earth to that which would have been received in free space. The discussion of this ground-wave propagation mode and the calculation of F are dealt with in chapter 6. including the ground-wave attenuation factors for both the transmitter to sea surface and sea surface to receiver paths gives:

$$\left.\begin{matrix} P_{RX} \\ \\ P_{RX(\omega)} \end{matrix}\right\} \quad \frac{P_{TX}G_{TX}G_{RX}\lambda^2 AF^2}{(4\pi)^3\, r^4} \quad \left\{\begin{matrix} \sigma \\ \\ \sigma(\omega) \end{matrix}\right. \qquad 3.27$$

In addition, the fact that we are now radiating into half-space rather than isotropically means that the antenna gains G_{TX} and G_{RX} must be redefined. According to BARRICK (1972b) 6dB must be subtracted from the gains. Thus G_{TX} for a quarter wave monopole would be -0.85dB rather than the usual figure of +5.15dB.

3.3 SPECTRAL ANALYSIS

We have seen that the spectrum of the range gated receiver output signal consists of copies of the Doppler spectrum of the echo from the range being observed. We now consider the techniques used to measure the spectrum of this signal. From the definition of power spectral density we estimate the power spectrum of a signal at some frequency, $P(\omega)$, by measuring the signal power present in a small range of frequencies about .

Traditionally, pulsed Doppler radars have used the scheme illustrated in figs. 3.2 and 3.6 . The signal is passed into a narrow bandpass filter centered on the frequency of interest. The filter output is passed through a square law device which effectively calculates the signal power. The detector output voltage, which is now proportional to the filter output power, is passed through a low pass filter which averages the signal over some time interval and thus reduces the statistical fluctuations due to noise. It can be shown (e.g. NEWLAND 1975) that the expected value of the output power is a direct measure of the power spectral density of the input signal at the center frequency of the bandpass filter. In order to measure the complete spectrum of the signal we need a bank of filters, one for each frequency of interest. Similarly the filter bank must be repeated for each range from which we wish to measure a Doppler spectrum. Not surprisingly there is some interest in replacing this analogue spectrum analysis technique with more efficient digital techniques. In radar oceanography

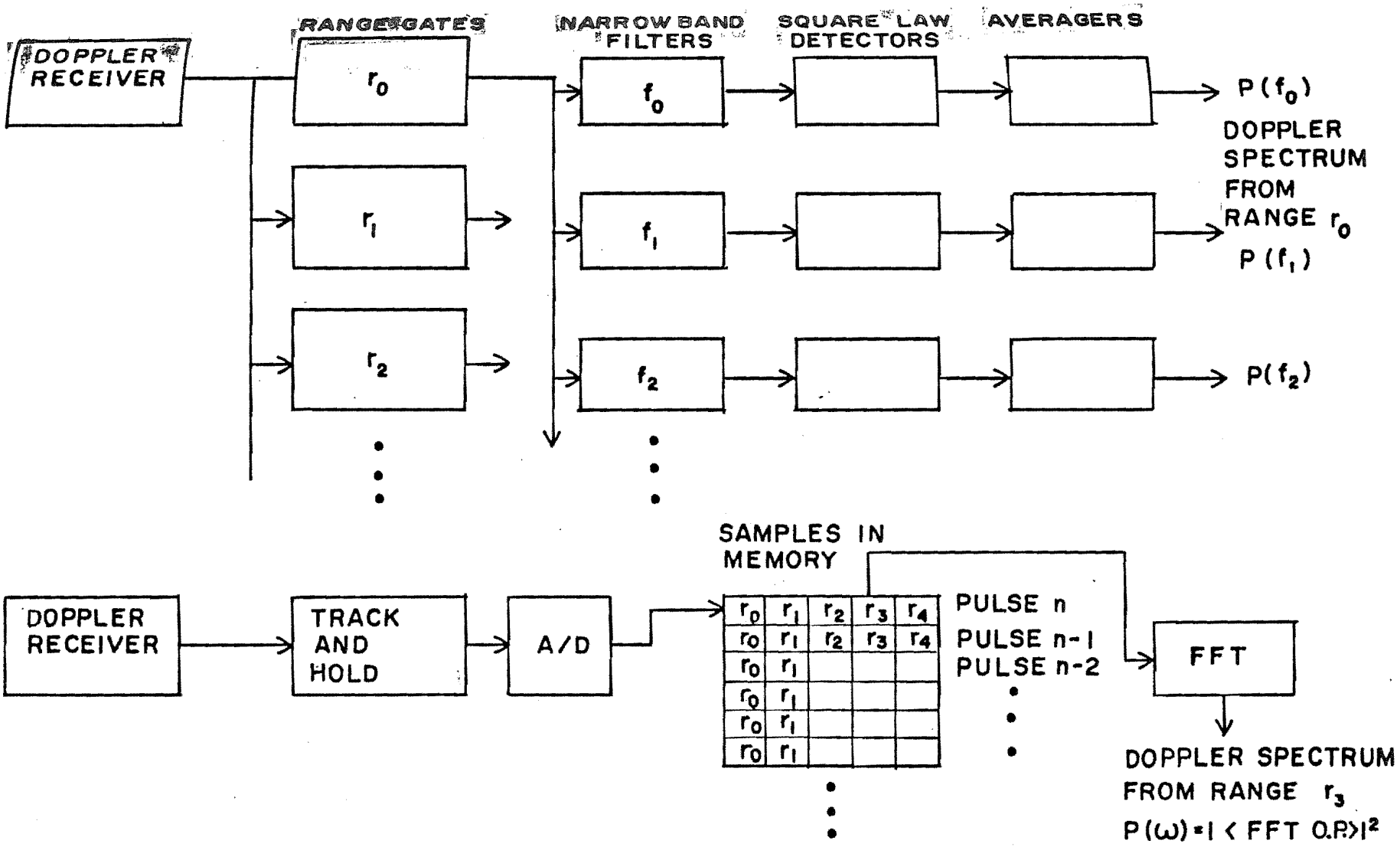

FIG. 3.6 ANALOGUE (TOP) AND DIGITAL (BOTTOM) SPECTRAL ANALYSIS TECHNIQUES

it is essential to use digital techniques as it is impossible to construct filters with the required bandwidths (~0.01Hz) and center frequencies (→ ←0.01 to 2Hz) using analogue techniques.

We mention the analogue system because many features of the digital system have direct counterparts in the analogue spectrum analyser. Many of the characteristics and limitations of digital spectral analysis can thus be simply understood in terms of the equivalent analogue system. In addition some of the terminology used in traditional aviation and military radar systems has carried over into oceanographic and geophysical systems.

The digital processing scheme is illustrated in fig. 3.6 . Samples from the range gated output (in the digital case range gating is performed by a sample and hold circuit) are converted into digital numbers by the A-D converters and accumulated in a computer memory for a time T seconds. The time series record in memory thus consists of $N = f_{pr} T$ samples. As the samples are complex values each will consist of two digital numbers, one from the real and one from the imaginary receiver output. The record in memory will therefore be 2N words long. This record is input to a fast Fourier transform (FFT) algorithm (COOLEY and TUKEY 1969) which calculates N complex values of the discrete Fourier transform of the record at frequencies spaced 1/T Hz apart from $- f_{pr}/2$ Hz to $+ f_{pr}/2$ Hz. (These are the Nyquist frequencies). If the echo samples are v(t) then the transform samples are given by:

$$V(f_i) = \frac{1}{N} \sum_{i=0}^{N-1} v(t_i) \exp(-j2\pi f_i t_i)$$

where

$$t_i = i\Delta t \qquad \Delta t = 1/f_{pr} \qquad 3.28$$

$$f_i = i\Delta f \qquad \Delta f = 1/T$$

The N/2 transform values with i in the range 0 to N/2-1 are the positive frequency points $f = f_i = i\Delta f$ with f in the range 0 to $+ f_{pr}/2$. The N/2 values with i in the range N/2 to N-1 are the negative frequency points with f = (N-i) Δf ranging from $- f_{pr}/2$ to 0 Hz. The discrete Fourier transform assumes that the record repeats itself indefinitely after the time, T. This results in the transform consisting of discrete samples Δf apart in the frequency domain, rather than a continuous spectrum for which all frequencies are present.

Estimates of the power spectrum are calculated from the squared magnitudes of the Fourier transform values by:

$$S(f_i) = [V(f_i)\ V^*(f_i)]\ T \qquad 3.29$$

Finally, as in the analogue case, it may be necessary to average the spectral estimates to reduce statistical fluctuations. This may be done by either averaging values from several seperate records or by averaging values from adjacent frequencies within a record.

Spectral density has units of "power" per unit frequency interval. "Power" is in units of A-D values

squared and is therefore not power in the physical sense. S(f) can be related to physical power spectral density at the receiver input by allowing for the gain factors of the various receiver stages, the A-D conversion factor and the receiver input impedance, which determines the conversion factor from input power to input voltage i.e.

$$P_{RX} = \frac{V_{RX}^2}{Z_{in}} \qquad 3.30$$

We combine these into a system gain factor, G_{sgs} , defined so that:

$$S(f) = |G_{sys}|^2 \, P_{RX}(f) \qquad 3.31$$

The calculation of G_{sgs} will be discussed in chapter 5. Due to the large range of spectral densities encountered in practice the output spectrum is usually plotted on a logarithmic scale. Traditionally, the quantity plotted is 10log(<spectral density>) with units refered to as decibels even though spectral density is not strictly a ratio. Spectral densities quoted in this manner can be thought of as decibels relative to an implied reference level of unit spectral density (0dB). Alternatively we can regard only the differences between decibel spectral densities, and not their absolute values, as having

meaning. The relation between hertz and radian frequency versions of the power spectrum is given by

$$S(f) = 2\pi S(\omega) \qquad 3.32$$

As previously mentioned the A-D converter sample and hold performs a function equivalent to the range gate of the analogue system. However a single sample and hold and A-D converter can take several range samples as samples from different ranges are easily unscrambled in the computer. A seperate FFT is performed on each set of N complex samples from a given range as illustrated in fig. 3.6 . Thus the duplication of hardware required by the analogue system is avoided, but at the expense of longer time required to calculate the spectra sequentially.

As is the case with all physical measurements the calculated power spectral density values, $S(f)$, are only estimates of the true signal power spectrum, $P(f)$. There are four main sources of error which result in the spectral estimates being different from the true spectrum:

(1) Aliasing - The true power spectrum is defined for a continuous signal whereas the input to the spectrum analyser stage is a sampled version of this continuous signal. The possibility of aliasing resulting from this was discussed earlier in this chapter. (section 3.1). It was shown there that aliasing may be easily avoided for the sea echo component of received spectrum. The same is

not true, however, for the random noise component.

We assume that the noise can be modeled by thermal noise with system noise temperature $N_{RX} = k\ T_{sys}$ (eqn. 3.22). The noise spectrum is then flat across the receiver bandwidth. In order to avoid aliasing this noise we must have:

$$f_{pr} > 2\ B_{RX} \qquad 3.33$$

The sampling rate is restricted by range ambiguity to:

$$f_{pr_{max}} = \frac{c}{2r_{max}} \qquad 3.11$$

while the receiver bandwidth must be great enough to provide the required range resolution:

$$B_{RX} = \frac{c}{2\Delta r} \qquad 3.34$$

Obviously we must have $\Delta r < r_{max}$ which requires that $B_{RX} < f_{pr_{max}}$ hence the Nyquist criterion for the noise component of the spectrum cannot be met. The effect of aliasing is to raise the estimated noise power spectral density above the true value as the total energy present in the bandwidth B_{RX} is now folded into a smaller bandwidth f_{pr}.

Consider a frequency, f, in the estimated spectrum. In addition to the power at this frequency the aliased spectrum will contain contributions from frequencies $f+f_{pr}$, $f+2f_{pr}$, $..f+nf_{pr}$ where n is the largest integer

such that $n f_{pr} \leq B_{RX}/2$. Similarly, contributions will come from the n negative frequencies $f-f_{pr}$, $f-2f_{pr}...f-nf_{pr}$. Hence the aliased noise power spectrum is:

$$S_{noise}(f) = G_{sys} \sum_{i=-n}^{n} N_{RX}(if_{pr} + f)$$
$$= (2n+1)\ \kappa\ T_{sys}\ G_{sys}^{2} \qquad 3.35$$

with

$$n = \text{entier}\left[\frac{B_{RX}}{2f_{pr}}\right]$$

If n is large (e.g. in our case $B_{RX} \sim 10^{5}H_z$ $f_{pr} \sim 10^{2}H_z \Rightarrow$ $n \sim 500$) we can make the approximations:

$$S_{noise}(f) = 2n\ k\ T_{sys}\ G_{sys}^{2}$$

and

$$S_{noise}(f) = \frac{B_{RX}\ k\ T_{sys}\ G_{sys}^{2}}{f_{pr}} \qquad 3.36$$

Showing that the aliased noise spectrum is still flat (i.e. independent of frequency) but that the estimated noise power spectral density is a factor of B_{RX}/f_{pr} larger than the true value $N_{RX} = k\,T_{sys}$. It is obviously desirable to sample at the highest possible rate consistent with the limit set by range ambiguity: eqn.

3.11.

(2) Finite record length - The spectrum is calculated from an input data record with finite length, T, whereas the Fourier transform is defined for an infinite record length. We can regard the finite length record as being an infinite length record multiplied by a rectangular "window" function of length T. In the frequency domain this is equivalent to convolving the true spectrum with the transform of the rectangular function. This transform has the form:

$$F(f) = \frac{\sin 2\pi fT}{2\pi f} \qquad 3.37$$

A signal with a delta function power spectrum will therefore produce a spectral estimate of the form:

$$S(f) = \frac{\sin^2 (2\pi fT)}{(2\pi f)^2} \qquad 3.38$$

The main peak of this function will have a width of the order of:

$$B = \frac{1}{T} \qquad 3.39$$

A single value of S(f) will therefore be the total power from all frequencies within this range. The bandwidth, B, can thus be likened to the bandwidth of the narrow band filters in the analogue spectrum analyser. (The actual shapes of the filter responses will, in general, be different). The record length, T, corresponds to the averaging time of the narrow band filter and is therefore often referred to as the coherent averaging time (or coherent integration time). In a conventional radar with a scanning beam this time is limited to the time for which the radar beam "dwells" on a particular target as it scans. Hence T is sometimes referred to as the dwell time (SHEARMAN 1983).

Since the total area under the $\sin^2 x/x^2$ function must equal the total power, P, in thje original delta function signal we can approximate the height of the peak by:

$$S(f_{peak}) = \frac{P}{B} = PT \qquad 3.40$$

This expression will only apply for a delta function signal or a signal with bandwidth less than B. For signals with bandwidths much greater than B (e.g. random noise) the spectral density will become independent of the coherent integration time.

We are now in a position to understand why spectral analysis can give much better range performance than

conventional detection techniques such as visual observation of the receiver output on an oscilloscope. If the echo consists of a delta function signal of total power, P_{sig} , together with noise of total power, P_{noise} , then clearly the signal will become undetectable on the oscilloscope when $P_{sig} \approx P_{noise}$. The spectral analysis process, however, spreads the noise power over the bandwidth f_{pr} and concentrates the signal power into the bandwidth B = 1/T. The ratio of signal to noise spectral densities is therefore (from eqn. 3.40 and eqn. 3.36) :

$$\begin{aligned} \frac{S_{sig}(f_{peak})}{P_{noise}} &= f_{pr}\, T\, \frac{P_{sig}}{P_{noise}} \\ &= n_{coh}\, \frac{P_{sig}}{P_{noise}} \end{aligned} \qquad 3.41$$

Where $n_{coh} = f_{pr}\, T$ is the number of samples coherently integrated in time T by the spectral analysis process.

Convolution of the spectrum with the $\sin^2 x/x^2$ function will result in a delta function signal being surrounded by sidelobes as well as being broadened. These sidelobes limit the dynamic range of the system. The sidelobes of a strong signal can obscure weak nearby signals. A considerable body of literature exists on this problem (see e.g. HARRIS 1978). The usual technique for reducing sidelobe levels is to multiply the data record by a window function before spectral analysis. This window function is chosen to have a transform with lower sidelobe levels than the $\sin(x)/x$ function resulting from a rectangular window. Usualy these smaller sidelobes are

obtained at the expense of a broader central peak and hence reduced resolution.

(3) Statistical fluctuations - The spectrum analyser output at a particular frequency is the sum of the signal power and noise power within the bandwidth B. Since the spectrum of white noise is flat it may appear that we could detect arbitrarily low signal levels in the noise. In practice calculated noise spectra show statistical fluctuations about the mean noise level. This results in the noise component of the spectrum having a "jagged" appearance rather than being a straight line (figs. 8.3a-k).

Consider the analogue spectrum analyser (fig. 3.6). As shown by NEWLAND (1975) the true power spectral density P(f) is proportional to the expected value of the output of the square law detector. We estimate this value by averaging the square law detector output for some time, T. This is known as incoherent (or post detection) averaging as the signal phase information is lost by the squaring process. The fluctuations in the power spectrum estimates result from the fact that we are calculating finite sample averages as opposed to the infinite average required to calculate the true expected value.

The fluctuations about the mean value can be modeled by a chi-square distribution (BARRICK and SNIDER 1977). This is the probability distribution of values of a variable, χ_n^2 , formed by squaring and adding n independent Gaussian random variables:

$$\chi_n^2 = x_1^2 + x_2^2 + \ldots\ldots x_n^2 \qquad 3.42$$

where n is referred to as the number of degrees of freedom. If each variable, x_i , has a variance of one then the expected value of χ_n^2 is clearly n. The variance , σ^2 , of χ_n^2 is given by:

$$\frac{\sigma}{m} = \sqrt{\frac{2}{n}} \qquad 3.43$$

In our case care is required calculating n as the variables to be added must be independent. If the width of the power spectrum of the narrow band filter output is B then the width of the output autocorrelation time function will be of the order

$$\tau = \frac{1}{B} \qquad 3.44$$

Hence samples of the output closer together in time than τ will be correlated and therefore not independent. If the squared filter output is incoherently averaged for a time T_{incoh} then we can estimate the number of independent samples averaged as:

$$n_{incoh} = \frac{T_{incoh}}{\tau} = B\, T_{incoh} \qquad 3.45$$

Each independent sample will contribute two degrees of freedom to the chi-square process as its real and imaginary parts are squared and added to produce an estimate of the power. The number of degrees of freedom is therefore:

$$n = 2\ B\ T_{incoh} \qquad 3.46$$

giving

$$\frac{\sigma}{m} = \frac{1}{\sqrt{B\ T_{incoh}}} = 1 \qquad 3.47$$

for the normalized variance of the spectral estimates. This same result can be derived more rigorously by using fourth order averages (NEWLAND, 1975; OTNES and ENOCHSON, 1972). The assumptions used are that the power P(f) does not change much within the bandwidth B and that the filter output is Gaussian.

The incoherent averaging time is limited to the maximum length of the data record available for analysis. This record length is limited, in turn, by practical factors such as the fact that the true power spectrum may change over longer periods of time. Given a maximum value of T_{incoh} eqn. 3.47 shows that a trade-off exists between frequency resolution and the accuracy of the spectral estimates. Thus a spectral estimate measured at high resolution will be the average of only a small number of independent samples and will therefore be subject to large statistical fluctuations.

BLACKMAN and TUKEY (1959) have shown that these same results apply to digital spectral analysis using the discrete Fourier transform provided that the bandwidth is replaced by the equivalent bandwidth of the digital calculation (eqn. 3.39). This gives:

$$\frac{\sigma}{m} = \frac{1}{\sqrt{B\ T}} = 1 \qquad 3.48$$

Showing that the raw spectral estimates calculated by eqn. 3.28 and eqn. 3.29 have considerable uncertainty. To reduce this uncertainty we must increase the amount of incoherent averaging. There are two common techniques for doing this. Firstly a running average over frequency can be performed. For example if 2n+1 adjacent spectral estimates are averaged together we have

$$S_{av}(f_k) = \frac{1}{2n+1} \sum_{m=-n}^{m=+n} S(f_{k+m}) \qquad 3.49$$

resulting in estimates with increased accuracy

$$\frac{\sigma}{m} = \sqrt{\frac{1}{2n+1}} \qquad 3.50$$

at the expense of reduced frequency resolution

$$B = \frac{2n+1}{T} \qquad 3.51$$

In radar oceanography a second technique is more common. In this technique the original data record with length T is subdivided into n segments with length T/n and each segment analysed separately. The n resulting spectra are then averaged together to produce a final spectrum. The coherent integration time is therefore $T_{coh} = T/n$ resulting, once again, in reduced resolution

$$B = \frac{1}{T_{coh}} = \frac{n}{T} \qquad 3.52$$

and increased accuracy

$$\frac{\sigma}{m} = \sqrt{\frac{1}{B\ T_{incoh}}} = \sqrt{\frac{1}{n}} \qquad 3.53$$

When using this technique care must be taken to ensure that the n spectral estimates to be averaged are independent. BARRICK and SNIDER (1977), in a study of the statistics of hf sea echo, have shown that spectral values seperated in time by more than 25s are essentially uncorrelated. The condition of independence thus sets an

upper limit to the bandwidth we can use:

$$B < \frac{1}{25s} = 0.04 \text{ Hz} \qquad 3.54$$

It is common practice in radar oceanography to average spectra from adjacent ranges and radar beam directions (BARRICK and LIPA 1977, LIPA and BARRICK 1983). Naturally, some range or angular resolution will be lost by this process but this may not be important if the sea conditions are spatialy homogeneous. BARRICK and SNIDER (1977) show that spectra from ranges 3km (20us) apart are independent and so may be averaged to improve their statistical reliability.

The number of incoherent averages may be increased still further by subdividing the data record into overlapping, rather than sequential, segments. (WELCH 1967, KANESEWICH 1975).For example if the data segments overlap by 50% twice the number of non-overlapping segments of the same length. The number of independent averages will be less than twice as great, however, due to the correlation between the segments resulting from the overlap. This correlation is a function of the extent to which the data window tapers off in the region of overlap and is given as a function of fractional overlap, r, by HARRIS (1978):

$$c(r) = \frac{\sum_{i=0}^{N-1} W(i)\, W(i + [1 - r]\, N)}{\sum_{i=0}^{N-1} W^2(i)} \qquad 3.55$$

for an N point data window w(i).

eqn. 3.47 for the normalized variance of the spectral estimates now becomes:

$$\left(\frac{\sigma}{m}\right)^2 = \frac{1}{n}\left[1 + 2c^2 - \frac{2c^2}{n}\right] \qquad 3.56$$

for the case of 50% overlap. As examples the Cooley, Welch and Lewis (Reisz) window has a 50% overlap correlation of 0.33 resulting in a normalized variance of :

$$\left(\frac{\sigma}{m}\right)^2 \approx \frac{11}{9n} \quad \left(n \approx \frac{2T}{T_{coh}}\right) \qquad 3.57$$

while the minimum 4 sample Blackmann - Harris window (HARRIS 1978) has negligible correlation (0.04) giving:

$$\left(\frac{\sigma}{m}\right)^2 = \frac{1}{n} \qquad 3.58$$

LIPA and BARRICK (1983) use overlapped processing to recover from the two-fold reduction in resolution with the Blackman - Harris window.

In order to use overlapped processing a continuous coherent data record must be collected. In contrast, the non-overlapped, sequential scheme allows short time gaps to be present between each segment (e.g. for FFT analysis

or writing data to magtape). The use of overlapped processing will therefore place additional constraints on the design of a data collection system. The ability to do overlapped processing was one of the criteria used to design the data collection and processing system used in this work.

(4) A-D quantization noise - A-D converters introduce quantization noise due to the continuously varying input voltage being rounded to a binary integer with a finite number of bits. A simple calculation (OTNES and ENOCHSON 1972) shows that this noise has a flat power spectrum with a variance of 1/12. In our case two A-D channels are used (real and imaginary receiver outputs) and the noise is spread over a bandwidth f_{pr} . The spectral density of quantization noise is therefore:

$$S_{qn}(f) = \frac{1}{6f_{pr}} \qquad 3.59$$

where the units of spectral density are (A-D counts)^2 /Hz.

Quantization noise will add to the spectral density for external and receiver noise eqn. 3.22. We can minimise this noise by choosing the receiver gain so that $S_{noise} >> S_{qn}$. For example if $S_{noise} = F_n S_{qn}$ then the overall noise level will be raised by a factor 1+1/Fn by quantization noise. However increasing receiver gain to make Fn large will reduce the dynamic range of the system. Consider a signal of the form $Ae^{j\omega t}$. The maximum

amplitude such a signal can have is limited by the word length of the A-D converter to

$$A_{max} = \frac{2^n - 1}{2} \qquad 3.60$$

where n is the number of bits in the A-D word. The peak power spectral density of this signal is therefore of the order:

$$S_{max} = \frac{A_{max}}{B} \approx \frac{2^{2n-2}}{B} \qquad 3.61$$

If we define the dynamic range, D, of the estimated spectrum as the ratio of maximum signal power spectral density to total noise power spectral density then clearly D is limited to

$$D = \frac{2^{2n-2}}{B} \quad \frac{6f_{pr}}{(F_{n+1})} = \frac{3.2^{2n-1}}{(F_{n+1})} \quad \frac{f_{pr}}{B} \qquad 3.62$$

We note that coherent integration has improved the dynamic range by a factor $f_{pr/B}$ over that given by the A-D converters thus reducing the number of bits neccessary to digitise the signal. This is illustrated in fig. 3.7 where a sea echo Doppler time series originally digitised to 10 bit accuracy has been rounded to 4 bits with no significant loss of information. Differences in the base-line noise level can be noticed as quantisation noise now significantly contributes to this noise.

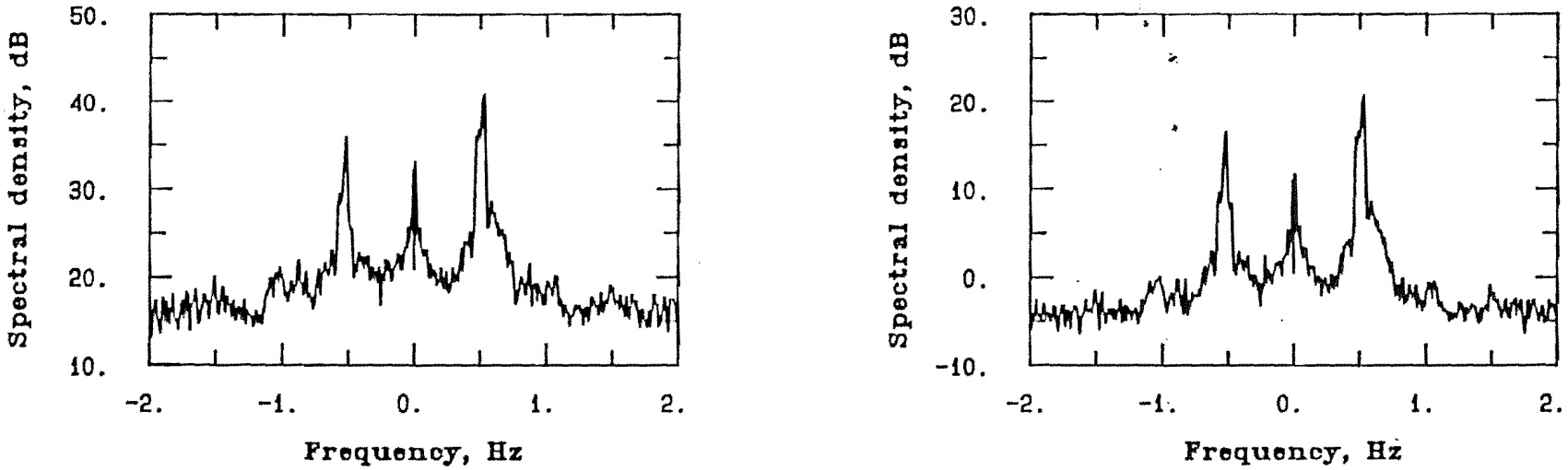

(a) Original spectrum (10 bit)

(b) Rounded spectrum

Fig. 3.7 Spectrum of 26MHz sea echo timeseries rounded to 4 bit accuracy.
(Date 1983/11/25 Time 1142 nzst Range 20km)

3.4 SUMMARY

In the previous sections we have seen how the performance of a pulsed Doppler radar system is determined by its various design parameters. We now summarise these results:

(1) To achieve a range resolution, Δr , the transmitter pulse width and receiver bandwidth must be

$$\tau_{TX} = \frac{2\ r}{c} = \frac{1}{B_{RX}} \qquad 3.63$$

(2) Range ambiguity limits the maximum pulse frequency to

$$f_{pr_{max}} = \frac{c}{2r_{max}} \qquad 3.64$$

where r_{max} is the greatest range from which signals can be detected.

(3) Aliasing (frequency ambiguity) sets a lower limit to the pulse repition frequency:

$$f_{pr_{min}} = 2f_{max} \qquad 3.65$$

where f_{max} is the highest frequency present in the

Doppler spectrum.

(4) The estimated spectral density of external and receiver noise in the final spectrum is determined by the unavoidable aliasing of this noise:

$$S_{noise} = kT_{sys} \frac{B_{RX}}{f_{pr}} G_{sys} \qquad 3.66$$

(5) Frequency resolution is determined by coherent integration time:

$$B = \frac{1}{T_{coh}} \qquad 3.67$$

(6) The uncertainty of the spectral estimates is determined by the incoherent averaging time. If n_{av} non-overlapped time series segments are used then:

$$n_{av} = T_{incoh}/T_{coh} \qquad 3.68$$

and

$$\frac{\sigma}{m} = \sqrt{\frac{1}{n_{av}}}$$

The number of incoherent averages can also be increased by averaging spectra from adjacent ranges, frequencies and beam directions etc. However the resolution in each of these quantities will be correspondingly reduced.

(7) If the maximum dynamic range of the spectrum is D and we require that this dynamic range be degraded by not more than a factor 1+1/Fn then A-D convertors with word length at least:

$$n = \frac{1}{2}\left[\frac{\ell n([F_{n+1}]\ D\ B/[3f_{pr}])}{\ell n\ 2} + 1\right] \qquad 3.69$$

will be required. The system gain, G_{sys}, is chosen so that

$$S_{noise} = F_n\ S_{qn} \qquad 3.70$$

giving:

$$G_{sys}^{\ 2} = \frac{F_n\ f_{pr}}{6kT_{sys}\ B_{RX}} \qquad 3.71$$

In order to use these results we need to be able to predict the signal strengths to be expected so that the maximum range, r_{max} , and maximum spectrum dyamic range,

D, can be calculated. Signal strengths can be calculated from the radar equation (eqn. 3.19) once the scattering cross sections of the sea surface, $\sigma, \sigma(\omega)$, and the ground wave attenuation factor, F, are known. The scattering cross sections will be discussed in chapter 4 while ground wave propagation and the complete calculation of radar performance is treated in chapter 6.

CHAPTER 4:

ELECTROMAGNETIC SCATTERING FROM OCEAN WAVES

4.1 HISTORICAL INTRODUCTION

In chapter 2 we discussed the basic principles of oceanography and saw that the properties of the ocean surface could be described by an ocean waveheight spectrum. In chapter 3 the principles of pulsed Doppler radar were discussed. It was shown here that the Doppler spectrum of the echoes from an extended moving target, such as the ocean surface, could be described by a frequency dependent scattering cross section, $\sigma(\omega)$. We start this chapter by combining these results and showing how the scattering cross section of the ocean surface, and hence the Doppler spectrum of radar sea echo, may be obtained from a knowledge of the ocean waveheight spectrum. However for radar remote sensing of the ocean surface it is the inverse problem that is of more importance. Namely, how do we obtain oceanographic information from measured sea echo Doppler spectra? The final section of this chapter discusses this problem.

From the time radar was invented before World War II it was noticed that the sea surface is a particularly strong reflector of radio waves. The pioneering study of this effect was made by CROMBIE (1955) while at the Dominion Physical Laboratory (now known as the Physics and Enginering Laboratory) of the New Zealand Department of Scientific and Industrial Research (DSIR). A research

report of this organisation, CROMBIE and PENTON (1954), describes the equipment Crombie used. The experiment was a ground wave pulsed Doppler radar operating at a frequency of 13.56MHz. The transmitter output was 1.3kW which, when fed into a corner reflector antenna with 30 degree beamwidth, gave a range of approximately 80 nautical miles (150km). The range gating system used could be set to sample any range between 13 and 185km with a resolution of 3.75km determined by the 25us transmitted pulse width. The Doppler time series from the selected range was recorded on a chart recorder and spectral analysis of this record performed with an Admiralty wave analyser. This device used electomechanical and electro-optical means to perform essentialy the same function as the analogue spectrum analyser discussed in chapter 3.

CROMBIE (1955, 1971) noticed three rather remarkable things about the sea echo data he obtained with this equipment. Firstly the amplitude of the echo was always constant regardless of sea state or wind conditions. The principal frequency present in the Doppler spectra was also constant at 0.38Hz, again irrespective of sea conditions. Thirdly most of the energy in the spectrum was concentrated in a very narrow region around this principal frequency of 0.38Hz. The strength of the echo also indicated an efficient scattering mechanism. Crombie correctly deduced that this mechanism was Bragg scattering

analogous to that observed in X-ray crystallography. Out of the entire mix of components in the ocean waveheight spectrum the radar wave is reflected most strongly from that component having a wavelength half the radar wavelength ($L = \lambda/2$). This is because if this condition is met reflections from one crest will be in phase, and therefore reinforce, reflections from subsequent crests. Furthermore in the monostatic radar geometry only those components travelling directly towards or away from the radar will be able to return echoes to the radar. The phase velocity of these waves is given by the gravity wave dispersion relation:

$$v = \sqrt{\frac{gL}{2\pi}} \qquad 4.2$$

and will result in the echo having two Doppler shifts from the carrier frequency:

$$\Delta f = \pm \frac{2v}{\lambda} = \pm\sqrt{\frac{g}{\pi\lambda}} \qquad 4.2$$

Where the positive Doppler shift is produced by the component advancing towards the radar and the negative Doppler shift produced by the receding component. For the frequency of 13.56MHz (λ = 22m) the Bragg scattering

ocean wave components will have a length of 11m, a period of 2.7s and a velocity of 4m/s. The Doppler shifts of the received echoes will be $\Delta f = \pm 0.376$Hz in excellent agreement with that observed. In any wind speed over 4m/s we will expect these Bragg components to be fully developed and hence of relatively constant amplitude (chapter 2) thus explaining the constant nature of the echo amplitude.

Two other features were apparent in Crombie's records. The first of these was a subsidiary peak at 0.54Hz which Crombie explained as being due to higher order Bragg scatter, in other words scatter with Doppler shifts given by:

$$\Delta f = \pm \sqrt{\frac{ng}{\pi\lambda}} \qquad 4.3$$

Where n is an integer which is equal to 2 for the 0.54Hz peak. Crombie also noticed that while the Bragg peak was narrow its width was still greater than that expected from spectral analysis. The explanation he proposed was that the Bragg scattering ocean waves existed in short trains of about six crests. It is now known that ocean currents contribute to this broadening (STEWART and BARNUM, 1975, BARRICK et. al., 1977).

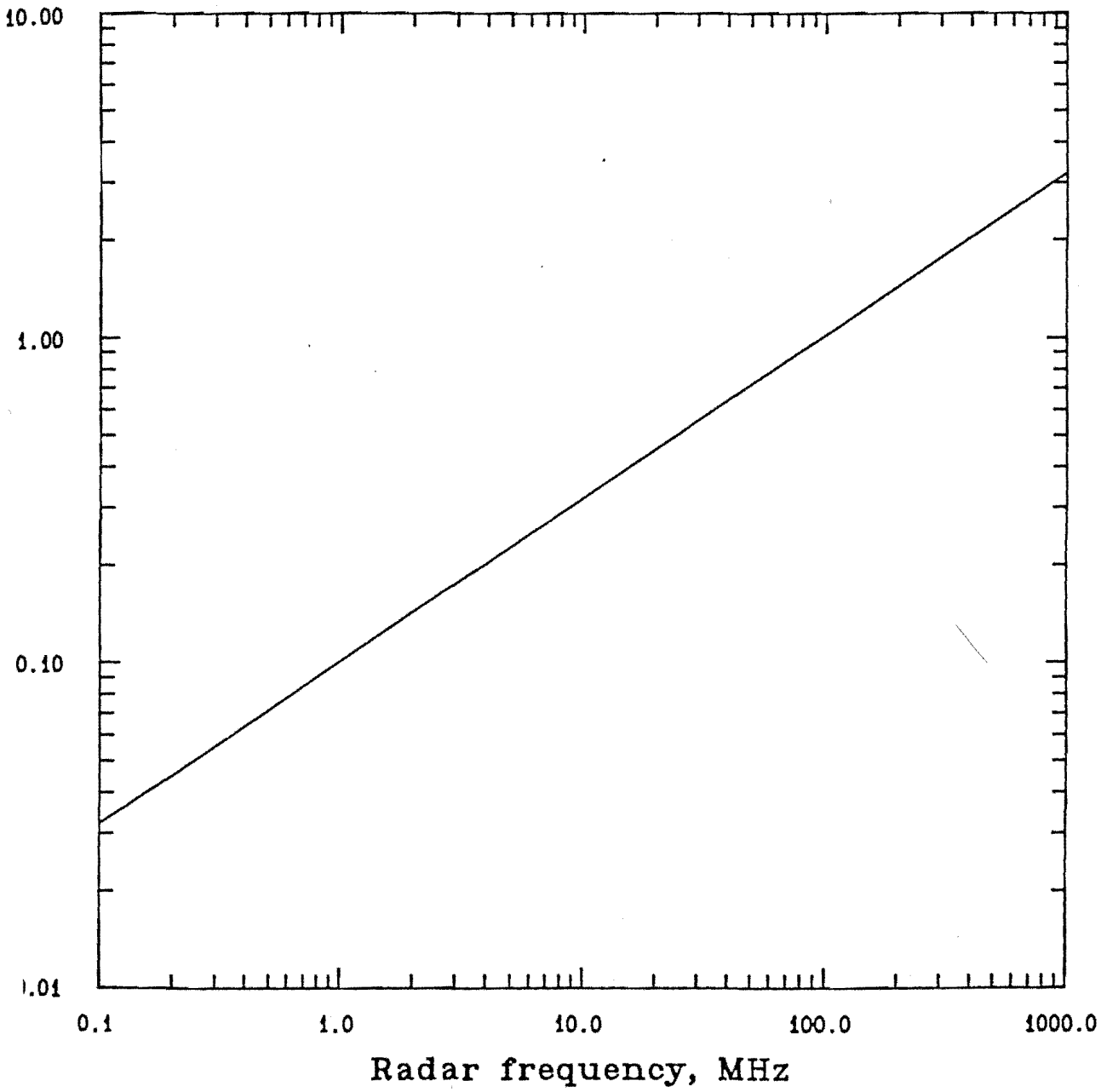

Fig. 4.1 Bragg relationship.

4.2 THE CALCULATION OF DOPPLER SPECTRA FROM OCEAN WAVEHEIGHT SPECTRA

Following Crombie's original work further progress came in the form of theoretical calculations of the radar cross section of the sea surface. PEAK (1959) used an electromagnetic scattering theory to derive a first order approximation to this cross section for a general rough surface. BARRICK (1972a) applied this result to the sea surface and showed (BARRICK and PEAK, 1968) that the result could be physically interpreted as Bragg scatter - confirming CROMBIE'S (1955) suggestion. A detailed derivation of this result may be found in JOHNSTONE (1975 Ph.D. thesis). Here we give a brief outline of the steps involved in the derivation:

(1) The calculation begins by considering a general rough surface which is described by a two dimensional series of Fourier coefficients. An electromagnetic field incident on this surface produces a field which consists of two components: A specularly reflected field, which is the field that would be produced by a plane surface in the absence of roughness and a scattered field which is due to the roughness. We calculate this scattered field by expressing it as a Fourier series of the same type used for the surface and then solving for the Fourier coefficients.

(2) The first step in the solution for these coefficients is to use the divergence equation for the electric field, $\nabla.\underline{E} = 0$. This eliminates some of the Fourier components and physically corresponds to the assumption that no free electric charges exist in the region.

(3) The remaining coefficients are found by applying the boundary conditions for the electric field at the surface. This condition is that the tangential component of the field on the surface must be zero.

(4) The resulting equations for the field components cannot be solved in closed form and so must be expanded in a perturbation series. This series is simplified by neglecting second and higher order terms. The conditions for the validity of this approximation are discussed by BARRICK (1972b). Generally the approximation holds for low sea states and low radar frequencies.

(5) At this point we have a first order solution for the field of a plane wave scattered by a rough surface . We need to relate this result to the radar cross section per unit area of surface. This is acheived by using the Stratton-Chu integral (JOHNSTONE 1975 Ph.D. thesis) to

calculate the field at some distant point (i.e. the radar receiver) due to the field on the surface.

(6) The result we have at this point is deterministic in that it is the cross section of one particular surface with a precise profile given by the two dimensional Fourier series. We obtain a result for a random rough surface by taking an ensemble average of surfaces of this kind. The result is that the Fourier series description of a the particular surface is replaced by the power spectrum of the ensemble of random surfaces.

(7) The results for rough surfaces are applied to the ocean surface by generalizing the Fourier series, and hence the random surface power spectrum, to include time variation. The dispersion relation for surface gravity waves is then used to restrict the result to first order. The radar cross section of the surface is now time dependent and is the same as the result for the time invariant rough surface but multiplied by a factor $e^{i\omega_B t}$ where ω_B is the Bragg frequency, $\omega_B = \sqrt{2g\kappa_o}$. The power spectrum of this time varying cross section, and hence the Doppler spectrum of the sea echo, thus consists of two delta functions at radian frequencies $\pm\omega_B$ exactly as observed by CROMBIE (1955):

$$\sigma_1(\omega) = 2^6\pi\kappa_o^4 \left[S(\underline{\kappa}_B)\ \delta\ (\omega - \sqrt{2g\kappa_o}) + S(-\underline{\kappa}_B)\ \delta\ (\omega + \sqrt{2g\kappa_o})\right]$$

Where $\kappa_o = 2\pi/\lambda$ is the radar wavenumber (rad/m) and $\underline{\kappa}_B = 2\kappa_o$ is the wavevector of the Bragg scattering component of the ocean waveheight spectrum, $S(\underline{\kappa})$. The total power in each delta function is proportional to the ocean waveheight spectral density at the Bragg frequencies. For radar frequencies above about 10MHz (see e.g. fig. 12.6 in BARRICK, 1972b) the Bragg scattering components are usually saturated and therefore of constant amplitude. This explains CROMBIE'S (1955) observation that the backscattered radar echo was constant in strength regardless of sea state. The total first order scattering cross section of the sea surface is readily estimated by integrating eqn. 4.4 over Doppler frequency with an appropriate model for the ocean waveheight spectrum. BARRICK (1972b) has performed this calculation for the Phillips spectrum (eqn.2.21) to obtain a result that is both surprising and useful:

$$\sigma_1 = 0.02 = -17\text{dB} \qquad 4.5$$

In other words the ω^{-5} dependence of the Phillips spectrum exactly cancels the radar frequency to yield a result that is independent of radar frequency. The first order portion of the sea echo can thus be used as a calibration target of known cross section. We use this result in chapter 6 to study the effect of ground wave

propagation on the performance of the radar. JOHNSTONE (1975 Ph.D. thesis) has examined this result for a variety of ocean waveheight spectrum models, including directional spectra. Under most conditions of wind speed and direction eqn. 4.5 still forms a good approximation.

Given that the total first order cross section is proportional to the amplitude of one particular ocean wave component it is obvious that the non-directional ocean waveheight spectrum could be determined by a series of measurements at multiple radar frequencies. Examples of this technique are given by CROMBIE (1971) and point to a major disadvantage of the system. The frequency range used, 2-30MHz, covers the high frequency, saturated region of the ocean waveheight spectrum but does not measure wave components with periods greater than about 7 seconds. These components include the interesting wind speed dependent cutoff region of the spectrum. In order to measure this region radar frequencies in the broadcast band would be required (fig. 4.1) raising the problem of mutual interference with broadcasting services. Furthermore antenna arrays become inconveniently large (hundreds of metres) at these frequencies, particularly if a narrow transmitted beam is required. A final problem is that absolute measurements of radar cross section are required. This in turn requires that receiver responses, path losses, antenna gains etc. be known at each of the

frequencies used. These quantities are difficult to measure accurately and often vary with weather conditions.

A potential solution to these problems was provided by HASSELMAN'S (1971) suggestion that non-linear hydrodynamic interactions between ocean wave components would allow the Bragg scattering components to be modulated by other components giving rise to continuous sidebands on either side of each Bragg peak. In contrast to the Bragg peaks, which result from only one ocean wave component, these sidebands contain information on the entire range of ocean wave component frequencies. In fact according to HASSELMAN (1971) each sideband should have the same form as the non-directional ocean waveheight spectrum thus allowing this spectrum to be determined by a single frequency radar. Hasselman also suggested that these sidebands could be divided by the total first order power in order to eliminate the effects of unknown path losses, system responses etc. One problem with this convenient normalisation is that the resulting spectrum points no longer obey the chi-square distribution (see chapter 3) hence we can no longer use chi-square statistics to estimate the uncertainties in parametrs derived from these normalised spectra. BARRICK (1980) shows that the spectra now obey the F distribution and presents graphs giving the error bounds on the spectrum points as functions of the number of independent spectra

averaged.

The existence of these sidebands was confirmed by accurate measurements of sea echo Doppler spectra with radar frequencies in the upper hf region (TYLER et.al., 1972). The sidebands appeared as broad peaks on either side of each Bragg peak and a higher than normal noise "floor" near 0Hz between the peaks. Standard tests established that these features were oceanographic in origin and not due to, for example, external interference. The sidebands were found to depend strongly on sea state and wind direction. They were not, however, symmetrical about each Bragg peak as predicted by HASSELMAN'S (1971) theory.

The problems of the asymmetry and directional dependence of the sidebands were resolved when BARRICK (1972b) developed a more advanced theory by extending the first order Bragg scattering theory to second order. As well as retaining second order electromagnetic scattering terms BARRICK'S (1972b) theory included second order hydrodynamic effects. Full mathematical details of this second order scattering theory may be found in JOHNSTONE (1975 Ph.D. thesis). A simplified derivation of both the first and second order scattering cross sections has been given by ROBSON (1984). The result for the second order part of the radar cross section is:

$$\sigma_2(\omega) = 2^6 \pi \kappa_o^4 \sum_{m_1, m_2 = \pm 1} \iint_{-\infty} |\Gamma|^2 \delta(\omega - m_1\sqrt{g\kappa_1} - m_2\sqrt{g\kappa_2})\, S(m_1\underline{\kappa}_1)\, S(m_2\underline{\kappa}_2)\, dpdq \qquad 4.6$$

This expression describes a double Bragg scattering process involving two ocean wave components:

$$\underline{\kappa}_1 = \tfrac{1}{2}\,\underline{\kappa}_B + (p,q)$$
$$\underline{\kappa}_2 = \tfrac{1}{2}\,\underline{\kappa}_B - (p,q) \qquad 4.7$$

The coupling coefficient, Γ , is the coherent sum of electromagnetic and hydrodynamic terms:

$$\Gamma = \Gamma_H + \Gamma_{Em} \qquad 4.8$$

Where

$$\Gamma_H = -\frac{j}{2}\left[\kappa_1 + \kappa_2 + m_1 m_2\left(1 + \frac{p^2+q^2-\kappa_o^2}{\kappa_1\kappa_2}\right)\left(\frac{1-2\omega^2}{\omega^2-\omega_B^2}\right)\right] \qquad 4.9$$

and

$$\Gamma_{EM} = \tfrac{1}{2}\left[(p^2+2q^2-\kappa_o^2)/(\sqrt{\kappa_o^2-p^2-q^2}+\kappa_o\Delta)\right] \qquad 4.10$$

Where Δ is the impedance of the sea surface divided by the impedance of free space. Physically, the electromagnetic terms describe a corner reflector effect in which the incident wave is Bragg scattered by $\underline{K_1}$ to produce an intermediate wave which is scattered back to the radar receiver by $\underline{K_2}$. The resulting Doppler shift is the sum of the individual Doppler shifts from the two components. This effect is most efficient if the two ocean wave components are traveling at $\pm$ 45 degrees to the radar beam. This condition gives rise to a peak in the second order Doppler spectrum at a frequency of $2^{3/4}\omega_B$. The hydrodynamic terms describe the non-linear interaction between the two ocean wave components, K_1 , K_2 , to produce a third wave which causes Bragg scattering of the incident radar beam. This third wave will not obey the first order dispersion relation and will therefore produce a different Doppler shift from first order scatter. A special case of these non-linear interactions is that of a wave interacting with itself to produce second, and higher order, harmonics. These harmonics travel at the same speed as the fundamental and give the basic wave component a trochoidal profile, in contrast to the sinusoidal profile resulting from first order hydrodyamic theory (Chapter 2). Scattering from the second harmonic of this trochoidal profile gives rise to a peak in the second order part of the spectrum at a frequency of $2^{1/2}\omega_B$.

Eqn. 4.6 allows the second order part of the sea echo Doppler spectrum to be calculated from a knowledge of the ocean waveheight spectrum. The delta function in the expression is used to reduce the double integral to a single integral which can then be evaluated numerically. Unfortunately the expression within the delta function has no closed form solution and so must be solved numericaly at each point in the integration. Several workers (BARRICK, 1977b; LIPA, 1977; JOHNSTONE, 1975 Ph.D. thesis) have overcome this problem by devising transformations which allow closed form solutions of the delta function argument.

The typical form of sea echo Doppler spectra, including both first and second order parts, is shown in fig. 4.2. There are three main second order sidebands. The two sidebands lying outside the Bragg peaks (i.e. $\omega < -\omega_B$ and $\omega > +\omega_B$) result from equal signs in the delta function argument (i.e. $m_1 = m_2$) and are therefore known as sum mode sidebands. The region between the Bragg peaks (i.e. $\omega_B < \omega < +\omega_B$) is produced by having opposite signs in the delta function argument (i.e. $m_1 \neq m_2$) and is known as the difference mode region. Second order spectra calculated by means of the above theory are in complete agreement with experimentally measured sea echo spectra (see e.g. the measured spectra in chapter 8). In particular the calculated spectra are found to depend

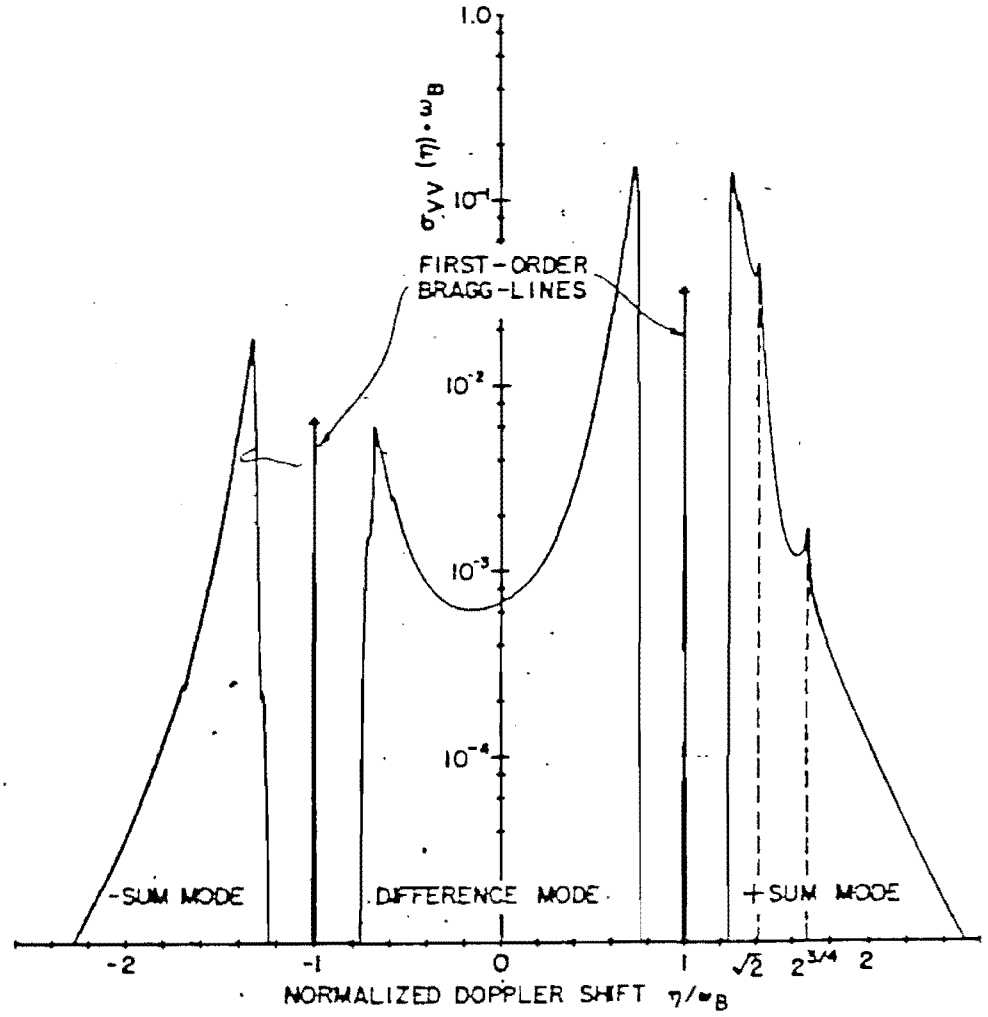

Fig. 4.2 Typical form of a sea-echo Doppler spectrum. (From JONSTONE, 1975).

strongly on wind speed and direction and are usually asymmetrical. Increasing wind speed increases the total energy in the second order spectrum and moves this energy closer to the Bragg peaks. Wind direction governs the asymmetry in the spectrum: cross-winds produce nearly symmetrical spectra, winds blowing towards the radar distribute the energy towards positive Doppler shifts while winds blowing away from the radar enhance the energy at negative Doppler shifts.

Second order cross sections also increase with increasing radar frequency. This fact leads to a convenient normalization. If $\sigma(\omega).\omega_B$ is plotted against ω/ω_B the resulting plot is constant if the parameter $u^2 f$ (u = windspeed, f = radar frequency) is constant. Thus if the radar frequency is multiplied by four the same graph is obtained at half the windspeed.

4.3 INFORMATION OBTAINABLE FROM SEA ECHO DOPPLER SPECTRA

In the previous sections we have examined the problem of predicting the sea echo Doppler spectrum from a knowledge of the ocean waveheight spectrum. In order to use hf Doppler radar as a remote sensing tool we must consider the inverse problem of obtaining oceanographic information from measured hf sea echo Doppler spectra. The ultimate goal is to obtain the complete directional ocean waveheight spectrum from the Doppler spectra. However this requires a considerable amount of complicated data processing with the result that much work has been done on extracting simpler parameters, such as significant wave height and dominant wave period, directly from the spectra. In this section we examine the important oceanographic quantities and outline the techniques that have been developed to obtain them from the Doppler spectra.

(1) The directional ocean waveheight spectrum. Given a means of calculating the second order Doppler spectrum from an ocean waveheight spectrum we can obtain the ocean waveheight spectrum from the Doppler spectrum by a "brute force" inversion technique. We first choose a trial ocean waveheight spectrum and calculate a second order Doppler spectrum from it. This spectrum is then compared with the measured Doppler spectrum and the trial ocean waveheight

spectrum adjusted to minimise the rms difference between the two. This process can be either manual or carried out by one of a number of common optimisation algorithms. An excellent discussion of these algorithms and their pitfalls is given by BEVINGTON (1969). TRIZNA et.al. (1977) have used this technique with reasonable success by using a simplified, corner reflector model of second order scatter. This model effectively ignores the hydrodynamic second order interactions.

As an alternative to these iterative optimisation techniques a number of standard matrix techniques for inverting integral equations exist. In these techniques the integral is converted by numerical quadrature into a matrix equation which is then solved subject to constraints imposed to minimise various problems such as ill-conditioning (WESTWATER and STRAND, 1972). Unfortunately these techniques cannot be directly applied to the inversion of second order sea echo due to the non-linear nature of the integrand in eqn. 4.6. LIPA (1977) has developed an inversion technique that overcomes this problem. The directional ocean waveheight spectrum is factorised into directional and non-directional parts in the manner of eqn. 2.24. In addition at high frequencies the non-directional spectrum is assumed to take the form of the Phillips saturation spectrum, eqn. 2.21. An iterative optimisation technique is used to find the

directional dependence. The directional dependence, together with the high frequency Phillips spectrum approximation, is then used to linearise the integral equation so that standard matrix inversion techniques may be used to solve for the low frequency part of the non-directional spectrum. Comparison of directional spectra obtained in this way with spectra measured by a pitch and roll buoy (chapter 2) show reasonable agreement (LIPA, 1978). Generally, wind directions agree to within 5 degrees and spectrum amplitudes agree to within about 20%.

(2) The non-directional ocean waveheight spectrum.

This can be estimated from the first order Bragg lines by using multi-frequency radar measurements (CROMBIE, 1971). However, as we have discussed previously, this method has severe practical disadvantages. BARRICK (1977a,b) has devised a technique which allows the non-directional spectrum to be obtained from the second order sidebands without requiring a full inversion process such as (1) above. The second order sidebands are divided by a weighting function, $W(\omega/\omega_B)$, and the result normalised by the total first order power, i.e.

$$S(\omega - \omega_B) = \frac{4\sigma_2(\omega)/W(\omega/\omega_B)}{\kappa_o^2 \int_0^\infty \sigma_1(\omega)\,d\omega} \qquad 4.11$$

The weighting function is obtained from the coupling coefficient, Γ , in eqn. 4.6 by integrating out its angular dependence. It is immediately apparent that this result bears a strong similarity to HASSELMAN'S (1971) original suggestion that the sidebands were due to modulation of the first order Bragg scattering components by other components in the ocean waveheight spectrum. A frequency, ω , in the Doppler spectrum thus corresponds to an ocean wave component with frequency, $\omega - \omega_B$. The difference with BARRICK'S (1977a,b) technique is the normalisation by the weighting function, $W(\omega/\omega_B)$.

(3) Wind measurements. Values of wind speed and direction are derived from measurements of sea conditions by assuming that the ocean waveheight spectrum is generated by the local wind and is in equilibrium with it. Hence wind speed is usually derived from some radar measure of significant wave height. Several techniques have been developed to extract significant wave height from sea echo Doppler spectra. MARESCA and GEORGES (1980) have investigated a semi-empirical method in which the rms waveheight is expressed as a function of the total, integrated second order power normalised by the first order power, i.e.

$$\kappa_o h = a\ R^b \qquad 4.12$$

where

$$R = \int_{-\infty}^{+\infty} \sigma_2(\omega)\,d\omega \;/\; \int_{-\infty}^{+\infty} \sigma_1(\omega)\,d\omega \qquad 4.13$$

Values of the coefficients a and b which give about 15% agreement (% agreement = % difference between the two measurements) between radar and buoy measurements have been found:

$$\kappa_o h = 0.8\ R^{0.6} \qquad 4.14$$

The rms waveheight, and hence the windspeed, may also be found by integrating the non-directional waveheight spectrum over frequency as in eqn. 2.13. The non-directional spectrum can, in turn, be found by using BARRICK'S (1977a,b) inversion technique. BARRICK (1977a) compares rms waveheights obtained in this way with measured data from a wave buoy. The results agree to within an accuracy of 23% - a figure which is consistent with the statistical uncertainty of the sea echo spectra used (33% from 9 incoherent averages). If a model non-directional spectrum is assumed then waveheight can be calculated once the appropriate parameters of the model are known (by substituting the model into eqn. 2.13). FORGET et. al. (1981) consider a Pierson-Moskowitz spectrum model with the frequency of the maximum of the

spectrum as the defining parameter. The significant waveheight is then given by:

$$H_{1/3} = 0.04/F_m^2 \qquad 4.15$$

The dominant frequency, F_m , of the spectrum is readily estimated from the second order sea echo spectrum by a technique that will be outlined below (see (4)). However the assumption of a model spectrum, together with the uncertainty in determining F_m , results in waveheight estimates that are not particularly accurate.

An interesting feature of sea echo Doppler spectra obtained at frequencies in the upper hf region is that the first order Bragg peaks are often much broader than would be expected from the coherent integration time of the radar. Furthermore this broadening is observed to increase with increasing sea states (see chapter 8) and may therefore be used to estimate wind speed (STEWART and BARNUM, 1975). The broadening is due to Doppler shifts caused by differing current velocities within the radar resolution cell (LIPA and BARRICK, 1983; LEISE, 1984). However at the resolution used by STEWART and BARNUM (1975) (12.8s coherent integration time) it is likely that part of the second order spectrum would have been included

within the region of the first order peaks, thus contributing to the windspeed dependence of the broadening. STEWART and BARNUM (1975) also suggest that wind speed can be estimated from the second order spectral density at 0Hz divided by the total first order energy. In this work, however, we find (see chapter 8) that the spectrum in the region of 0Hz is strongly influenced by receiver offset voltages and long term variations in these offsets. In addition echoes from land masses will produce peaks at 0Hz (SHEARMAN, 1981). We therefore conclude that this technique is likely to be unreliable unless considerable care is taken to avoid these effects.

Wind direction is obtained by assuming that it corresponds to the maximum in the directional dependence of the ocean waveheight spectrum. Inversion techniques for obtaining the directional ocean waveheight spectrum (e.g. LIPA, 1977) can therefore estimate wind direction as a by product. A simpler method, however, has been suggested by LONG and TRIZNA (1973) and is based on the fact that first order Bragg scattering occurs from only those wave components travelling directly towards or away from the radar. The first order echoes thus sample the ocean waveheight spectrum directional dependence at an angle equal to the difference between the wind direction (directional maximum) and the radar beam direction. If a model for this directional dependence is assumed the wind

direction can be determined from the ratio of the strengths of the advancing to receding first order peaks. This process is illustrated in fig. 4.3. The 180 degree ambiguity in wind direction can be resolved if the overall wind circulation pattern is known. This is usually the case with skywave radar measurements which cover an area of the ocean surface comparable in size to typical weather patterns.

Discussions of these wind measuring techniques have been given by STEWART and BARNUM (1975) and DEXTER and THEODORIDIS (1982). STEWART and BARNUM (1975) conclude, by comparison with buoy data, that skywave wind direction measurements are accurate to ±16 degrees and wind speed measurements to ±4m/s. DEXTER and THEODORIDIS (1982) extend BARRICK'S (1977a) wind speed inversion technique to include the effect of fetch limited seas.

(4) The cutoff frequency and dominant frequency of the spectrum. HASSELMAN'S (1971) suggestion that second order echoes are modulation sidebands can be used to readily estimate some important parameters of the ocean waveheight spectrum without having to obtain this spectrum by means of a full inversion process. BARRICK (1977b) has shown that HASSELMAN'S (1971) suggestion is a good approximation if the second order sidebands are multiplied by a weighting function. This weighting function, however,

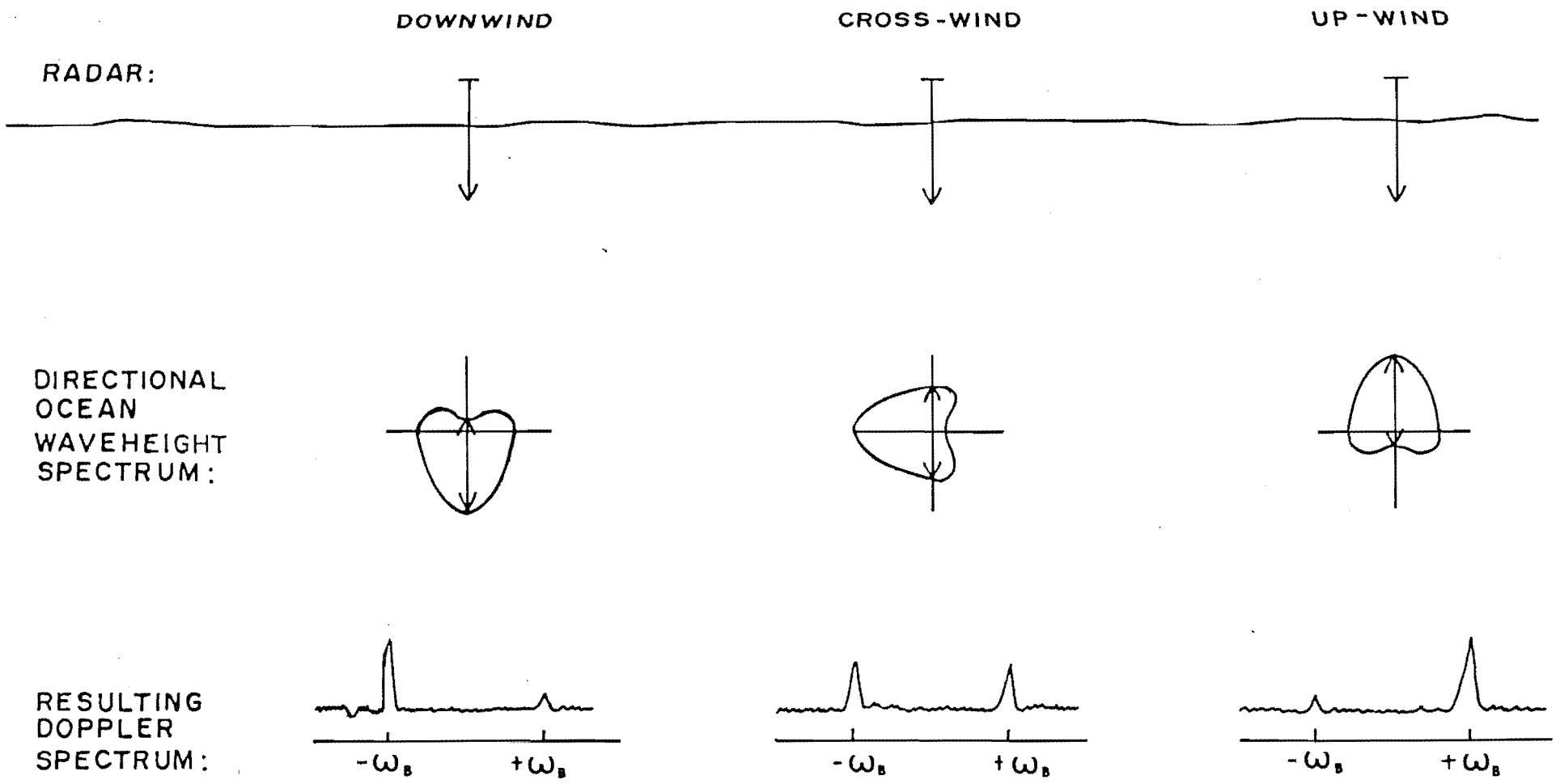

FIG. 4.3 WIND DIRECTION FROM BRAGG LINE RATIO.

only corrects the amplitude of the spectrum, leaving the Doppler frequencies unchanged. The result of this is that a direct interpretation of these Doppler shifts in terms of ocean wave frequencies is possible. In other words a frequency, F_o , in the ocean waveheight spectrum gives rise to Doppler shifts

$$f_o = \pm f_B \pm F_o \qquad 4.16$$

in the second order part of the sea echo spectrum. Low frequency ocean wave components thus influence the second order sidebands close to the Bragg peaks while higher frequencies influence those parts further away from the Bragg peaks. Therefore if the ocean waveheight spectrum has a low frequency cutoff at some frequency, F_c , we expect that a gap of width aproximately F_c will exist between the Bragg peaks and the second order sidebands. Most sea echo Doppler spectra, including those obtained in this work, clearly show this seperation between the Bragg peaks and the second order echoes. FORGET et.al. (1981) have used these ideas to estimate the cutoff frequency and dominant frequency (frequency of the spectrum maximum) of the ocean waveheight spectrum. If L_c is the width of the region of the sea echo Doppler spectrum between the Bragg peaks then the cutoff frequency of the ocean waveheight spectrum can be estimated by:

$$F_c = f_B - L_c/2 \qquad 4.17$$

Similarly if L_m is the width of this region of the spectrum measured between its maxima then the dominant ocean wave frequency is estimated by:

$$F_m = f_B - L_m/2 \qquad 4.18$$

FORGET et.al. (1981) find that the accuracy of these techniques improves as F_m becomes smaller (i.e. waveheights become greater).

(5) Properties of swell. The techniques we have discussed up to this point have assumed that the ocean waveheight spectrum causing the radar scattering has been generated by the local wind within the radar resolution cell. This assumption will clearly be incorrect if swell from some distant storm is present. We recall from chapter 2 that swell has a very narrow band spectrum due to the dispersive properties of the first order gravity wave solution. If we apply HASSELMAN'S (1971) modulation sideband theory we expect that swell will produce four

narrow spikes in the second order spectrum. These spikes will be arranged as one spike on either side of each Bragg peak. The frequency seperation between each peak and its associated Bragg peak will be the swell frequency. TYLER et. al. (1972) have estimated swell periods in this manner and have found that they agree with values obtained by visual observations of waves arriving on a nearby beach.

LIPA and BARRICK (1980) have predicted the sea echo spectrum resulting from swell by using a mathematical model of the swell waveheight spectrum in the equation for the second order radar cross section (eqn. 4.6). Their results confirm that four peaks are generated. However these peaks are not symmetrically distributed about the Bragg peaks as implied by HASSELMAN'S (1971) modulation sideband theory. The frequencies of the swell peaks depend on the direction of arrival of the swell, as well as its period. If the frequency seperation of the swell peaks surrounding the $+\omega_B$ Bragg peak is $\Delta\omega^+$ and the corresponding value for the $-\omega_B$ Bragg peak is $\Delta\omega^-$ then the swell wavenumber, κ_s, and direction of arrival (relative to the radar beam), θ_s, are given by:

$$\kappa_s = \left(\frac{1}{16g}\right) (\Delta\omega^+ + \Delta\omega^-)^2$$

$$\theta = \cos^{-1}\left[8\omega_B \frac{\Delta\omega^+ - \Delta\omega^-}{(\Delta\omega^+ + \Delta\omega^-)}\right]$$

The swell frequency, ω_s , is found by applying the first order dispersion relation:

$$\omega_s = \sqrt{g\kappa_s} \qquad 4.20$$

Equivalent expressions in terms of the absolute frequencies of the peaks, rather than their frequency seperations, have been given by FORGET et. al. (1981).

(6) Ocean surface currents. The Doppler shifts of the first order Bragg peaks are due to the characteristic phase velocity of the ocean wave components responsible for first order Bragg scatter. The phase velocity of the component is relative to the body of water in which the wave exists. A current in this body of water will therefore transport the Bragg scattering waves with it thus changing the velocity of these waves with respect to the radar. The result is that the Bragg peaks will be shifted from their theoretical positions, $\pm\omega_B$, by an amount, $\Delta\omega$, given by:

$$\Delta\omega = 2\kappa_o v_{cr} \qquad 4.21$$

Where v_{cr} is the radial component of the current velocity. If several different radial current velocities exist within the radar resolution cell multiple Doppler shifts will occur, sometimes giving rise to multiple Bragg peaks. Usualy, however, the finite Doppler frequency resolution of the radar will merge these peaks together to produce a single peak broadened from the value given by the radar resolution. The different radial components can arise because the actual current velocity varies within the resolution cell or because of a broad-beam radar viewing a uniform current from different directions. Each Doppler frequency point in the current broadened first order echo corresponds to a unique value of radial current velocity given by eqn. 4.21. If the direction of arrival of each of these frequencies can be determined then a map of radial current velocities can be determined. If two radars seperated by some distance are used to examine the same area of sea surface then the resulting radial current maps may be combined to yeild a vector current velocity map. BARRICK et. al. (1977) have developed a compact antenna system which allows the direction of arrival of first order echoes to be accurately determined.

This antenna system uses the fact that a typical current pattern will produce echoes from at most two directions at any given Doppler shift. By measuring the phase of these echoes received on a number of spaced

antennas their direction of arrival can be determined. The accuracy of such a system would decrease considerably if echoes from more than two directions were present. In contrast the traditional phased array antenna works by synthesizing a narrow beam receive response and electronically scanning this beam over the required area of sea. An extremely large array is thus required if the directional accuracy of Barrick's interferometer system (1-2 degrees) is to be approached. The phased array system can, however, resolve echoes arriving from a large number of different directions at once. An even more compact direction finding antenna system has been developed by LIPA and BARRICK (1983). This system uses a computer to synthesize a narrow, scanning beam from the directional responses of two crossed loop antennas. As a result of this work the measurement of current velocity maps has become one of the most successful applications of hf radar oceanography. The equipment described by BARRICK et. al. (1977), LIPA and BARRICK (1983) and LEISE (1984) is almost at the stage of commercial production and has been used in a variety of oceanographic studies (SHEARMAN 1983).

CHAPTER 5:

EQUIPMENT DESIGN

5.1 BIRDLINGS FLAT FIELD STATION

This is the first of three closely related chapters dealing with the design of the pulsed Doppler radar system. In this chapter we concentrate on hardware aspects of the system while chapter 7 deals with the development of computer software for data collection and processing. The calculation of the performance of the radar system, a neccesary part of the design process, is treated in chapter 6 along with the study of the ground wave propagation problem we encountered during the initial testing and prototyping stage of the work. Unless otherwise mentioned the system described in these chapters is the final, working version of the radar, the prototype system is not described. Relatively few hardware differences exist between the prototype and the final system, the main difference being in the data collecting software. The radar system was installed and operated at the University of Canterbury's field station for atmospheric/ionospheric research at Birdlings Flat. We begin this chapter with a description of this field station and the facilities available there.

Research in ionospheric, atmospheric and space physics has a long tradition at Canterbury with studies being concentrated in three major areas:

(a) Measurements of ionospheric electron densities by means of the differential absorption and phase between the two modes (o and x) of radio propagation in the ionosphere.

(b) Measurements of ionospheric wind speeds by correlating ionospheric radar echoes received by three spaced antennas. This is known as the drifts experiment.

(c) Radar studies of meteors.

The ionospheric studies have concentrated largely on the D region (approximately 70-100km) of the atmosphere. From time to time other studies have been conducted within the atmospheric group. notable among these is KRENEK'S (1977 Ph.D. thesis) development of a pulse compression radar system for high resolution ionospheric studies. Some of Krenek's hardware formed the basis for our system. The ionospheric studies use 2.4MHz as a main frequency with 4.8MHz as a second frequency. Radar meteor experiments use 26.36MHz.

Ionospheric work was originaly carried out in the late 1930's and 40's at the University's town site. Later, this work was moved to a field station at Rolleston, about 30km south of Christchurch. However lack of space,

combined with increasing electrical interference, prompted a move to the Birdlings Flat site. Birdlings Flat is located on a shingle spit approximately 50km by road from Christchurch (fig. 5.1) and offers large amounts of flat, treeless ground for the construction of antenna arrays. In addition the site is well removed from sources of electrical interference (apart from fishing trawlers off the coast) and is shielded from Christchurch by the hills of Banks Peninsula. We will see later that the level of background noise at Birdlings Flat is close to the minimum values reported in the literature.

The move to Birdlings Flat started about 1961 with the differential absorption electron density studies. The transfer was finaly completed during 1983-1984 with the shift of the meteor radar group to Birdlings Flat. The field station at Rolleston has now been closed down.

The original experiments at Birdlings Flat were housed in caravans and relied on manual data gathering by tedious and time consuming techniques such as visual measurements from oscilloscope traces. The first step towards a more automated system was provided by FRASER (1965) who developed a hardware data collection system for the ionospheric winds (Drifts) experiment. This system recorded data from the three receivers on paper tape. These paper tapes were read into an IBM 1620 mainframe

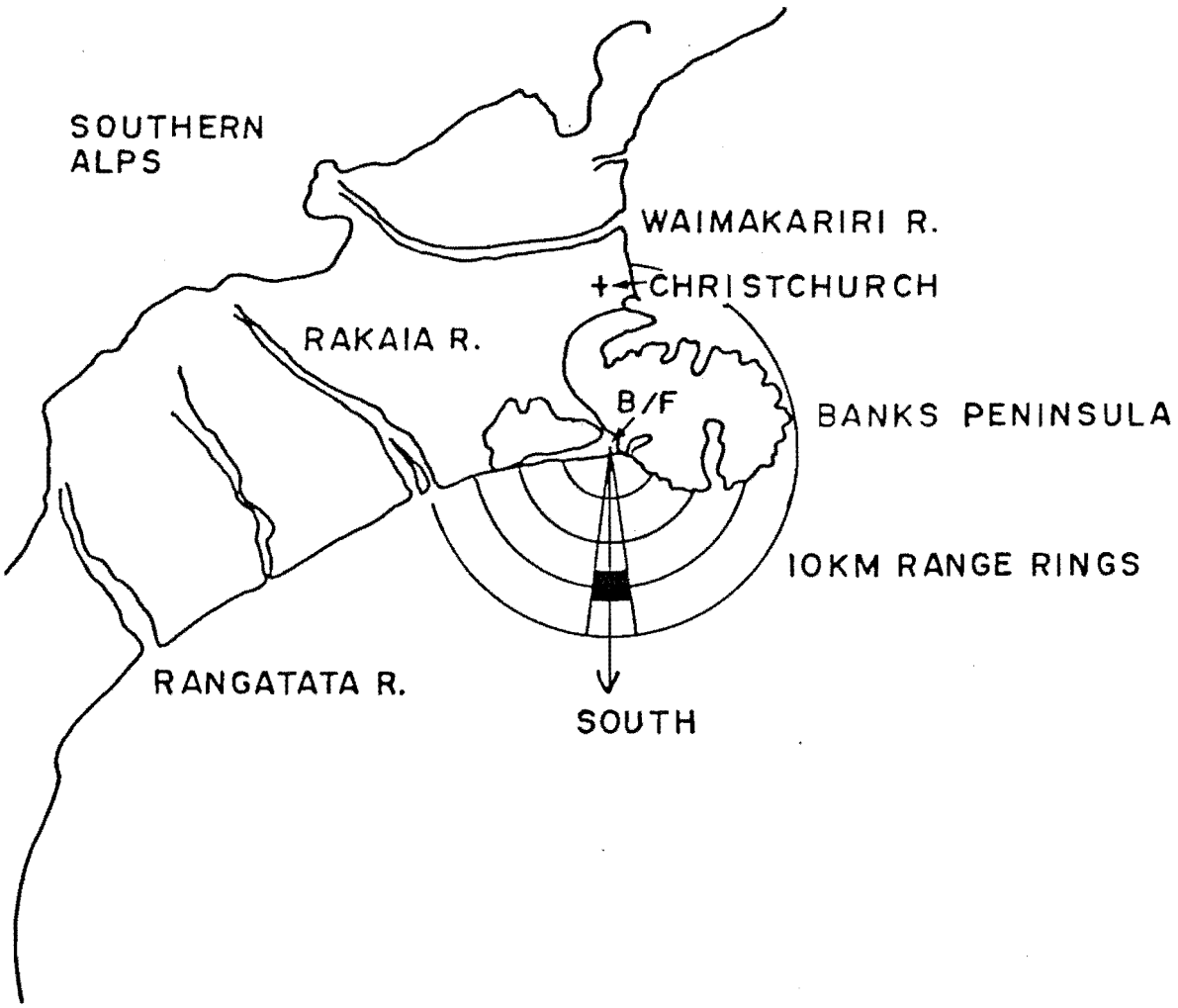

FIG.5.1 LOCATION OF THE BIRDLINGS FLAT (B/F) FIELD STATION WITH 15° ANTENNA BEAM AND RADAR RESOLUTION CELL AT 30KM.

where the wind speeds were calculated by means of one-bit correlations between the three receiver voltages. The next significant improvement was the construction of a permanent building at Birdlings Flat in 1968. This was followed in 1972 by a major improvement - the installation of a DEC PDP 8/e minicomputer. This computer allowed the station to be run automatically and left unattended while data collection progressed. The data are recorded on 7 track magnetic tape (magtape) which is changed about once every five days. The PDP-8 allows some processing of data to be done at Birdlings Flat with a resulting saving in magtape storage space and subsequent processing time on the mainframe computers at Canterbury (Burroughs B6930 and Prime P750). During 1980-1983 two new permanent buildings were constructed at Birdlings Flat. The main building replaces the old receiver hut and houses most of the equipment including the PDP-8, the receivers and the frequency generation system. The second building (approximately 1/2km away towards the sea) houses the radar transmitters.

A simplified diagram of the current layout at Birdlings Flat is given in fig. 5.2. Of major interest to us is the coherent 2.4MHz system. The master frequency standard is a temperature controlled 9.6MHz crystal in the receiver building. This 9.6MHz is divided by 2 to generate 4.8MHz which is sent to the transmitter building via an

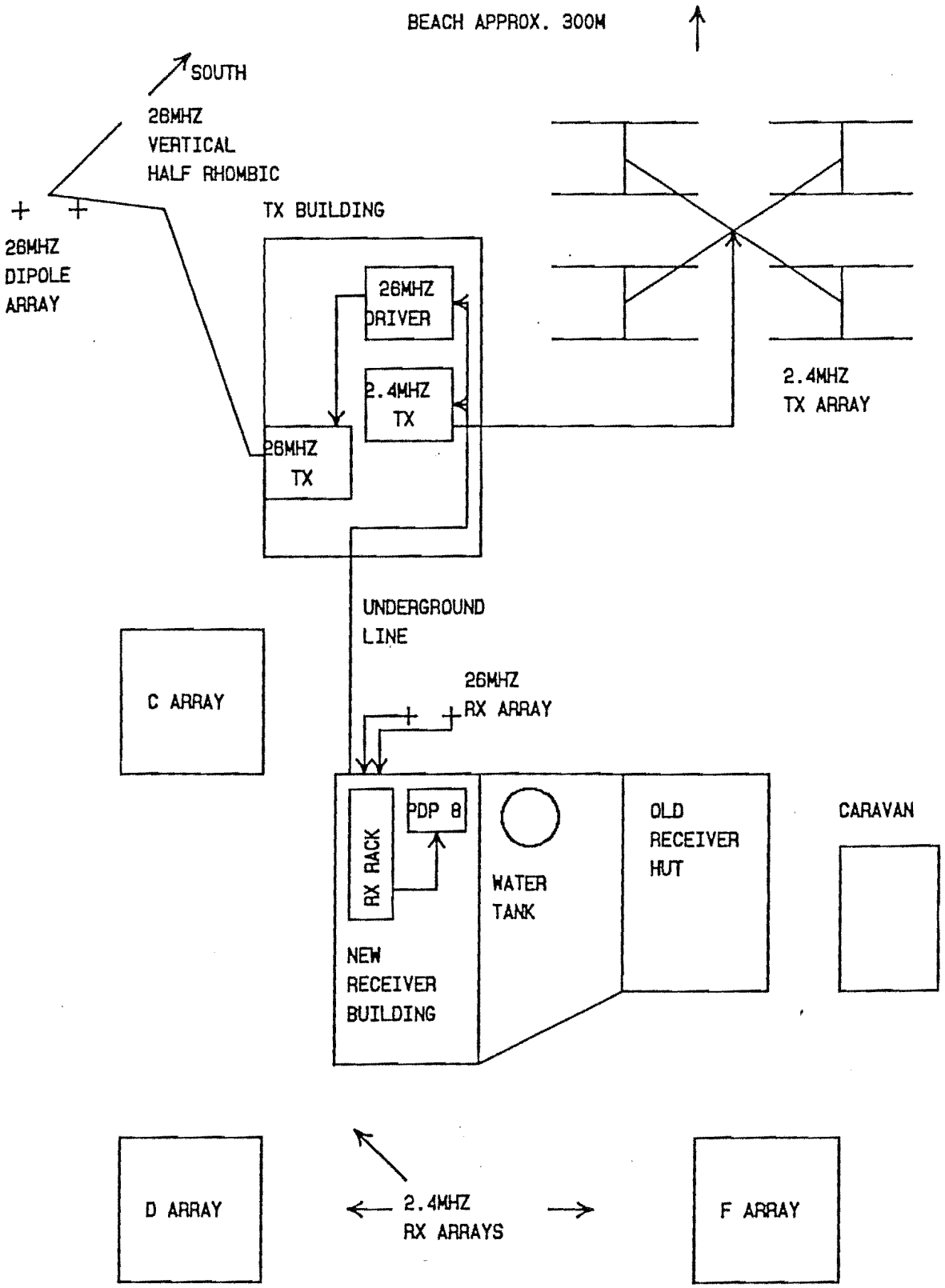

Fig. 5.2 Layout of Birdlings Flat field station (not to scale).

underground line. At the transmitter building a further division by 2 yeilds the 2.4MHz carrier frequency for the transmitter. The 2.4MHz ionospheric radar system does not use phase coherence - the receivers having their own reference oscillators to shift the 2.4MHz echoes down to 0Hz. However the receivers designed by KRENEK (1977 Ph.D. thesis) for his pulse compression radar can accept 9.6MHz from an external source and divide this by 4 to produce two SIN and COS 2.4MHz signals, which, when multiplied by the received signal produce inphase (real) and quadrature (imaginary) components of this signal at 0Hz. Given these facilities a 2.4MHz coherent pulse radar is relatively easy to construct.

The PDP-8 computer system and related hardware is shown in fig.5.3. Peripherals attatched to the computer include a decwriter, dual dectape, paper tape punch/reader and a Kennedy 7 track, 800bpi magtape. Data is input from the experiments via two A-D converter systems. The "slow" A-Ds have 3 non-multiplexed inputs and are used for the drifts and early versions of the electron density experiments. They sample at 2.5km range increments and input data to the PDP-8 via a direct memory access (DMA) interface. The "fast" A-Ds were built for KRENEK'S (1977 Ph.D. thesis) system as spatial resolution greater than 2.5km was required. In their original form they were capable of sampling at 0.5km range increments. This data

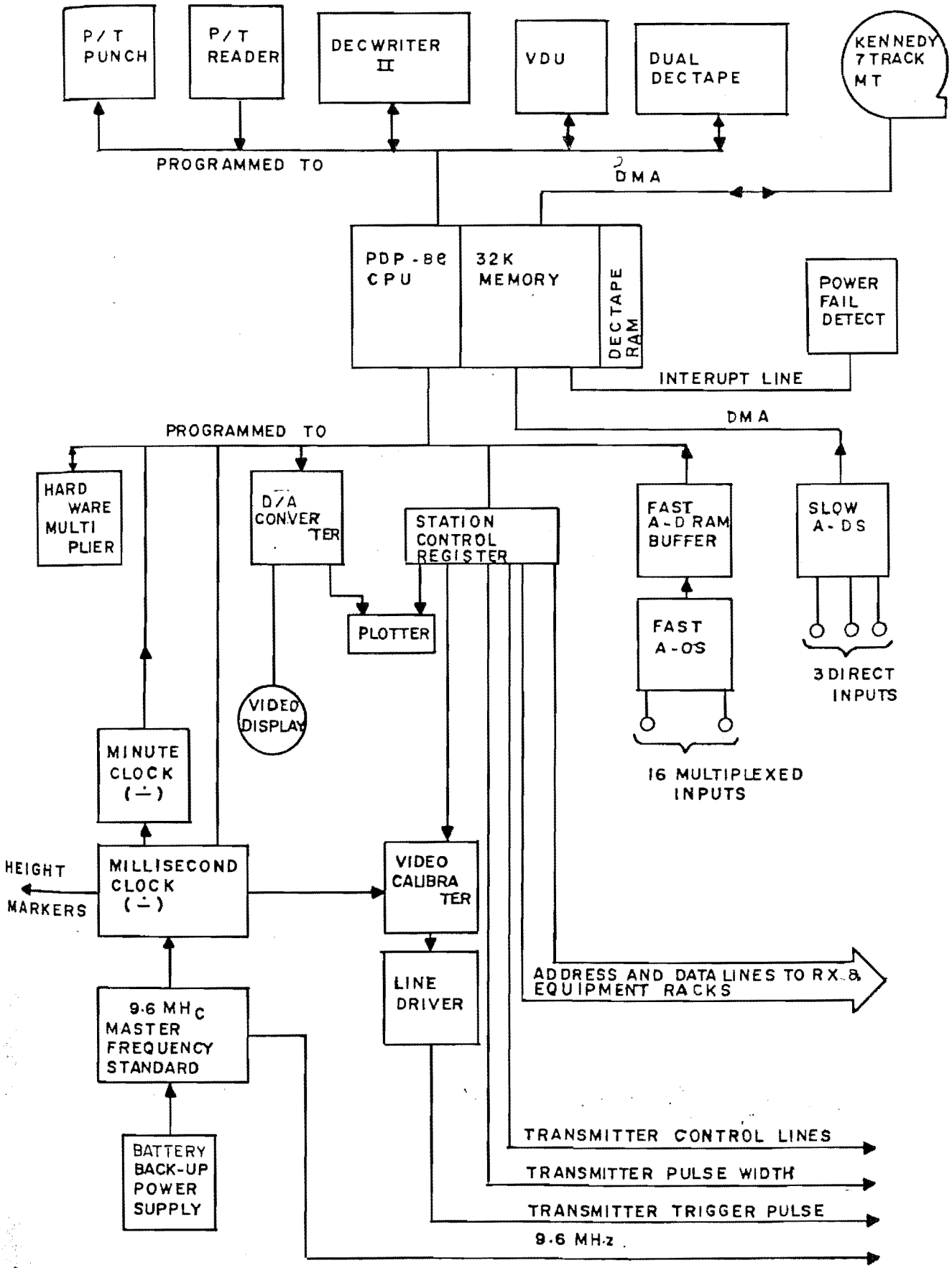

FIG. 5.3 PDP-8e COMPUTER SYSTEM AND ASSOCIATED HARDWARE.

transfer rate considerably exceeds the capabilities of the DMA system so the A-D data is first stored in a RAM buffer and then transferred to the PDP-8 by programmed IO at a slower speed.

Equipment is controlled by the PDP-8 through a station control register. Some of the station control register bits are used to address bin positions in the rack containing receivers and other equipment. The rest of the bits are data for the addressed device in the rack. The transmitters are also addressable devices in this scheme. Transmitter data triggers the transmitters, sets their pulse width and switches their power supplies.

All system timing and synchronization is controlled by a millisecond (1kHz) clock driven from the 9.6MHz master crystal. A battery backup for the 9.6MHz crystal ensures that time of day information can be maintained through a power failure (a frequent occurrence at Birdlings Flat). As an example of this timing and synchronization scheme consider a typical transmitter trigger / A-D conversion sequence: A program running in the PDP-8 sends a command (through the station control register) to trigger the transmitter and then enters a loop waiting for a flag to be raised by the next pulse from the millisecond clock. The transmitter trigger command enables the video calibrator box (see fig. 5.3)

to send the actual trigger pulse to the transmitter at the next millisecond pulse. When this millisecond pulse arrives the PDP-8 program exits its waiting loop and starts the A-D convertors (also through a synchronising flip-flop). The A-D conversion process is thus synchronized to the transmitted pulse - a neccessary condition for an A-D sample to correspond to a particular range. The pulses that cause the A-Ds to sample at regular range increments are also derived from the millisecond clock. (These range gate pulse are known as height markers - a term which reflects the ionospheric bias of the work at Birdlings Flat).

The considerable age of the PDP-8 was a problem during this work. In fact this is the last experiment that will be implemented on this system. A completely new system, based on a recently purchased PDP-11 (LSI-11/23), is currently under development and, at the time of writing, is being used to run the electron density experiment. When completed, the new system will run both drifts and electron density measurements together. Peripherals attatched to the PDP-11 include a Winchester hard disk (20Mbyte), a dual 8 inch floppy disk drive, a 9 track magnetic tape drive and a Visual V55 terminal. Completion of this system will considerably upgrade the facilities available at Birdlings Flat.

5.2 DESIGN PHILOSOPHY

The major objective of this work is to conduct an investigation into the feasibility of radar oceanography at Canterbury. Two consequences arise from this objective: Firstly the system we build should be flexible rather than specialised. In other words the system should allow many different kinds of experiments to be performed in the future and should obtain data in a form that will be useful to a wide variety of different oceanographic studies (The ionospheric drifts radar system follows this philosophy). Secondly the system should be simple and capable of producing, at an early stage, some initial results from which the future course of the work can be planned. It was for these reasons that ground wave hf pulsed Doppler radar was chosen as the technique for our system. Ground wave, as opposed to skywave, propagation was chosen because of the simpler antenna systems and cleaner Doppler spectra that it gives. (Skywave Doppler spectra are often contaminated by ionospheric motion). On the basis of simplicity we also decided to limit the system to one, or at most two, frequencies as opposed to using more esoteric multiple frequency or swept frequency systems.

There is an obvious and considerable advantage to be gained by integrating our system as much as possible with

the existing system at Birdlings flat rather than building a stand-alone system from scratch. Many of the problems inherent in the design of a computerised data collection system have already been solved by the designers of the ionospheric radar system. In addition the ionospheric radar contains much of the hardware we need. A consequence of this approach is that we are limited to the frequencies 2.4 and 26MHz. However as BARRICK et. al. (1977) point out (and for reasons we will dicuss shortly) frequencies in the range 25-30MHz are the optimum frequencies for a general purpose oceanographic radar system. In the USA a frequency band within this range has been allocated for radar oceanography. We therefore choose 26MHz as our main frequency of operation.

We have previously noted that it is a simple matter to convert the 2.4MHz ionospheric radar to coherent operation. We have also mentioned that sea echoes are often observed on this system during appropriate weather conditions. It thus appears that a 26MHz system integrated with the existing 2.4MHz system could easily have 2.4MHz as a useful second frequency. From radar scattering theory (chapter 4) we expect an interesting contrast between the Doppler spectra obtained on these two frequencies.

The first order Bragg frequency at 26MHz is 0.5Hz.

The Bragg scattering waves at this frequency are almost always present in fully saturated form. This implies that 26MHz first order echoes will be of relatively constant amplitude. As second order scattering cross sections increase rapidly with increasing frequency we expect second order echoes to be relatively strong compared to those at 2.4MHz. Doppler shifts due to currents etc. will also be larger at higher radar frequencies. In contrast the Bragg frequency at 2.4MHz is 0.16Hz. Bragg waves at this frequency are down in the low frequency cutoff region of the ocean waveheight spectrum. The amplitudes of first order echoes will therefore be highly variable and strongly dependent on sea state. We expect second order echoes at this fequency to be much weaker than at 26MHz and possibly not observable at all.

After the construction af the radar system had been completed these differences in character between 2.4 and 26MHz sea echoes were readily apparent even from visual observation of an oscilloscope trace. 26MHz echoes had an oscillation period of about 2s (0.5Hz) and were of constant amplitude regardless of sea state. With increasing sea state, however, they changed from regular oscillations to an irregular random variation indicating the presence of additional frequency components provided by second order scatter. 2.4MHz echoes varied considerably in amplitude from day to day. Often they were not visible

while at other times they were visible to 60km range and interfered with ionospheric measurements. Their period of oscillation was about 6s, corresponding to the Bragg frequency of 0.16Hz, and their oscillations were always regular indicating an absence of second order echo.

5.3 COHERENT FREQUENCY GENERATION SYSTEM

From the discussion of the preceding section it is apparent that our main hardware task is the construction of a 26.36MHz coherent frequency generation system integrated with the existing coherent 2.4MHz system. A diagram of this frequency generation system is given in fig.5.4. The major difference between this system and the pulsed Doppler radar systems illustrated in the figures of chapter 3 is that the downshift in frequency from 26.36MHz to 0hz occurs in two steps. The received echoes with a center frequency of 26.36MHz are first mixed with 23.96MHz from a local oscillator. This shifts the echoes down to the difference frequency of 2.4MHz. The echoes can now be input to the coherent 2.4MHz system based on Krenek's receivers and shifted down to 0Hz. Alternatively the 26.36 to 2.4MHz convertor can be disconnected and a 2.4MHz ionospheric antenna plugged into Krenek's receiver to obtain 2.4MHz Doppler spectra. The transmitter carrier frequency is generated by a similar two step process. 23.96MHz from the local oscillator is sent to the transmitter building via the underground line. The 23.96MHz is then mixed with 2.4MHz derived from the 9.6MHz master oscillator. This time the sum, rather than the difference, output from the mixer is used generating the carrier frequency of 26.36MHz.

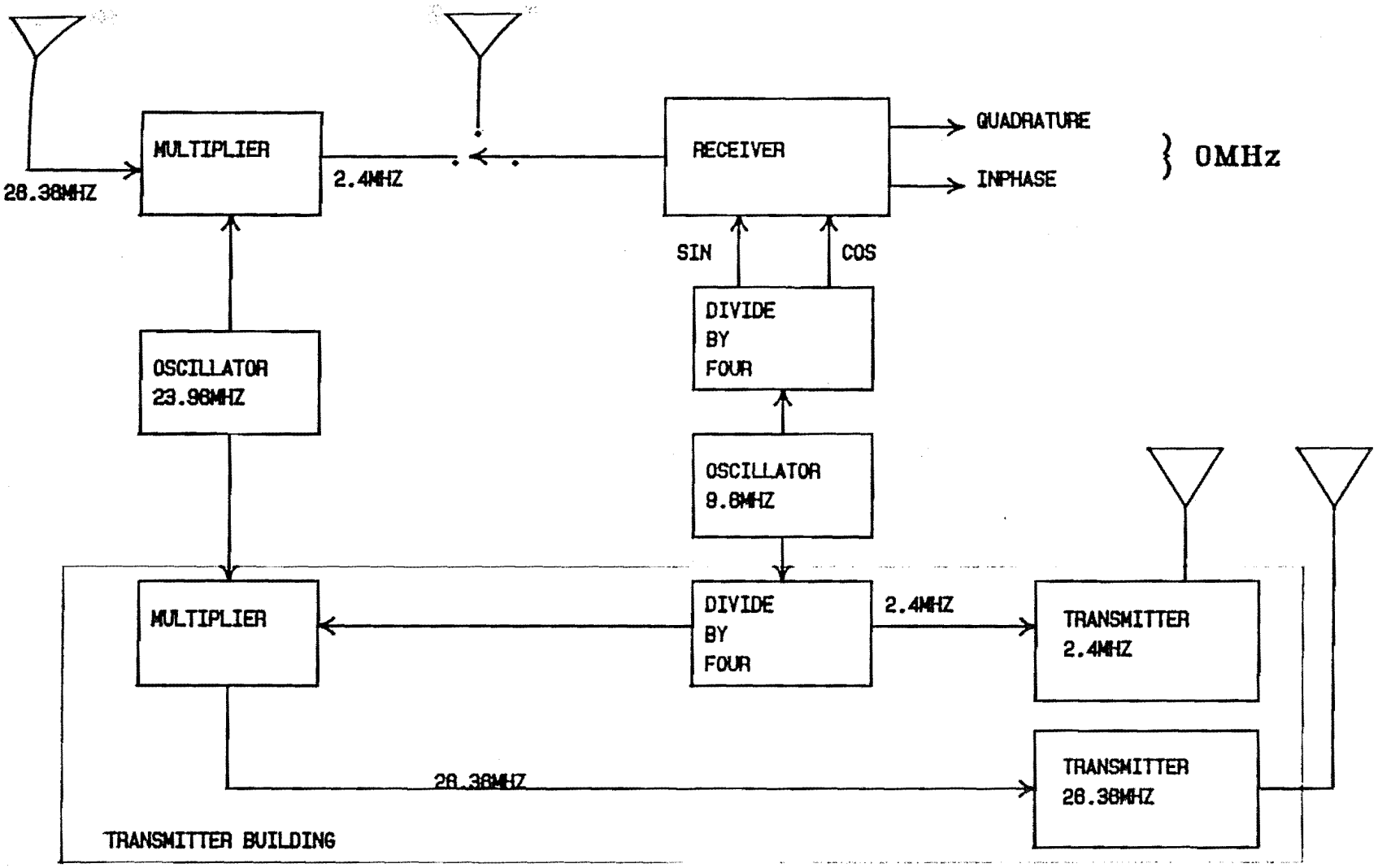

Fig. 5.4 Coherent frequency generation system.

The first problem to be dealt with in the design of this fequency generation system is that of the quality of the oscillators outputs. Up until now we have assumed that the spectrum of the carrier signal is a perfect delta function in frequency. A real crystal oscillator will, however, vary slightly in frequency producing a spectral line with finite width. In addition this line may be surrounded by sidelobes and/or random noise. When this signal is mixed with an echo signal in a multiplier stage the result (as shown in chapter 3) is the convolution of the echo spectrum with the oscillator spectrum. A delta function echo will, therefore, appear as the oscillator spectrum and may have its linewidth, sidelobe and noise levels considerably degraded. A detailed study of these effects has been given by RAVEN (1966). For our purposes we require that a line in the echo spectrum be broadened by no more than the broadening due to the spectral processing. This is simply the Doppler frequency resolution given by B = 1/Tcoh which in our case is of the order of 0.01Hz. Furthermore we require that noise and sidelobes in the oscillator spectrum be low enough that the overall system noise level is not raised.

At first sight it might appear that the oscillator must not deviate by more than 0.01Hz in the coherent integration time (100s) - an extremely stringent requirement. We recall, however, the discussion in chapter

3 that by using the same ocillator to generate the transmitted pulse and to shift the echo from this pulse down to 0Hz we can overcome this long term stability requirement. The important quantity now becomes the stability of the oscillator during the transit time of a pulse from the transmitter to the ocean and back to the receiver (approx. 100us). Since crystal data in this form are not normally available a direct test was used to assess the quality of the oscillator outputs. For this purpose we make use of the fact that we expect the Bragg lines at 2.4MHz to be a good approximation to delta functions. Measured sea echo Doppler at 2.4MHz (see chapter 8) show first order Bragg lines with a width of 0.01Hz - a figure which agrees exactly with that expected from the coherent integration time of 100s. We conclude from this that no significant degradation of the signal has occured because of 9.6MHz oscillator frequency instability. As we discuss in section 5.5 the background noise spectral density in the output spectra is in good agreement with the value calculated from receiver noise level measurements. These noise levels are, in turn, close to the minimum values quoted in the literature (e.g. ITT CORP. 1968). It is therefore likely that no significant noise or sidebands have been introduced by either the 23 or 9.6MHz oscillators. Assessing the frequency stability of the 23MHz oscillators is more difficult as the Bragg lines at 26MHz are broadened considerably from 0.01Hz. We cannot use the received carrier line at 0Hz as this will

be effected by drifts in receiver output voltages (This line is removed during processing by subtracting the average value of the Doppler timeseries). Since frequency fluctuations on a time scale of 100us are usually the product of mechanical vibration, rather than thermal fluctuations (RAVEN 1966), we expect the frequency stability of the 23MHz crystal to be similar to that of the 9.6MHz master crystal.

The second problem encountered in the design of the frequency generation system concerns the underground cable connecting the transmitter and receiver buildings. This was installed to carry the 4.8MHz carrier frequency to the 4.8 and 2.4MHz transmitters. At 23MHz the attenuation of this cable is appreciable. The attenuation calculated from the frequency response of the cable was 32dB making it still preferable to use this cable as opposed to direct free space transmission (54dB attenuation). However some "brute force" is required to overcome this attenuation and for this purpose a VMOS amplifier was used to raise the level of the 23.96MHz signal to about 7-10W before transmission down the cable. At the other end of the cable Schmitt triggers and limiter circuits were used to clean up the signal before feeding it into the mixer and transmitter.

5.4 TRANSMITTERS

The purpose of a transmitter is to raise a single frequency signal to a high enough power level that the received echoes from this signal will be above the external noise level. In addition the transmitter must be responsible for applying pulse modulation to the carrier signal. As with all amplifiers the signal power level is increased by means of an active device which uses the weak signal to control a much larger flow of power from a power supply to the output. In order to maximise the output power and minimise heating of the device high conversion efficiency from input to output power is important. Operating the device as a linear amplifier (i.e. the input voltage is effectively multiplied by a constant gain factor) results in poor efficiency (usually 50-60% maximum). For single frequency, constant amplitude work this efficiency can be raised considerably by using square, rather than sinusoidal, waveforms and operating the active device more as an on-off switch than a linear amplifier (i.e. class C operation). The high power square wave output is then converted to a single frequency sinusoid by passing it through a filter which removes the high frequency harmonics and passes only the fundamental frequency. The circuit of a high power rf amplifier or transmitter can thus be simply understood by noting that the additional circuitry surrounding the amplifying device

performs the following three functions:

(a) Power supply circuitry to apply to apply the correct voltages to the device.

(b) Impedance matching circuitry to match the device's input and output impedances to those of following stages.

(c) Circuitry to filter unwanted harmonics from input and output signals. In addition some types of transmitting valves require circuitry to prevent them breaking into parasitic oscillation.

The final output power level in any system is usually reached in a number of amplifying stages. For example in our system the carrier signal is first raised from TTL levels to about 10W by an amplifier based on a VMOS transistor as an active device. The power VMOS transistor is a recent innovation which combines the advantages of small size and convenient power supply voltages when compared to a thermionic valve together with good thermal overload protection and convenient impedances when compared to an rf power transistor. From the VMOS stage the signal is amplified to approximately 1kW by a driver stage using a TT21 valve. The final amplification, up to a

power level of 10-100kW is performed by the transmitter final amplifier which uses 4PR60 valves as active devices.

Four transmitters were used at various stages of this project. Initial tests of the system were made with a 10kW, 26MHz transmitter from a meteor radar experiment at the old Rolleston field station. This transmitter used a single 4PR60A valve in its final stage and has been described by WEBB (1980 Ph.D. thesis). The final system used a 100kW meteor radar transmitter described by POULTER (1978 Ph.D. thesis). The final stage of this transmitter consisted of two push-pull amplifiers in parallel, using four 4PR60 valves. The actual power output of this transmitter was estimated from the power input to the final stage and an estimated conversion efficiency of 60% including any antenna impedance mismatch losses. Using the values of 8kV for the anode voltages and 10mA for the total anode current together with a 1 : 1000 duty cycle (20us pulses at 50Hz) gives 80kW for the input power and 48kW for the estimated power into the antenna. A problem with this transmitter is that it is normally run in incoherent mode from a 26MHz carrier provided by its own local oscillator. The rf drive to the final stage could be easily disconnected, however, to allow an external carrier source to be used. Thus conversion of the transmitter to coherent operation was accomplished by constructing a new driver stage to take 26.36MHz from our frequency

generation system and inject it into the final amplifier in place of the local driver output.

This coherent driver stage, which was built from the TT21 driver stage of the 10kW transmitter, also doubled as the 1kW test transmitter used for the field strength experiments mentioned in chapter 6. When the decision to move to the higher powered transmitter was made it was realised that the requirements for a coherent driver stage were similar to those for the test transmitter. (i.e. approximately 1kW, coherent pulsed output). The major difference between these applications was in the load impedance seen by the driver stage. The antenna for the field strength experiment was expected to have an impedance of about 50 ohms whereas the input impedance of the 100kW transmitter final amplifier was unknown. The output stage of the coherent driver was therefore rebuilt as a pi-coupler so that it could easily be matched to a wide range of different loads. It is at this stage that the pulse modulation is applied to the 26.36MHz carrier. A block diagram of the phase coherent transmitting system is given in fig. 5.5.

The transmitter used for 2.4MHz operation is the transmitter used for the drifts and electron density experiments. This transmitter has a nominal output of 100kW and has a final amplifier stage consisting of two

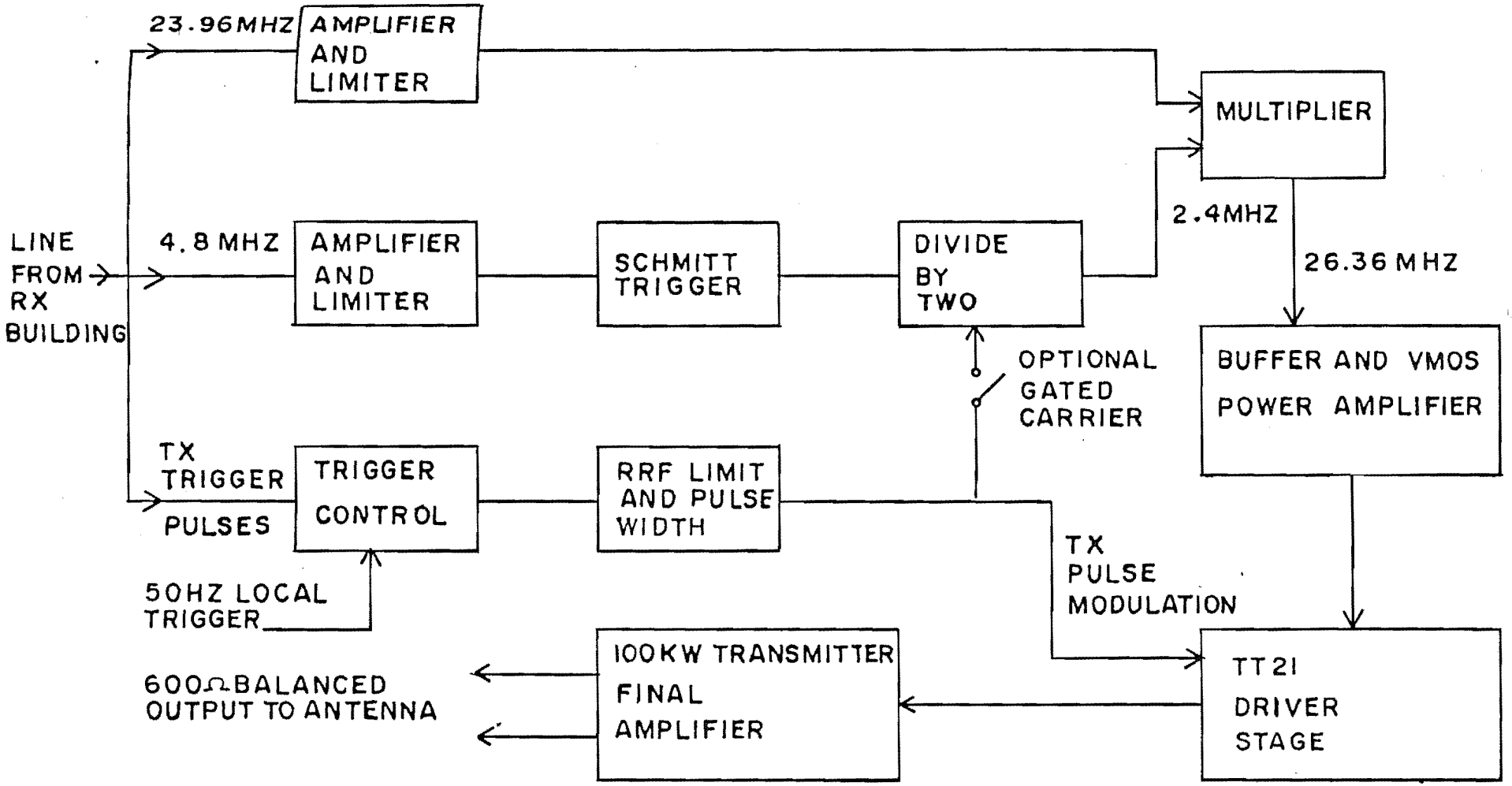

FIG. 5.5 BLOCK DIAGRAM OF COHERENT 100KW TRANSMITTER SYSTEM.

push-pull amplifiers in parallel - a similar configuration to the meteor radar transmitter. No modifications were needed to this transmitter as it is already set up for coherent operation. Unfortunately simultaneous operation on 2.4 and 26MHz was not possible as radiation from the 2.4MHz transmitter interfered with the 26MHz circuitry giving rise to phase instabilities. This problem could be simply cured, however, if future experiments require simultaneous operation on both frequencies.

5.5 RECEIVERS AND MULTIPLIERS

A block diagram of the coherent receiving system is given in fig. 5.6. Both this figure and fig. 5.5 may be regarded as low level expansions of fig. 5.4 which is an overall picture of the complete coherent transmission, reception and carrier frequency generation system. The purpose of a receiver is to reduce the frequency and increase the level of an incoming signal to values that can be handled by following devices (e.g. oscilloscopes, loudspeakers, A-D converters). In our case the signal is shifted down to a center frequency of 0Hz and increased in power by about 94dB.

The frequency shifting is performed by Motorola 1496 analogue multipliers. These can be thought of as amplifiers whose gain is proportional to an externally applied voltage. The output is thus the product of the input signal and the external voltage, which, in our case, is a local oscillator or carrier frequency. Our discussion of the multiplication process in chapter 3 assumed complex signals as inputs to a "black-box" multiplier which produced only the difference frequency at the output. The 1496 multipliers use real signals and thus produce the sum of the frequencies, as well their difference. The multiplier output must therefore be filtered to select the desired output frequency. The

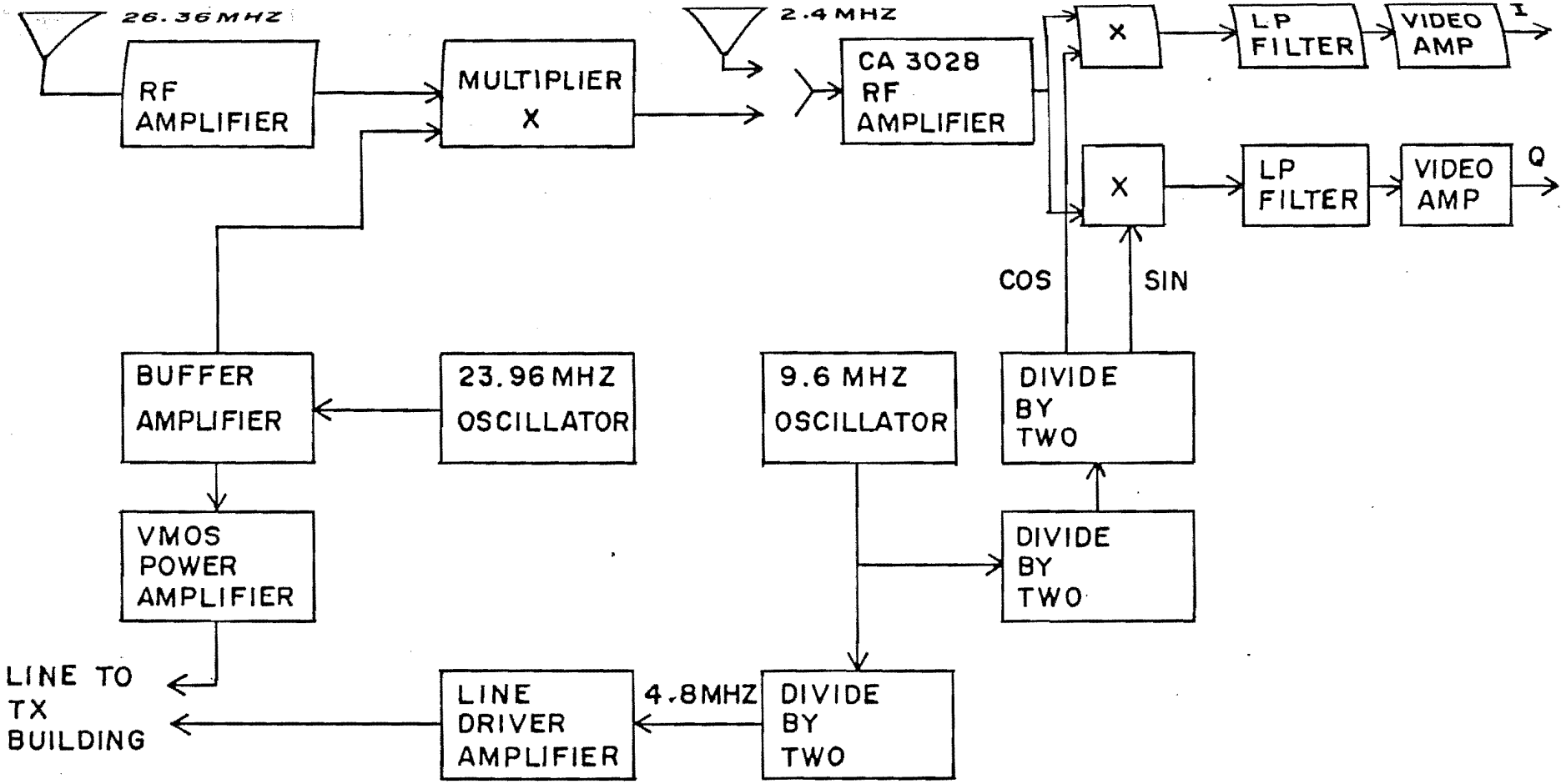

FIG 5.6 BLOCK DIAGRAM OF COHERENT RECEIVING SYSTEM.

carrier input to the multiplier is operated in saturated mode with a square wave input. This has the important advantage of making the multiplier output independent of variations in the carrier amplitude (within reasonable limits). The harmonics of the square wave are removed by the same filter that selects the sum or difference output frequency.

The complex multiplier "black-box" is synthesised by feeding the 2.4MHz signal into two 1496 multipliers. Each of these multipliers is fed with a 2.4MHz carrier in the usual manner. These carriers, however, differ in phase by 90 degrees and form two orthogonal basis vectors on a phasor diagram. Multiplication by these carriers thus projects out the real and imaginary components of the complex signal phasor. These components are often referred to as the inphase (real) and quadrature (imaginary) receiver outputs. The orthogonal carrier signals are generated by the logic circuitry that performs the division by four to generate 2.4MHz from 9.6MHz.

The inphase and quadrature multipliers are followed by low-pass filters to select only the difference mode frequencies. In KRENEK'S (1977 Ph.D. thesis) original design these filters determined the overall frequency response of the receiver. Each filter had a 3dB cutoff frequency of 100kHz resulting in an overall receiver

bandwidth of 200kHz (-100kHz to +100kHz). For our application this bandwidth was reduced to 100kHz (-50kHz to +50kHz) allowing a maximum range resolution of 1.5km with a transmitter pulse width of 10us. This resolution was chosen mainly because 100kHz was the minimum bandwidth to which Krenek's receivers could be easily modified. We also anticipate future studies that require high spatial resolution, for example studies of wave growth with an off-shore wind and detailed measurements of the variation of echo strength with range under varying sea conditions. However much oceanographic work does not require this resolution and would benefit from a system with narrower bandwidth e.g. 25 to 50kHz, and correspondingly reduced noise level.

The final receiver output levels are determined by video amplifiers. These adjust the multiplier output voltages to the -5V to +5V range required by the A-D converters. The signal input levels required by the multipliers are provided by broad band rf amplifiers. The general principle here is that the overall noise level is largely determined by the noise level of the first stage. Thus, if the multiplier is proceded by a properly designed rf amplifier with lower noise level, an improvement in the overall noise level will result. Using this technique the receiver's internal noise level was reduced to such an extent (approx. 0.1uV) that external noise was the main

contributor to the overall noise level (1-4uV).

Receiver performance measurements were made by observing the receiver output levels on an oscilloscope and comparing these with levels produced by a signal generator connected to the receiver input. The voltage gain from 26MHz input to 0Mhz output was thus found to be:

$$G_R = 4.71 \times 10^4 \qquad 5.1$$

giving a single channel gain of 94dB. An input to the A-D converter of +5V results in the full scale output of 2047. The A-D conversion factor is therefore:

$$F_{A-D} = 409 \qquad 5.2$$

resulting in a gain of 146dB from the receiver input to A-D output (i.e. 20log (<A-D output value>/<voltage across RX input impedance>) = 146dB). The system gain G_{sys} we have been using is the ratio between the power dissipated by a complex received signal in the receiver input impedance and the power in the resulting output spectrum. To calculate this quantity from our measurements

we must take into account the fact that we are now dealing with complex signals rather than single channel real signals and the conversion between physical power in the receiver input impedance and spectral power defined as the square of the A-D output. A complex signal $Ae^{j\omega t}$ across the input impedance, Zin, will result in a complex receiver output voltage $G_R Ae^{j\omega t}$ and complex spectrum input $G_R F_{AD} Ae^{j\omega t}$. The input power is:

$$P_{RX} = \frac{A}{Z_{in}} \qquad 5.3$$

and the output power is:

$$P = (G_R F_{AD})^2 A^2 \qquad 5.4$$

giving:

$$G_{sys} = (G_R F_{AD}) \quad Z_{in} = 165 \text{ dB} \qquad 5.5$$

for the system gain.

Background noise in the Doppler spectra typicaly had a power spectral density of 11dB. Spectra from close ranges often have higher noise levels, probably due to the disturbing effects of the transmitted pulse. This power spectral density is equivalent to a system noise temperature of 32,700K and an rms voltage across the receiver input impedance of 1.84uV. This is in good agreement with the measured values of noise voltage which varied between 1 and 4 uV. These values are typical of very quiet sites where most of the external noise is of galactic origin (ITT CORP. 1968). In our case the fact that most of the received energy is arriving from below the critical penetration angle of the ionosphere (about 12 degrees at 26MHz) will influence these noise levels.

5.6 ANTENNAS

The choice of antenna systems was governed by two conflicting requirements. In order to be able to interpret second order sea echo a narrow transmitted beam is required so that the electromagnetic energy hits the sea surface at a single, well defined angle with respect to the wind direction. Other experiments were envisaged, however, which required a broad transmitted beam. One idea was to measure the phase difference between echoes received on two spaced antennas in order to determine their direction of arrival. There is only one practical solution to this problem and that is to build two antenna systems, one broad beam - the other narrow beam. Because the radar echoes are produced by a distributed target the beamwidth of the transmitting antenna has little effect on the radar range.

The narrow beam antenna was a vertical half rhombic as described by BRUCE (1931). This type of antenna is very simple to construct and gives quite high gain. The gain and beamwidth of this antenna were esimated from published curves (BRUCE 1931) to be 10dB and 15 degrees respectively. The 10dB figure includes the 3dB loss in the 800 ohm load resistor. The measured impedance of this antenna was 607 ohms with a phase angle of -20 degrees. The antenna is thus a good match to the 600 ohm

transmitter output and was fed by means of a 600 ohm open wire line. As this line was several wavelengths long no balun was neccessary to convert the convert the balanced transmitter output into the unbalanced input required by the antenna - the twin wire line isolated the transmitter from the antenna earth because of its length.

The broad beam antenna consisted of an array of two 300 ohm folded dipoles connected in series to provide a good match to 600 ohms. No difference in radar range was observed between this antenna and the narrow beam rhombic. This confirms that transmitted beamwidth has little effect on the radar's range performance. As the dipole array is a balanced antenna system its similar performance to the rhombic, and other grounded systems, eliminated poor grounding of these antennas as a possible explanation of the propagation problem we discovered (chapter 6). Receiving antennas were standard 50 ohm 1/4 wave monopoles chosen for simplicity and compatability with both transmitting systems. The directional pattern of the receiving antenna can have an important effect on the performance of the radar by eliminating sources of interference (e.g. radio stations) that come from specific directions. In the case of different receive and transmit antenna patterns the area of the radar resolution cell on the sea surface is the product of that given by each beam. Thus maximum signal strength is obained when the transmit

and receive patterns match. As 2.4MHz operation is obtained purely as a by product of the ionospheric radar system the standard ionospheric antenna system was used.

CHAPTER 6:

GROUND WAVE PROPAGATION

6.1 INTRODUCTION

Radio propagation between the radar and the ocean surface radar resolution cell is via the groundwave mode. In general this mode is a combination of the direct free-space wave, a wave reflected from the ground and a surface wave. The surface wave is a special mode of propagation which is trapped by the interface between the surface and the air and guided around the curved surface of the earth in a similar manner to a wave propagating on a transmission line.

The ground wave field strengths at the contact patch and back at the receiver will obviously differ from those that would occur with free space propagation. The radar performance equation developed in chapter 3 assumed free space propagation and corrected for ground-wave propagation by means of a factor, F, the ground wave attenuation factor.

During the initial design phase of this project field strength calculations were made by assuming no difference between free space and ground wave propagation, i.e. the attenuation factor was set to unity. The justification for this is that in the limit of low frequencies and high surface conductivity , ground wave field strengths are not appreciably different from free space values. Further, the calculations show that a transmitter of approximately 1kW peak pulse power should be adequate for most ground

wave experiments in the upper hf region. This result is in good agreement with power levels used by other workers in the field.

It was somewhat of a surprise, therefore, that an initial test at 26MHz, using a 10kW transmitter, failed to reveal any visible trace of sea echo. In contrast to this, strong sea echo has always been observed from the 2.4MHz ionospheric radar under appropriate sea conditions (Well developed first order Bragg waves). This is in spite of the fact that this radar, with its vertically pointing horizontally polarized antennas, has a highly unfavourable configuration for observing sea echo.

Careful checks of the equipment (e.g. measurements of receiver gain and noise level and estimation of transmitter power output) failed to reveal any problems in this area. This evidence points to a frequency dependent propagation effect being to blame. Since we do not expect the properties of the sea surface or the atmosphere to be appreciably different from those encountered by other workers only one possibility is left and that is propagation over the ground between the antenna system and the sea surface. At Birdlings Flat this distance is large (approx. 500-800m) compared to that found in other systems. Furthermore the ground consists of shingle and sand covered by a thin layer of earth. This type of ground has a low conductivity and is generally considered to be poor from the point of view of ground wave radio

propagation (FLOCK, 1979; CROOKES and FLEMMING, 1909).

Additional evidence supporting this hypothesis is provided by BARRICK et.al. (1977). They found that attempts to increase the range of the radar by placing the antennas back from the sea on the roofs of buildings were counterproductive and that the optimum locations for the antennas were as close to the water's edge as possible. LYONS and BARRICK (1984) mention that the performance of many ground wave oceanographic radars often falls short of their predicted performance. It thus appears that the system described in this work may suffer from an extreme form of a problem which has affected other systems through- out the world.

Further supporting evidence is provided by published curves of ground wave attenuation (fig. 5 from CROOKES and FLEMMING, 1909). The curve for ground of poor conductivity shows appreciable attenuation even at distances of only 1km from the transmitter. Naturally, it would be interesting to extend these results to shorter distances (e.g. a few hundred metres). Care must be taken, in these cases, to ensure that the mathematical models used still apply. It was felt that the most convincing proof of this would be a direct comparison of theoretical results with an experimental measurement of attenuation over the ground at Birdlings Flat.

These observations provided the motivation for the

subject of this chapter: A detailed study of ground wave propagation and its effect on the radar system. The invesigation proceeded from both a theoretical and an experimental point of view. The first section of this chapter reviews the theory of ground wave propagation over a homogeneous spherical earth and leads up to the description of a computer program for calculating the ground wave attenuation factor, F.

The results of this theoretical study are then compared with an experimental measurement of ground wave attenuation. The conclusion reached is that poorly conducting ground between the antenna system and the sea can introduce attenuation of sufficient magnitude to explain the poor performance of the original test system.

The remainder of the chapter is concerned with the extension of the ground wave propagation program to the accurate calculation of radar system performance and the development of strategies for overcoming the propagation problem.

6.2 THE CALCULATION OF GROUND WAVE FIELD STRENGTHS.

The mathematical problem involved in the calculation of ground wave propagation over the curved surface of the earth is the problem of the diffraction of a wave by a sphere. This problem has been worked on for considerable time and has wide applicability to many fields other than radio propagation. (See RAYLEIGH, 1871; MIE, 1908; VAN DER POL and BREMMER, 1937). Examples include the scattering of light by particles such as air molecules and raindrops, scattering problems in quantum mechanics, acoustics and seismology and the Schumann electromagnetic resonances of the earth-ionosphere waveguide.

The solution to the problem was obtained in terms of a series expansion which, in the case of light scattering problems, converged rapidly facilitating early solutions (RAYLEIGH, 1871; MIE, 1908). The radio propagation problem, however, converged poorly and a solution amenable to numerical calculation was not obtained until WATSON (1919) developed a transformation that yielded a more rapidly converging version of the series.

A survey of early work on the subject is given by LOGAN (1965) while PRYCE (1953) gives a survey of work on the radio propagation problem. More detailed treatments of the radio case are given by BREMMER (1949) and VAN DER POL and BREMMER (1937). BREMMER (1949) is particularly useful for providing physical insight into the meaning of

the mathematics. At close ranges the effect of the earth's curvature can be neglected yielding a flat earth approximation. WAIT (1971) provides a summary of the history of the development of this approximation as well as a treatment of the general problem in modern mathematical notation. The following overview of the problem is largely based on WAIT'S (1971) work.

The geometry of the problem is shown in fig. 6.1. The earth is represented by a sphere of radius, a, consisting of material with dielectric constant, ε , and conductivity, σ . The transmitter is an infinitesimal dipole situated above the "north pole" of the spherical coordinate system (b,0). The field is received at a point P (r, θ, ϕ).

The problem consists of solving Maxwell's equations given the boundary conditions imposed by this geometry. Considerable simplification is provided by the use of a radial Hertz vector, $\underline{r}\, U$, from which the various electromagnetic field components can be derived by:

$$
\begin{aligned}
E_r &= \left(\kappa^2 + \frac{\partial}{\partial r^2}\right)(r\ U) \\
E_\theta &= \frac{1}{r}\frac{\partial^2}{\partial r \partial \theta}\ (r\ U) \\
H_\phi &= -i\varepsilon\omega \frac{\partial U}{\partial \theta} \qquad\qquad 6.1 \\
E_\phi &= H_r = H_\theta = 0 \\
&\text{for } r > a\ .
\end{aligned}
$$

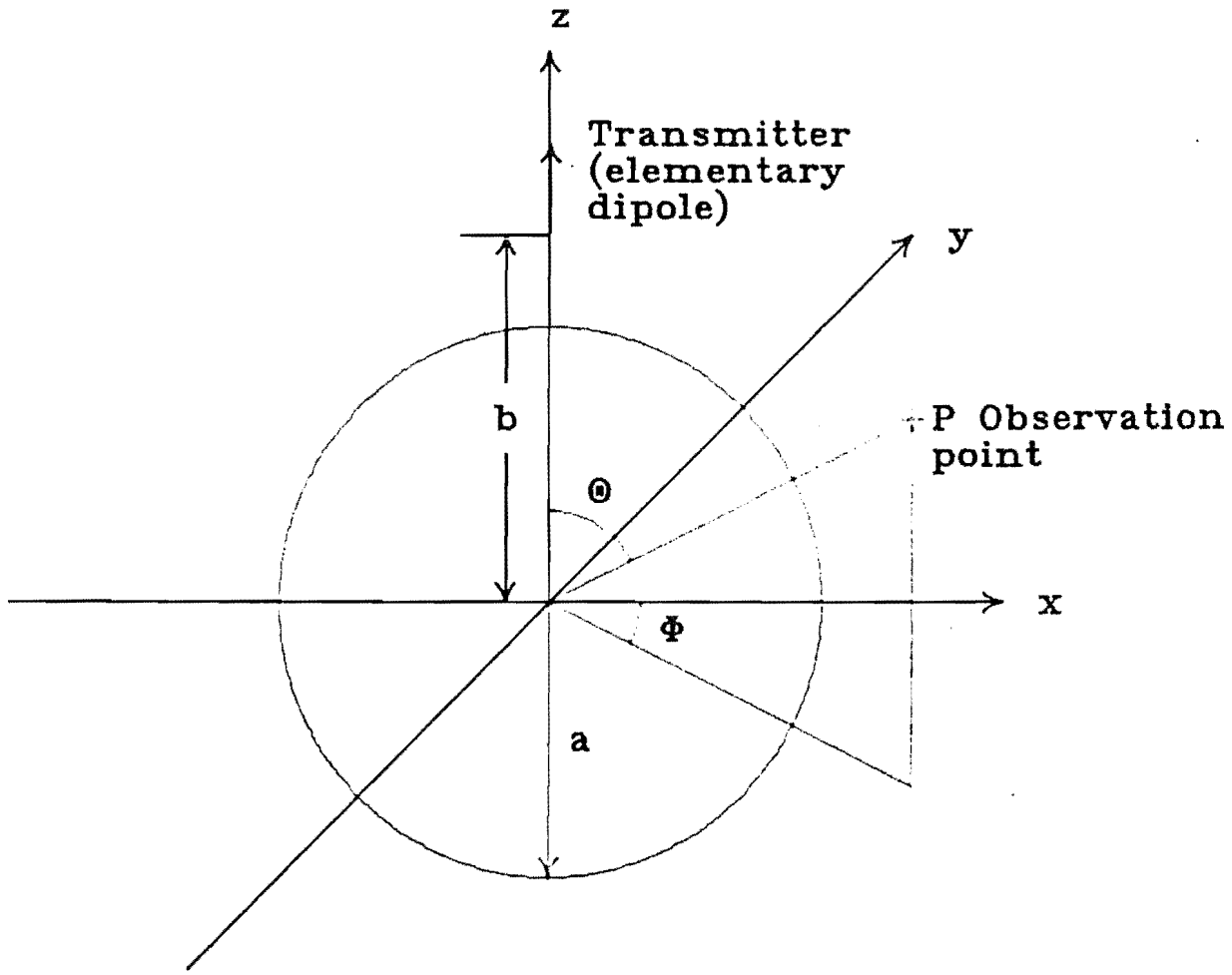

Fig. 6.1 Geometry of the propagation problem.

The eight equations that result from Maxwell's equations (VAN DER POL and BREMMER, 1937) now reduce to one scalar wave equation:

$$(\nabla^2 + \kappa^2)\, U = 0 \qquad 6.2$$

We now assume that the field can be written as the sum of two parts, $U_1 + U_2$, where U_1 is the field from the transmitter in free space and U_2 is the correction due to the presence of the earth. The free space transmitted field has the form:

$$U_1 = \frac{-\,Ids}{4\pi i\varepsilon\omega}\ \frac{\exp(-i\kappa R)}{bR} = \frac{-C_o \exp(-i\kappa R)}{bR} \qquad 6.3$$

where Ids is the elementary transmitter current and $R^2 = r^2+b^2-2br\cos\theta$ is the line of sight distance between the transmitter and the receiver.

Since a closed form (algebraic) solution of these equations is not possible the analysis proceeds by expanding both parts of the field $U_1 + U_2$ as series of spherical harmonics of the form:

$$h_n^{(2)}(\kappa r)\, P_n(\cos\theta) \qquad 6.4$$

where we introduce the spherical Hankel functions as follows:

$$h_n^{(1)} = -(-1)^n x^n \left(\frac{d}{x dx}\right)^n \left(\frac{e^{ix}}{x}\right)$$

$$h_n^{(2)} = i(-1)^n x^n \left(\frac{d}{x dx}\right)^n \left(\frac{e^{-ix}}{x}\right) \qquad 6.5$$

The expansion of U_1 is completely determined (using the expansion of $\exp(-i\kappa R)/R$ in spherical harmonics)

$$U_1 = \frac{i\kappa C_o}{2} \sum_{n=0}^{\infty} (2n+1) h_n^{(1)}(\kappa r) h_n^{(2)}(\kappa b) P_n(\cos\theta) \quad r<b$$

$$U_1 = \frac{i\kappa C_o}{2} \sum_{n=0}^{\infty} (2n+1) h_n^{(2)}(\kappa r) h_n^{(1)}(\kappa b) P_n(\cos\theta) \quad r>b \qquad 6.6$$

whereas the expansion for U_2 involves unknown coefficients, A_n :

$$U_2 = \frac{i\kappa C_o}{2} \sum_{n=0}^{\infty} (2n+1) A_n h_n^{(2)}(\kappa r) P_n(\cos\theta) \qquad 6.7$$

The A_n coefficients are found by applying the boundary condition at r = a:

$$E_\theta = - ZH\phi$$

or

$$\frac{1}{r} \frac{\partial}{\partial r} rU = Zi\varepsilon\omega U \qquad 6.8$$

Where Z is the surface impedance which is given from the dielectric constant and conductivity of the surface by:

$$Z = 120\pi \left[\frac{i\kappa}{\gamma} \sqrt{1 + \frac{\kappa^2}{\gamma^2}} \right] \qquad 6.9$$

with

$$\gamma = \sqrt{i\sigma\omega - \varepsilon\omega^2} \qquad 6.10$$

The result is:

$$A_n = - \frac{h_n^{(1)}(\kappa a)}{h_n^{(2)}(\kappa a)} \left[\frac{\frac{d}{dx} \log x h_n^{(1)}(x) - i\varepsilon\omega Z/\kappa}{\frac{d}{dx} \log x h_n^{(2)}(x) - i\varepsilon\omega Z/\kappa} \right]_{x=\kappa a} h_n^{(2)}(\kappa b) \qquad 6.11$$

and hence the field is of the form

$$U = U_1 + U_2 = \sum_{n=0}^{\infty} (2n+1)\ f(n)\ P_n(\cos\theta) \qquad 6.12$$

where $f(n)$ is a function which can be calculated from the properties of the medium, σ , ε .

The series converges slowly in this form. As PRYCE (1953) points out important terms are in the range

$$\kappa a - (\kappa a)^{1/3} < n < \kappa a + (\kappa a)^{1/3} \qquad 6.13$$

Hence the case of light scattering from atmospheric particles is easy to deal with. RAYLEIGH (1871) derived his $1/\lambda^4$ law of light scattering from the first term of a series like this. In contrast the problem of light dispersion from raindrops to form a rainbow is harder (VAN der POL and BREMMER, 1937) while the problem of radio propagation over the earth's surface remained intractable until the work of WATSON (1919). (Although WAIT (1971) mentions that JOHLER and BERRY (1961) have programmed a series like this on a computer).

The essence of WATSON'S (1919) method is the residue theorem (see e.g. ARFKEN 1970) which states that the integral of a function over a contour in the complex plane can be expressed as a sum of residues (coefficients of a

series expansion of the function) at the poles of the function enclosed by the contour. Thus the series (Eqn. 4.12) can be considered as a sum of residues and transformed into a complex integral. The contour of integration can be topologically transformed into a new contour giving the same result but this time enclosing a new set of complex poles at the points $\nu = \nu_s$ given by:

$$\frac{d}{dx} \log x h^{(2)}_{\nu_s}(x) - iZ/120\pi = 0 = M(\nu) \qquad 6.14$$

where $x = \kappa a$. We note that the Hankel and Legendre functions have been generalised to be of complex order. The original series used functions of integral order corresponding to the original set of poles n=1,2,3..... on the real axis. The new integral can now be expressed as another residue series of the form:

$$U \propto \sum_s \frac{(\nu_s+\frac{1}{2}) h^{(2)}_{\nu_s}(\kappa b) h^{(2)}_{\nu_s}(\kappa r) P_{\nu_s}[\cos(\pi-\theta)]}{\sin(\pi\nu_s) \left[\frac{\partial M(\nu)}{\partial \nu}\right]_{\nu=\nu_s} \left[h^{(2)}_{\nu_s}(\kappa a)\right]^2} \qquad 6.15$$

The spherical Hankel functions may be approximated by

ordinary Hankel functions of order 1/3 to give:

$$U = 2U_o(2\pi X)^{1/2} e^{-i\pi/4} \sum_s \frac{f_s(h_1) f_s(h_2) e^{-i\tau_s x}}{2\tau_s - 1/\delta^2}$$

where:

$$U_o = \frac{I\mathrm{d}s\, e^{-i\kappa s\theta}}{4\pi i\varepsilon\omega a(a\sin\theta)^{1/2}}$$

$$f_s(h_i) = \left[\frac{X_i^2 - 2\tau_s}{-2\tau_s}\right] \frac{H_{1/3}^{(2)}\left[\frac{1}{3}(X_i^2 - 2\tau_s)^{3/2}\right]}{H_{1/3}^{(2)}\left[\frac{1}{3}(-2\tau_s)^{3/2}\right]}$$

$h_1 = r - a \qquad h_2 = b - a$ 6.16

$X = (\kappa a)^{1/3}\theta \qquad X_i = (\kappa a)^{1/3}(2h_i/a)^{1/3} \quad i = 1, 2.$

$= \frac{-i120\pi}{(\kappa a)^{1/3} Z} \qquad \tau_s = \frac{\nu_s - \kappa a + \frac{1}{2}}{(\kappa a)^{1/3}}$

This series converges much more rapidly than the original series; In fact eleven terms suffice for most problems in

radio propagation (GERKS 1962).

An alternative deriveation is given by PRYCE (1953) by using a transformation which flattens part of the earth's surface and considers rays with upward concave curvature. The spherical harmonic expansions are replaced by Fourier transforms and the final result for the field is expressed in terms of Airy integrals. WAIT (1971) shows that these two methods of approach yield identical results.

Each term of the series decays away exponentially with distance. Far into the shadow region, beyond the radio horizon, one term is adequate for convergence of the series. Hence the field ultimately decays exponentially with range - a factor which limits the maximum range of a ground wave radar. (BARRICK et. al. 1977).

Conversely, at close ranges, an increasing number of terms are required for convergence so an approximate formula, valid for a flat earth, is used. Historicaly this flat earth problem was the first ground wave propagation problem to be considered and resulted in the well known flat earth solution of SOMMERFELD (1909). PRYCE (1953) shows that this flat earth approximation may be derived from the full spherical earth solution by means of a geometrical ray theory approximation.

The flat earth approximation is given in terms of the

ratio of free space field strength, E_o , to the field strength in the presence of the ground by:

$$\frac{E}{E_o} = 1 + R_v e^{-j\theta} + (1-R_v) F e^{-j\theta} \qquad 6.17$$

where:

$$R_v = \frac{(\varepsilon - jx)\sin\psi - \sqrt{\varepsilon - 1 - jx}}{(\varepsilon - jx)\sin\psi + \sqrt{\varepsilon - 1 - jx}} \qquad 6.18$$

$$x = 60\sigma\lambda$$

$$\tan\psi = \frac{h_1 + h_2}{d} \qquad \theta = \frac{4\pi h_1 h_2}{\lambda d}$$

and h_1 , h_2 are the transmitter and antenna heights and d is the distance between the antennas. Physically, the first two terms of the solution represent the direct space wave and a wave reflected from the surface of the earth with reflection coefficient, R_v , while the third term represents a surface wave trapped in the interface between

the surface and the air. When the antennas are at the earth's surface, i.e. $h_1 = h_2 = 0$, the direct and reflected waves cancel ($R_V = -1$) leaving only the surface wave. The surface wave attenuation factor, F, is given by:

$$F = 1 - j\sqrt{\omega}\ e^{-\omega}\ \mathrm{erfc}\ (\sqrt{-\omega}) \qquad 6.19$$

where erfc is the complimentary error function and:

$$\omega = \frac{4P_1}{(1-R_V^2)} = P e^{-jB}$$

$$P_1 = pe^{-jb} \qquad p = \frac{\pi d}{\lambda}\,\frac{\sqrt{(\varepsilon-1)^2+x^2}}{\varepsilon^2+x^2} \qquad 6.20$$

$$\tan b = \frac{\varepsilon+1 + (\varepsilon-1)(\varepsilon/x)^2}{x + (\varepsilon-2)(e/x)}$$

P is the numerical distance introduced by SOMMERFELD (1909).

The range at which the flat earth approximation breaks down and the spherical earth solution becomes applicable is given in various forms by several of the above workers. The form used in this work is:

$$d = (1.609)\ 50/f_o^{1/3} \qquad 6.21$$

where f_o is the transmitted frequency in MHz and d is the distance, in km, beyond which the flat earth approximation breaks down. As examples the flat earth approximation is valid to 60km at 2.4MHz and 27km at 26MHz.

Computer calculation of these expressions (Eqn. 6.16) requires series expansions for the Hankel funcitons and a numerical method for solving the root determining equation (Eqn. 6.14). Suitable series are provided by GERKS (1962) and a correction note: GERKS (1962b). A computer program based on this work was written and a listing is provided in appendix A.

The input data to the program are the radio frequency, the conductivity and dielectric constant of the earth (or sea) and the heights of the transmitting and receiving antennas above ground. The program then determines the ratio of ground wave to free space field strength for a number of ranges from the transmitter. If a particular range is less than that given by Eqn. 6.21 the flat earth approximation is used (Eqn. 6.17) otherwise the spherical earth residue series expansion (Eqn.6.16) is used. The results of the program were checked against published attenuation curves, e.g. GERKS (1962) and JASICK (1961), and found to agree exactly for the cases given.

The general features that emerge from these results

are that ground wave attenuation increases rapidly with increasing frequency and decreasing ground conductivity.(This explains the difference in sea echo field strengths between 2.4 and 26 MHz mentioned in the introductory paragraphs (6.1)). Close to the transmitter the field strength decreases with the familiar 1/r dependence while over the radio horizon the field strength decreases with successively higher powers of 1/r until the field finally decays exponentially with range.

Of particular interest is the case (fig.6.2) for very short ranges (0-1km) and very poor ground conductivity ($\sigma = 0.001 \Omega m^{-1}$, $\varepsilon = 4$). This case was designed to simulate propagation over the ground between the transmitter and the sea at Birdlings Flat. It can be seen that even at these short ranges suprisingly high attenuation of the field, when compared with free space values, can occur. An interesting comparison can be made between this case and the case for the same situation but with a frequency of 2.4MHz instead of 26MHz. We see here that the field strengths are much closer to their free space values showing the strong frequency dependence of this short range poor ground attenuation effect. As mentioned in the introductory section this frequency dependence was a noticeable feature of experiments at Birdlings Flat.

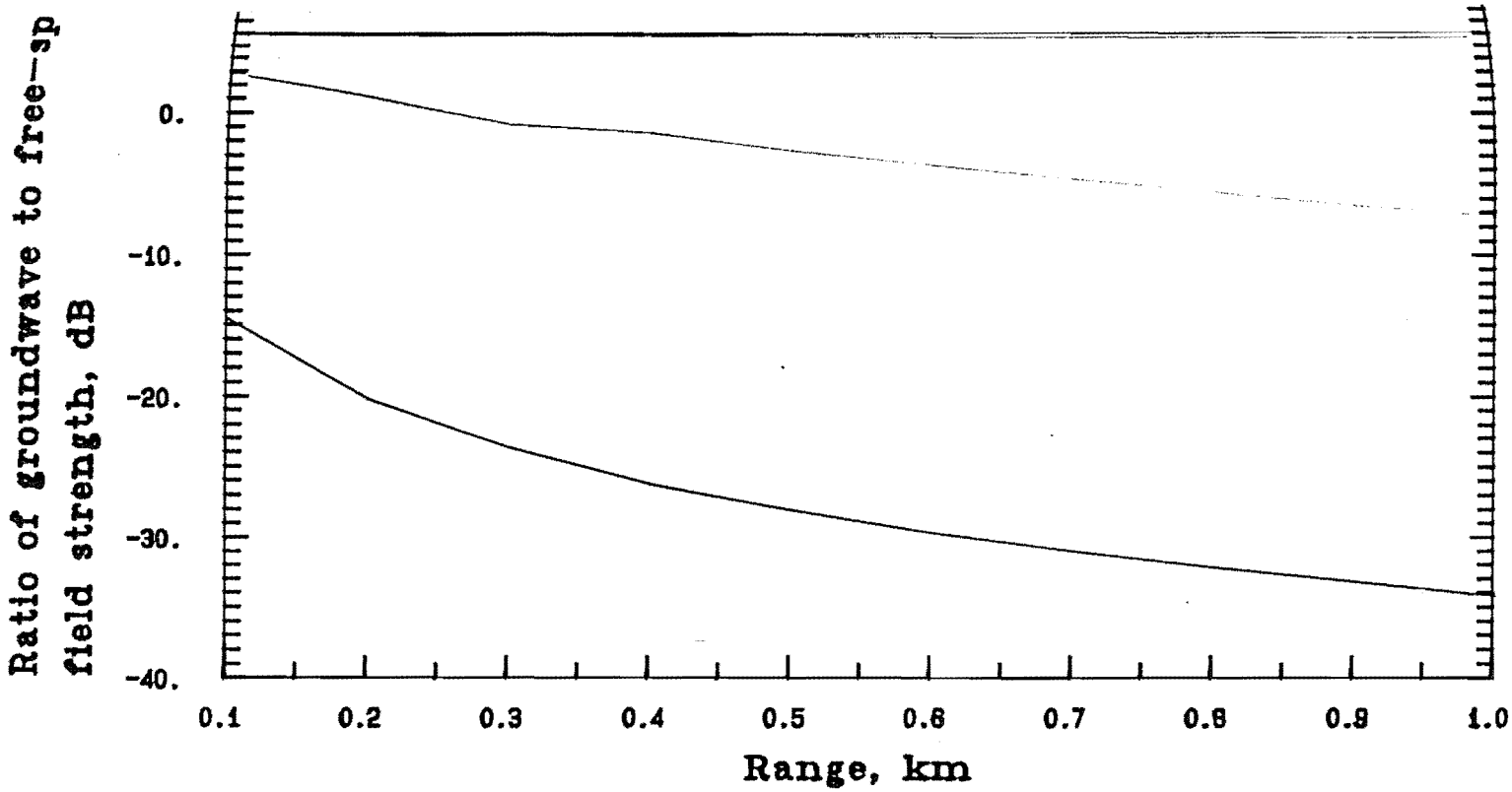

Fig. 6.2 Short range ground wave attenuation.

6.3 EXPERIMENTAL MEASUREMENTS

The theoretical calculations of the previous sections show that high ground wave attenuation (up to 34dB above the free space value) is possible at very short ranges (0-1km) from a transmitter at upper hf. We expect that the methods used to perform these calculations should be valid for all ranges outside the near field of the antenna (λ/D ,about 10m in our case). It is desirable, however, to confirm these theoretical results with direct experimental measurements. One good reason for this is that we do not know the electrical properties of the ground at Birdlings Flat - the assumed values of dielectric constant = 4 and conductivity = 0.001 S/m are educated guesses.

Unfortunately numerous uncertainties, systematic errors and subtleties are present in any attempt to measure rf field strengths. (e.g. impedance mismatches, varying ground conditions, effects due to receiver frequency responses and non-linearities). We emphasise the uncertain nature of field strength measurements by expressing the field strengths in decibels. If we conservatively estimate that measured or calculated field strengths will be correct to within an order of magnitude this translates into an uncertainty of ± 5dB. Similarly a systematic error of a factor of two becomes an error of 3dB. We find, however, that the range of field strengths encountered in practice is large enough (several tens of decibels) that the uncertainties are relatively small in comparison and useful conclusions can therefore be drawn

from the measurements.

Ideally we would like a series of field strength measurements extending from the transmitter near field zone to several km out to sea. Unfortunately this is not feasible given currently available equipment and the facilities available at Birdlings Flat. Instead of this a single field strength measurement over an all land path was used. The experiment is illustrated in fig. 6.5.

A transmitter with nominally 1kW output power transmits 20us 50Hz pulses over a 500m path to the main coherent receiving system. The received power is measured by using a calibrated attenuator in front of the receiver to adjust the receiver output pulses to a known constant level as indicated on an oscilloscope. The power in the receiver input impedance neccessary to produce this same output level can then be found by connecting a signal generator to the receiver input. We assume that the response of the receiver to the pulses is the same as its response to the steady state generator output. This is reasonable as a 20us pulse will easily fit within the 100kHz receiver bandwidth. This technique avoids uncertainties due to receiver non-linearities and simplifies the calibration of the receiver.

The power radiated from the transmitter is estimated by measuring the rf voltage across the transmitting antenna terminals and calculating the voltage that would appear across the assumed antenna radiation resistance of 35 ohms. The rms antenna input voltage was measured by using an rf probe connected to an oscilloscope and found

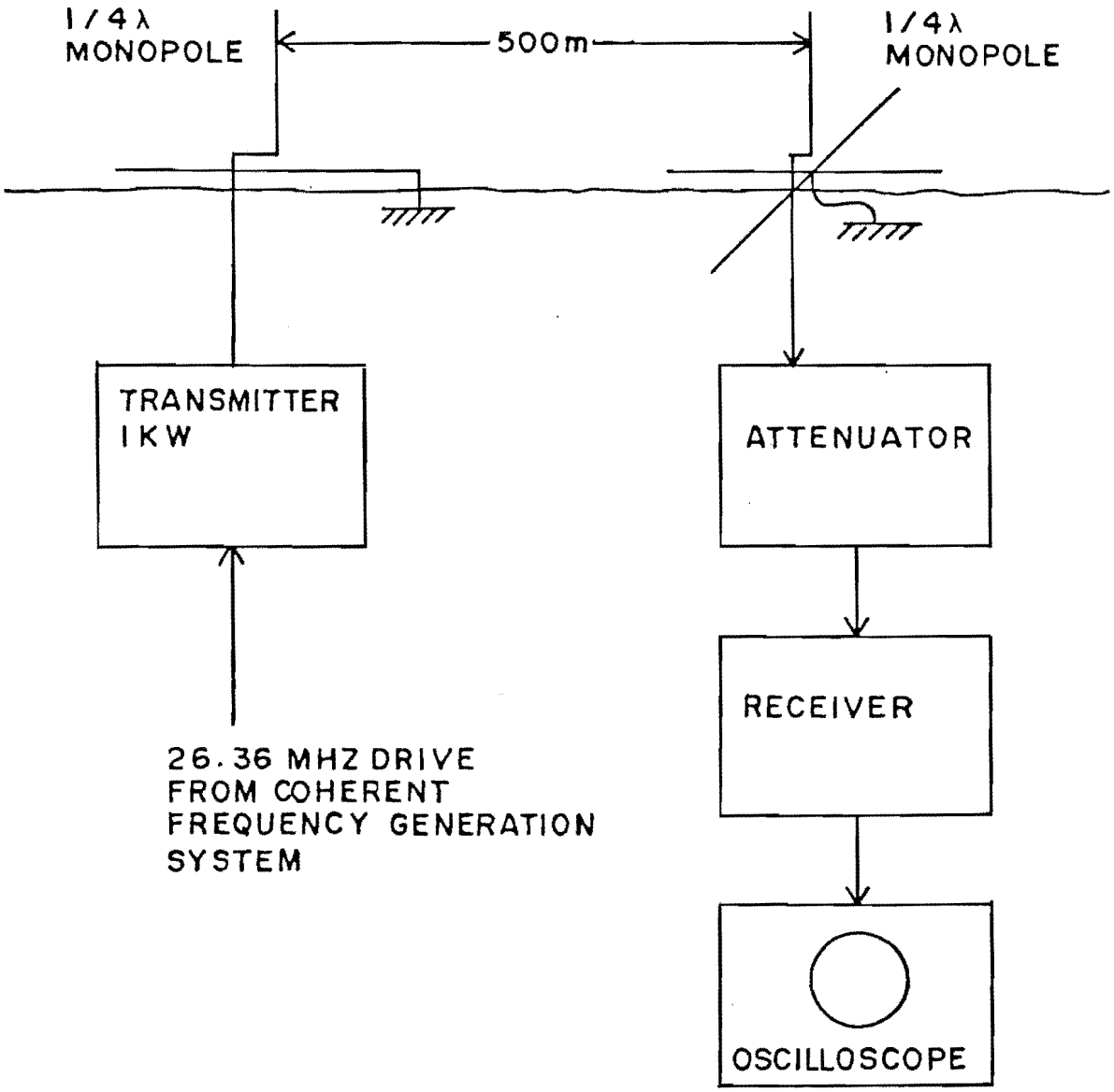

FIG.6.5 EXPERIMENTAL SETUP FOR FIELD STRENGTH MEASUREMENTS AT BIRDLINGS FLAT.

to be 322V. The antenna impedance was measured as 68.5 - j 50.1 ohms. We assume that this consists of 35 ohms from the standard radiation resistance of a 1/4 monopole with the rest of the impedance comming from the wire mesh ground mat under the antenna. This is a lossy capacitor connecting the antenna to the "true" ground. From these measurements we calculate that the voltage across the radition resitance is 132.74V resulting in a radiated power of 503W (for the duration of each pulse). In decibels relative to 1 Watt this is 27dBW. The equivalent isotropic radiated power (EIRP) is calculated by adding the equivalent free space gain of the antenna (-0.85dB). The received power is calculated by adding the gain of the receiving antenna (also -0.85dB) and subtracting the free space attenuation over the 500m path (54.85dB). The power we expect to receive assuming free space propagation is therefore -29.5dBW.

The voltage across the 75 ohm receiver input impedance was 11.3mV (measured by the technique outlined earlier. The 35 ohm receiving monopole was matched to the receiver input impedance by a 5-1/4 wavelength 50 ohm coax line acting as a transmission line transformer). The power actually received was therefore:

$$\frac{V_{RX}^2}{Z_{in}} = 1.7\times10^{-6}\text{W} = -57.7\ \text{dBW} . \qquad 6.22$$

Comparing the free space calculation with the measured power reveals that propagation over 500m of ground has introduced an additional loss of 28dB. The value

predicted by the ground wave field strength program for this case is 28.2dB. The theoretical and experimental values of attenuation are thus in very good agreement.

6.4 RADAR PERFORMANCE PREDICTION

We are now in a postion to calculate the performance of a ground wave pulsed Doppler radar system. We use the expressions developed in chapter 3 and calculate the ground wave attenuation factor, F^2 , by using the methods of the previous section. The received echo power is given by:

$$\left.\begin{matrix} P_{RX} \\ \\ P_{RX(\omega)} \end{matrix}\right\} = \frac{P_{TX}G_{TX}G_{RX}\lambda^2 AF^2}{(4\pi)^3 r^4} \left\{\begin{matrix} \sigma \\ \\ \sigma(\omega) \end{matrix}\right. \qquad 3.27$$

and the received noise power is given by:

$$P_n = k\ T_{sys}\ B_{RX} \qquad 3.23$$

These received powers result in output spectral densities given by:

$$S(\omega) = G_{sys}^{\ 2}\ P_{RX}(\omega) \qquad 3.31$$

$$S_{noise} = k\ T_{sys}\ \frac{B_{RX}}{f_{pr}}\ G_{sys}^{\ 2} \qquad 3.36$$

Given the theoretical calculation of $\sigma(\omega)$ we can predict the final received echo spectrum from these

equations. The result, however, would be specific to the sea conditions used to calculate $\sigma(\omega)$. The calculation of second order cross sections from ocean waveheight spectra is also a complicated task (JOHNSTONE 1975 Ph.D. thesis). A simpler and more general measure of radar performance uses the observation (chapter 4) that the total first order cross section is almost always -17dB (i.e. 1/50th of the sea surface acts as a perfect first order radar reflector). JOHNSTONE (1975 Ph.D. thesis) discusses the conditions under which this approximation is applicable. The most important condition is that the Bragg components be saturated. The first order portion of the sea echo thus provides us with a useful calibration target for studying radar performance. Several previous studies have made use of this fact. (LYONS and BARRICK 1984, DeMAISTRE et. al. 1978).

The peak spectral density of the first order echo can be estimated by dividing the total first order received power by the equivalent bandwidth of the echo:

$$S_{max} = \frac{G_{sys} \; P_{RX}}{B_e} \qquad 6.23$$

This assumes that all the power is contained in one Bragg peak. If the power is equally distributed between each of the Bragg peaks then S_{max} will be reduced by 3dB. As mentioned previously, at 2.4MHz the equivalent echo bandwidth is the value given by the spectral processing

i.e.

$$B_e = \frac{1}{T_{coh}} \qquad 6.24$$

which is $\sim$ 0.01Hz in this work. At 26MHz the Bragg lines are considerably broadened from this value, probably because of different current velocities at different positions within the radar resolution cell. Typical values are 0.05Hz during quiet conditions and 0.1Hz during storms.

999an simplify and generalise the radar performance prediction process stilll further by considering single parameters analagous to the maximum range of a conventional radar with visual output. In the case of our system, however, experience has shown that there are several "maximum ranges" that are useful indicators of radar performance.

(1) r_{vis} - The maximum range of a visible echo: This is the maximum range from which sea echoes are visible on an A-scope oscilloscope display attached to the receiver output. In this case we are effectively using the radar system as a conventional radar and, from chapter 3, the maximum range is obtained when the total received echo power is equal to the total noise power i.e.

$$B_e S_{max} = S_{noise} f_{pr} \qquad 6.25$$

(2) r_{2nd} - The maximum range of useful second order echo. This is a fairly subjective parameter that depends somewhat on the use to which the second order echo spectrum is to be put. From experience with data gathered at Birdlings Flat good second order spectra are obtained out to the maximum range of the visible echo. Thus we set $r_{2nd} = r_{vis}$. Due to the strong dependence of second order cross sections on radar frequency this result will only apply at upper hf (25-30MHz).

(3) r_{1st} - The maximum range of useful first order echo: Once again this depends on the intended application of the Doppler spectrum. In this work we arbitrarily use 10dB signal to noise ratio as the criterion for this maximum range. This gives:

$$S_{max} = 10\ S_{noise}$$

This definition agrees with the maximum range of a ground wave pulsed Doppler radar as defined by BARRICK et. al. (1977).

(4) r_{lim} - The limiting range: This is the maximum range from which a first order echo can be detected with reasonable probability - regardless of the usefuleness of this echo for subsequent processing. This range is found by considering the statistics of the sea

echo Doppler spectrum. The statistical fluctuations in the Doppler spectrum are given by Eqn. 3.53 :

$$\frac{\sigma}{m} = \sqrt{\frac{1}{N}} \qquad 3.53$$

Where N is the number of independent spectra averaged to produce the final spectrum. For typical sea echo spectra N is large enough (N > 10) that the Gaussian approximation to the chi-squared distribution can be used. Since a typical spectrum has of the order of 1000 points we desire that the probability of getting a noise fluctuation as large as the first order echo be of the order of 1/1000. From Gaussian statistics a probability level of 0.001 corresponds to 3.1 standard deviations from the mean noise level. This gives:

$$S = m + 3.1\sigma = m(1 + 3.1\,\frac{\sigma}{m})$$

or 6.27

$$S(dB) = S_{noise(dB)} + 10 \log\,(1 + 3.1\,\frac{\sigma}{m})$$

Using Eqn. 3.53 with N = 10 as a typical value gives:

$$S_{max}(dB) = S_{noise(dB)} + 2.97 \qquad 6.28$$

The output spectral densities in a measured spectrum are

signal + noise whereas the predicted values are purely signal. The condition for the limiting range is therefore that the first order signal spectral density is equal to the noise spectral density.

The computer program listed in appendix B uses these principles to predict the performance of oceanographic ground wave radar systems. The ground wave field strength program in appendix A is called as a procedure to calculate the ground wave attenuation factor. The program reads in input data consisting of basic radar parameters and calculates the peak first order spectral density at 5km range increments starting at 5km. At each step the program tests the conditions for the maximum range parameters and, if one is met, prints out a message. The program terminates when the limiting range is reached. It is assumed that all the energy is contained in a single Bragg peak. This is a good approximation if the difference between the $+\omega_B$ and $-\omega_B$ peaks is greater than about 10dB. If the peaks are equal in magnitude then they will be 3dB lower than the computer prediction.

Example radar performance plots are given in fig. 6.3. In both of these cases a common system gain of 146dB was used. (This is the gain of the Birdlings Flat system). The purpose of this is to allow spectral density plots to be directly compared. It must be remembered, however, that signal to noise ratios, rather than absolute signal strengths, are the important

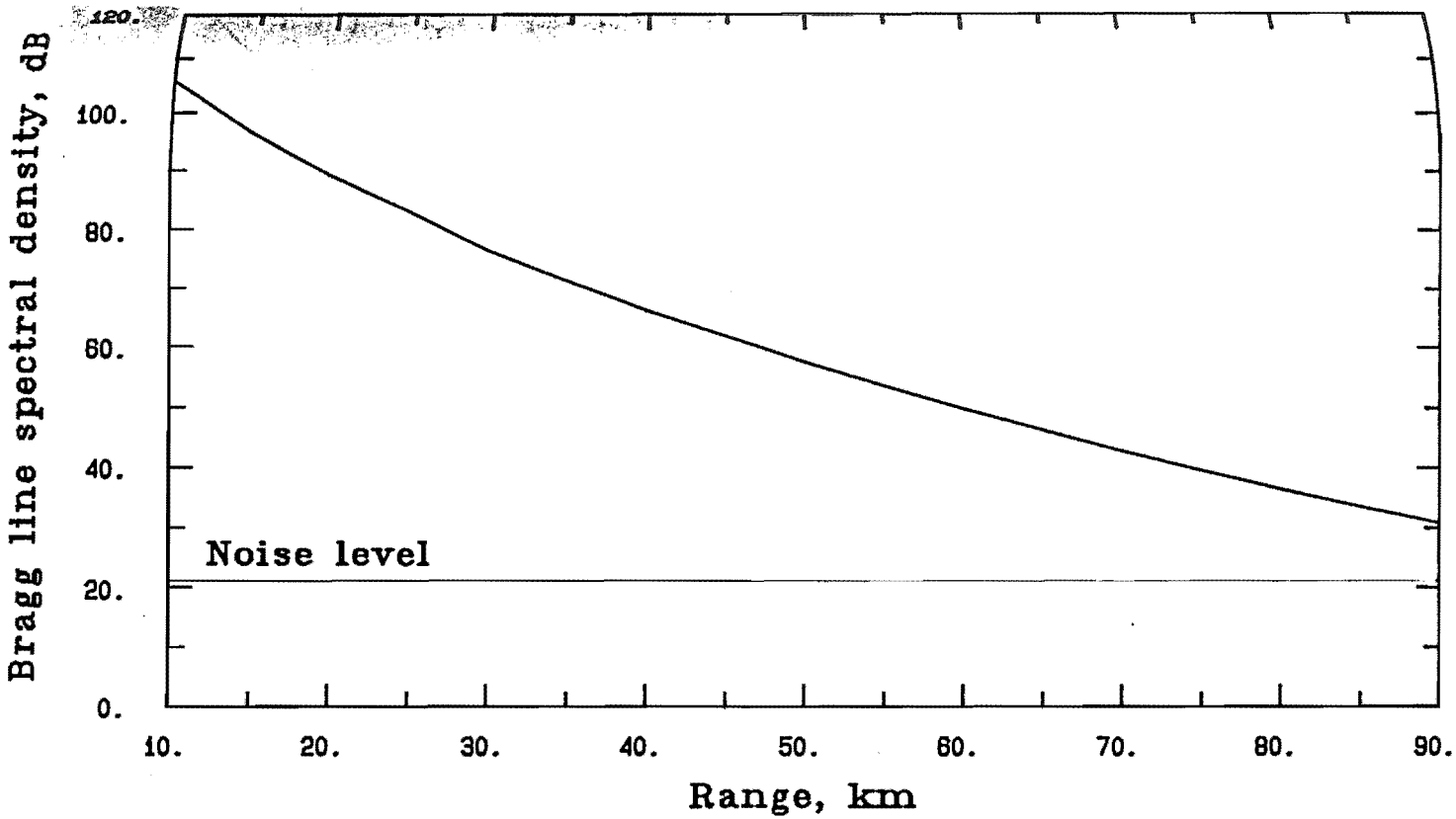

Radar frequency 26MHz	Transmitter power 2.5kW
TX antenna gain −0.85dB	RX antenna gain −0.85dB
Antenna heights 0 m	Noise temperature 1,000,000K
Pulsewidth 20μs	Pulse repetition frequency 333Hz
Bragg line width 0.05Hz	Receiver bandwidth 100kHz

Fig. 6.3a Radar performance analysis.

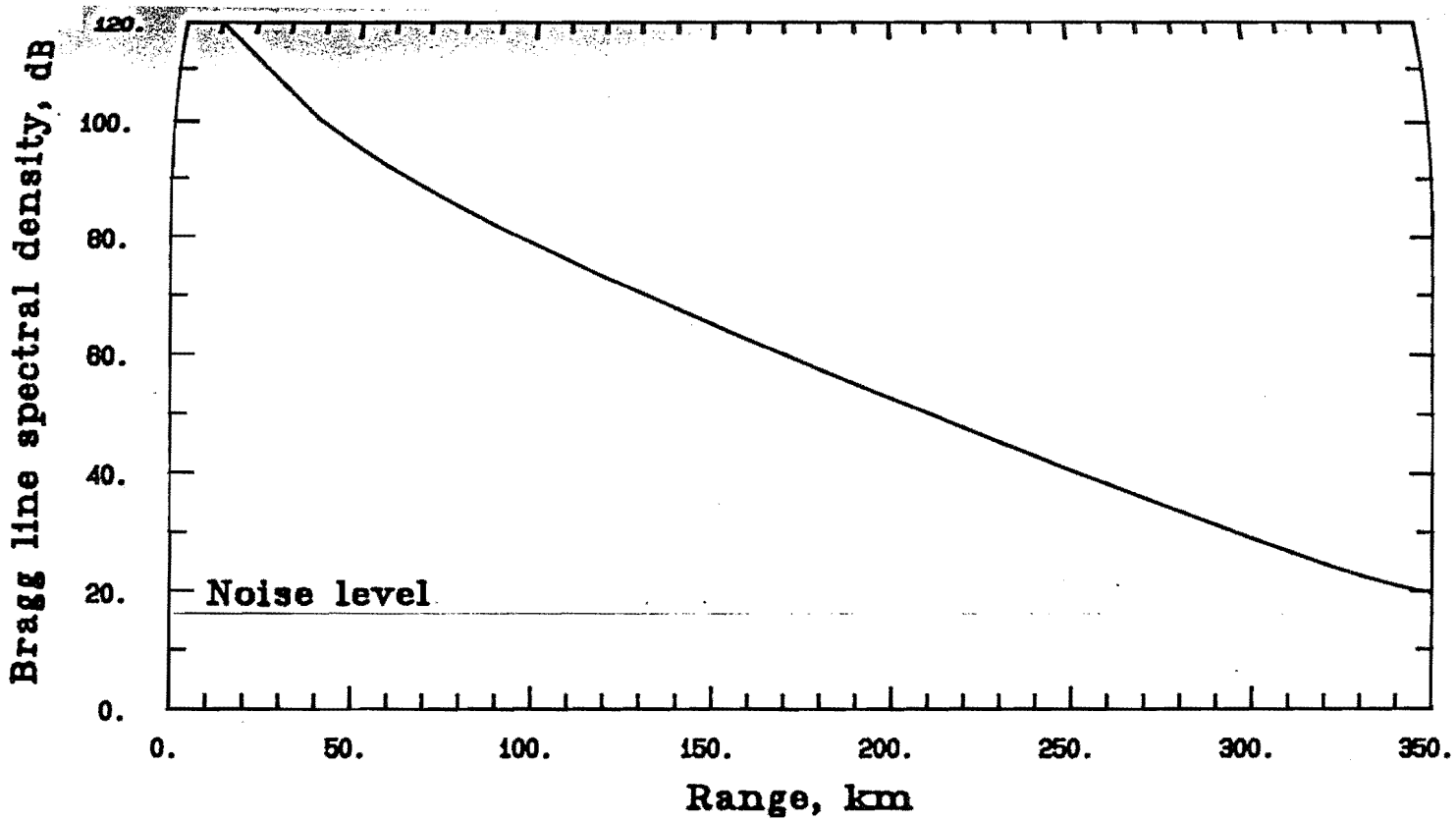

Radar frequency 10MHz	Transmitter power 1.0kW
TX antenna gain −0.85dB	RX antenna gain −0.85dB
Antenna heights 0 m	Noise temperature 100,000K
Pulsewidth 20us	Pulse repetition frequency 100Hz
Bragg line width 0.01Hz	Receiver bandwidth 100kHz

Fig. 6.3b Radar performance analysis.

quantities for determining radar performance.

Fig 6.3 (a) was designed to simulate the upper hf, approx. 1kW systems typicaly used by other workers (e.g. BARRICK et. al. 1977). We see that the maximum range of this system (70-100km) is consistent with the values reported by these workers. Fig. 6.3 (b) (10MHz) was chosen to be typical of systems using the lower end of the hf band (e.g. SHEARMAN 1981). Due to the frequency dependence of ground wave attenuation the maximum range of these systems for first order echo is much greater (approx. 300km) than that of the upper hf systems. Second order cross sections, however, are very much smaller relative to the first order cross section at these frequencies. As a result second order echoes were not observed on our 2.4MHz system and the observational rule of thumb that the maximum visible echo range equals the maximum range for good second order echo does not apply. Additionaly, the assumption that the first order cross section is a constant -17dB also does not apply as Bragg waves at lower frequencies are near the cutoff region of the ocean waveheight spectrum and, therefore, are not often saturated.

Fig. 6.4 is a comparison of theoretical versus experimental first order echo strengths from the Birdlings Flat system. The experimental points are the total first order power spectral density, i.e. the spectral density that would result if the total echo power

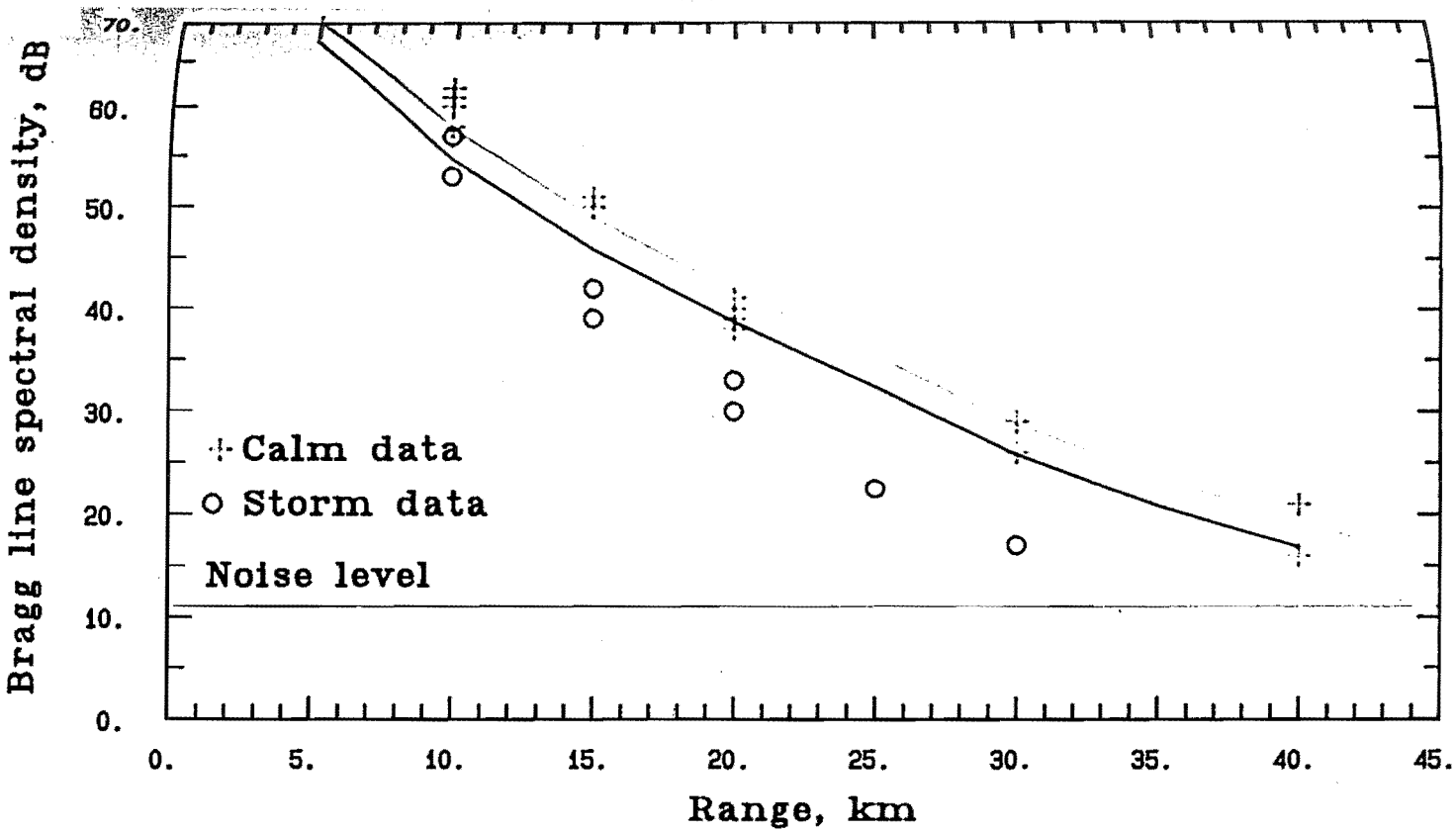

Radar frequency 26MHz
TX antenna gain 10dB
Antenna heights 0 m
Pulsewidth 20μs
Bragg line widths — 0.05Hz
— 0.1Hz
Transmitter power 48kW
RX antenna gain −0.85dB
Noise temperature 32,700K
Pulse repetition frequency 100Hz
Receiver bandwidth 100kHz

Fig. 6.4 Comparison of measured and predicted echo strengths. 60dB subtracted from theoretical curves.

present in both Bragg peaks was present in only one peak with the same width. The points are grouped into two sets, one set from normal, calm sea conditions, the other set from a southwesterly storm (1983/12/14). Similarly, two theoretical curves are provided: One assuming a Bragg line equivalent bandwidth of 0.05Hz, typical of calm conditions, the other assuming a Bragg line width of 0.1Hz corresponding to storm conditions. A discussion of the uncertainties inherent in these signal strength measurements and predictions was given in the previous section. The ground wave propagation loss was modelled by adding a constant 60dB attenuation to the theoretical curves.

Several conclusions can be drawn from fig. 6.4:

(1) Excellent agreement is obtained between the points corresponding to calm conditions and their theoretical curve. Since the additional 60dB attenuation figure was chosen for good fit to the experimental data it is the variation of signal strength with range, rather than the absolute signal strengths, that we have successfully predicted. This agrees with the findings of LYONS and BARRICK (1984) that the rate of attenuation of ground wave signals is more readily predicted than the absolute value of signal strength.

(2) Following on from (1) we see that the

propagation problem in our system is accurately modelled by a constant 60dB loss. This reinforces the theory that the cause of the problem is high attenuation due to propagation over the poorly conducting ground seperating the antennas from the sea. Other possible explanations, such as tropospheric ducting, now seem less likely as these would produce attenuations that vary with range, time and meteorological conditions.

(3) The results from the storm do not agree with their predicted curve. The attenuations are higher and they vary with range. This is because the ground wave field strength calculation assumes that the sea surface is smooth rather than rough. BARRICK (1971) shows that sea surface roughness may be accounted for by replacing the sea surface impedance derived from a conductivity of 4 S/m and dielectric constant of 80 with a new value derived from the ocean waveheight spectrum. BARRICK's (1971) curves for the additional loss due to sea state are entirely consistent with the observed values shown in fig. 6.4 and indicate a wind speed of about 25 knots.

Until this point all our discussions have assumed propagation over a homogeneous surface i.e. a surface consisting entirely of land or sea. The actual radar propagation path is clearly a two section path consisting of about 300m of poorly conducting ground followed by several tens of km of sea. A semi-empirical solution to the problem of propagation over inhomogeneous ground has

been given by MILLINGTON (1949). This solution was based on an earlier method due to ECKERSLEY (1930) which simply combined the attenuations from the various sections of the path that consisted of different media. The difficulty with this approach was that it did not obey the reciprocity condition that the same field strength must be obtained if the positions of the transmitter and receiver are interchanged. MILLINGTON (1949) solved this problem by writing the field strength as the geometric mean (or arithmetic mean with field strengths in dB) of the forward and reciprocal path field strengths. Thus for a path consisting of two sections of length d_1 and d_2 the field strength $\varepsilon(d) = (d_1 + d_2)$ is given by:

$$\varepsilon(d) = \left[\frac{\varepsilon_1(d_1)}{\varepsilon_2(d_1)} \varepsilon_2(d_1+d_2) \frac{\varepsilon_2(d_2)}{\varepsilon_1(d_2)} \varepsilon_2(d_1+d_2) \right]^{\frac{1}{2}} \qquad 6.29$$

where $\varepsilon_1(d)$ is the field strength resulting from propagation for a distance, d, over the medium of section 1 and $\varepsilon_2(d)$ is the corresponding field strength for section 2. This method can be extended to a path consisting of any number of sections. Analytical solutions to the problems of two and three section paths over a spherical earth have been developed by WAIT (1971).

A surprising prediction of these theories concerns the change in field strength that results when the boundary between two media is crossed. If the propagation

is from a medium with high attenuation (e.g. poorly conducting ground) to one with low attenuation (e.g. sea water) a "recovery effect" is predicted in which the field strength increases with distance for a short distance after the coast is passed. Theoretically, this is explained by energy being fed downwards into the wave field from higher levels where the effect of the transition in surface media is less noticeable. A similar "converse effect" in which the field strength is rapidly attenuated following a transition from sea to land is also predicted by these theories. Both of these effects have been experimentaly verified. ANDERSEN (1963), for instance, measured a drop of 12-14dB in the strength of a 25MHz signal 200-300m after crossing a coastline.

To apply these results to the Birdlings Flat system we consider a 300m path from the transmitter over land to the coast followed by 20km of sea and a return path with 800m of land from the coast to the receiving antenna. Application of Eqn. 6.29 gives 33dB higher attenuation than would be the case for an all sea path of the same length. This is significantly less than the observed value of 60dB. From the curves given by MILLINGTON (1949) and WAIT (1971) some variation of this attenuation with range in the region 0-20km is expected. This is due to the influence of the recovery and converse effects. No significant variation of attenuation with range was observed in our results. A simpler approach is to consider the ground as an attenuator with attenuation as

calculated by the ground wave field strength program. This method gives 55dB attenuation on top of the all-sea value - a figure which is in reasonably good agreement with the observed results.

6.5 CONCLUSIONS

Computer methods have been developed that enable predictions of the performance of ground wave pulsed Doppler radars to be made. When applied to our system these predictions show that received first order spectral densities are 57dB lower than expected. This results in a reduction in maximum range from 120km to 35-40km. Experimental measurements, confirmed by theoretical calculations, have shown that the attenuation over the poorly conducting ground between the antennas and the sea is of sufficient magnitude to account for this poor performance.

Attempts to extend this work to include MILLINGTON's (1949) recovery effect were not as successful and further work is required on this topic. The most productive approach would be to combine theoretical predictions with detailed field strength measurements extending across the land - sea boundary.

The first order portion of the sea echo Doppler spectrum provides a useful calibration target. Measurements of first order echo strengths are sensitive and accurate enough to detect variations in ground wave attenuation due to different sea states. This could form the basis of a method for obtaining sea state information from first order sea echo Doppler spectra.

We conclude this chapter with a discussion of the strategies used to overcome the propagation problem. The obvious solution to the problem is to place both receiving and transmitting antennas as close to the water's edge as

possible. This suggestion was first put forward by BARRICK et.al. (1977) who found that trying to increase the signal strength by placing antennas back from the water's edge on the roofs of buildings was generaly counter-productive. Unfortunately it was impossible, for various practical reasons, to move the antennas at Birdlings Flat any closer to the sea. Increasing the gain of the transmitting antenna, a standard method for increasing radio signal strengths, has surprisingly little effect on sea echo signal strengths. This is because an increase in gain is neccessarily accompanied by a reduction in antenna beamwidth and, therefore, a corresponding reduction in the scattering area of the sea surface. Correct choice of the receiving antenna's directional response can have a large effect on radar performance by eliminating the reception of unwanted noise sources. For the purposes of this work it was felt that a highly directional receiving antenna system would greatly reduce the flexibility of the radar system as several potential applications of the radar require broad coverage (e.g. determining the direction of arival of first order echoes by measuring the phase difference between two spaced receiving antennas).

Two methods for improving the range of the radar system were finally chosen. The first method was to increase the transmitted power by replacing the prototype system's 10kW transmitter with a meteor radar transmitter with a nominal output of 100kW. This increased the signal strength by about 10dB and enabled sea echos to be seen on

an oscilloscope connected to the receiver output. The second, and more important, improvement involved raising the maximum pulse repetition frequency of the radar. An important conclusion from chapter 3 was that the performance of a pulsed Doppler radar increases with transmitted prf due to an increase in coherent integration resulting in a reduction in aliased noise. The prf of the original test system was limited to about 5-10Hz by the speed of the PDP-8 data collection software. New software was written and minor hardware modifications were made to enable data to be collected using interrupt driven I/O instead of the standard programmed I/O system. The new data collection system was capable of operating at a prf of 500Hz. The actual prf used was 100Hz, however, as the maximum pulse rate of the transmitter was limited to 100-200Hz. Idealy a prf close to the limit imposed by range ambiguity (1000-2000Hz) should be used. These improvements resulted in a marked increase in the quality of the sea echo Doppler spectra. (see chapter 8 for examples of these spectra). The signal to noise ratios of the spectra are now comparable to those published by other workers. The new data collection system will be described in the next chapter.

CHAPTER 7:

DATA PROCESSING SYSTEM

7.1 INTRODUCTION

The design of a software system for data collection and processing formed a major part of this work. The design philosophies discussed in chapter 5 with respect to the hardware also apply to the design of this data processing system. In other words our system is an initial investigation which should be flexible enough to allow many different experiments and investigations to be carried out. From the point of view of software this means that we should be able to gather and permanently store sea echo data in a form that will be useful to as wide a range of future research projects as possible. In addition our data processing system must allow as high a pulse repetition frequency as possible in order to limit the effects of the propagation problem discussed in chapter 6. Consideration of these points led to the following design descisions being made:

(1) The raw sea echo Doppler time series will be the form in which the data will be permanently stored. These time series will be continuous rather than broken into segments of length equal to the coherent integration time. A convenient unit with which to deal with the collected data will therefore be a single run containing complex time series from all of the ranges sampled. By storing data in this format we are not committed to any particular

subsequent data processing method. It is possible for the data to be re-analysed several times with different spectral analysis parameters to optimise the extraction of different oceanographic information. For example a wide range of different coherent integration times can be used and the coherent data segments may be overlapped to increase the amount of incoherent averaging (chapter 3). In addition new spectral analysis techniques, such as the maximum entropy method (MEM) (CHILDERS 1978), may be applied as they are developed.

(2) Data will be collected on the PDP-8 and recorded on magtape in the form discussed above. All subsequent processing will be done on mainframe computers as software development on these machines is considerably easier than it is on a PDP-8 at a remote site. Initial results can thus be obtained far more rapidly than with a system that relied on the PDP-8 to do all the processing. The mainfame computers are also considerably more powerful than the PDP-8 - an important consideration for some data analysis techniques (e.g. MEM spectral analysis and inversion techniques for obtaining ocean waveheight spectra from sea echo Doppler spectra (LIPA 1977)). The University of Canterbury has two mainframe computers: A Burroughs B6930 and a Prime P750. The B6930 is much better suited to our task than the P750 due to the ability of the powerful Burroughs extended Algol language to perform low level

operations such as the manipulation of individual bits within a computer word. Unfortunately only the P750 has a 7 track magtape drive - those on the B6930 being incompatible 9 track drives. The extra step of reading 7 track tapes on the P750 and writing the data to Burroughs compatible 9 track tape was considered, however, to be worth the effort in order to gain the advantages of the B6930 over the P750 for this application.

(3) We adopt the technique of storing data as direct binary numbers (i.e. 12 bit PDP-8 words) rather than converting the values to strings of ASCII or EBCDIC characters. This saves processtime on both the PDP-8 and the mainframes and brings about a considerable reduction in data storage space. The 10-bit A-D values have a range of -2048 to +2047. By adding 2048 we can store these values as four 8 bit characters giving a total of 32 bits per A-D value. In binary format an A-D value is stored in one 12 bit PDP-8 word. Binary format thus occupies 12/32 = 0.38 of the space of character string format. The B6930 has a 48 bit word length allowing four A-D samples to be packed exactly into one word with no waste space left over. In character string format it is easier to put one 32 bit A-D value into one 48 bit B6930 word than to split A-D values across word boundaries. Direct binary format would occupy 1/4 of the space of this system.

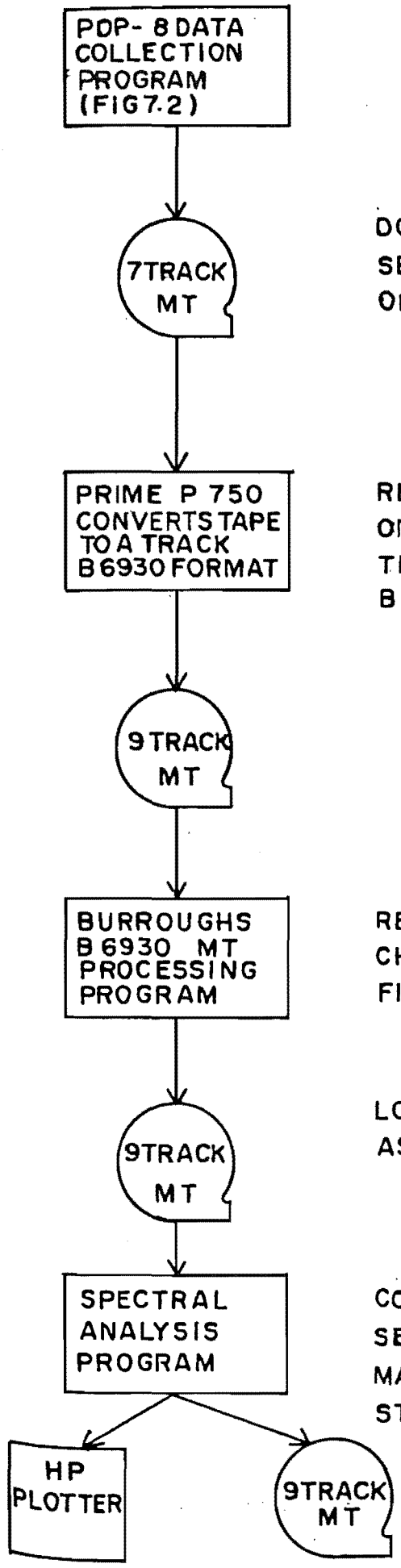

FIG 7.1 OVERALL DATA COLLECTION AND PROCESSING SYSTEM

In order to estimate the likely storage requirement of our system we assume that four ranges will be sampled in each run. Given that the maximum range of our system is of the order of 40km (chapter 6) a probable set of ranges would be 10, 20, 30 and 40km. We note from typical published spectra (e.g. BARRICK and LIPA 1979, SHEARMAN 1981) that sea echo Doppler spectra are almost always entirely contained within the band -2Hz to +2Hz. On the basis of this we choose 4Hz as our design sampling rate for the Doppler time series. Since we are recording four time series (one from each range) simultaneously our data collection program will generate 16 complex numbers, or 32 PDP-8 words, per second. We choose 1000 seconds (17 minutes) as the total length of a time series. With times longer than 1 hour the sea echo spectra may become non-stationary (BARRICK and SNIDER 1977) and interesting trends may be averaged out. In contrast shorter times will allow less incoherent averaging and, therefore, will result in spectra with greater statistical uncertainty. We thus arrive at an estimated storage requirement per run of 32K 12 bit words or 48KB (1KB = 1 kilobyte = 1024 8-bit words). A 1200 foot, 1600 bit per inch magtape has a storage capacity of approximately 20MB thus allowing 400 runs to be stored on one magtape. Using character string, rather than binary format would reduce this to about 100-200 runs. Another important advantage of binary format is that it results in data files of a more convenient size for subsequent handling and processing. 48KB is 267 B6930

disk segments. A four-fold increase in this amount (1068 segments) is a substantial fraction of an individual users normal disk allocation (3000 segments = 540KB).

We now consider how the data processing system can reduce the effects of the high ground wave attenuation present in our system. The pulse repetition frequency of the prototype system was limited to about 5-10Hz by the performance of the original data collection software. Recalling the discussions of chapter 3 we need to increase this prf as much as possible up to the limit of about 2kHz imposed by range ambiguity. In our system the prf is ultimately limited by the 26MHz transmitter. Above 100Hz this transmitter becomes unreliable and produces phase instabilities resulting in a loss of phase coherence. (Planned improvements to this transmitter for the meteor radar system will probably raise this limit to about 400Hz). We therefore choose 100Hz prf as our design goal and try to acheive this with improved data collection software.

The immediate problem that results from this higher prf is a 25-fold increase in data storage requirement. Furthermore the extra data stored is for the purpose of reducing the aliasing of noise and does not contain useful sea echo information. We solve this problem by passing the time series samples, as they are collected, through a

digital low pass filter with a cutoff frequency of 2Hz. This reduces the time series bandwidth from the range ± 50Hz (determined by the prf) to our design value of ± 2Hz. By the Nyquist theorem the filter output will now be fully specified by samples taken at 4Hz rate even though the filter output is updated at 100Hz. Our scheme is therefore to transfer one filter output value to magtape for every 100/4 = 25 transmitted pulses, discarding the redundant intermediate values. The equations of chapters 3 and 6 can be extended to include digital filtering by noting that the time series sampling rate, f_{samp}, is now no longer equal to the pulse repetition frequency, f_{pr}. The only modification to the pulsed Doppler radar design rules (section 3.5) is that step 3 now becomes:

$$f_{samp} = 2f_{max} \qquad 7.1$$

The digital filter cutoff frequency is then $f_{samp/2}$. It is convenient to arrange for f_{pr}/f_{samp} to be an integer, n_{av}, so that we record one filter output value or every n_{av} transmitted pulses. By using digital filtering we have gained the advantage of minimum data storage requirements reulting from a low prf together with the low aliased noise level that results from a prf near the maximum value.

Of course the digital filter will place an extra demand on processing power. The problem of providing additional performance to raise the prf and do digital filtering was solved by changing from the traditional programmed IO data gathering system to an interrupt driven system. The interrupt system allows seperate tasks, such as A-D conversion, digital filtering and writing data to magtape to proceed in parallel rather than sequentially as is the case with the programmmed IO system. A-D conversion and magtape writing are done by hardware external to the PDP-8 CPU so, once started, they can proceed independently of a CPU program. As an example we consider a write to magtape. Under programmed IO a program initiates the write and then enters a waiting loop continually checking for a flag indicating that the data transfer is complete. Only when this flag is raised can the program stop the magtape drive and resume its original task. Since a magtape write takes about 250 milliseconds considerable valuable time is wasted in this loop.

Under interrupt driven IO the program starts the magtape write and immediately resumes the original task. When the data transfer to magtape is complete the magtape interface hardware generates an interrupt which causes program control to switch from the interrupted task to a short routine that stops the magtape drive. When this

routine finishes the original task is resumed at the point where it was interrupted. In a similar manner an A-D conversion (taking approximately 1.2ms) can proceed while the digital filter is processing the data from the previous A-D conversion. Interrupt driven IO was implemented by making some simple modifications to the PDP-8 interface boards.

A further significant increase in performance resulted from re-writing the fast A-D driver program. It will be recalled from chapter 5 that these A-Ds store data into a local RAM buffer. In addition the A-Ds start sampling at the millisecond clock pulse before the transmitted pulse and continue sampling at 2.5km range intervals until shortly after the following millisecond pulse. Thus the RAM buffer contains considerably more range samples (approx. 100) than the 4-10 ranges that we need. The original fast A-D driver transferred all of these samples to the PDP-8 - a time consuming task. The A-D program was therefore re-written so that only the required range samples would be transferred.

7.2 DATA COLLECTION AND PROCESSING SOFTWARE

(1) The PDP-8 data collection program The data collection program consists of a machine code kernel which is called from a driver program written in Rogalgol, a dialect of Algol 60 (ABBOT, 1980). The machine code kernel performs the high speed data collection and filtering while the driver communicates with the operator and calculates parameters and tables required by the kernel. In this way we combine the advantages of high speed with an assembler language and the ease of programming associated with high level languages.

The machine code routine consists of a main foreground program and a set of interrupt service routines. When an interrupt occurs the foreground program is interrupted and the appropriate service routine is executed. When this routine finishes the foreground program resumes at the point at which it was interrupted. A block diagram of this arrangement is given in fig. 7.2. The heart of the program is a timer routine driven by interrupts from the millisecond clock. As illustrated by the timing diagram, fig. 7.3, this routine synchronises the operation of the rest of the program. Every time a millisecond interrupt occurs the millisecond interrupt routine increments a counter. When this counter equals the number of milliseconds between transmitted pulses (10 in

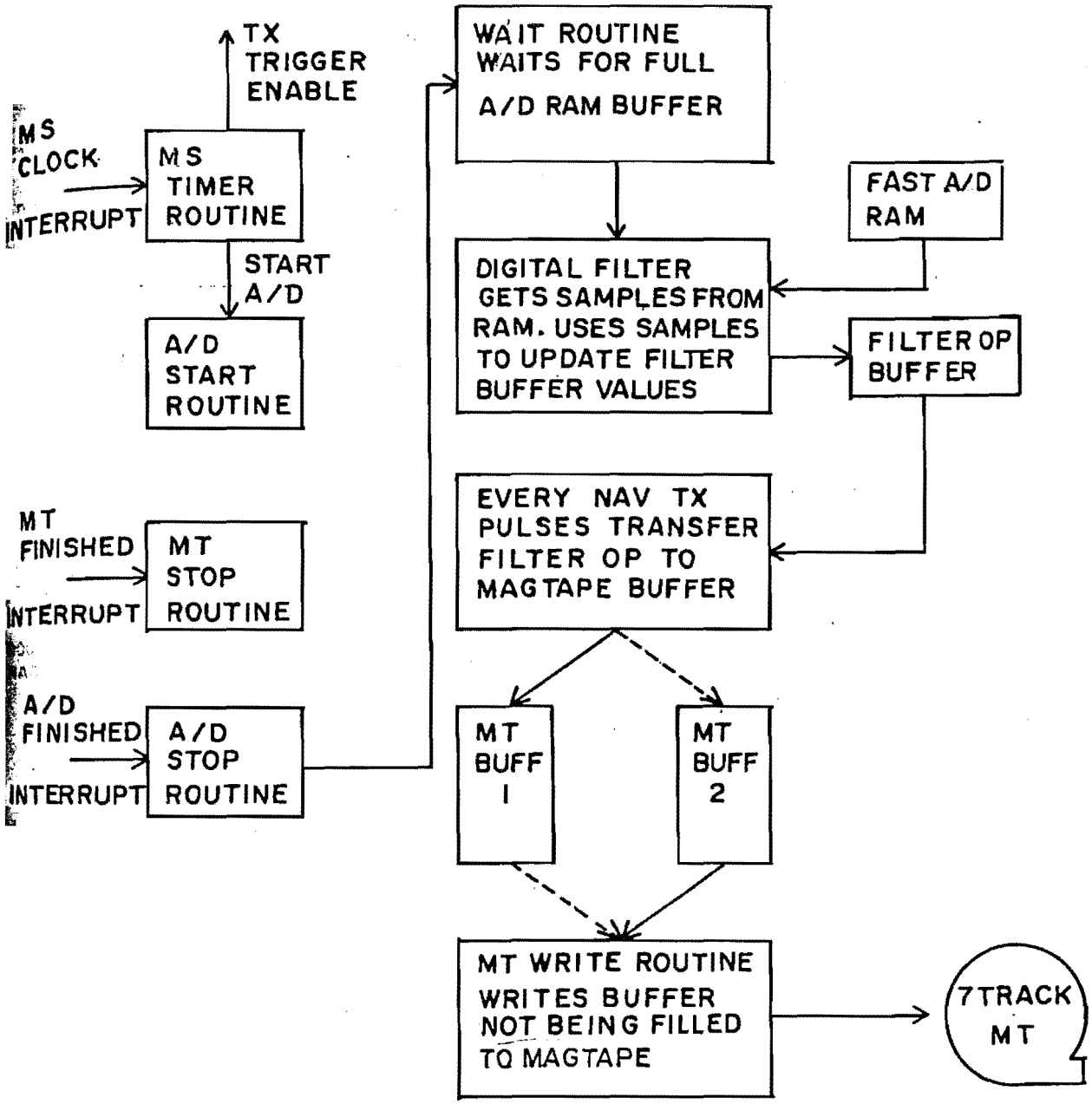

FIG 7.2 PDP-8 DATA COLLECTION PROGRAM.

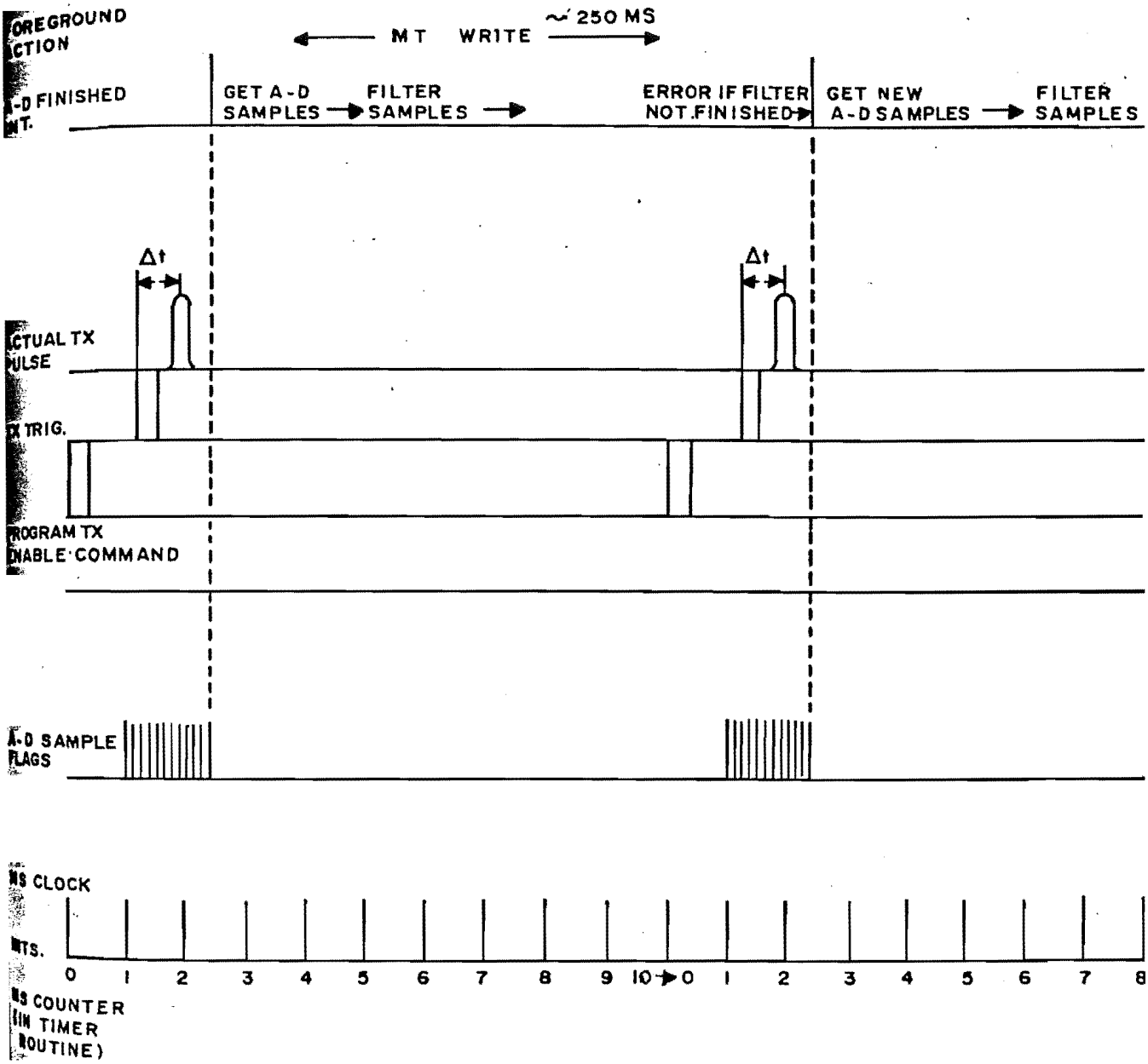

FIG 7.3 DATA COLLECTION PROGRAM TIMING DIAGRAM.

this example) the counter is reset to zero and a command sent to trigger the transmitter. On the next millisecond interrupt (counter = 1) the timer routine jumps to another routine that starts the A-D converters. At the same time the transmitter trigger (in a box known as the video calibrator box), which was enabled by the transmitter command, sends the trigger pulse to the transmitter. After a fixed delay, equivalent to about 40 A-D range samples, the transmitter pulse occurs and A-D samples taken after this are valid sea echo data. The A-D samples and transmitted pulse are thus synchronised to the millisecond interrupt and hence to each other.

The A-D conversion finishes about 1.2ms after it was started and causes an interrupt. The A-D interrupt routine shuts down the A-D converter and sets a software flag (semaphore) that indicates to the interrupted foreground program that the A-D RAM buffer contains a new set of samples to be processed. By this time the foreground program should have finished processing the previous set of A-D samples and will be in a wait loop checking this software flag. When the flag is set by the A-D interrupt routine the foreground program exits the wait loop and starts the digital filter algorithm.

The filter output values are stored in a small memory buffer. New filter output values are calculated

recursively from the old output values and the A-D samples. The filter obtains the A-D samples directly from the RAM buffer. For this purpose the RAM addresses containing the required range and A-D channel samples are pre-computed and stored in a table before the machine code kernel is started. The filter routine simply retrieves these addresses from the table. This saves the routine from performing an array address calculation each time an A-D sample is required.

Every $n_{av} = f_{pr}/f_{samp}$ transmitted pulses (25 in this example) the filter output buffer is transferred to a magtape buffer. When this buffer is full it is written out to magtape. Since it takes approximately 250ms to write out the 314 word buffer a double buffering scheme must be used to enable the magtape write to proceed in parallel with the rest of the program. In this scheme two magtape buffers are used. While buffer 1 is being written to magtape buffer 2 is being loaded with filter output samples. When buffer 2 is full the roles of the buffers are switched so that buffer 2 is written to magtape while further filter samples are written to buffer 1. The filtered time series are thus stored on tape as a sequence of 314 word blocks.

The Algol driver program is written as an interpreter which accepts and performs commands typed in by the

operator. In addition to the command that starts the kernel there are commands that call test routines for checking various parts of the system (such as the fast A-D converter) and commands that enable the operator to change basic system parameters such as prf, filter bandwidth, the ranges to be sampled and the length of the run. The driver calculates further information from these parameters (e.g. the filter coeficients and the RAM range address table) and loads all of this information into appropriate locations in the kernel when the kernel is started. For this work the A-D multiplexer was set at two channels per range sample so as to sample both the real and imaginary receiver outputs. Provision has been made for increasing this to six channels, allowing up to three phase sensitive receivers to be sampled simultaneously. Error trapping routines are also included in the driver. These report on anything that went wrong during the operation of the kernel and check that input values are sensible. (e.g. that the prf is not so high that it will damage the 26MHz transmitter).

The ultimate performance of the data collection software was tested by disabling the transmitter and increasing the prf until a timing error occurred. With four ranges the maximum prf was 500Hz - a considerable improvement over the original software. This 500Hz limit is probably due to the one millisecond resolution of the

timer routine.

(2) The digital filter algorithm.

The criteria used for selecting a filter algorithm were simplicity and low process time. On this basis a simple recursive RC low pass filter was chosen. At each transmitted pulse a new filter output value, y_i , is calculated from the previous value, y_{i-1}, and the A-D sample, x_i , by:

$$y_i = Ay_{i-1} + (1 - A)\, x_i \qquad 7.2$$

Where the filter coefficient, A, determines the 3dB cutoff frequency, B_{3dB} , of the filter by:

$$A = e^{-2\, t_{pr}\, B_{3dB}} \qquad 7.3$$

and with $t_{pr} = 1/f_{pr}$ as the filter sampling interval. Since we must apply this filter to both the real and imaginary parts of the complex time series eqn. 7.2 must be evaluated twice for each range sampled. Four ranges thus require eqn. 7.2 to be evaluated eight times for each transmitted pulse. For reasons that will be discussed

shortly the filter output values are double precision so, in this example, the filter output buffer is sixteen PDP-8 words long. The recursive form of the digital filter thus has the advantages over the non-recursive form of reducing filter buffer storage and, more importantly, of distributing the process time used by the filter over a large number of pulses.

A non-recursive filter would accumulate $n_{av} = f_{pr}/f_{samp}$ complex samples from each range in a filter buffer and then operate on all of these samples in the time between two transmitted pulses, producing eight double precision output values. Thus with $n_{av} = 25$ a 400 word buffer would be required and eqn. 7.2 would have to be evaluated 200 times in 10ms - an impossible task. Of course double buffering could be used but this would require 800 words of storage.

According to the Nyquist theorem we must set f_{samp} to be twice the highest frequency present in the filter output spectrum. As a rough approximation we choose B_{3dB} as the filter cutoff frequency and set $f_{samp} = 2B_{3dB}$ thus:

$$B_{3dB} = \tfrac{1}{2} f_{samp} = \frac{f_{pr}}{2n_{av}} \qquad 7.4$$

giving a simple form for the filter coefficient:

$$A = e^{-\pi/n_{av}} \qquad 7.5$$

Since the filter is not an ideal low pass filter this approximation will result in some aliasing but, provided our assumption that the sea echo part of the spectrum lies entirely within 2Hz is correct, it is only the noise component of the spectrum alias at f_{samp} that will be folded into our spectrum. Due to the 6dB per octave filter cutoff we neglect contributions from the higher frequency copies of the spectrum. We can readily estimate the likely effect of this aliasing by assuming that the original spectrum is flat and of unit amplitude over the receiver passband. The aliased spectrum in the range $0 < f < f_{samp/2}$ is therefore the sum of the RC filter response and its copy at f_{samp}:

$$V(f) = \frac{1}{1+f/B_{3dB}} + \frac{1}{\frac{1+2B_{3dB}-f}{B_{3dB}}} \qquad 7.6$$

giving:

$$V(f) = \frac{4}{3+\frac{2f}{B_{3dB}}-\left(\frac{f}{B_{3dB}}\right)^2} \qquad 7.7$$

Calculated values of this expression show that the maximum error is only 1.2dB and occurs at 0Hz. The error falls to 0dB at 2Hz (we are adding two values with 3dB attenuation) and is negligible (< 0.05dB) for a large region surrounding this point. Our choice of an RC filter with $f_{samp} = 2B_{3dB}$ thus has the interesting property of preserving the flat noise level near the edges of the spectrum (this would otherwise have been 3dB down). This property is noticeable in the measured spectra (chapter 8) and proved very useful for the estimation of background noise levels from the spectra.

The filter calculations are performed in double precision as the multiplicaton of two n bit quantities produces, in general, a 2n bit result. Rounding this value back to single precision by retaining only the higher order word can introduce round-off errors as some intermediate values in the filter calculation can be very small quantities. For example if A is close to 1.0 (a typical value is 0.8) and the A-D values are small $(1-A)x_i$ may lie entirely within the low order word of the multiplier output. The double precision filter output values are rounded back to single precision on transfer to the magtape buffer as we expect the filtered values to be of the same order of magnitude as the original A-D samples.

(3) Data file format.

Data from one run consists of a filtered Doppler time series from each of the ranges sampled. Each run is stored as a seperate file consisting of a sequence of 314 word magtape blocks. The Algol program opens this file by writing a beginning of file (BOF) block containing a complete set of information on the run. The Algol program then calls the machine code data collecting program which writes the sequence of data blocks in the manner described previously. Upon completion of the run the Algol program writes an end of file (EOF) block which may contain comments typed in by the operator. In this way any notes about, for example, unusual conditions during the run are permanently stored with the run data and are automatically written out by the mainframe data processing programs. This proved to be an extremely useful feature.

All blocks start with a common header consisting of a start title ("BIRDLING" in 6 bit stripped ASCII characters), a block number and a time stamp giving the date and time of the start of the run. The start title is used to synchronise the reading of data within a magtape block. Sometimes a few stray bits can be written or read at the start of each block thus an erroneous value may result if, for example, a program expects to find the block number 4 words from the start of the block. This problem is solved by the program looking for the start

title "BIRDLING" and counting words from this point on. The block number is used to indicate the type of a block as well as to count blocks. Thus a block number of 0 indicates a BOF block and the start of a new run on the 7 track tape while a block number of -1 indicates an EOF block. Data blocks are numbered 1 to the maximum number of blocks as indicated by the BOF block. The time stamp is used to uniquely identify a given run. When the file is converted to a B6930 file for permanent storage this time stamp is incorporated into the filename, e.g. TSDATA/1984/11/27/1722. The date and time are written in the strict high to low order sequence year/month/day/hour:minute to avoid the confusion that exists, on our computers, between British and American conventions for writing dates.

(4) Mainframe programs.

Mainframe software consists of three programs. The first of these is a Prime Pascal program that transfers the 7 track data to 9 track magtape. The resulting 9 track tape is then read on the B6930 by the Burroughs extended Algol program MTPROCESS. This program converts the data into the B6930 compatible TSDATA/= files for permanent storage. A substantial amount of error checking is performed by this program as the 7 track transfer between the PDP-8 and the Prime is a weak link in our system: Both the PDP-8 and Prime 7 track magtape systems

are known to cause errors. MTPROCESS must also allow for the possibility of incomplete runs or old runs partly overwritten by new runs existing on the tape. As MTPROCESS reads each block it accomplishes these tasks by applying a number of rules, in the form of IF...THEN...ELSE statements, to decide its future course of action. These rules may be easily updated if new error conditions are discovered in the future.

The final program, DPSPECTRUM (written in Burroughs exended Algol), accepts the TSDATA/= files as input and computes the Doppler spectrum of each time series in the manner discussed in chapter 3. In other words each time series is broken into a number of segments each overlapping by 50% with its neighbours. The segments are then multiplied by one of a number of data windows and operated on by a fast Fourier transform routine. The transforms of all the segments are then averaged together to produce the final sea echo Doppler spectrum which is output on an X-Y plotter. Selected spectra may be saved as disk or magtape files.

CHAPTER 8:

RESULTS, CONCLUSIONS AND SUGGESTIONS FOR FURTHER WORK

8.1 RESULTS

In this chapter we discuss a selection of spectra obtained with our system and suggest some topics for further research. The discussion of the results obtained proceeds firstly from the point of view of the performance of the system. We then discuss, in a semi-quantitative manner, the oceanographic features of the Doppler spectra. Even though the reduction of radar data beyond the point of Doppler spectra was not a primary aim of this work such a discussion is nevertheless worthwhile as an illustration of the variety of oceanographic information that can be extracted from sea echo Doppler spectra.

A selection of sea echo Doppler spectra measured with our system is shown in fig 8.3. These spectra are comparable to those published by other workers (e.g. JOHNSTONE,1975; SHEARMAN,1981; BARRICK and LIPA, 1979) and are a significant improvement over those obtained by prototype versions of the system. The main improvement is a reduction in background noise level from 30-40dB to a minimum value of 11dB. This reduction is a result of the higher prf allowed by the new data processing system. As predicted the noise level is flat to the edges of the spectrum at +2Hz and -2Hz rather than being 3dB down at these frequencies. This is due to partial aliasing of the digital filter response (see chapter 7). The minimum noise

level of 11dB is obtained only under quiet conditions and at ranges greater than or equal to 20km. At closer ranges the noise level increases to as much as 30dB. This is probably the result of the receiver failing to recover from the effects of the transmitted pulse. Fortunately, at these ranges the signal strength is high enough to overcome the effects of this additional noise. Additional background noise due to lightning and CB radio transmissions is also evident in some of the spectra. Man-made radio transmissions sometimes appear as a "hump" in the noise level about 0.5-1Hz wide - this indicates a single frequency of high stability (i.e. an unmodulated carrier) which has been aliased down into the spectrum from somewhere within the 100kHz receiver passband.

Artifacts near 0Hz Doppler shift are common in the spectra. These are often attributed to echoes from stationary targets such as land and surrounding hills etc. (TYLER et. al. 1972). In our case this explanation is unlikely for the following reasons: a) The artifacts have considerable width and structure. Land echoes would be single lines with width determined by the spectral resolution of the system (approx. 0.01Hz). In the time domain such an echo would appear as a constant dc level and would therefore be removed when the spectral analysis program subtracts the average from each data segment. b) The strength of these artifacts does not appear to depend

on range in any reasonable manner. The artifact varies considerably from run to run and is often seen at ranges from which no sea echo is observed. When these points are considered the most likely explanation for the artifact is long term drift in the receiver offset voltage. This could be reduced by removing linear trends, as well as average values, from the time series data segments. Improved receiver output stages would achieve the same effect.

Further artifacts in the spectra are small peaks at ± 1.05Hz. These are second harmonics of the Bragg peaks at ± 0.524Hz. These harmonics are due to non-linearities in receiver response and appear above the noise level when the Bragg peaks exceed 50dB. When the Bragg peaks reach 60dB third harmonics at ± 1.57Hz become visible. The second harmonic peaks are typically 25dB down from the main Bragg peaks. From this figure we can estimate the total harmonic distortion figure of the receiver as 0.25%. Since this is a reasonable figure the presence of second harmonics is more a reflection of the sensitivity of the spectral analysis technique than an indication of poor receiver performance. When the receiver gain measurements were made (chapter 5) no deviations from linearity could be detected in the receiver response.

In chapter 3 it was mentioned that selection of data windows for spectral analysis almost always involves a

trade-off between various aspects of performance. For instance a window giving high frequency resolution will probably have high sidelobe levels and vice versa. In figs. 8.3 i,j we compare two windows at the extremes of this trade-off range by using them to analyse the same data record. The Cooley, Welch and Lewis (Reisz) window preserves frequency resolution and peak spectral density (B = 1.2/T- chapter 3) but has rather high sidelobe levels with the highest sidelobe level being only 21dB below the peak. On the other hand the minimum 4-sample Blackman-Harris window has extremely low sidelobe levels (91dB below the peak) but degrades frequency resolution by a factor of two (B = 2/T). The difference between these windows, while noticeable, is not great. We conclude the choice of data windows for our application is not critical. LIPA and BARRICK (1983) discuss an application for which the choice of data windows is critical. In the inversion of waveheight spectra from second order spectra low sidelobe levels are very important and require the use of the Blackman-Harris window. The major difference between the spectra is the increased smoothness and loss of fine detail due to the lower resolution of the Blackman-Harris window. The amplitudes and heights of the Bragg peaks are not affected as they are already broadened considerably from the value determined by coherent integration time and thus appear as narrow band noise-like signals to the windows. The fact that no noticeable sidelobes are present in either spectrum shows that the

sidelobe level of the Cooley, Welch and Lewis window is acceptable for our purposes. We expect this as even under calm conditions peak second order spectral densities are about 15dB down from the Bragg peaks. Sidelobes would be visible in the spectra if a rectangular window was used (-13dB sidelobes).

From the point of view of oceanography our spectra show all of the features mentioned in the literature. In particular we have:

(1) First order Bragg peaks. These are always visible and, at 26MHz, are of relatively constant total power. The relative difference in strength between the advancing and receding Bragg peaks in all cases correctly corresponded to the component of wind velocity in the radar beam direction. For most of our measurements this wind component was onshore. Offshore winds are relatively rare due to the shielding effects of the hills of Banks Peninsula.

(2) Second order echoes were again almost always present at 26MHz but, in contrast to the first order echoes, their total energy was strongly dependant on sea state, wind speed and wind direction. No second order echoes were observed at 2.4MHz.

(3) The peaks at $2^{1/2}\,\omega_B$ and $2^{3/4}\,\omega_B$ in the second order spectrum were observed in most of the 26MHz spectra, although the $2^{1/2}\,\omega_B$ peak often appears only as a discontinuity in the overall second order continuum.

(4) Effects due to current induced Doppler shifts were very noticeable in the 26MHz spectra. These were most readily seen as a splitting of the first order echoes into multiple peaks at about 20km range. In addition current effects are the most likely explanation for the broadening of the Bragg peaks from their 0.01Hz theoretical widths. This can be illustrated by means of a simple model. Firstly the assumption that current induced Doppler shifts have broadened the Bragg peaks implies that the current pattern must produce a continuous range of radial velocity components within the radar resolution cell. Secondly we note that the peaks of the broadened first order spectra are not noticeably shifted from their theoretical positions (during calm weather). This means that in the beam maximum direction the radial component of current velocity must be close to zero and the current must therefore flow perpendicular to the radar beam maximum direction. The predominant current off the Canterbury coast flows from the south to the north approximately parallel to the coast (KIRK 1983 private communication). It is likely, therefore, that in the

vicinity of Birdlings Flat (see fig. 5.1) the current is approximately perpendicular to the radar beam direction. Our simple model for this situation is illustrated in fig. 8.1 (a). We assume that a uniform current with constant velocity, v_c , and constant direction perpendicular to the beam maximum, exists throughout the radar resolution cell. The projection of this current velocity vector onto the various radial directions from the radar produces the continuous range of Doppler shifts:

$$-\frac{2f}{c} v_c \sin(\theta_B/2) \text{ to } +\frac{2f}{c} v_c \sin(\theta/2) \qquad 8.1$$

Where θ_B is the beamwidth. We can thus estimate the current velocity from the broadening of the first order peaks. Using the nominal beamwidth of 15 degrees gives 1m/s for the current velocity. This agrees with typical values measured by ships in this region. (KIRK 1983 private comunication). However precise measurements of the antenna beam patterns would be neccessary in order to obtain accurate and reliable current measurements using this technique. Alternatively the direction of arrival of various parts of the first order spectrum could be measured by the standard technique of multiple, spaced receiving antennas (see e.g. BARRICK et. al. 1977). The present system could easily be set up to do this.The existence of a more complicated line structure in the

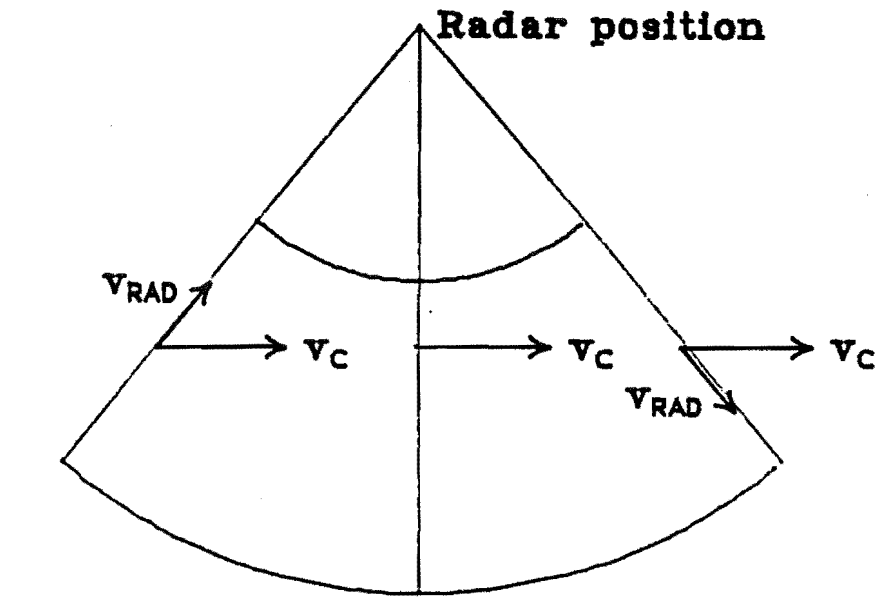

(a) Cross-beam current

(b) Head-on current

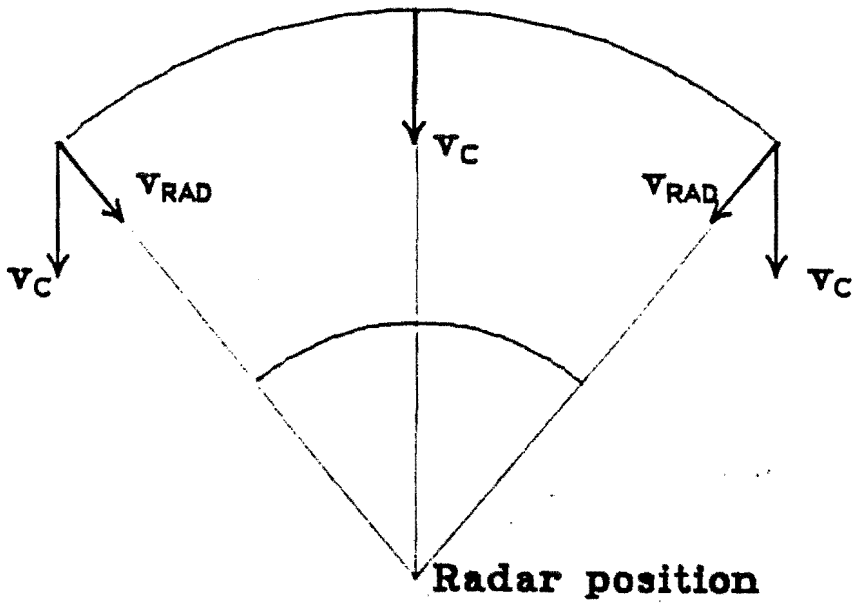

Fig. 8.1 Current broadening of Bragg lines by the variation in the radial component of the current velocity across the radar resolution cell.

first order spectrum near 20km indicates that this simple model has broken down due to a different current pattern. Here we are probably observing the current turning outwards around Banks peninsula. This is supported by the fact that the new peaks are shifted down in frequency indicating a large mass of water with a velocity component away from the radar.

It is interesting to compare results measured under calm conditions (e.g. 1983/11/25) with those taken during a storm (1983/12/14). The wind for the 1983/11/25 results was a light onshore sea breeze with strength not more than about 1m/s. The storm on 1983/12/14 followed the passage of a cold front at 1330 NZST and was accompanied by gale force southerly winds with speeds estimated to be of the order of 20m/s. The first point to note is the high degree of asymmetry between advancing and receding Doppler shifts in the storm spectra. This is to be expected given a wind/wave direction 180 degrees to the radar beam. The presence of a receding Bragg peak indicates that there is still some wave energy propagating in the upwind direction. Interestingly, this upwind Bragg peak is smaller than its associated second order peak. The spectra recorded under calm conditions show a more symmetrical distribution of energy between positive and negative Doppler shifts, with the larger amplitude of the $\pm \omega_B$ Bragg peak indicating an onshore wind component.

In all storm spectra both Bragg peaks are shifted 0.07Hz higher in frequency than the Bragg frequencies. This is in contrast to the calm results in which the Bragg peaks were at their theoretical positions. The radial component of current velocity corresponding to this Doppler shift was calculated to be 0.4m/s. This current is probably generated by the wind. The Bragg peaks are also broadened to about 0.1Hz which is twice the value observed under calm conditions (0.05Hz). We have seen previously that the broadening of the Bragg peaks is consistent with a simple model in which a uniform current flows at 90 degrees to the radar beam direction. We can extend this model to the storm case by considering a uniform current flowing directly towards the radar (fig. 8.1b). In this case the model predicts an asymmetrical peak with a maximum (corresponding to the radar beam maximum) having the greatest Doppler shift, $2fv_c/C$, from the Bragg frequency. Away from the beam maximum direction the echo strength, and Doppler shift from the Bragg frequency, are progressively reduced until at the edges of the beam the Doppler shift is:

$$f - f_B = \frac{2f}{c} v_c \cos(\theta_B/2) \qquad 8.2$$

The advancing first order peaks from the storm spectra show asymmetrical features of precisely this form. These features, however, contribute only a small fraction (approximately 0.06Hz) of the total broadening observed, indicating that other processes, such as turbulence in the current field, contribute to the overall width of the peaks.

We now consider the second order parts of these spectra. The predominant second order echoes observed under calm conditions are narrow band peaks surrounding each Bragg peak. The frequencies of these peaks imply a modulation period of about 10 seconds. Given the low windspeed this is likely to be well below the cutoff frequency of the locally generated wind/wave spectrum. We therefore interpret these peaks as being due to swell from distant storms. Applying the methods outlined in chapter 4 we calculate the period of the swell to be 10 seconds and its direction to be ± 140 degrees to the radar beam direction. The swell propagation direction is thus either 40 degrees or 320 degrees with respect to north. Two radar beams would be neccessary to resolve this ambiguity. In addition to these swell peaks there are further second order echoes present in the region near 0Hz between the Bragg peaks. These are probably due to the local wind generated sea.

In contrast the second order echoes from the storm spectra are broad-band and contain considerable energy indicating a high sea state. In addition there is considerable asymmetry in the second order spectra with advancing Doppler shifts having much greater energy than receding Doppler shifts. This is consistent with the existence of a high wind speed in a direction close to 180 degrees to the radar beam. The period of the wave components at the cutoff frequency of the ocean waveheight spectrum was estimated from the second order spectra to be 5-7 seconds showing that at the time of measurement (1410 NZST) the spectrum had not had time to develop to equilibrium with the wind. We note also that the $\omega_B^{1/2}$ and $\omega_B^{3/4}$ peaks have been shifted upwards in frequency by the same amount as the first order Bragg peaks (0.07Hz). This is to be expected as the current will increase the radial components of the phase velocity of all ocean wave components by the same amount (although longer wave components are more sensitive to current velocities at greater depths beneath the surface).

8.2 SUGGESTIONS FOR FURTHER WORK

The primary aim of this work has been the development of a ground wave pulsed Doppler radar system for the remote sensing of ocean surface conditions. The results presented in this chapter demonstrate that this aim has been achieved in that a system has been developed which has the potential to gather large quantities of oceanographic information from a large area of the sea surface. The obvious extension to this work is the further analysis of the Doppler spectra to obtain this oceanographic information and the subsequent use of this information for oceanographic research. In addition more work needs to be done on the ground wave propagation problem. In particular we need to understand the role played by the Millington recovery and converse effects in this problem. We conclude this chapter by discussing some other interesting topics for further research:

(1) Other systems. Our system was designed as an initial investigation and was required to be flexible and easily integrated into the existing Birdlings Flat system. As outlined in chapters 5 and 7 design decisions for this system were made largely as a consequence of this philosophy. However other, future systems - especialy those dedicated to some particular oceanographic experiment - could benefit from the use of different

techniques and design parameters. For instance if high range resolution is not required the receiver bandwidth could be substantially reduced (e.g. to as little as 15kHz) to improve signal to noise ratios. A further benefit would come from optimising the antenna beam patterns. In other words the transmit pattern would be matched to the physics and geometry of the particular experiment then the receiving array pattern matched to the transmit pattern. The digital filter algorithm for this system was chosen to give flat, predictable noise levels near the spectrum edges. This property was required for the radar performance measurements of chapter 6. A system not requiring this property could use the simpler filtering scheme of averaging groups of received pulses. The time consuming multiplication operations would thus be eliminated. Some degree of portability would be a desirable feature of any future system. This would be acheived by building a microcomputer based stand-alone system. The operation of such a system could be made much more convenient by using the microcomputer to perform the spectral analysis of the echo time series in close to real time. In this way rapid feedback on system performance and sea conditions could be obtained. A further advantage of performing spectral analysis on the microcomputer is a reduction in data storage space by a factor equal to the number of segments averaged to produce the final spectrum (about 10). In a microcomputer environment this is important if data are to be stored on floppy disks at some

stage in the analysis process. For a system with the performance described below approximately 80KB of storage will be required for the raw time series data from one run. This is a substantial fraction of the size of a typical 5-1/4 inch floppy disk (140KB). Processing of this data to the stage of the final, incoherently averaged Doppler spectra (approximately 8KB of storage) will thus be a much more convenient route to follow with a floppy disk based system.

The use of a microcomputer to do the digital filtering presents some immediate problems, however. Firstly we note that any system not subject to our propagation problem will have a maximum range in the vicinity of 100km and will therefore generate about 10 complex range samples for each transmitted pulse. Secondly we have noted that the optimum prf for an upper hf system is of the order of 2kHz. The computer has, therefore, only 500us in which to retrieve 20 samples from the A-D convertor buffer, perform the filter algorithm on each of these samples and, if neccessary, transfer the filter outputs to a magtape or output buffer. A detailed consideration of the steps required to perform these tasks reveals that approximately 200-300 machine code instructions would have to be excecuted during this 500us period. This is at the absolute limit of performance of most currently available microprocessors. (A discussion of

the performance of various microprocessors for digital filtering may be found in WITWORTH, 1984). It is, therefore, probable that dedicated hardware will have to be used for digital filtering once this level of performance is approached. A possible scheme is to use an external RAM buffer as in the fast A-D system. Instead of loading the A-D samples directly into this buffer hardware between the A-Ds and the buffer would add each A-D sample to the contents of its corresponding RAM memory location. About once every 250ms the computer would read the accumulated sums from the RAM buffer and zero the buffer ready for the next set of averages. This would leave the computer with the relatively easy task of transfering samples at a 4Hz rate.

A further problem arises if the spectral analysis is to be performed by the microcomputer. The fast Fourier transform algorithm requires data to be scaled at regular intervals to prevent intermediate values in the calculation overflowing the computer's word size. This scaling introduces round-off error that appears as additional noise in the final spectrum. On the basis of the typical signal to noise ratios that we have observed and a discussion of this problem given by COOPER (1977) it appears that a word size of at least 16 bits will be required in order to ensure that the spectra are not degraded by FFT round-off error. On an 8 bit machine the

FFT will therefore have to be computed in double precision at considerable cost in program development and execution time. The performance advantage of 16 bit over 8 bit machines is highlighted further by the fact that most of the new 16 bit machines have built-in hardware for performing the time consuming multiplication operations whereas most 8 bit machines do not.

We summarise this section by making the following observations about stand-alone microcomputer based systems:

(1) The technique used in this work of storing data in the form of raw time series is likely to be inconvenient if access to a mass storage device, such as a hard disk or a magtape drive, is not available.

(2) While it is possible to develop a radar system based on an 8 bit microcomputer the advantages of using 16 bit machines (e.g. DEC LSI-11/23, Motorola 68000) will probably outweigh their extra cost.

(3) Hardware digital filtering will be required if prfs approaching the range ambiguity limit (2kHz) are envisaged.

(2) Ionospheric propagation. In this work ground wave propagation was used in favour of ionospheric propagation due to its simplicity and the higher quality Doppler spectra that it provides. In the ionospheric propagation technique (e.g. SHEARMAN 1983, MARESCA 1979) sea echo Doppler spectra are obtained by reflection of the radar beam off ionized layers at altitudes of 100-400km in the earth's atmosphere. Even though some contamination of the Doppler spectra results from the movement of these layers the range of the radar is increased to as much as 3000km. The result of this is that wind speeds and directions and wave properties may be measured over very large areas of the ocean's surface - a region where it is difficult to get wind measurements by other means. Skywave radar oceanography could thus have an important impact on weather forecasting in countries, such as New Zealand, surrounded by large areas of ocean.

The system at Birdlings Flat could easily be extended to skywave operation by constructing appropriate antenna systems. In order to investigate this possibility further a simple hf ionosperic propagation program was written based on the work of FRICKER (1981). Our aim here is to obtain general results from a few typical ionospheric parameters rather than to obtain accurate hf propagation predictions. On 26MHz reflection is from the F region at a height of approximately 300km resulting in a maximum range

of 3200km. As any wave launched higher than about 12 degrees above horizontal will penetrate the layer without reflection there is also a minimum usable range which is 1900km. The maximum propagation loss is about 4dB higher than the free space loss due to absorption in the D region of the ionosphere. At 2.4MHz reflection is from the E region at a height of about 100km, although the F region can be used at night when the solar ultra-violet induced ionization of the E region decreases. During the day 2.4MHz is usualy below the penetration frequency of the E region so that all vertical beam angles, up to 90 degrees, can be used. D region absorption is much higher than at 26MHz and increases rapidly as the beam angle approaches horizontal. If we arbitrarily choose 60dB as the maximum tolerable absorption the range will be limited to about 400km by this effect. The geometrical range limit is 1600km due to the lower height of the E region. 26MHz is thus the preferred frequency for skywave operation at Birdlings Flat. No ionospherically propagated sea echoes were observed with our system during the course of this work although CB radio transmissions from the west coast of the United States were readily received. This is probably a result of the fact that the transmitting antenna does not have a narrow enough beam, in the vertical plane, for ionospheric work. This is supported by the observation of ionospherically propagated sea echoes by BAGGALEY (1983, private communication) using the meteor radar system. This system has a very high gain

transmitting antenna with a beam directed about 30 degrees above horizontal. The echoes were observed as a result of reflection of the beam from a sporadic E layer.

(3) The use of vhf (30-300MHz) frequencies. At present radar oceanography uses two regions of the electromagnetic spectrum: The hf region (3-30MHz), where scattering is by the first and second order Bragg mechanisms (chapter 4) and the uhf/microwave region (> 1GHz) where scattering is modelled by a two scale process in which scattering from short capillary waves is modulated by the longer gravity waves (BARRICK, 1972b; PLANT, 1977). Little use has been made of the intermediate vhf region. The most probable reason for this is the poor range available at vhf when compared with hf due to the strong frequency dependance of ground wave attenuation. In addition no reliable skywave propagation mode is available at vhf although KEYS (1983, private communication) has observed sea echo with a 50MHz auroral radar via sporadic E reflection. There are, however, many conceivable oceanographic studies that do not need data from long ranges and could therefore benefit from the advantages of higher frequencies. Examples are coastal erosion studies and the routine monitoring of sea state at present performed by visual observation. From a purely academic point of view it would be interesting to examine the transition from the Bragg scattering model to the

microwave two scale model that must occur somewhere within the vhf region.

There are several interesting advantages that come with the use of frequencies in the vhf region:

(1) Antennas at vhf are much smaller (a few metres) than those at hf (tens of metres). The size of antenna arrays is one of the major disadvantages of hf radar oceanography with several studies being aimed at producing more compact antenna systems (BARRICK et. al., 1977; BARRICK and LIPA, 1979a). Reduced antenna size will allow more portable equipment to be produced.

(2) In the region around 150MHz noise levels are the minimum observed anywhere within the radio part of the electromagnetic spectrum. At higher frequencies internal receiver noise increases while at lower frequencies external background noise increases. Typical noise temperatures given by ITT CORP. (1968) for 150MHz are 1500K for quiet conditions to 600,000K for noisy urban areas.

(3) The wide bandwidth available at vhf allows high spatial resolution to be obtained with short transmitted pulses. This is important in, for example, coastal erosion

and sediment transport studies where wave energy must be measured close in to the shore - preferably in to the surf zone.

(4) At vhf current induced Doppler shifts and second order effects will be larger than at hf and will therefore allow more accurate measurements to be made given the same coherent integration time.

(5) If the antennas are raised above ground level the field strength increases much more rapidly with height at vhf than at hf. The ground wave propagation mode consists of a surface wave (strongly attenuated at vhf) together with a direct wave and a ground reflected wave. At heights less than a wavelength above the surface the direct and reflected waves cancel leaving the surface wave whereas at heights of more than a wavelength this cancellation effect is reduced allowing direct line of sight propagation. Even though vhf will be much more susceptible to the propagation problems we have encountered it will be much easier to avoid these problems by using elevated antennas. This fact was experimentally verified during the construction of a 40MHz telemetry link for the meteor radar at Birdlings Flat. A large gain in field strength was obtained by raising the antennas for this system about 20m above ground on poles.

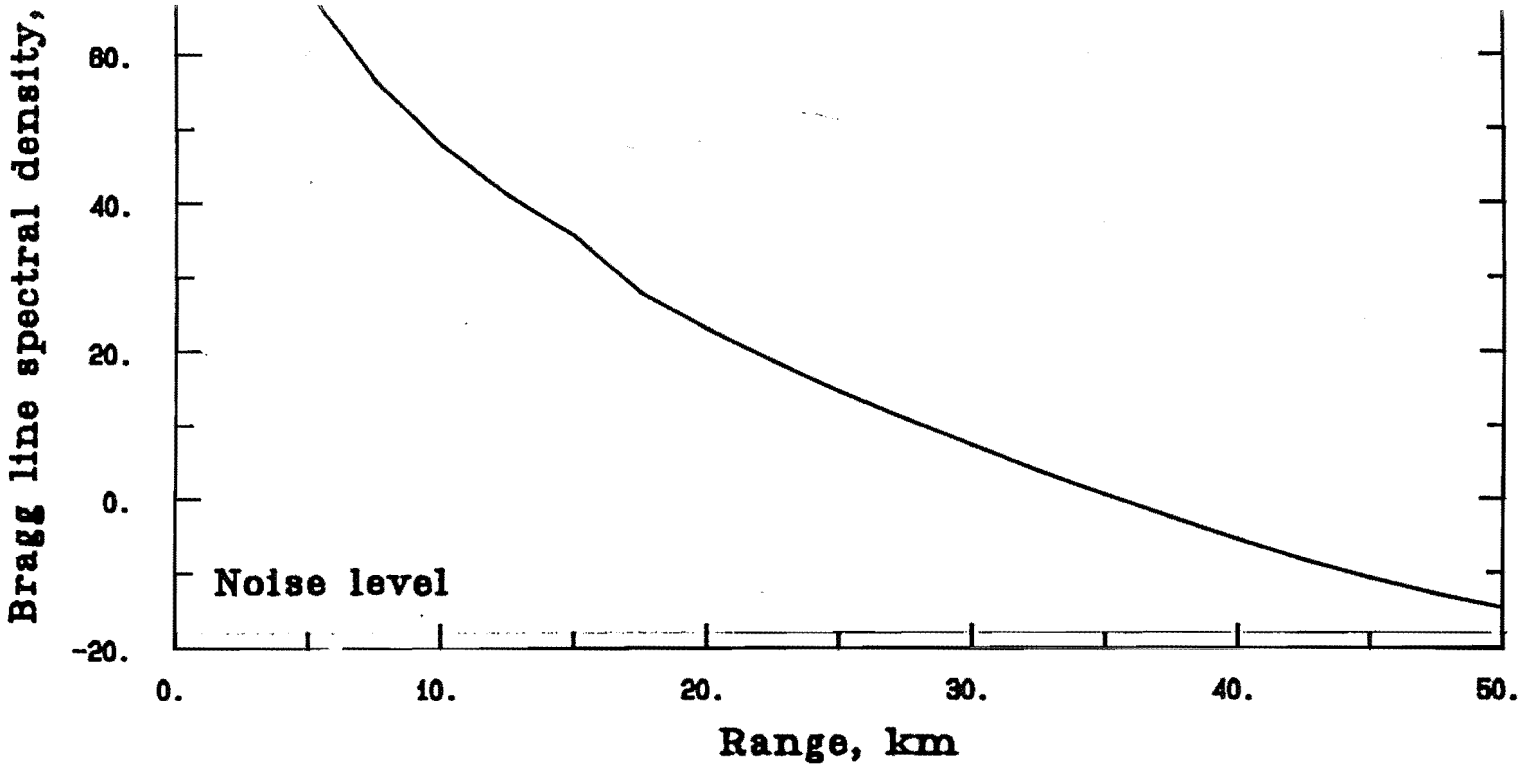

Radar frequency 150MHz	Transmitter power 5.0kW
TX antenna gain 10dB	RX antenna gain 10dB
Antenna heights 20m	Noise temperature 1500K
Pulsewidth 20us	Pulse repetition frequency 2000Hz
Bragg line width 0.2Hz	Receiver bandwidth 50kHz

Fig. 8.2 Performance of a typical vhf radar system.

The major disadvantage of the vhf region is, as we have mentioned, the poor range (about 30km - see fig. 8.2). However in some circumstances this may actually be an advantage as the high ground wave attenuation will help prevent mutual interference between the radar and other users of these frequencies.

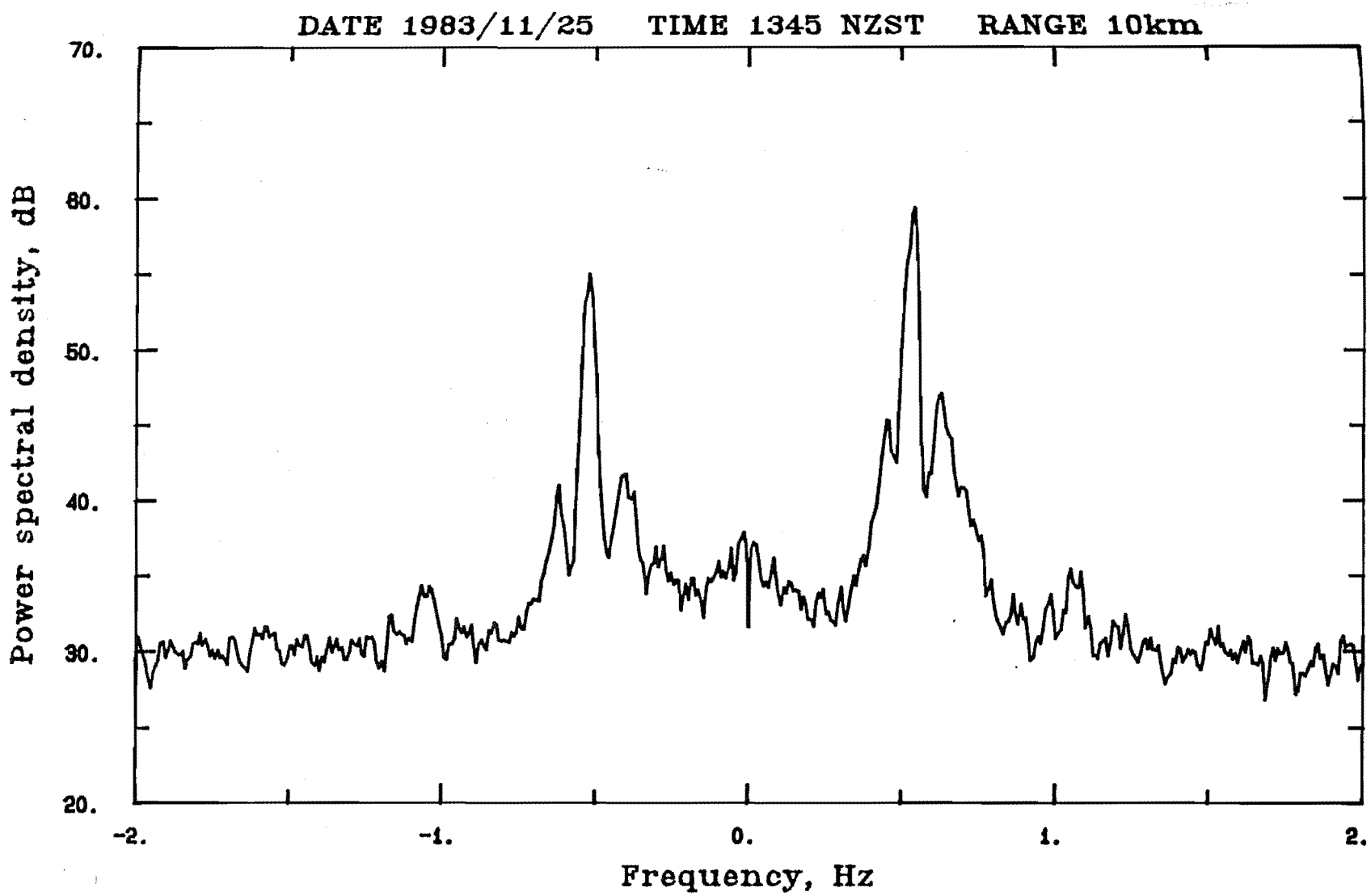

Fig. 8.3a Doppler spectrum of sea echo at 26MHz.
Calm conditions.

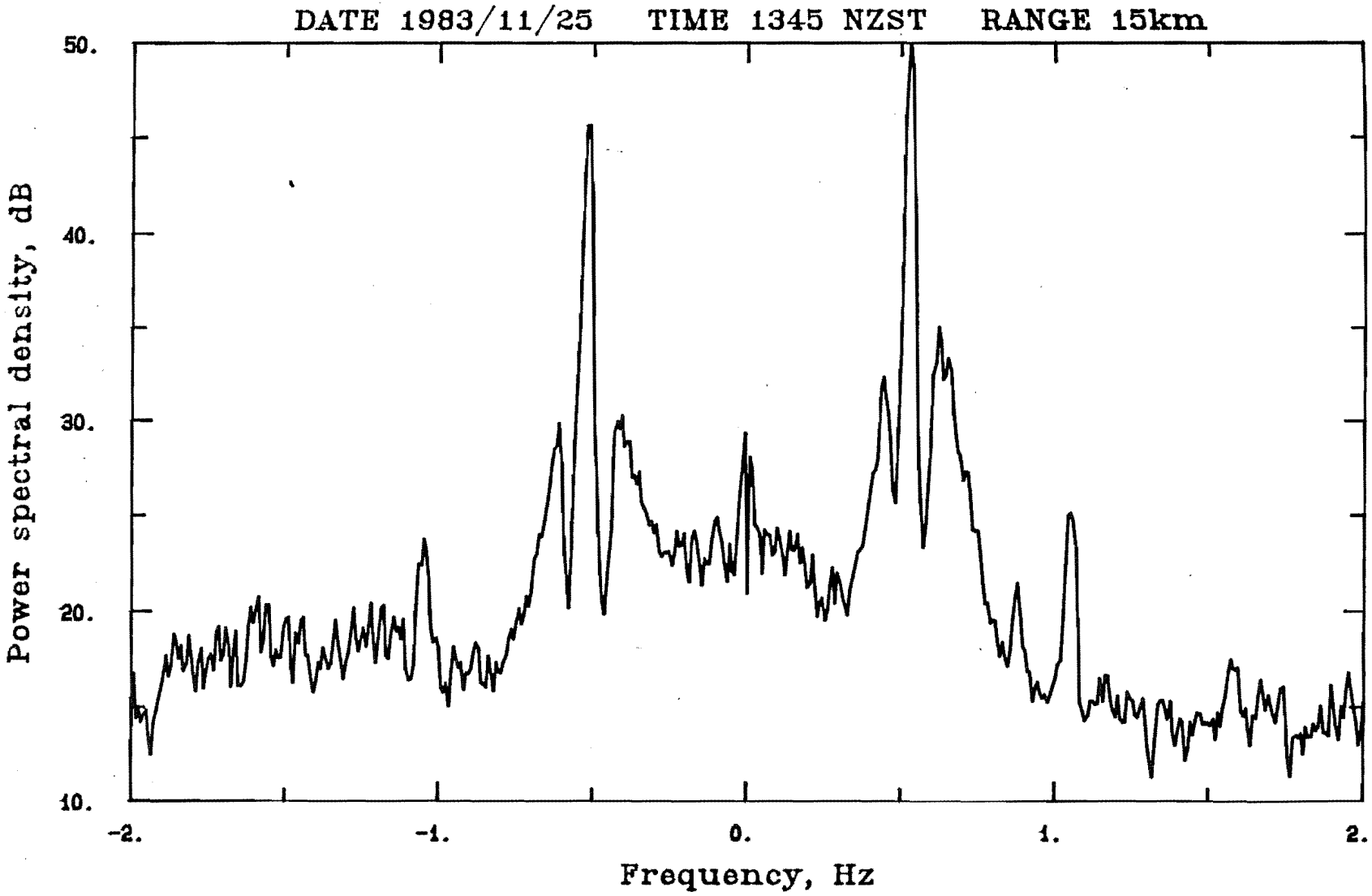

Fig. 8.3b Doppler spectrum of sea echo at 26MHz.
Calm conditions.

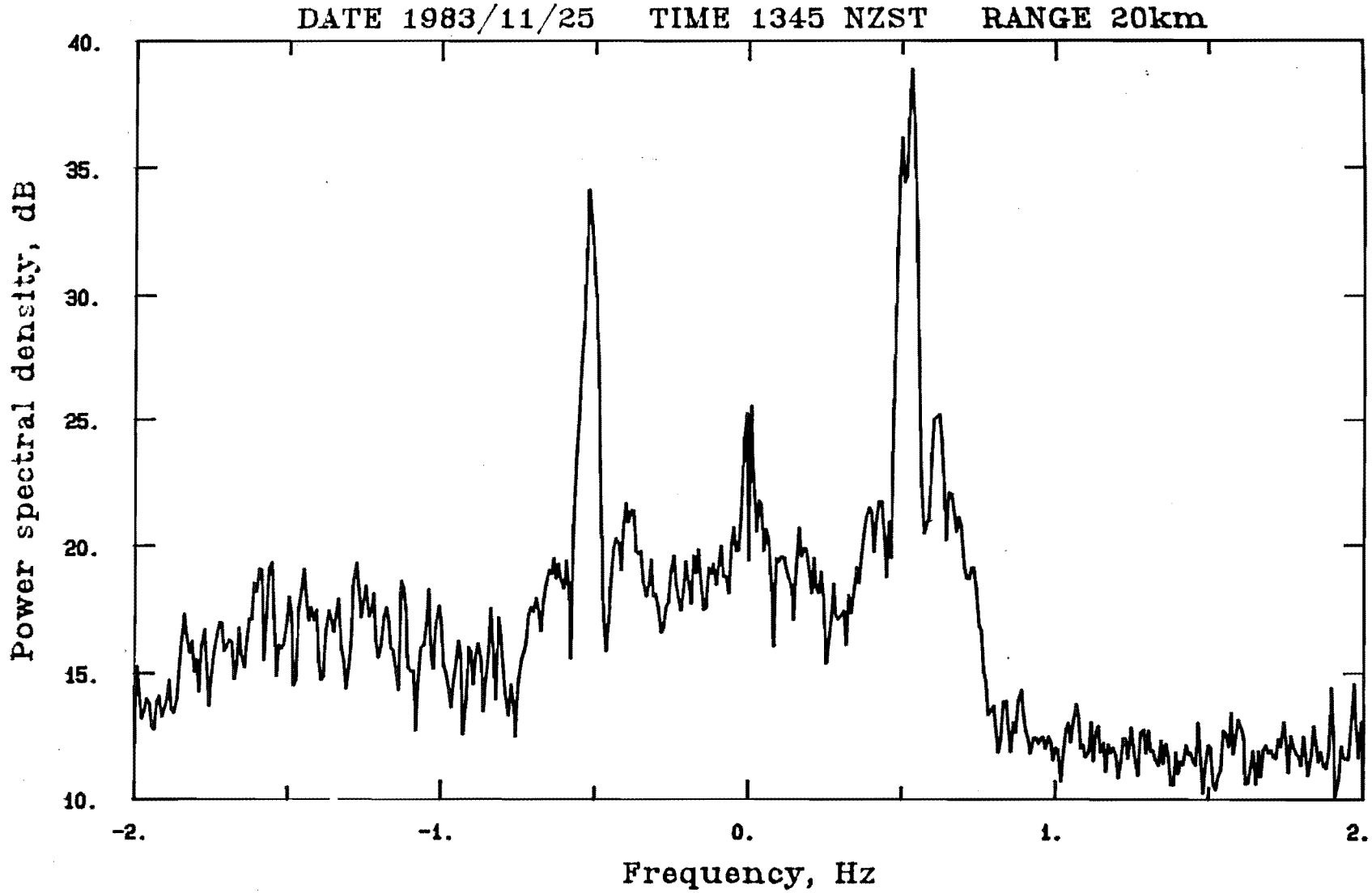

Fig. 8.3c Doppler spectrum of sea echo at 26MHz.
Narrow band interference.

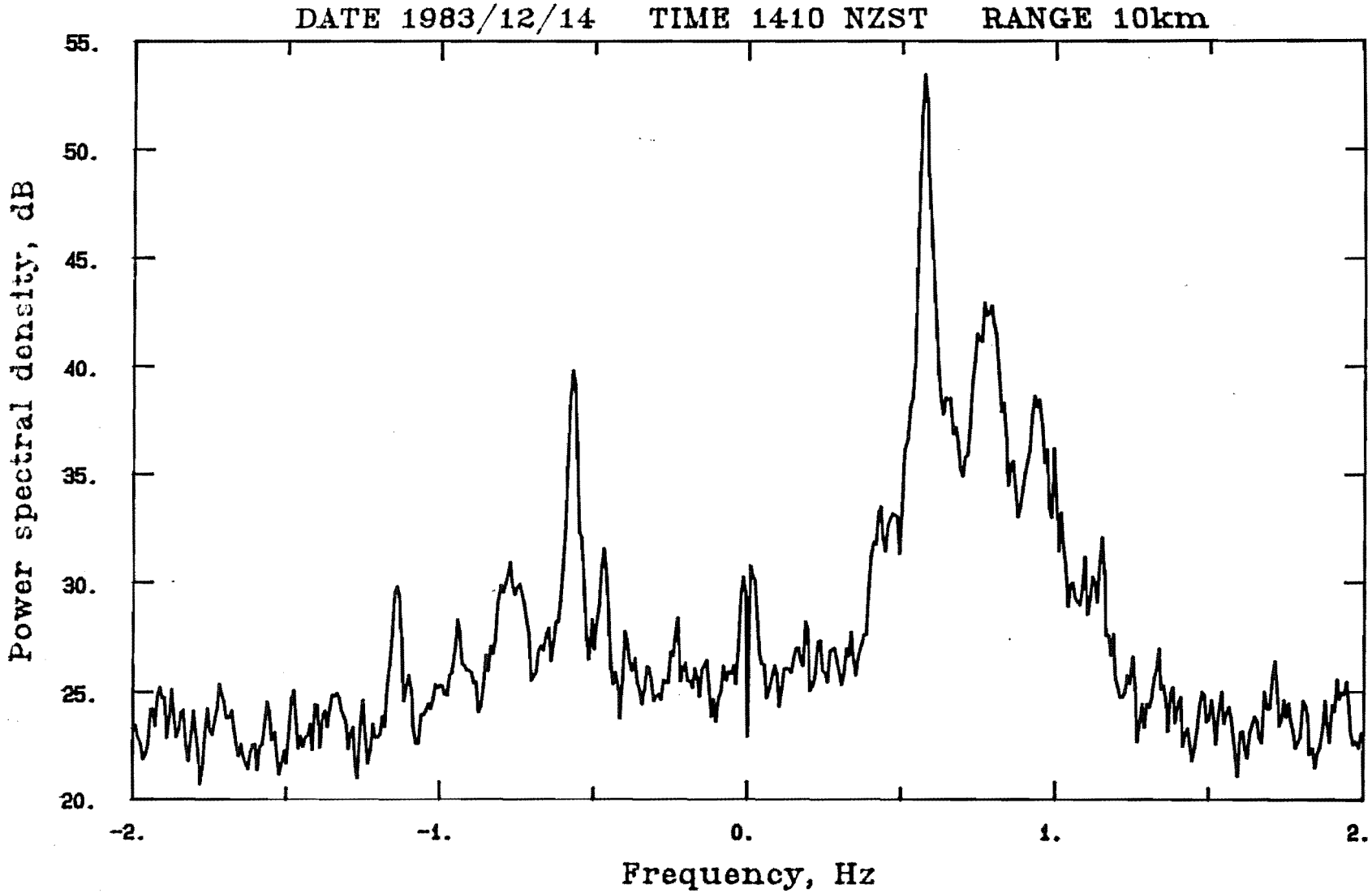

Fig. 8.3d Doppler spectrum of sea echo at 26MHz.
South westerly storm.

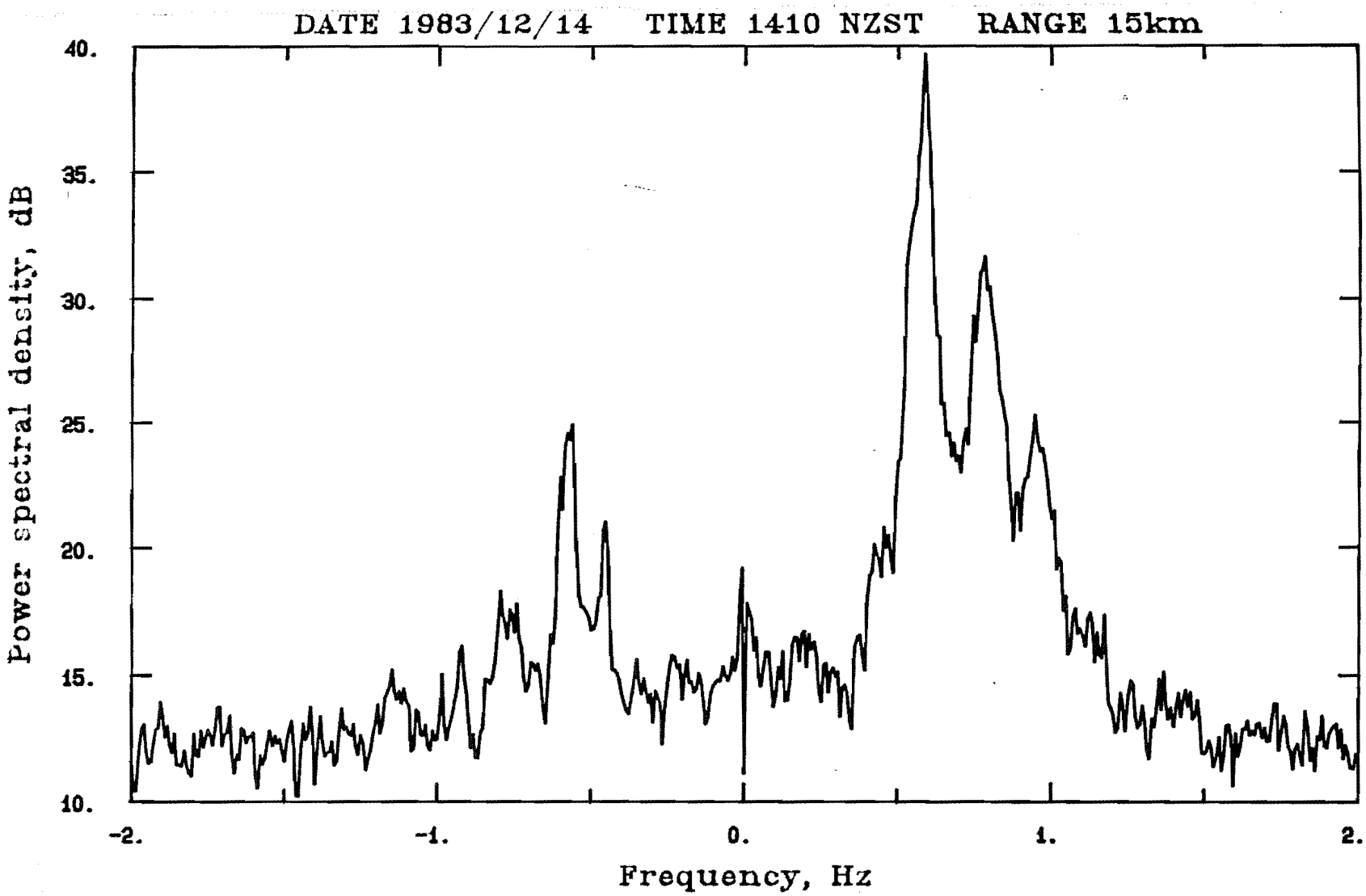

Fig. 8.3e Doppler spectrum of sea echo at 26MHz.
South westerly storm.

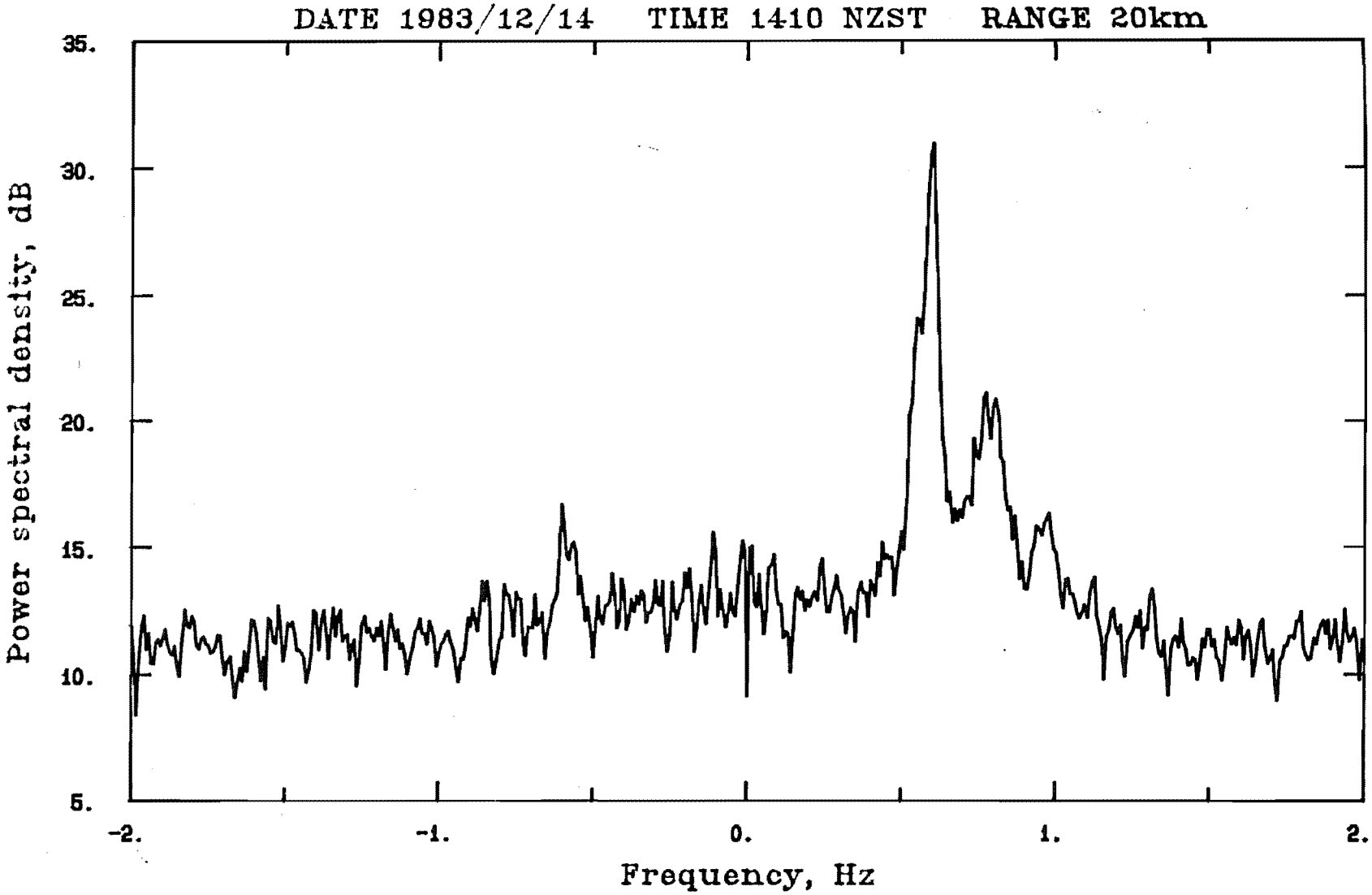

Fig. 8.3f Doppler spectrum of sea echo at 26MHz.
South westerly storm.

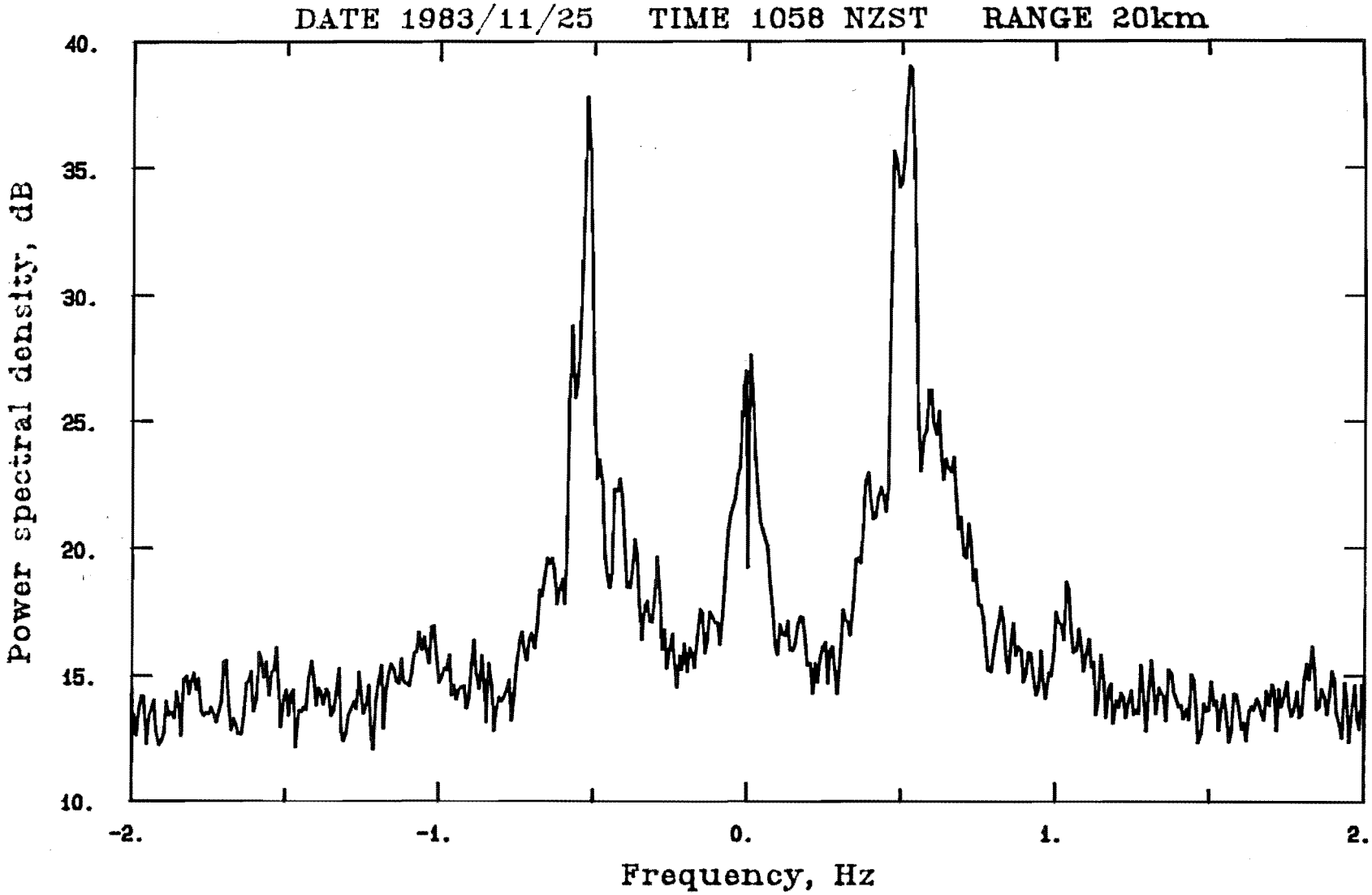

Fig. 8.3g Doppler spectrum of sea echo at 26MHz.
Bragg peaks split by current induced Doppler shifts.

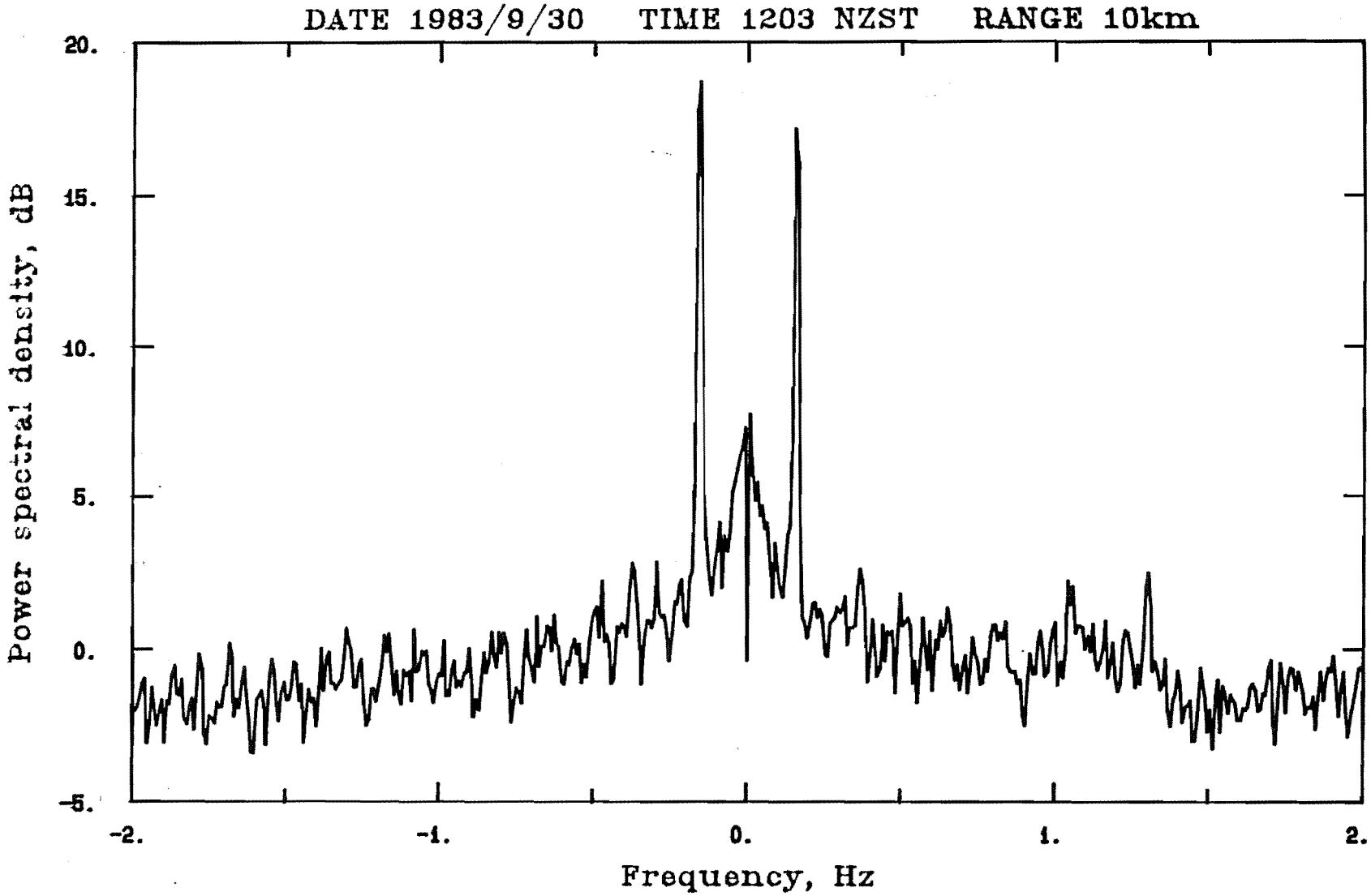

Fig. 8.3h Doppler spectrum of sea echo at 2.4MHz.

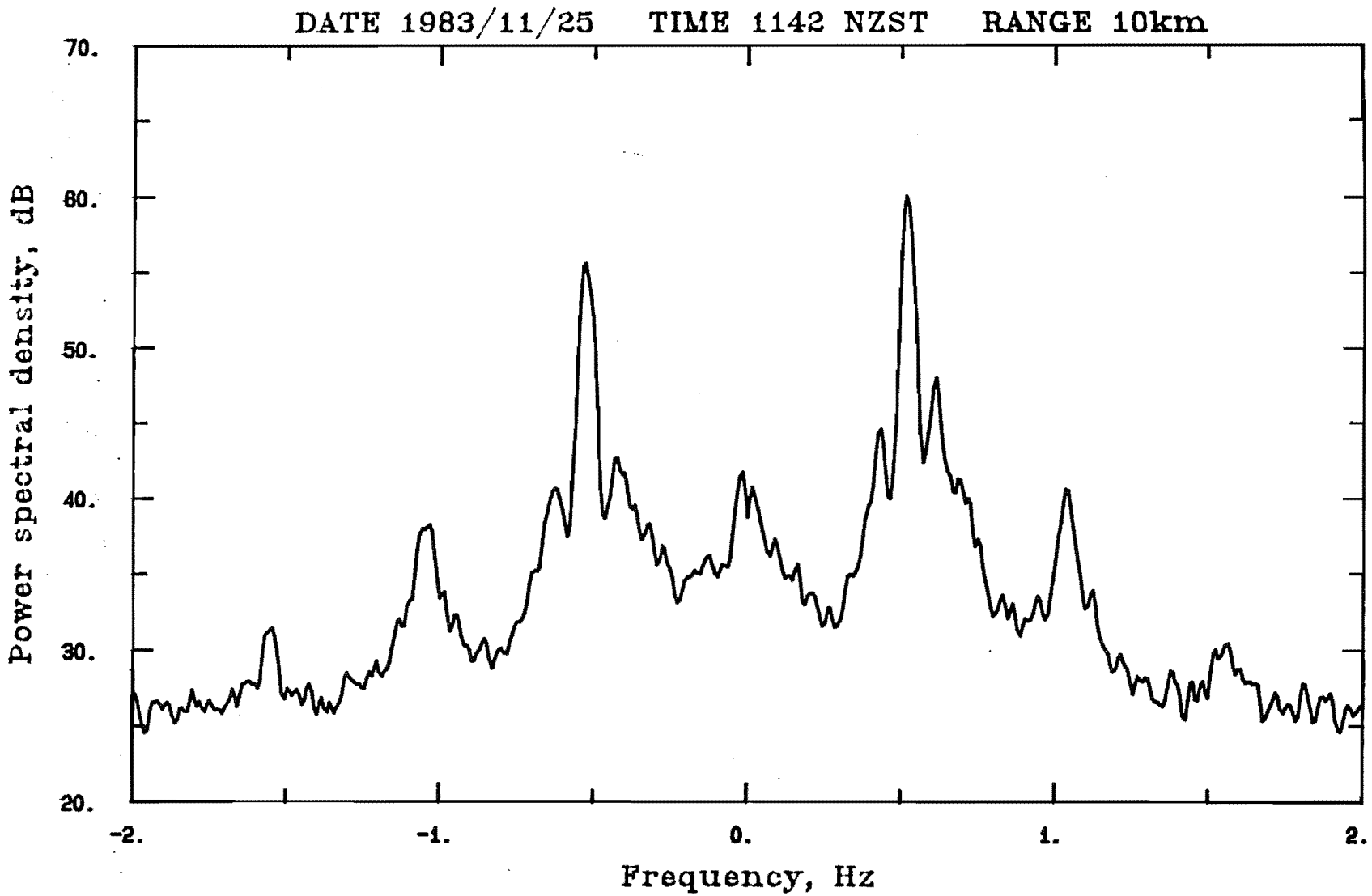

Fig. 8.3i Doppler spectrum of sea echo at 26MHz.
Analysed with Blackman Harris data window.

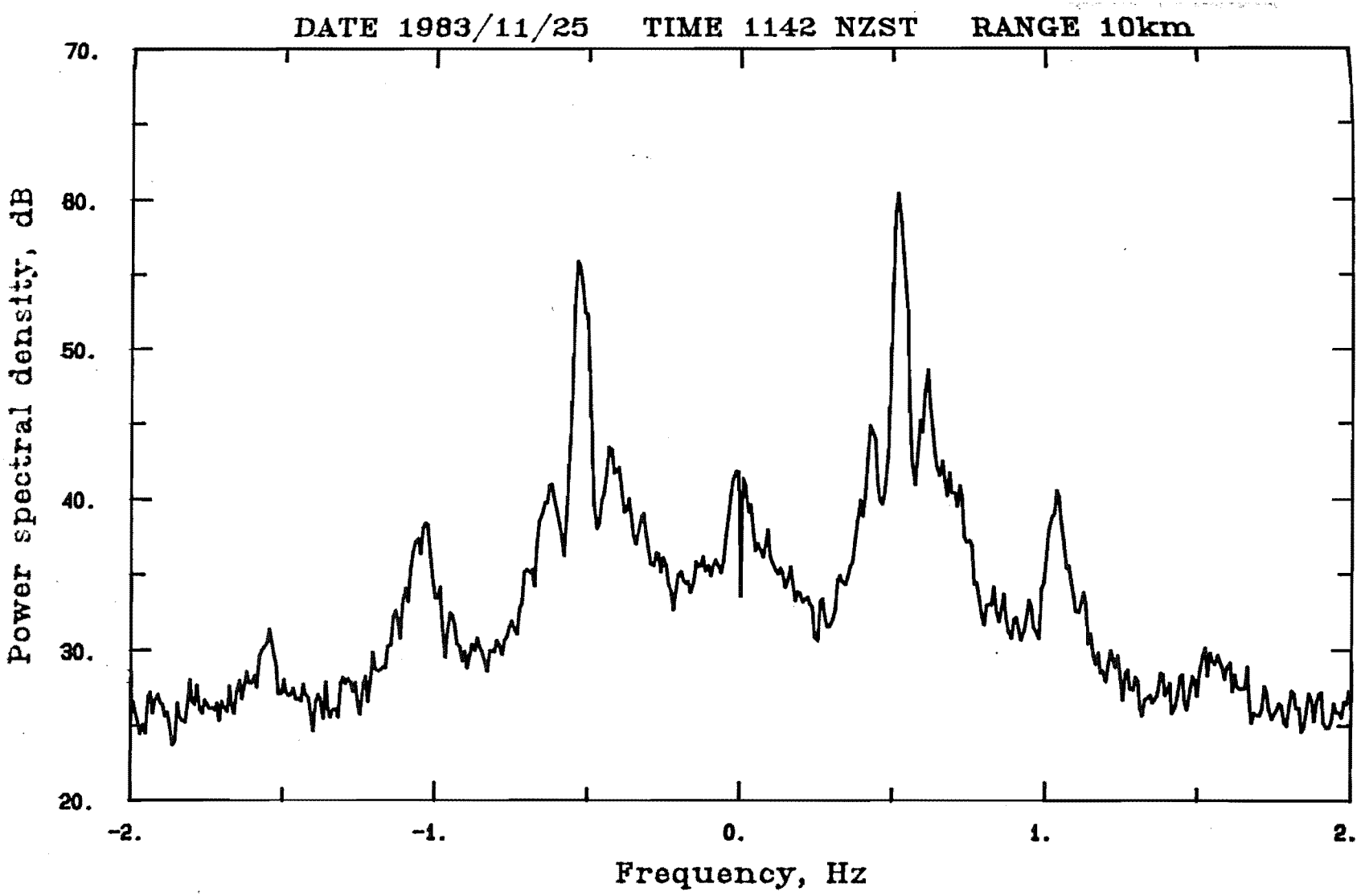

Fig. 8.3j Doppler spectrum of sea echo at 26MHz.
Analysed with Cooley, Welch and Lewis data window.

ACKNOWLEDGEMENTS

I would like to thank the following people for help given during the course of this work:

Professors A.G. McLellan and B.G. Wybourne for providing the opportunity and facilities to do this work and for financial support in the form of a teaching fellowship.

Dr. G.J. Fraser for his excellent supervision of this project.

Dr. R.G.T. Bennett for many helpful and entertaining discussions relating to this project.

Graham Lees for help with various aspects of the Birdlings Flat field station and for teaching me, over the years, to view computers in their correct perspective.

The electronics technicians, John de Voil and Greg Haslett for constucting the equipment and for helpful discussions concerning this equipment.

Mrs. B.Bristowe for typing those parts of the thesis (equations, Greek symbols etc.) unable to be dealt with by the word processing system.

Finally I would like to thank my family for their support and encouragement over the years.

John McGregor

May 1985

REFERENCES

ABBOT, R.H., 1980 : The role of Algol-60 in computer education. Computer Educ. no.35, p.24.

ANDERSEN,J.B.,1963: Reception of skywave signals near a coastline. J. Res. NBS. 67D, 325-330.

BARBER, N.F. and URSEL, F.,1948 : The generation and propagation of ocean waves and swell. I. Phil. Trans. Roy. Soc. A 240, 527-560.

BARRICK, D.E., 1971 : Theory of HF/VHF propagation across the rough sea, Parts I and II. Rad.Sci. 6, 517-533.

_____ 1972a: First order theory and analysis of MF/HF/VHF scatter from the sea. IEEE Trans. Ant. Prop. AP.20, 2-10.

_____ 1972b: Remote sensing of the sea state by radar. Ch.12 of Remote sensing of the troposphere, V.E. Derr (ed.). U.S. Government Printing Office,Washington, D.C. 20402.

_____ 1977a: Extraction of wave parameters from measured hf radar sea-echo Doppler spectra. Rad. Sci. 12, 415-424.

_____ 1977b: The ocean waveheight non-directional spectrum from inversion of the hf sea-echo Doppler spectrum. Remote sensing of Environment 6, 201-227.

_____ 1980: Accuracy of parameter extraction from sample-averaged sea-echo Doppler spectra. IEEE trans. Ant. Prop. AP-28, 1-11.

BARRICK, D.E. and EVANS, M.W., WEBER, B.L., 1977 : Ocean surface currents mapped by radar. Science 198, 138-144.

BARRICK, D.E. and LIPA, B.J., 1979a : A compact transportable hf radar system for directional coastal wave field measurements. P153-201 in Ocean Wave Climate, Earle and Malahoff (eds). Plenum Press, New York.

_____ 1979b : Ocean surface features observed by hf coastal ground-wave radars : A progress review. In: Ocean Wave Climate, Earle and Malahoff (eds).,p.129-152. Plenum Press, New York.

BARRICK, D.E. and PEAKE, W.H., 1968 : A review of scattering from surfaces with different roughness scales. Rad. Sci. 3, 865-868.

BARRICK, D.E. and SNIDER, J.B., 1977 : The statistics of hf sea-echo Doppler spectra. IEEE trans. Ant. Prop. AP-25, 19-28.

BARTON, D.K. (ed), 1977 : Radars. Vols. 1-7. Artech House Inc., Massachusetts.

BEVINGTON, P.R., 1969 : Data reduction and error analysis for the physical sciences. McGraw-Hill, New York.

BLACK, K.P. and HEALY, T., 1981 : Computer programs for wave analysis, wind wave generation, wave retraction diagrams and fast Fourier analysis. Occasional report no. 6, 1981, Dept. of Earth Sciences, University of Waikato.

BLACKMAN, R.B. and TUKEY, J.W., 1959 : The measurement of power spectra. Dover, N.Y.

BRACEWELL, R.N., 1965 : The Fourier transform and its applications. McGraw-Hill Inc., U.S.A.

BREMMER, H., 1949 : Terrestrial radio waves. Elsevier publishing Co. New York and Amsterdam.

BRUCE, E., 1931 : Developments in short-wave directive antennas. Proc. IRE 19, 1406-1433.

BURDIC, W.S., 1968 : Radar signal analysis. Prentice-Hall Inc.

CHILDERS, D.G.,1978: Modern spectrum analysis IEEE Press. Published by John Wiley and Sons, N.Y.

COOLEY, J.W. and TUKEY, J.W., 1965 : An algorithm for the machine calculation of complex Fourier series. Math. Comp. 19, 297-301.

COOPER, J.W., 1977 : The minicomputer in the laboratory. John Wiley and Sons Inc., U.S.A.

CROMBIE, D., 1955 : Doppler spectrum of sea-echo at 13.56 mc/s. Nature 175, 681.

_____ 1971 : Backscatter of hf radio waves from the sea, p.131-162 in Electromagnetic probing in geophysics. J.R. Wait (ed). The Golem Press, Boulder, Colorado, U.S.A.

CROMBIE, D.D., HASSELMANN, K., SELL, W., 1978 : High-frequency radar observations of sea eaves travelling in opposition to the wind. Boundary Layer Meteor., 13, 45-54.

CROMBIE,D.D. and PENTON, W.A., 1954 : A simple coherent pulse radar system. Report no. R.222, DSIR (Dominion Physical Laboratory), Lower Hutt, New Zealand.

CROOKES, W. and FLEMING, J.A., 1909 : Researches in radiotelegraphy. In Wireless Telegraphy. The Royal Institution Library of Science. Applied Science Publishers, London.

DeMAISTRE, J.C., BROCHE, P., CROCHET, M., 1978 : Off-shore wind measurements by HF Doppler ground-wave radar. Boundary Layer Meteor., 13, 55-60.

DEXTER, P.E. and THEORDORIDIS, S., 1982 : Surface wind speed extraction from HF sky-wave Doppler spectra. Rad. Sci. 17, 643.

DOWDEN, R.L., 1957 : Short-range echoes observed on ionospheric recorders. J. Atmos. Terr. Phys. 11, 111-117.

ECKERSLEY, P.D.,1930: The calculation of the service area of broadcast stations. Proc. IRE. 18 1160-1193 (1930).

FLOCK, W.L., 1979 : Electromagnetics and the environment. Remote sensing and elecommunications. Prentice Hall Inc., Englewood Cliffs, N.J.

FORGET, P., BROCHE, P., DeMAISTRE, J.C., FONTANEL, A., 1981 : Sea state frequency features observed by ground wave hf Doppler radar. Rad. Sci. 16, 917-925.

FRASER, G.J. and VINCENT, R.A., 1970 : A study of D-region irregularities. J. Atmos. Terr. Phys. 32, 1591-1607.

FRICKER, R., 1981 : An hp 97 calculator method for hf sky-wave field strength prediction. P.237-240 in International conference on Antennas and Propagation. Part 2. Propagation. IEE, London.

GERKS, I.H., 1962 : Use of a high-speed computer for ground-wave calculations. IRE TRans. Ant.Prop. AP-10 292-299. Correction note: AP-14, 406-407.

HALL, W.M., 1956 : Prediction of pulse radar performance. Proc. IRE 44, 224-231.

HARRIS, F.J., 1978 : On the use of windows for harmonic analysis with the discrete Fourier transform. Proc. IEEE 66, 51-83.

HASSELMAN, K., 1971: Determination of ocean wave spectra from Doppler radio return from the sea surface. Nature 229, 16.

ITT CORP., 1968 : Reference data for radio engineers (5th ed). Howard W. Sams and Co., U.S.A.

JASIK, H.(ed).,1961: Antenna engineering handbook. McGraw-Hill, N.Y.

JOHNSTONE, D.L.,1975: Second order electromagnetic and hydrodynamic effects in high-frequency radio-wave scattering from the sea. Ph.D. Thesis, Standford University.

KANASEWICH, E.R.,1975: Time sequence analysis in Geophysics. University of Alberta Press., Edmonton, Alberta, Canada.

KINSMAN, B., 1965 : Wind waves. Prentice-Hall Inc., N.J., U.S.A.

KRAUS, E.B., 1972 : Atmosphere-ocean interaction. Clarendon Press, Oxford.

KRENEK, S.H., 1977 : A pulse compression radar system for high-resolution ionospheric sounding. Ph.D. Thesis, University of Canterbury.

LeBLOND, P.H. and MYSAK, L.A., 1978 : Waves in the ocean. Elsevier, N.Y.

LEISE, J.A., 1984 : The analysis and digital signal processing of NOAA's surface current mapping system. IEEE J. Oceanic Eng. OE-9 106-113.

LIPA, B.J., 1977 : Derivation of directional ocean-wave spectra by integral inversion of second-order radar echoes. Rad. Sci. 12 (3), 425-434.

_____ 1978 : Inversion of second-order radar echoes from the sea. J. Geophys. Res. 83, 959-962.

LIPA, B.J. and BARRICK, D.E., 1980 : Methods for the extraction of long-period ocean wave parameters from narrow beam hf radar sea-echo. Rad. Sci. 15, 843-853.

_____ 1983 : Least-squares methods for the extraction of surface currents from CODAR crossed-loop data : Application at ARSLOE. IEEE J. Oceanic Eng. OE-8, 226-253.

LOGAN, N.A., 1965 : Scurvey of some early studies of the scattering of plane waves by a sphere. Proc. IEEE 53, #8, Aug.

LONG, A.E. and TRIZNA, D.B., 1973 : Mapping of North Atlantic winds by hf radar sea backscatter interpretation. IEEE trans. Ant. Prop. AP-21, 680-685.

LYONS, R.S. and BARRICK, D.E., 1984 : Attentuation rates of coastal radar signals at 25 MHz. Rad. Sci. 19, 319-324.

MARESCA, J.W., 1979: High frequency skywave measurements of waves and currents associated with tropical and extra-tropical storms. P.221-234. In Ocean Wave Climate. Earle and Malahoff (eds). Plenum Press, N.Y.

MARESCA,J.W. and GEORGES, T.M., 1980 : Measuring rms waveheight and the scalar ocean wave spectrum with hf skywave radar. J. Geophys. Res. 85C, 2759-2771.

MEI, Chiang C., 1983 : The applied dynamics of ocean surface waves. John Wiley and Sons, U.S.A.

MIE, G., 1908 : Beiträge zur optik trüber medien, speziell Kolloidaler metallösungen. Ann. Phys. 25, 377-445.

MILLINGTON, G., 1949: Ground wave propagation over an inhomogeneous smooth earth. Part I. Proc. IEE 96, 53 (Part III).

MUNK, W.H., MILLER, G.R., SNODGRASS, F.E. and BARBER, N.F.,1963: Directional recording of swell from distant storms. Phil. Trans. Roy. Soc. A, 255, 505-584.

NEWLAND, D.E.,1975 : An introduction to random vibrations and spectral analysis. Longman, London.

OTNES, R.K. and ENOCHSON, L., 1972 : Digital time series analysis. Wiley, N.Y.

PEAK, W.H., 1959 : Theory of radar return from terrain. Part I. IRE Int. Conv. Record 7, 27-41.

PHILLIPS, O.M., 1958 : The equilibrium range in the spectrum of wind generated waves. J. Fluid Mech. 4, 426-434.

_____ 1966 : The dynamics of the upper ocean. Cambridge University Press.

PIERSON, W.J. and MOSKOWITZ, L., 1964 : A proposed spectral form for fully developed wind seas based on the similarity theory of S.A. Kitaigorodski. J. Geophys. Res. 69, 5181-5190.

PLANT, W.J., 1977 : Studies of back scattered sea return with a cw, dual-frequency, x-band radar. IEEE trans. Ant. Prop. AP-25, 28-36.

POULTER, E.M.,1978 : Radio-meteor investigations of atmosphere motion. Ph.D. thesis, University of Canterbury.

PRYCE, M.H.L., 1953: The diffraction of radio waves by the curvature of the earth. Advances in Physics (Supplement to Phil. Mag.) 2, 67-95.

RAVEN, R.S., 1966 : Requirements for master oscillators for coherent radar. Proc. IEEE 54, 237-243.

RAYLEIGH, J.W., 1871 : On the light from the sky, its polarization and colour. Phil.Mag.41, 107.

ROBSON, R.E., 1984 : Simplified theory of first- and second-order scattering of hf radio waves from the sea. Rad. Sci. 19, 1499-1504.

SHAW, R., 1982 : Wave energy : A design Challenge. Ellis Horwood Ltd. Distributed by John Wiley and Sons Inc., N.Y.

SHEARMAN, E.D.R., 1981 : Remote sensing of ocean waves, currents and surface winds by dekametric radar. Ch.21 in Remote Sensing in Meteorology, Oceanography and Hydrology. A.P. Cracknell, ed. Ellis Horwood, Chichester.

_____ 1983 : Radio science and oceanography. Rad. Sci. 18, 299-320.

SNODGRASS, F.E., GROVES, G.W., HASSELMAN, K.F., MILLER, G.R., MUNK, W.H. and POWERS, W.H., 1966 : Propagation of ocean swell across the

SOMMERFIELD, A., 1909 : Ueber die ausbreitung der wellen in der drahtlosen telegraphie. Ann. d. Phys. (4) 28, 665.

STEWART, R. H., 1980 : Ocean wave measurement techniques. In Air Sea Interaction. Instruments and Methods. Dobson et al. (eds). Plenum Press, New York.

STEWART, R.H. and BARNUM, J.R., 1975 : Radio measurements of oceanic winds at long ranges : an evaluation. Rad. Sci. 10, 853-857.

STEWART. R.H. and TEAGUE, C., 1980 : Dekameter radar observations of ocean wave growth and decay. J. Phys. Oceanog. 10, 128-143.

TRIZNA, D.B., MOORE, J.C., HEADRICK, J.M. and BOGLE, R.W., 1977: Directional sea spectrum determination using hf Doppler radar techniques. IEEE trans. Ant. Prop. AP-25, 4-11.

TYLER, G.L., FAULKERSON, W.E., PETERSON, A.M. and TEAGUE,C.C., 1972 : Second order scattering from the sea : Ten meter radar observations of the Doppler continuum. Science 177, 349-351.

TYLER, G.L. et al. 1974 : Wave directional spectra from synthetic apeture observations of radio scatter. Deep Sea Res. 21, 989-1016.

VAN DER POL, B. and BREMMER, H., 1937 : The diffraction of electromagnetic waves from an electrical point source round a finitely conducting sphere, with applications to radiotelegraphy and the theory of the rainbow. Phil. Mag. 24, 825-864.

WAIT, J.R., 1971 : Theory of ground wave propagation. Chapter 5 in Electromagnetic Probing in Geophysics. J.R. Wait (ed). The Golem Press, Boulder, Colorado, U.S.A.

WATSON, C.N., 1918 : The diffraction of radio waves by the earth. Proc. Roy. Soc. A95, 83-99.

_____ 1919 : The transmission of electric waves around the earth. Proc. Roy. Soc. A95, 546-563.

WEBB, T.H., 1980 : Diffusion of meteoric plasma. Ph.D. thesis, University of Canterbury.

WELCH, P.D., 1967 : The use of fast Fourier transform for the estimation of power spectra: A method based on time averaging over short, modified periodograms. IEEE trans. Audio and Electroacoust.

WESTWATER, E.R. and STRAND, O.N., 1972 : Inversion techniques. In : Remote sensing of the troposphere. V.E. Derr (ed). Ch. 16 U.S. Government Printing Office, Washington, D.C.

WITWORTH, I.R., 1984 : 16-bit microprocessors. Granada, London.

APPENDIX A:
THE GROUND WAVE FIELD STRENGTH PROGRAM

```
BEGIN
   %CALCULATES GROUND WAVE FIELD STRENGTHS OVER A SPHERICAL
   %EARTH BY USING A RESIDUE SERIES EXPANSION. SEE GERKS I.H.
   %1962: USE OF A HIGH SPEED COMPUTER FOR GROUND WAVE
   %CALCULATIONS. IRE TRANS. AP 10 292-299.
   %AT CLOSE RANGES THE FLAT EARTH APPROXIMATION
   %IS USED.

   INTEGER I,S;
   REAL H0,D0,F0,KA,L,PI,MODT,ARGT,E,X,SIGMA,H1,H2,D,GRWAVE,
   DMIN,DMAX,DSTEP,PHASE,SPATIAL;
   COMPLEX SUM,T,TA,CORREC,C,J,MINUSJ;
   REAL ARRAY TMAX,TMIN,TCRIT[1:11],TABLE[1:11];
   COMPLEX ARRAY AS[1:11],A[0:11,1:11],B[0:10,1:11];
   REAL C1,C2,C3,C4,D1,D2,D3,D4;
   REAL Y,W;
   REAL PHI,THETA,P;
   COMPLEX RV,AX,BX,WD,REFWAVE,SURFWAVE;

   %I/O DECLARATIONS:
   %*****************

   FILE LP(KIND=PRINTER,MAXRECSIZE=22);
   FILE PLOTFILE(KIND=DISK);
   FILE SCREEN(KIND=REMOTE,MAXRECSIZE=14,MYUSE=IO);
   FILE ATABLE(KIND=DISK,FILETYPE=7);
   FILE BTABLE(KIND=DISK,FILETYPE=7);
   SWITCH FILE OUTPUT := LP,SCREEN;
   INTEGER SELECT;
   BOOLEAN LPOUT,SCREENOUT;
   DEFINE INFORM = FOR SELECT := (IF LPOUT THEN 0 ELSE 1 )
   STEP 1 UNTIL (IF SCREENOUT THEN 1 ELSE 0 ) DO
   WRITE(OUTPUT[SELECT]#; % DETERMINES WHERE THE OUTPUT GOES.
   DEFINE OSCR = IF SCREEN.KIND=3 THEN WRITE(SCREEN#; %OUTPUT TO
   %SCREEN IF IN INTERACTIVE MODE.


   COMPLEX PROCEDURE F(W);
   VALUE W;
   COMPLEX W;
   BEGIN
      %CALCULATES THE SURFACE WAVE ATTENUTATION FUNCTION BY
      %USING EITHER A CONVERGENT OR AN ASYMPTOTIC EXPANSION
      %FOR THE COMPLIMENTARY ERROR FUNCTION.

      COMPLEX DUM;
      INTEGER I;
      REAL COEF;

      COEF := 105;


      IF CABS(W) <= 10 AND CABS(W) > 0 THEN
      BEGIN
         DUM := 1 - J*CSQRT(PI*W)*CEXP(-1*W) - 2*W
         +(2*W)**2/3 - (2*W)**3/15;
         IF CABS(W) >= 1 THEN
         FOR I := 4 STEP 1 UNTIL 40 DO
         BEGIN
            DUM := DUM + (-1)**I*(2*W)**I/COEF;
```

```
         COEF := COEF*(2*(I+1)-1)
      END
   END
   ELSE
   DUM := -1*( 1/(2*W) + 3/(2*W)**2 + 15/(2*W)**3 );

   F := DUM
END OF F;


COMPLEX PROCEDURE HANKEL(Z);
VALUE Z;
COMPLEX Z;
BEGIN
   %USES A SERIES EXPANSION TO CALCULATE THE SPHERICAL HANKEL
   %FUNCTION FOR A COMPLEX ARGUMENT.

   COMPLEX ZX,A,B,C;
   REAL ALFA;

   ZX := MINUSJ*Z**(3/2);
   ALFA := 0.85366722;

   A := 1 + C1/ZX + C2/ZX**2 + C3/ZX**3 + C4/ZX**4;
   B := 1 - C1/ZX + C2/ZX**2 - C3/ZX**3 + C4/ZX**4;

   C := CEXP(2*ZX/3)*A + J*CEXP(-2*ZX/3)*B;
   HANKEL := ALFA*Z**(-1/4)*CEXP( J*5*PI/12 )*C

END OF HANKEL;


COMPLEX PROCEDURE HANKELDERIV(Z);
VALUE Z;
COMPLEX Z;
BEGIN
   %USES A SERIES EXPANSION TO CALCULATE THE DERIVATIVE OF THE
   %SPHERICAL HANKEL FUNCTION.

   COMPLEX ZX,A,B,C;
   REAL ALFA;

   ZX := MINUSJ*Z**(3/2);
   ALFA := 0.85366722;

   A := 1 - D1/ZX - D2/ZX**2 - D3/ZX**3 - D4/ZX**4;
   B := 1 + D1/ZX - D2/ZX**2 + D3/ZX**3 - D4/ZX**4;

   C := CEXP(2*ZX/3)*A - J*CEXP(-2*ZX/3)*B;
   HANKELDERIV := MINUSJ*ALFA*Z**(1/4)*CEXP( J*5*PI/12 )*C

END OF HANKELDERIV;



%INITIALIZATION SECTION.

%
%SET DEFAULT OUTPUT DIRECTION.
IF SCREEN.KIND=3 THEN
BEGIN %INTERACTIVE MODE.
   SCREENOUT := TRUE;
   LPOUT := TRUE
```

```
END
ELSE
BEGIN %BATCH MODE.
   SCREENOUT := FALSE;
   LPOUT := TRUE
END;

PI := 4*ARCTAN(1);
J := COMPLEX(0,1);
MINUSJ := COMPLEX(0,-1);

C1 := 0.10416667;        D1 := 0.14583333;
C2 := 0.08355035;        D2 := 0.09874132;
C3 := 0.12822657;        D3 := 0.14331205;
C4 := 0.29184903;        D4 := 0.31722720;


TMAX[1] := 0.4627;       TMIN[1] := 1.044;        TCRIT[1] := 0.7181;
TMAX[2] := 0.3275;       TMIN[2] := 0.9202;       TCRIT[2] := 0.5167;
TMAX[3] := 0.2909;       TMIN[3] := 0.6858;       TCRIT[3] := 0.4376;
TMAX[4] := 0.2695;       TMIN[4] := 0.5660;       TCRIT[4] := 0.3933;
TMAX[5] := 0.2539;       TMIN[5] := 0.4913;       TCRIT[5] := 0.3611;
TMAX[6] := 0.2422;       TMIN[6] := 0.4393;       TCRIT[6] := 0.3382;
TMAX[7] := 0.2330;       TMIN[7] := 0.4004;       TCRIT[7] := 0.3191;
TMAX[8] := 0.2252;       TMIN[8] := 0.3701;       TCRIT[8] := 0.3048;
TMAX[9] := 0.2186;       TMIN[9] := 0.3455;       TCRIT[9] := 0.2925;
TMAX[10] := 0.2129;      TMIN[10] := 0.3251;      TCRIT[10] := 0.2815;
TMAX[11] := 0.2079;      TMIN[11] := 0.3078;      TCRIT[11] := 0.2725;

FOR I := 0,1,3 STEP 1 UNTIL 11 DO
BEGIN
   READ(ATABLE,//,FOR S := 1 STEP 1 UNTIL 11 DO TABLE[S],PHASE);
   PHASE := PHASE*PI/180;
   FOR S := 1 STEP 1 UNTIL 11 DO
   A[I,S] := TABLE[S]*CEXP(J*PHASE)
END;

FOR I := 0 STEP 1 UNTIL 10 DO
BEGIN
   READ(BTABLE,//,FOR S := 1 STEP 1 UNTIL 11 DO TABLE[S],PHASE);
   PHASE := PHASE*PI/180;
   FOR S := 1 STEP 1 UNTIL 11 DO
   B[I,S] := TABLE[S]*CEXP(J*PHASE)
END;

KA := 8.504@6;      %EARTH RADIUS WITH CORRECTION FACTOR OF 4/3
%FOR ATMOSPHERIC REFRACTION.

OSCR[STOP],<"Line printer output? (true or false)- ">);
READ(SCREEN,//,LPOUT);


%READ IN THE INPUT DATA.

OSCR[STOP],<"Enter frequency (MHz): ">);
WHILE NOT READ(SCREEN,//,F0) DO
BEGIN
   L := 2.99792458@8/(F0*1@6);

   OSCR,<"Enter ground constants. Dielectric constant">);
   OSCR[STOP],<"and conductivity (S/m): ">);
   READ(SCREEN,//,E,SIGMA);

   OSCR[STOP],<"Enter TX and RX heights (m): ">);
   READ(SCREEN,//,H1,H2);
```

```
%WRITE INPUT DATA TO PRINTER.

WRITE(LP[SKIP 1]);
IF LPOUT THEN
BEGIN
   WRITE(LP,<"Frequency is ",F10.2," MHz">,F0);
   WRITE(LP,<"Dielectric constant of ground is ",F10.1>,E);
   WRITE(LP,<"Conductivity of ground is ",F10.4," S/m">,SIGMA);
   WRITE(LP,<"TX height is ",F10.1," m">,H1);
   WRITE(LP,<"RX height is ",F10.1," m">,H2);
   WRITE(LP[SPACE 5])
END;

X := 60*SIGMA*L;

%CALCULATE HEIGHT AND DISTANCE NORMALIZING FACTORS.

H0 := 1/2*(KA*L**2/PI**2)**(1/3);
D0 := (KA**2*L/PI)**(1/3);

%CALCULATE THE PARAMETER FOR THE ROOT DETERMINING EQUATION.

Y := SQRT(  (E-1)**2 + X**2  );
W := E**2 + X**2;
Y := SQRT( W/Y );
MODT := ( L/PI/KA )**(1/3)*Y;

ARGT := -3*PI/4 + ARCTAN(E/X) - 1/2*ARCTAN( (E-1)/X );

T := MODT*CEXP(J*ARGT);

%CALCULATE THE AS PARAMETERS FOR THE HEIGHT GAIN AND DISTANCE
%FUNCTIONS. THESE PARAMETERS ARE RELATED TO THE ZEROS OF THE
%ROOT DETERMINING EQUATION.

FOR S := 1 STEP 1 UNTIL 11 DO
BEGIN
   %ONE As PARAMETER FOR EACH TERM IN THE RESIDUE SERIES.

   IF MODT <= TMAX[S] THEN
   BEGIN
      AS[S] := A[0,S];
      FOR I := 1,3 STEP 1 UNTIL 11 DO
      AS[S] := AS[S] + A[I,S]*T**I
   END ELSE
   IF MODT >= TMIN[S] THEN
   BEGIN
      AS[S] := B[0,S];
      FOR I := 1 STEP 1 UNTIL 10 DO
      AS[S] := AS[S] + B[I,S]/T**I
   END ELSE
   BEGIN
      %T NEAR CRITICAL VALUE SO CALCULATE AN INITIAL VALUE AND
      %USE INTERPOLATION TO GET A BETTER VALUE.

      IF MODT > TMAX[S] AND MODT <= TCRIT[S] THEN
      BEGIN
         TA := TMAX[S]*CEXP(J*ARGT);

         AS[S] := A[0,S];
         FOR I := 1,3 STEP 1 UNTIL 11 DO
         AS[S] := AS[S] + A[I,S]*TA**I
      END ELSE
      BEGIN
         TA := TMIN[S]*CEXP(J*ARGT);
```

```
            AS[S] := B[0,S];

            FOR I := 1 STEP 1 UNTIL 10 DO
            AS[S] := AS[S] + B[I,S]/TA**I
         END;


         DO
         BEGIN
            CORREC := ( T - TA )/( 1 + AS[S]*TA*T );
            AS[S] := AS[S] + CORREC;

            TA := HANKEL(AS[S])/HANKELDERIV(AS[S])

         END
         UNTIL CABS(CORREC) < 1@-4
      END
   END;


OSCR[STOP],<"Enter minimum range, step and maximum range (km): ">);
   READ(SCREEN,//,DMIN,DSTEP,DMAX);
   DMIN := DMIN*1@3;        DSTEP := DSTEP*1@3;
   DMAX := DMAX*1@3;

   INFORM,<"DISTANCE      GND.WAVE    SPATIAL      TOTAL">);
   INFORM,<"      km            dB          dB         dB">);
   INFORM[SPACE 2]);


   FOR D := DMIN STEP DSTEP UNTIL DMAX DO
   BEGIN

      IF D < 1609*50/F0**(1/3) THEN
      BEGIN
         %USE FLAT EARTH APPROXIMATION AT CLOSE RANGES.

         %CALCULATE GROUND REFLECTION COEFFICIENT.

         PHI := ARCTAN(  (H1+H2)/D  );
         THETA := 4*PI*H1*H2/L/D;
         X := 60*SIGMA*L;
         AX := (E - J*X)*SIN(PHI);
         BX := CSQRT(E - 1 - J*X);

         RV := (AX - BX)/(AX + BX);

         %CALCULATE SOMMERFELD'S NUMERICAL DISTANCE.

         P := SQRT( (E-1)**2 + X**2 );
         P := P/(E**2 + X**2);
         P := P*PI*D/L;

         PHASE := E + 1 + (E-1)*(E/X)**2;
         PHASE := PHASE/( X + (E-2)*(E/X) );
         PHASE := ARCTAN(PHASE);

         WD := 4/((1-RV)**2)*P*CEXP(MINUSJ*PHASE);

         %CALCULATE THE RATIO OF GROUND WAVE TO FREE SPACE
         %FIELD STRENGTH AND THE FREE SPACE AND TOTAL ATTENUATION.

         SPATIAL := 20*LOG(4*PI*D/L);
         REFWAVE := RV*CEXP(MINUSJ*THETA);
         SURFWAVE := (1-RV)*F(WD)*CEXP(MINUSJ*THETA);
```

```
            GRWAVE := 20*LOG(CABS(1 + REFWAVE + SURFWAVE))

         END ELSE
         BEGIN
            %AT LARGER DISTANCES, WHERE THE EARTH'S CURVATURE IS
            %IMPORTANT, USE THE ELEVEN TERM RESIDUE SERIES SUM.

            SUM := 0;
            FOR S := 1 STEP 1 UNTIL 11 DO
            BEGIN

               C := HANKEL( AS[S] + H1/H0 );
               C := C*T**2/(1 + AS[S]*T**2);
               C := C*HANKEL( AS[S] + H2/H0 );
               C := C*CEXP( J*AS[S]*D/D0 );
               C := C/HANKEL(AS[S])**2;

               SUM := SUM + C

            END OF ELEVEN TERM RESIDUE SERIES SUM;

            GRWAVE := 20*LOG( SQRT(L*D)/H0*CABS(SUM));
            SPATIAL := 20*LOG(4*PI*D/L)
         END;

         WRITE(PLOTFILE,//,LOG(D/1000),GRWAVE);
         INFORM,<4F10.1>,D/1000,GRWAVE,SPATIAL,SPATIAL-GRWAVE)

      END;
      OSCR[SPACE 5]);
      OSCR[STOP],<"Enter frequency (MHz): ">)
   END;
   WRITE(PLOTFILE,<"*">);
   LOCK(PLOTFILE,CRUNCH)
END.
```

APPENDIX B:
THE RADAR PERFORMANCE PREDICTION PROGRAM

```
BEGIN
   %RADAR PERFORMANCE PREDICTION FOR FULLY DEVELOPED
   %FIRST ORDER SEA SCATTER.
   %CALCULATES GROUND WAVE FIELD STRENGTHS OVER A SPHERICAL
   %EARTH BY USING A RESIDUE SERIES EXPANSION. SEE GERKS I.H.
   %1962: USE OF A HIGH SPEED COMPUTER FOR GROUND WAVE
   %CALCULATIONS. IRE TRANS. AP 10 292-299.
   %AT CLOSE RANGES THE FLAT EARTH APPROXIMATION
   %IS USED.
%WARNING: SYSTEM GAIN DOES NOT CORRESPOND WITH THESIS DEFINITION.
%-------------------------------------------------------------------


   INTEGER I,S;
   REAL H0,D0,F0,KA,L,PI,MODT,ARGT,E,X,SIGMA,H1,H2,D,
   DMIN,DMAX,DSTEP,PHASE,SPATIAL;
   COMPLEX SUM,T,TA,CORREC,C,J,MINUSJ;
   REAL ARRAY TMAX,TMIN,TCRIT[1:11],TABLE[1:11];
   COMPLEX ARRAY AS[1:11],A[0:11,1:11],B[0:10,1:11];
   REAL C1,C2,C3,C4,D1,D2,D3,D4;
   REAL Y,W;
   REAL PHI,THETA,P;
   COMPLEX RV,AX,BX,WD,REFWAVE,SURFWAVE;
   REAL TXPOWER,PULSEWIDTH,GTX,BEAMWIDTH,HTX,GRX,
   HRX,BANDWIDTH,LOSSES,EIRP,CROSSECTION,ATTEN,
   PSCAT,PRX,SPECDENSITY,SYSGAIN;
   REAL PRF,BRX,SYSTEMP,SNOISE;
   BOOLEAN MAXVIS,MAXR;


   %I/O DECLARATIONS:
   %*****************

   FILE LP(KIND=PRINTER,MAXRECSIZE=22);

   FILE SCREEN(KIND=REMOTE,MAXRECSIZE=14,MYUSE=IO);
   FILE ATABLE(KIND=DISK,FILETYPE=7);
   FILE BTABLE(KIND=DISK,FILETYPE=7);
   SWITCH FILE OUTPUT := LP,SCREEN;
   INTEGER SELECT;
   BOOLEAN LPOUT,SCREENOUT;
   DEFINE INFORM = FOR SELECT := (IF LPOUT THEN 0 ELSE 1 )
   STEP 1 UNTIL (IF SCREENOUT THEN 1 ELSE 0 ) DO
   WRITE(OUTPUT[SELECT]#; % DETERMINES WHERE THE OUTPUT GOES.
   DEFINE OSCR = IF SCREEN.KIND=3 THEN WRITE(SCREEN#; %OUTPUT TO
   %SCREEN IF IN INTERACTIVE MODE.


%PLOT DECLARATIONS:
%*****************

FILE PLOTFILE(KIND=DISK,MAXRECSIZE=14,BLOCKSIZE=420);
INTEGER INDEX;
REAL ARRAY YDATA[0:200];


   PROCEDURE OUTPUTBLOCK;
   BEGIN
      %WRITES DATA TO THE OUTPUT PLOT FILE
      %IN COMPRESSED FORMAT.
```

```
   INTEGER I,MRSIZE;

   I := 0;
   MRSIZE := 14;

   WRITE(PLOTFILE,//,INDEX,DSTEP/1000,DSTEP/1000);
   DO
   BEGIN
      WRITE(PLOTFILE,MRSIZE,YDATA[I]);
      I := I+MRSIZE
   END
   UNTIL I > INDEX OR I > 200
END OF OUTPUTBLOCK;


COMPLEX PROCEDURE F(W);
VALUE W;
COMPLEX W;
BEGIN
   %CALCULATES THE SURFACE WAVE ATTENUTATION FUNCTION BY
   %USING EITHER A CONVERGENT OR AN ASYMPTOTIC EXPANSION
   %FOR THE COMPLIMENTARY ERROR FUNCTION.

   COMPLEX DUM;
   INTEGER I;
   REAL COEF;

   COEF := 105;


   IF CABS(W) <= 10 AND CABS(W) > 0 THEN
   BEGIN
      DUM := 1 - J*CSQRT(PI*W)*CEXP(-1*W) - 2*W
      +(2*W)**2/3 - (2*W)**3/15;
      IF CABS(W) >= 1 THEN
      FOR I := 4 STEP 1 UNTIL 40 DO
      BEGIN
         DUM := DUM + (-1)**I*(2*W)**I/COEF;
         COEF := COEF*(2*(I+1)-1)
      END
   END
   ELSE
   DUM := -1*( 1/(2*W) + 3/(2*W)**2 + 15/(2*W)**3 );

   F := DUM
END OF F;



COMPLEX PROCEDURE HANKEL(Z);
VALUE Z;
COMPLEX Z;
BEGIN
   %USES A SERIES EXPANSION TO CALCULATE THE SPHERICAL HANKEL
   %FUNCTION FOR A COMPLEX ARGUMENT.

   COMPLEX ZX,A,B,C;
   REAL ALFA;

   ZX := MINUSJ*Z**(3/2);
   ALFA := 0.85366722;

   A := 1 + C1/ZX + C2/ZX**2 + C3/ZX**3 + C4/ZX**4;
   B := 1 - C1/ZX + C2/ZX**2 - C3/ZX**3 + C4/ZX**4;
```

```
   C := CEXP(2*ZX/3)*A + J*CEXP(-2*ZX/3)*B;
   HANKEL := ALFA*Z**(-1/4)*CEXP( J*5*PI/12 )*C

END OF HANKEL;


COMPLEX PROCEDURE HANKELDERIV(Z);
VALUE Z;
COMPLEX Z;
BEGIN
   %USES A SERIES EXPANSION TO CALCULATE THE DERIVATIVE OF THE
   %SPHERICAL HANKEL FUNCTION.

   COMPLEX ZX,A,B,C;
   REAL ALFA;

   ZX := MINUSJ*Z**(3/2);
   ALFA := 0.85366722;

   A := 1 - D1/ZX - D2/ZX**2 - D3/ZX**3 - D4/ZX**4;
   B := 1 + D1/ZX - D2/ZX**2 + D3/ZX**3 - D4/ZX**4;

   C := CEXP(2*ZX/3)*A - J*CEXP(-2*ZX/3)*B;
   HANKELDERIV := MINUSJ*ALFA*Z**(1/4)*CEXP( J*5*PI/12 )*C

END OF HANKELDERIV;



REAL PROCEDURE GRWAVE(D);
REAL D;
BEGIN
   %CALCULATES THE RATIO OF THE GROUNDWAVE FIELD AT
   %DISTANCE, D, TO THE FIELD THAT WOULD EXIST IN
   %FREE SPACE AT THIS DISTANCE. RETURNED QUANTITY
   %IS RATIO OF POWER DENSITIES = (RATIO OF FIELD
   %STRENGTHS)**2.

   REAL DUM;

   IF D < 1609*50/F0**(1/3) THEN
   BEGIN
      %USE FLAT EARTH APPROXIMATION AT CLOSE RANGES.

      %CALCULATE GROUND REFLECTION COEFFICIENT.

      PHI := ARCTAN(  (H1+H2)/D  );
      THETA := 4*PI*H1*H2/L/D;
      X := 60*SIGMA*L;
      AX := (E - J*X)*SIN(PHI);
      BX := CSQRT(E - 1 - J*X);

      RV := (AX - BX)/(AX + BX);

      %CALCULATE SOMMERFELD'S NUMERICAL DISTANCE.

      P := SQRT( (E-1)**2 + X**2 );
      P := P/(E**2 + X**2);
      P := P*PI*D/L;

      PHASE := E + 1 + (E-1)*(E/X)**2;
      PHASE := PHASE/( X + (E-2)*(E/X) );
      PHASE := ARCTAN(PHASE);

      WD := 4/((1-RV)**2)*P*CEXP(MINUSJ*PHASE);
```

```
      SPATIAL := 20*LOG(4*PI*D/L);
      REFWAVE := RV*CEXP(MINUSJ*THETA);
      SURFWAVE := (1-RV)*F(WD)*CEXP(MINUSJ*THETA);
      DUM := CABS(1 + REFWAVE + SURFWAVE)

   END ELSE
   BEGIN
      %AT LARGER DISTANCES, WHERE THE EARTH'S CURVATURE IS
      %IMPORTANT, USE THE ELEVEN TERM RESIDUE SERIES SUM.

      SUM := 0;
      FOR S := 1 STEP 1 UNTIL 11 DO
      BEGIN

         C := HANKEL( AS[S] + H1/H0 );
         C := C*T**2/(1 + AS[S]*T**2);
         C := C*HANKEL( AS[S] + H2/H0 );
         C := C*CEXP( J*AS[S]*D/D0 );
         C := C/HANKEL(AS[S])**2;

         SUM := SUM + C

      END OF ELEVEN TERM RESIDUE SERIES SUM;

      DUM :=  SQRT(L*D)/H0*CABS(SUM)
   END;

   GRWAVE := DUM**2
END OF GRWAVE;



%INITIALIZATION SECTION.

%
%SET DEFAULT OUTPUT DIRECTION.
IF SCREEN.KIND=3 THEN
BEGIN %INTERACTIVE MODE.
   SCREENOUT := TRUE;
   LPOUT := TRUE
END
ELSE
BEGIN %BATCH MODE.
   SCREENOUT := FALSE;
   LPOUT := TRUE
END;

PI := 4*ARCTAN(1);
J := COMPLEX(0,1);
MINUSJ := COMPLEX(0,-1);
MAXVIS := FALSE;   MAXR := FALSE;

C1 := 0.10416667;        D1 := 0.14583333;
C2 := 0.08355035;        D2 := 0.09874132;
C3 := 0.12822657;        D3 := 0.14331205;
C4 := 0.29184903;        D4 := 0.31722720;



TMAX[1] := 0.4627;       TMIN[1] := 1.044;        TCRIT[1] := 0.7181;
TMAX[2] := 0.3275;       TMIN[2] := 0.9202;       TCRIT[2] := 0.5167;
TMAX[3] := 0.2909;       TMIN[3] := 0.6858;       TCRIT[3] := 0.4376;
TMAX[4] := 0.2695;       TMIN[4] := 0.5660;       TCRIT[4] := 0.3933;
TMAX[5] := 0.2539;       TMIN[5] := 0.4913;       TCRIT[5] := 0.3611;
```

```
TMAX[6] := 0.2422;      TMIN[6] := 0.4393;      TCRIT[6] := 0.3382;
TMAX[7] := 0.2330;      TMIN[7] := 0.4004;      TCRIT[7] := 0.3191;
TMAX[8] := 0.2252;      TMIN[8] := 0.3701;      TCRIT[8] := 0.3048;
TMAX[9] := 0.2186;      TMIN[9] := 0.3455;      TCRIT[9] := 0.2925;
TMAX[10] := 0.2129;     TMIN[10] := 0.3251;     TCRIT[10] := 0.2815;
TMAX[11] := 0.2079;     TMIN[11] := 0.3078;     TCRIT[11] := 0.2725;

FOR I := 0,1,3 STEP 1 UNTIL 11 DO
BEGIN
   READ(ATABLE,//,FOR S := 1 STEP 1 UNTIL 11 DO TABLE[S],PHASE);
   PHASE := PHASE*PI/180;
   FOR S := 1 STEP 1 UNTIL 11 DO
   A[I,S] := TABLE[S]*CEXP(J*PHASE)
END;

FOR I := 0 STEP 1 UNTIL 10 DO
BEGIN
   READ(BTABLE,//,FOR S := 1 STEP 1 UNTIL 11 DO TABLE[S],PHASE);
   PHASE := PHASE*PI/180;
   FOR S := 1 STEP 1 UNTIL 11 DO
   B[I,S] := TABLE[S]*CEXP(J*PHASE)
END;

KA := 8.504@6;      %EARTH RADIUS WITH CORRECTION FACTOR OF 4/3
%FOR ATMOSPHERIC REFRACTION.

OSCR[STOP],<"Line printer output? (true or false)- ">);
READ(SCREEN,//,LPOUT);


%READ IN THE INPUT DATA.

OSCR[STOP],<"Enter frequency (MHz): ">);
WHILE NOT READ(SCREEN,//,F0) DO
BEGIN
   L := 2.99792458@8/(F0*1@6);

   OSCR,<"TRANSMITTER:">);
   OSCR[STOP],<"      Power (kW) ">);
   READ(SCREEN,//,TXPOWER);
   OSCR[STOP],<"      Pulse width (us) ">);
   READ(SCREEN,//,PULSEWIDTH);
   OSCR[STOP],<"      prf (Hz) ">);
   READ(SCREEN,//,PRF);

   OSCR,<"TX ANTENNA: ">);
   OSCR[STOP],<"      Gain (dB) ">);
   READ(SCREEN,//,GTX);
   OSCR[STOP],<"      Beamwidth (degrees) ">);
   READ(SCREEN,//,BEAMWIDTH);
   OSCR[STOP],<"      Height (m) ">);
   READ(SCREEN,//,HTX);

   OSCR,<"RX ANTENNA: ">);
   OSCR[STOP],<"      Gain (dB) ">);
   READ(SCREEN,//,GRX);
   OSCR[STOP],<"      Height (m) ">);
   READ(SCREEN,//,HRX);



   OSCR[STOP],<"System gain (dB) ">);
   READ(SCREEN,//,SYSGAIN);
   OSCR[STOP],<"Bandwidth of echo (Hz) ">);
   READ(SCREEN,//,BANDWIDTH);
   OSCR[STOP],<" Additional losses (dB) ">);
```

```
      READ(SCREEN,//,LOSSES);
      OSCR[STOP],<"     Receiver bandwidth (kHz) ">);
      READ(SCREEN,//,BRX);
      OSCR[STOP],<"     System noise temperature (K) ">);
      READ(SCREEN,//,SYSTEMP);


      EIRP := 1000*TXPOWER*10**(GTX/10);
      SNOISE := (10**(SYSGAIN/10))*(BRX*1000)*(1.381@-23)
      *SYSTEMP*75/PRF;

      IF LPOUT THEN
      BEGIN
WRITE(LP,<"                         RADAR PERFORMANCE PREDICTION">);
WRITE(LP,<"                         ****************************">);
         WRITE(LP,<"TRANSMITTER">);
         WRITE(LP,<"-----------">);
         WRITE(LP,<"     Frequency:",F10.2," MHz">,F0);
         WRITE(LP,<"     Power:",F10.1," kW">,TXPOWER);
         WRITE(LP,<"     EIRP:",F10.1," kW",F10.0," dB">,EIRP/1000,
         10*LOG(EIRP));
         WRITE(LP,<"     Pulsewidth:",F10.0," us">,PULSEWIDTH);
         WRITE(LP,<"     prf:",F10.0," Hz">,PRF);
         WRITE(LP,<"TX ANTENNA">);
         WRITE(LP,<"-----------">);
         WRITE(LP,<"     Gain:",F10.2," dB">,GTX);
         WRITE(LP,<"     Beamwidth:",F10.1," degrees">,BEAMWIDTH);
         WRITE(LP,<"     Height:",F10.0," m">,HTX);
         WRITE(LP,<"RX ANTENNA">);
         WRITE(LP,<"-----------">);
         WRITE(LP,<"     Gain:",F10.2," dB">,GRX);
         WRITE(LP,<"     Height:",F10.0," m">,HRX);
         WRITE(LP[SPACE 2]);
         WRITE(LP,<"System gain:",F10.2," dB">,SYSGAIN);
         WRITE(LP,<"Echo bandwidth:",F10.3," dB">,BANDWIDTH);
         WRITE(LP,<"Additional losses:",F10.0," dB">,LOSSES);
         WRITE(LP,<"Receiver bandwidth:",F10.0," kHz">,BRX);
         WRITE(LP,<"System noise temperature:",F10.0," K">,SYSTEMP);
         WRITE(LP,<"Spatial resolution:",F10.1," km">,2.9979458@8*
         (1@-9)/2*PULSEWIDTH);
         WRITE(LP,<"Spectral density of noise:",F10.0," dB">,
         10*LOG(SNOISE));
         WRITE(LP[SPACE 10])
      END;

      OSCR,<"Power spectral density of noise is: ",F10.0," dB">,
      10*LOG(SNOISE));

      TXPOWER := TXPOWER*1000;
      GTX := 10**(GTX/10);
      GRX := 10**(GRX/10);
      SYSGAIN := 10**(SYSGAIN/20);
      LOSSES := 10**(-1*LOSSES/10);


      E := 80;       SIGMA := 4;
      X := 60*SIGMA*L;

      %CALCULATE HEIGHT AND DISTANCE NORMALIZING FACTORS.

      H0 := 1/2*(KA*L**2/PI**2)**(1/3);
      D0 := (KA**2*L/PI)**(1/3);

      %CALCULATE THE PARAMETER FOR THE ROOT DETERMINING EQUATION.

      Y := SQRT(  (E-1)**2 + X**2  );
```

```
W := E**2 + X**2;
Y := SQRT( W/Y );
MODT := ( L/PI/KA )**(1/3)*Y;

ARGT := -3*PI/4 + ARCTAN(E/X) - 1/2*ARCTAN( (E-1)/X );

T := MODT*CEXP(J*ARGT);

%CALCULATE THE AS PARAMETERS FOR THE HEIGHT GAIN AND DISTANCE
%FUNCTIONS. THESE PARAMETERS ARE RELATED TO THE ZEROS OF THE
%ROOT DETERMINING EQUATION.

FOR S := 1 STEP 1 UNTIL 11 DO
BEGIN
   %ONE As PARAMETER FOR EACH TERM IN THE RESIDUE SERIES.

   IF MODT <= TMAX[S] THEN
   BEGIN
      AS[S] := A[0,S];
      FOR I := 1,3 STEP 1 UNTIL 11 DO
      AS[S] := AS[S] + A[I,S]*T**I
   END ELSE
   IF MODT >= TMIN[S] THEN
   BEGIN
      AS[S] := B[0,S];
      FOR I := 1 STEP 1 UNTIL 10 DO
      AS[S] := AS[S] + B[I,S]/T**I
   END ELSE
   BEGIN
      %T NEAR CRITICAL VALUE SO CALCULATE AN INITIAL VALUE AND
      %USE INTERPOLATION TO GET A BETTER VALUE.

      IF MODT > TMAX[S] AND MODT <= TCRIT[S] THEN
      BEGIN
         TA := TMAX[S]*CEXP(J*ARGT);

         AS[S] := A[0,S];
         FOR I := 1,3 STEP 1 UNTIL 11 DO
         AS[S] := AS[S] + A[I,S]*TA**I
      END ELSE
      BEGIN
         TA := TMIN[S]*CEXP(J*ARGT);

         AS[S] := B[0,S];

         FOR I := 1 STEP 1 UNTIL 10 DO
         AS[S] := AS[S] + B[I,S]/TA**I
      END;


      DO
      BEGIN
         CORREC := ( T - TA )/( 1 + AS[S]*TA*T );
         AS[S] := AS[S] + CORREC;

         TA := HANKEL(AS[S])/HANKELDERIV(AS[S])

      END
      UNTIL CABS(CORREC) < 1@-4
   END
END;


OSCR[STOP],<"Enter range step (km): ">);
READ(SCREEN,//,DSTEP);
DSTEP := DSTEP*1000;
```

```
      INFORM,<"DISTANCE      SPECTRAL">);
      INFORM,<"      km     DENSITY,dB">);
      INFORM[SPACE 2]);

INDEX := -1;

      FOR D := DSTEP,D+DSTEP WHILE SPECDENSITY >= SNOISE DO
      BEGIN
         %CALCULATE FIRST ORDER SCATTERRING CROSS-SECTION.

         CROSSECTION := 0.02*2.99792458@8*(PULSEWIDTH*1@-6)/2
         *(BEAMWIDTH*PI/180)*D;

         %CALCULATE THE POWER SCATTERRED FROM THE CONTACT PATCH.

         H1 := HTX;       H2 := 0;
         ATTEN := GRWAVE(D);
         PSCAT := EIRP/(4*PI*D**2)*ATTEN*CROSSECTION;

         %CALCULATE THE RECEIVED POWER.

         H1 := 0;         H2 := HRX;
         IF HRX NEQ HTX THEN ATTEN := GRWAVE(D);

         PRX := PSCAT/(4*PI*D**2)*ATTEN*LOSSES*(L**2)*GRX/4/PI;

         %CONVERT TO SPECTRAL DENSITY.

         SPECDENSITY := (SYSGAIN**2)*PRX*75/BANDWIDTH;


         IF NOT MAXVIS AND (BANDWIDTH*SPECDENSITY <= PRF*SNOISE) THEN
         BEGIN
            MAXVIS := TRUE;
INFORM,<"                          Max. range of visible echo">)
         END;

         IF NOT MAXR AND (SPECDENSITY <= SNOISE*10) THEN
         BEGIN
            MAXR := TRUE;
INFORM,<"                          Max. range of useful 1st order echo">)
         END;

INDEX := INDEX+1;
YDATA[INDEX] := 10*LOG(SPECDENSITY + SNOISE);

         INFORM,<2F10.1>,D/1000,10*LOG(SPECDENSITY + SNOISE));


      END;
OUTPUTBLOCK;
      MAXVIS := FALSE;   MAXR := FALSE;
      OSCR[SPACE 5]);
      OSCR[STOP],<"Enter frequency (MHz): ">)
   END;  CLOSE(PLOTFILE,CRUNCH)
END.
```

APPENDIX C:
THE PDP8 DATA COLLECTION PROGRAM MACHINE CODE KERNEL

```
/                TIMESERIES COLLECTING PROGRAM
/                ****************************

/BASIC THEORY:   IN PULSED DOPPLER RADAR THE DOPPLER SPECTRUM OF
/-------------   THE ECHO FROM SOME RANGE IS THE POWER SPECTRUM
/               OF THE TIMESERIES OF ECHO VOLTAGES FROM THIS
/               RANGE. IF THE MAXIMUM FREQUENCY IN THIS SPECTRUM
/               IS B Hz THEN THE TIMESERIES POINTS MUST BE SPACED
/               DELTS = 1000/2B MILLISECONDS APART IN TIME. I.E.
/               THE PULSE REPITITION FREQUENCY MUST BE AT LEAST
/               2B Hz.

/PURPOSE OF THIS PROGRAM:       TO COLLECT AND RECORD ON MAGTAPE
/------------------------       SIMULTANEOUS TIMESERIES OF ECHO
/               VOLTAGES FROM A NUMBER OF PRE-SPECIFIED RANGES
/               USING A NUMBER OF PRE-SPECIFIED A-D CONVERTOR
/               CHANNELS.

/METHOD:        THE TIMESERIES ARE COLLECTED AT HIGH PRF
/-------        (DELTX = 1000/PRF > DELTS) AND DIGITALY FILTERED
/               DOWN TO THE REQUIRED BANDWIDTH TO REDUCE THE EFFECTS
/               OF ALIASED BACKGROUND NOISE. THUS ONE TIMESERIES
/               POINT IS THE RESULT OF AVERAGING DATA FROM NAV =
/               DELTX/DELTS TRANSMITTED PULSES IN THE DIGITAL FILTER.
/               THE PROCESSES OF A-D CONVERSION, DIGITAL FILTERING
/               AND MAGTAPE WRITING ARE CARRIED OUT IN PARALLEL UNDER
/               INTERRUPT CONTROL. IN ADDITION, INTERRUPTS FROM THE
/               MILLISECOND CLOCK ARE USED TO CONTROL THE TIMING
/               OF THE TRANSMITTER A-D CONVERSION SEQUENCE.
/               TO ENABLE DATA COLLECTION TO CONTINUE THROUGH A
/               MAGTAPE WRITE A DOUBLE BUFFERING SCHEME IS USED.


/                     IOT DEFINITIONS
/                     ***************

/STATION IOTS:
/-------------
                LSCR=6726       /LOAD STATION CONTROL REGISTER.
                CLSK=6727       /SKIP ON MILLISECOND CLOCK FLAG.
                CLCF=6707       /CLEAR MILLISECOND CLOCK FLAG.
                MSE=6013        /ENABLE MILLISECOND INTERRUPT.
                MSD=6015        /DISABLE MILLISECOND INTERRUPT.

/FAST A-D IOTS:
/--------------
                ADIE=6730       /ENABLE FAST A-D INTERRUPT.
                FASF=6731       /SKIP ON WORD COUNT OVERFLOW.
                ADCL=6732       /CLEAR ALL FLAGS.
                ADLC=6733       /LOAD COMMAND REGISTER.
                ADEN=6734       /ENABLE OR DISABLE A-D.
                ADIM=6735       /INCREMENT RAM MEMORY ADDRESS.
                ADLA=6736       /LOADS RAM MEMORY INTO ACCUMULATOR.
                ADID=6737       /DISABLE FAST A-D INTERRUPT.

/MAGTAPE IOTS:
/-------------
                CLT=6712        /CLEAR TRANSPORT.
```

```
                CLF=6725        /CLEAR FLAGS.
                RMSR=6714       /READ MAGTAPE STATUS REGISTER.
                SKJD=6723       /SKIP ON JOB DONE.
                SKEF=6721       /SKIP ON ERROR FLAG.
                LCMR=6705       /LOAD MAGTAPE COMMAND REGISTER.

/DMA INTERFACE IOTS:
/-------------------
                LWCR=6701       /LOAD DMA WORD COUNT REGISTER.
                LCAR=6703       /LOAD CURRENT ADDRESS REGISTER.
                SDBF=6717       /SET BUFFER FIELD FOR DMA TRANSFER.

/HARDWARE MULTIPLIER IOTS:
/-------------------------
                CLRMUL=6540         /CLEAR MULTIPLIER.
                LOADX=6541          /LOAD X REGISTER.
                LOADY=6542          /LOAD Y REGISTER.
                MULT=6543           /MULTIPLY X AND Y.
                GETL=6545           /GET LOW WORD OF RESULT.
                GETM=6546           /GET MEDIUM WORD OF RESULT.
                GETH=6547           /GET HIGH WORD OF RESULT.



/                       ALGOL IO DEVICE PATCH
/                       *********************

/THE MACHINE CODE ROUTINES IN THIS PROGRAM CAN BE CALLED AS IO
/DEVICES FROM AN ALGOL PROGRAM BY PUTTING THEIR ADDRESSES IN
/THE ALGOL IO DEVICE TABLE.


FIELD 6
/******

*265
        IN28
*304
        DEV26
        DEV27
        OUT28

/LINKS FROM ALGOL IO DEVICE MECHANISM TO MACHINE CODE ROUTINES
/IN FIELD 5.

*3000

DEV26,  0               /CHOUT(26,0) DOES MAGTAPE WRITE FROM
        CDF CIF 50      /ALGOL.
        JMS I XMTWR
        JMP I DEV26

DEV27,  0               /CHOUT(27,0) STARTS THE TIMESERIES COLLECTING
        CDF CIF 50      /ROUTINE.
        JMS I XTSWR
        JMP I DEV27

OUT28,  0               /CHOUT(28,0) TRIGGERS TRANSMITTER AND DOES
        CDF CIF 50      /AN A-D CONVERSION.
        JMS I XADTR
        JMP I OUT28

IN28,   0               /ADVALUE := CHIN(28) GETS A VALUE FROM THE A-D
        CDF CIF 50      /RAM BUFFER. RAM ADDRESS PREVIOUSLY SET USING
```

```
        JMS I XADGT     /PUTLOC(5,XRAMADR,RAMADR).
        JMP I IN28

XMTWR,  MTWRITE
XTSWR,  TSWRITE
XADTR,  ADTRIG
XADGT,  ADGET


/                       INTERRUPT SERVICE SKIP CHAIN
/                       ****************************


FIELD 0
/******

/DETERMINE CAUSE OF INTERRUPT AND JUMP TO APPROPRIATE
/SERVICE ROUTINE.

*0
INTSV,  0           /MILLISECOND CLOCK INTERRUPT.
        CLSK
        JMP ADCHK
        CDF CIF 50
        JMP I XCLSV

ADCHK,  FASF        /A-D FINISHED INTERRUPT.
        JMP MTCHK
        CDF CIF 50
        JMP I XADSV

MTCHK,  SKJD        /MAGTAPE WRITE FINISHED INTERRUPT.
        JMP EXIT
        DCA SAVAC
        CDF 50
        DCA I XMTRUN        /CLEAR MAGTAPE RUNNING SOFTWARE FLAG
        CDF                 /AND STOP MAGTAPE.
        LCMR
        TAD SAVAC

EXIT,   RMF         /GO BACK TO INTERRUPTED PROGRAM.
        ION
        JMP I 0

SAVAC,  0
XCLSV,  CLSERVE
XADSV,  ADSERVE
XMTRUN, MTRUN


FIELD 5
/******


/                       PAGE ZERO VARIABLES, LITERALS ETC.
/                       **********************************

*100

/SOFTWARE FLAGS & SWITCHES.
BUFRDY, 0               /RAM BUFFER FULL OF DATA TO BE PROCESSED.
ADRUN,  0               /A-D CONVERSION IN PROGRESS.
SWITCH, 0               /SWITCHES BETWEEN MT BUFFERS.
```

```
MTRUN,   0                /MAGTAPE WRITE IN PROGRESS.
NOFILT,  0                /DISABLES FILTER ON FIRST PULSE OR IF NAV = 1.
MARK,    1                /MARK END OF EACH FILTER BUFF. O.P. IN MT BUFF.
MTEN,    0                /ENABLES MT WRITE ON NEXT MS INTERRUPT.

/COUNTERS.
CNTPLS,  0                /COUNTS TRANSMITTED PULSES.
CNTBLK,  0                /COUNTS MAGTAPE BLOCKS.
CNTSMP,  0                /COUNTS A-D SAMPLES.

/BUFFER POINTERS.
HFPTR,   0                /POINTER TO HIGH PART OF FILTER BUFFER.
LFPTR,   0                /POINTER TO LOW PART OF FILTER BUFFER.
MTPTR,   0                /MAGTAPE BUFFER POINTER.
RAMPTR,  0                /A-D RAM BUFFER POINTER.

/ADDRESSES.
XMTDATA,0                 /ADDRESS OF DATA SECTION OF CURRENT MT BUFFER.
XBLOKNO,0                 /ADDRESS OF BLOCK NO. IN MT BUFFER.
XTAB,    RAMTAB           /ADDRESS OF TABLE OF REQUIRED A-D SAMPLE NUMBERS
XHFBUF,  HFLTBUF          /ADDRESSES OF HIGH AND LOW PARTS OF DIGITAL
XLFBUF,  LFLTBUF          /FILTER BUFFER.
MTTAB,   MTBUF1           /TABLE OF ADDRESSES OF THE MAGTAPE BUFFERS.
         MTBUF2
XMTAB,   MTTAB            /ADDRESS OF TABLE OF MT BUFFER ADDRESSES.
ADDR,    0                /STORES ADDRESS OF MT BUFFER.
XMTRAN,   MTRAN              /ADDRESS OF MAGTAPE SUBROUTINE.
XNMS,       NMS              /ADDRESS OF TIME SINCE LAST TX PULSE.
XDELTX,     DELTX          /ADDRESS OF TIME BETWEEN TX PULSES.
XFILTER,FILTER            /ADDRESS OF DIGITAL FILTER ROUTINE.
XDTRANS,DRTRAN            /ADDRESS OF DIRECT TRANSFER ROUTINE.
GOHOME,  L4               /ERROR RETURN ADDRESS.
XMTBUF,  0                /ADDRESS OF CURRENT MAGTAPE BUFFER.
XMTCA,   MTCA             /ADDRESS OF CURRENT ADDRESS FOR MT ROUTINE.

/CONSTANTS.
N4,      4
M0001,1
A4000,   4000
A6000,  6000

/OTHERS.
NAV,     15               /NO.OF TX PULSES FILTERED PER TIMESERIES SAMPLE.
NBLOKS,  100              /TOTAL NUMBER OF MT BLOCKS.
 HEDLEN,  HEDWC              /LENGTH OF MT BUFFER HEADER.
DATALEN,DATAWC             /LENGTH OF MT BUFFER DATA SECTION.
TABLEN,   6               /LENGTH OF RAM ADDRESS TABLE.
ERROR,    0                 /ERROR STATUS WORD.
MTDEL,   1                /DELAYS TO FINE TUNE TIMING OF A-D AND
ADDEL,   1                /MT START.



/                         INTERRUPT SERVICE ROUTINES
/                         **************************

*200

/FAST A-D INTERRUPT ROUTINE
/--------------------------

ADSERVE,DCA SAVAC1
        ADEN              /STOP A-DS AND DISABLE INTERRUPT.
        ADID
        ADCL              /CLEAR FAST A-D FLAG.
        IAC               /SET FLAG INDICATING THAT A-D RAM CONTAINS
```

```
        DCA I XBUFRDY   /DATA TO BE PROCESSED.
        DCA I XADRUN    /RESET A-D RUN FLAG.
        TAD SAVAC1
        CDF CIF
        JMP EXIT
SAVAC1, 0               /STORES ACCUMULATOR.
XBUFRDY,BUFRDY
XADRUN, ADRUN


/MILLISECOND CLOCK INTERRUPT SERVICE ROUTINE
/-------------------------------------------

CLSERVE,DCA SAVAC3      /SAVE ACCUMULATOR AND LINK.
        RAR
        DCA SAVL
        CLCF            /CLEAR MILLISECOND CLOCK FLAG.

        ISZ NMS         /INCREMENT TIME.
        TAD NMS
        CIA
        TAD DELTX       /TIME FOR ANOTHER TRANSMITTER PULSE?
        SZA CLA
        JMP CL1
        DCA NMS         /YES. CLEAR TIME AND TRIGGER TRANSMITTER.
        TAD TXFLAG
        LSCR
        CLA
        LSCR
        JMP CL2

CL1,    TAD NMS         /TIME TO START A-D CONVERSION?
        CIA
        TAD STMARKER
        SZA CLA
        JMP CL2
        TAD I XBUFRDY   /YES. CHECK THAT PREVIOUS RAM BUFFER HAS
        SZA CLA         /BEEN READ OUT.
        JMP ERR1
        TAD I XADRUN    /CHECK THAT A-DS NOT STILL RUNNING.
        SZA CLA
        JMP ERR2
        IAC
        DCA I XADRUN    /SET A-D RUNNING FLAG.
        JMS ADSTART     /START A-D CONVERSION AND EXIT.
        JMP CL2

/SIGNAL ERROR CONDITIONS TO FOREGROUND PROGRAM.

ERR1,   TAD ERROR       /READING OF PREVIOUS A-D BUFFER NOT COMPLETE.
        IAC
        DCA ERROR
        JMP I GOHOME

ERR2,   TAD ERROR
        IAC
        IAC             /PREVIOUS A-D CONVERSION NOT YET FINISHED.
        DCA ERROR
        JMP I GOHOME

/SYNCHRONIZE MAGTAPE WRITE TO MILLISECOND MARKER
/TO ENSURE STABLE TIMING.

CL2,    CLA
        TAD MTEN                /IF MT ENABLED THEN DO MT WRITE.
        SNA CLA
```

```
        JMP CL3                 /NOT ENABLED. RETURN FROM MS ROUTINE.
        DCA MTEN                /RESET ENABLE FLAG.

        TAD MTDEL               /DELAY LOOP TO FINE TUNE POSITION
        CIA                  /OF MT INTERRUPT.
        DCA COUNT
        ISZ COUNT
        JMP .-1

        JMS I XMTRAN            /START MAGTAPE WRITE.
        WCOUNT                  /TOTAL NO. OF WORDS IN BUFFER.
MTCA,   0                       /ADDRESS OF START OF BUFFER.
        2142                /WRITE+GO+ODD PARITY+INT. ENABLE COMMAND.
        CLA                     /CHECK FOR ERRORS.
        TAD ERROR
        SZA CLA
        JMP I GOHOME

CL3,    CLA CLL             /RESTORE SAVED ACCUMULATOR AND LINK.
        TAD SAVL
        RAL
        TAD SAVAC3
        CDF CIF
        JMP EXIT

SAVAC3, 0                   /STORES ACCUMULATOR.
SAVL,   0                   /STORES LINK.
NMS,    0                   /NO. OF MILLISECONDS SINCE LAST TX PULSE.
DELTX,  24                 /TIME BETWEEN TX PULSES IN MILLISECONDS.
TXFLAG, 7700                /THE COMMAND THAT TRIGGERS THE TRANSMITTER.
STMARKER,1                  /TIME FROM TX TRIG. TO A-D START.

/ROUTINE TO START THE FAST A-DS
/------------------------------

ADSTART, 0                  /VARIABLE DELAY LOOP TO PREVENT A-DS
        CLA                 /FROM STARTING ON A HEIGHT MARKER.
        TAD DELAY              /CHANGE DELAY TO VARY.
        CIA
        DCA COUNT
        ISZ COUNT
        JMP .-1

        ADCL                /CLEAR FLAGS.
        TAD RAMCA           /LOAD RAM CURRENT ADDRESS REGISTER.
        ADLC
        CLA
        TAD FADWC           /LOAD WORD COUNT REGISTER.
        ADLC
        CLA
        TAD ADMUX           /LOAD MULTIPLEXER COMMAND.
        ADLC
        CLA
        TAD ADFCN           /LOAD FUNCTION COMMAND.
        ADLC
        CLA
        ADIE                /ENABLE WORD COUNT OVERFLOW INTERRUPT.
        TAD A1000
        ADEN                /START A-DS.
        JMP I ADSTART
RAMCA,  0                   /STARTING ADDRESS OF RAM MEMORY.
FADWC,  1467                 /FAST A-D WORD COUNT. (10 BIT).
ADMUX,  0       /MULTIPLEXER COMMAND. BITS 3-6 ARE STARTING CHANNEL.
ADFCN,  33      /BIT 8 = 2.5KM. BIT 9 = 1KM. 3-7=NO. OF MUX. CHANNELS
A1000,  1000                /COMMAND THAT STARTS A-DS.
COUNT, 0           /DELAY LOOP COUNTER.
```

```
DELAY,     5                /DELAY FOR FINE TUNING A-D START TIMING.


/                           TSWRITE FOREGROUND PROGRAM
/                           **************************

*400

/INITIALIZATION SECTION.

TSWRITE, 0
        CLA CMA             /RESET COUNTERS, FLAGS ETC.
        TAD I XDELTX
        DCA I XNMS
        DCA BUFRDY
        DCA ADRUN
        DCA MTRUN
        DCA ERROR
        TAD NAV
        CIA
        DCA CNTPLS
        DCA SWITCH

        TAD MTTAB           /INITIALIZE MAGTAPE BUFFER.
        DCA XMTBUF
        TAD MTTAB
        TAD HEDLEN
        DCA XMTDATA
        TAD MTTAB
        TAD N4
        DCA XBLOKNO
        TAD NBLOKS
        CIA
        DCA CNTBLK
        TAD XMTDATA
        DCA MTPTR
        IAC                 /NO DIGITAL FILTERING ON FIRST PULSE.
        DCA NOFILT

        CLCF                /TURN ON THE INTERRUPT SYSTEM.
        MSE
        KIE
        ION

/WAIT FOR A FULL FAST A-D RAM BUFFER.

L1,     CLA
        TAD BUFRDY
        SNA CLA
        JMP L1

/GET SAMPLES FROM RAM AND DO DIGITAL FILTERING.

        CLA                 /MAKE POINTER TO RAM ADDRESS TABLE AND
        TAD XTAB            /HIGH AND LOW PARTS OF FILTER BUFFER.
        DCA RAMPTR
        TAD XHFBUF
        DCA HFPTR
        TAD XLFBUF
        DCA LFPTR
        TAD TABLEN
        CIA
        DCA CNTSMP
```

```
        ADCL            /SET A-DS TO RAM READ MODE.

        CLA             /IF FIRST TIME THROUGH THEN TRANSFER SAMPLES
        TAD NOFILT      /DIRECTLY TO FILTER BUFFER OTHERWISE DO
        SZA CLA         /DIGITAL FILTERING.
        JMP L5
        JMS I XFILTER
        JMP L6
L5,     JMS I XDTRANS
        CLA CMA         /DISABLE FILTER IF NAV = 1.
        TAD NAV
        SZA CLA
        DCA NOFILT
L6,     CLA             /CLEAR A-D BUFFER SOFTWARE FLAG.
        DCA BUFRDY

/EVERY NAV = DELTS/DELTX PULSES THE FILTER OUTPUT IS WRITTEN
/TO THE MAGTAPE BUFFER.

        ISZ CNTPLS      /NAV PULSES YET?
        JMP L1          /NO. GO BACK AND WAIT FOR ANOTHER PULSE.

        CLA             /YES. REINITIALIZE PULSE COUNTER.
        TAD NAV
        CIA
        DCA CNTPLS

        CLA             / INITIALIZE FOR TRANSFER FROM FILTER
        TAD XHFBUF      /BUFFER TO MAGTAPE BUFFER.
        DCA HFPTR
        TAD TABLEN
        CIA
        DCA CNTSMP

L3,     TAD I HFPTR     /TRANSFER FILTER OUTPUT VALUE.
        DCA I MTPTR

        ISZ HFPTR       /INCREMENT POINTERS.
        ISZ MTPTR
        ISZ CNTSMP
        JMP L3          /GO BACK FOR NEXT VALUE.
        TAD MARK        /MARK OPTION PUTS -1 IN MAGTAPE BUFFER
        SNA CLA         /AFTER EACH FILTER BUFFER OUTPUT.
        JMP L7
        CMA
        DCA I MTPTR
        ISZ MTPTR

/CHECK TO SEE WHETHER ENOUGH SPACE REMAINS IN THE MAGTAPE BUFFER
/FOR THE NEXT SET OF FILTER OUTPUT VALUES.

L7,     CLA
        TAD MTPTR
        TAD TABLEN       /LENGTH OF FILTER BUFFER.
        TAD MARK
        CIA
        TAD XMTDATA     /ADDRESS OF MT BUFFER DATA SECTION.
        TAD DATALEN     /LENGTH OF MT BUFFER DATA SECTION.
        SMA CLA
        JMP L1          /ENOUGH SPACE SO GO BACK.

        TAD CNTBLK      /RECORD BLOCK NUMBER ON MAGTAPE.
        IAC
        TAD NBLOKS
        DCA I XBLOKNO
```

```
        TAD XMTBUF      /SET MAGTAPE CURRENT ADDRESS.
        DCA I XMTCA
        ISZ MTEN        /ENABLE MT WRITE ON NEXT MS INTERRUPT.

        ISZ SWITCH      /SWITCH TO ALTERNATE BUFFER.
        TAD SWITCH
        AND M0001       /SWITCH MOD 2.
        DCA SWITCH
        TAD XMTAB
        TAD SWITCH
        DCA ADDR
        TAD I ADDR
        DCA XMTBUF
        TAD XMTBUF
        TAD HEDLEN
        DCA XMTDATA
        TAD XMTBUF
        TAD N4
        DCA XBLOKNO
        TAD XMTDATA
        DCA MTPTR

        ISZ CNTBLK      /LOOP OVER REQUIRED NO. OF MT BLOCKS.
        JMP L1

L4,     TAD MTEN        /WAIT FOR PENDING MAGTAPE WRITE
        SZA CLA         /TO START.
        JMP .-2
        MSD             /WAIT FOR MAGTAPE WRITE TO FINISH.
        TAD MTRUN
        SZA CLA
        JMP .-2

        IOF             /TURN OFF INTERRUPT AND GO BACK
        CDF CIF 60      /VIA FIELD 6 LINK.
        JMP I TSWRITE


/                       DIGITAL FILTER ROUTINE
/                       **********************

/A RECURSIVE DIGITAL RC FILTER. THE FILTER OUTPUTS FOR EACH RANGE
/AND CHANNEL ARE STORED IN A BUFFER, FLTBUF. THE A-D SAMPLE FOR
/A PARTICULAR RANGE AND CHANNEL, X, IS READ FROM THE A-D RAM BUFFER
/AND COMBINED WITH THE PREVIOUS OUTPUT FROM THIS RANGE AND CHANNEL
/BY: <NEW OUTPUT> = (1-COEFF)*X + COEFF*<PREVIOUS OUTPUT>. THIS IS
/REPEATED FOR ALL THE RANGES AND CHANNELS.
/COEFF IS A COEFFICIENT DETERMINED BY THE FILTER BANDWIDTH AND SAMPLING
/INTERVAL. IT IS REPRESENTED IN SIGNED BINARY FRACTION FORMAT AND MAY
/NOT BE NEGATIVE.
/MULTIPLICATIONS ARE PERFORMED IN DOUBLE PRECISION TO KEEP ROUND OFF
/ERROR LESS THAN A-D LEAST SIGNIFICANT BIT.

*600

FILTER, 0
F3,     CLRMUL          /MULTIPLY PREVIOUS OUTPUT BY FILTER COEF.
        CLA
        DCA MFLAG
        TAD I HFPTR             /GET PREVIOUS OUTPUT FROM BUFFER.
        SMA
        JMP F1
        ISZ MFLAG
        CIA
```

```
F1,     LOADX
        CLA
        TAD A                   /MULTIPLY BUFFER OUTPUT BY FILTER COEFF.
        LOADY
        MULT
        NOP
        NOP
        CLA CLL
        GETL                    /GET DOUBLE PRECISION RESULT AND STORE IT.
        RAL                     /LEFT SHIFT AS A IS A SIGNED BINARY FRACTION
        DCA L
        GETM
        RAL
        DCA M
        TAD MFLAG               /CORRECT FOR SIGN OF BUFFER VALUE.
        SZA
        JMS NEG1

        CLRMUL          /GET A-D VALUE AND MULTIPLY BY 1-COEFF ( = B ).
        CLA
        DCA MFLAG
        ADCL
        TAD I RAMPTR    /GET A-D VALUE FROM RAM BUFFER.
        ADLC
        CLA
        ADLA
        CIA             /VALUE IS TWO'S COMPLIMENT.
        TAD A4000
        SNA             /CORRECT +5V VALUE.
        CMA
        TAD A4000
        SMA
        JMP F2
        ISZ MFLAG
        CIA
F2,     LOADX
        CLA
        TAD B
        LOADY
        MULT
        NOP
        NOP
        CLA CLL
        GETL
        RAL
        DCA LA
        GETM
        RAL
        DCA MA
        TAD MFLAG
        SZA
        JMS NEG2

        CLA CLL         /ADD THE TWO DOUBLE PRECISION MULTIPLY RESULTS.
        TAD L
        TAD LA
        DCA I LFPTR
        RAL
        TAD M
        TAD MA
        DCA I HFPTR
        ISZ LFPTR               /INCREMENT POINTERS AND COUNTER.
        ISZ HFPTR
        ISZ RAMPTR
        ISZ CNTSMP
        JMP F3
```

```
        JMP I FILTER
A,      3050
B,      730
L,      0
M,      0
LA,     0
MA,     0
MFLAG,  0


NEG1,   0
        CLA CLL
        TAD L
        CIA
        DCA L
        RAL
        DCA ST
        TAD M
        CMA
        TAD ST
        DCA M
        JMP I NEG1
ST,     0


NEG2,   0
        CLA CLL
        TAD LA
        CIA
        DCA LA
        RAL
        DCA ST
        TAD MA
        CMA
        TAD ST
        DCA MA
        JMP I NEG2

/                       MAGTAPE WRITE ROUTINE
/                       **********************

*1000

MTRAN,  0
        CLA CLL
        RMSR    /READ STATUS
        AND (2002)
        SZA     /REWINDING OR RUNNING?
        JMP .-4 /YES
        RMSR    /WHY DID IT STOP?
        AND (0010)      /EOT TEST
        SZA
        JMP MTERR1
        RMSR    /CHECK IF TRANSPORT READY
        AND (0402)
        TAD (-0400)
        SZA     /ON LINE AND NO WRITE LOCK
        JMP MTERR2
        CLT
        CLF
        CLA CLL IAC     /ACC = +1
        TAD I MTRAN     /GET WORD COUNT
        CMA IAC
        LWCR
        ISZ MTRAN
        CLA CLL CMA     /ACC = -1
```

```
        TAD I MTRAN
        LCAR
        CLA
        TAD N5
        SDBF
        CLA
        ISZ MTRAN
        TAD I MTRAN     /GET COMMAND
        LCMR
        ISZ MTRUN
        ISZ MTRAN
        JMP I MTRAN
N5,     5
N10,    10

/SET MAGTAPE ERROR BITS.

MTERR1, CLA             /MAGTAPE AT END OF TAPE.
        TAD ERROR
        TAD N4
        DCA ERROR
        ISZ MTRAN
        ISZ MTRAN
        ISZ MTRAN
        JMP I MTRAN

MTERR2, CLA             /MAGTAPE OFF LINE OR WRITE LOCKED.
        TAD ERROR
        TAD N10
        DCA ERROR
        ISZ MTRAN
        ISZ MTRAN
        ISZ MTRAN
        JMP I MTRAN




/                       ALGOL MAGTAPE WRITE IO DEVICE
/                       ****************************

*1200

/CHOUT(26,0)

MTWRITE, 0
        CLA             /DISABLE MILLISECOND AND KEYBOARD INTERRUPTS.
        MSD
        KIE
        ION             /TURN ON THE INTERRUPT SYSTEM.

        JMS I XMTRAN
        WCOUNT
        MTBUF1
        2142
        CLA

M1,     TAD MTRUN               /WAIT FOR MT WRITE TO FINISH.
        SZA CLA
        JMP M1

        IOF             /TURN OFF INTERRUPT AND GO BACK THROUGH
        CDF CIF 60      /FIELD 6 LINK.
        JMP I MTWRITE
```

```
/                       TX TRIG. A-D CONVERSION ALGOL IO DEVICE
/                       ***************************************

/CHOUT(28,0)

ADTRIG, 0
        CLA
        CLCF
        MSE             /ENABLE MILLISECOND INTERRUPT.
        KIE             /DISABLE KEYBOARD INTERRUPT.
        ION             /TURN ON INTERRUPT AND WAIT FOR FULL
                        /A-D RAM BUFFER.
AD1,    CLA
        TAD BUFRDY
        SNA CLA
        JMP AD1

        IOF             /GO BACK THROUGH FIELD 6 LINK.
        CDF CIF 60
        JMP I ADTRIG


/                       ALGOL A-D RAM READ DEVICE
/                       *************************

/READS A VALUE FROM THE A-D RAM BUFFER. ADDRESS OF VALUE IS IN
/RAMADR. VALUE IS RETURNED IN ACCUMULATOR.

ADGET,  0
        CLA
        DCA BUFRDY      /RESET A-D SOFTWARE FLAG.

        ADCL            /SET A-DS TO READ MODE.

        CLA             /SET RAM ADDRESS.
        TAD RAMADR
        ADLC

        CLA             /GET VALUE.
        ADLA

        CIA             /VALUE IS TWO'S COMPLIMENT.
        TAD A4000       /CORRECT +5V VALUE.
        SNA
        CMA
        TAD A4000

        CDF CIF 60      /RETURN WITH VALUE IN ACCUMULATOR.
        JMP I ADGET
RAMADR, 0


/                       DIRECT RAM TO FILTER BUFFER TRANSFER ROUTINE
/                       *******************************************

DRTRAN, 0

D1,     CLA
        ADCL
        TAD I RAMPTR            /GET A-D SAMPLE.
        ADLC
        CLA
```

```
        ADLA
        CIA                     /CORRECT IT.
        TAD A4000
        SNA
        CMA
        TAD A4000
        DCA I HFPTR             /STORE IT IN FILTER BUFFER.
        ISZ HFPTR               /INCREMENT POINTERS AND GO BACK.
        ISZ LFPTR
        ISZ RAMPTR
        ISZ CNTSMP
        JMP D1
        JMP I DRTRAN


/                       BUFFERS AND TABLES
/                       ******************

*1400

/A-D RAM ADDRESS TABLE.
/----------------------

RAMTAB, 100             /CONTAINS RAM ADDRESSES OF REQUIRED A-D SAMPLES.
        101             /THESE NUMBERS ARE DEFAULT VALUES.
        102
        103
        104
        105


*2000

/MAGTAPE BUFFER NO. 1.
/---------------------

HEDWC=12
DATAWC=454
WCOUNT=HEDWC+DATAWC+4

MTBUF1, TEXT "BIRDLING"
*MTBUF1+HEDWC+DATAWC
        TEXT "FINISHED"


/MAGTAPE BUFFER NO. 2.
/---------------------

*3000

MTBUF2, TEXT "BIRDLING"
*MTBUF2+HEDWC+DATAWC
        TEXT "FINISHED"


*4000

/DIGITAL FILTER OUTPUT BUFFER.
/-----------------------------

HFLTBUF,0       /BUFFER FOR HIGH WORDS OF DOUBLE PRECISION RESULT.

*4400

LFLTBUF,0       /BUFFER FOR LOW WORDS OF DOUBLE PRECISION RESULT.
```

```
/ROUTINE TO STOP RUNAWAY MAGTAPE.
/---------------------------------

FIELD 4
/******

*44

        CLA
        CLT
        CLF
        LCMR
        HLT
$
```

APPENDIX D

PROGRAM TO COMPUTE DOPPLER SPECTRA FROM SEA ECHO TIMESERIES DATA

```
 $RESET BINDER LIST
 $SET AUTOBIND
 $BIND = FROM PLOTA/=,OBJECT/GRAPH
BEGIN
   %
   %PERFORMS SPECTRAL ANALYSIS ON A SERIES OF RADAR ECHO VOLTAGES
   %STORED ON THE TSDATA/<TIMESTAMP> FILES. (INTERNAL NAME TSFILE).
   %THE TIMESERIES OF N COMPLEX DATA POINTS
   %IS DIVIDED INTO NSEGS OVERLAPPING SEGMENTS EACH OF LENGTH
   %LSEG. EACH SEGMENT IS ADJUSTED TO ZERO MEAN, MULTIPLIED BY
   %A WINDOW FUNCTION AND FOURIER TRANSFORMED. THE FOURIER
   %TRANSFORMS OF THE SEGMENTS ARE THEN CONVERTED TO ESTIMATES
   %OF POWER SPECTRAL DENSITY AND AVERAGED TO PRODUCE THE FINAL
   %SPECTRUM. THE SPECTRUM CAN BE OUTPUT TO EITHER A DISK
   %FILE OR THE PLOTTER.
   %
   %                          DATA FILE FORMAT:
   %                          -----------------
   %
   %DATA IS STORED AS A THREE DIMENSIONAL ARRAY OF A-D SAMPLES
   %EACH ONE PDP8 WORD (12 BITS) LONG. E.G FOR TWO RANGES,
   %THREE A-D CHANNELS:
   %
   %        PDP8 WORD                          CONTENTS
   %        ---------                          --------
   %
   %            0                    PULSE 0    RANGE 1    CHANNEL 1
   %            1                      P1         R1         CH2
   %            2                      P1         R1         CH3
   %            3                      P1         R2         CH1
   %            4                      P1         R2         CH2
   %            5                      P1         R2         CH3
   %            6                      P2         R1         CH1
   %                                     .
   %                                     .
   %                                     .
   %                                   ETC.
   %
   %                       TIMESERIES FORMAT:
   %                       ------------------
   %
   %THE TIMESERIES CONSISTS OF SUCCESSIVE PULSES FROM ONE RANGE
   %AND TWO A-D CHANNELS (REAL AND IMAGINARY PARTS OF COMPLEX
   %TIMESERIES).  E.G.
   %
   %    TIMESERIES SAMPLE          REAL PART          IMAGINARY PART
   %    -----------------          ---------          --------------
   %
%           0              P0   R1    CH1          P0   R1    CH2
%           1              P1   R1    CH1          P1   R1    CH2
%           2              P2   R1    CH1          P2   R1    CH2
   %           .                    .                       .
   %           .                    .                       .
   %           .                    .                       .
%           N-1            PN-1 R1    CH1          PN-1 R1    CH2


   %DATA FILE DECLARATION
   %**********************
```

```
  FILE TSFILE(KIND=DISK,MAXRECSIZE=14,BLOCKSIZE=420);

  %I/O DECLARATIONS:
  %*****************

  FILE LP(KIND=PRINTER,MAXRECSIZE=22);
  FILE SCREEN(KIND=REMOTE,MAXRECSIZE=14,MYUSE=IO);
  FILE PLOTFILE(KIND=DISK,MAXRECSIZE=14,BLOCKSIZE=420,
  TITLE="PLOTFILE.",SECURITYUSE=IO);
  SWITCH FILE OUTPUT := LP,SCREEN;
  INTEGER SELECT;
  BOOLEAN LPOUT,SCREENOUT;
  DEFINE INFORM = FOR SELECT := (IF LPOUT THEN 0 ELSE 1 )
  STEP 1 UNTIL (IF SCREENOUT THEN 1 ELSE 0 ) DO
  WRITE(OUTPUT[SELECT]#; % DETERMINES WHERE THE OUTPUT GOES.
  DEFINE OSCR = IF SCREEN.KIND=3 THEN WRITE(SCREEN#; %OUTPUT TO
  %SCREEN IF IN INTERACTIVE MODE.
  DEFINE NEWPAGE = IF LPOUT THEN WRITE(LP[SKIP 1])#;

  REAL ARRAY SCREENBUFF[0:13];
  POINTER PB;
  INTEGER CHARS;

  DEFINE
  FIRSTWORD = SCAN PB:PB FOR CHARS:70 UNTIL NEQ " "#,

  NEXTWORD = SCAN PB:PB FOR CHARS:CHARS UNTIL = " ";
  SCAN PB:PB FOR CHARS:CHARS WHILE = " "#,

  SKIPWORD = SCAN PB:PB FOR CHARS:CHARS UNTIL = " "#;

$ USE SCREEN FOR FILE5;


  %DATA BUFFER:
  %************

  REAL ARRAY BUFFER[0:1023];%STORES COMPRESSED DATA FROM ONE 7 TRACK
  %MAGTAPE BLOCK.
  DEFINE
  WORD(I) = BUFFER[(I) DIV 4].[(47-((I) MOD 4)*12):12]#;
  %GETS PDP8 WORD FROM BUFFER.


  %VARIABLES
  %*********

  INTEGER N; %TOTAL NUMBER OF DATA POINTS USED.

  INTEGER LSEG; %LENGTH OF DATA SEGMENT.

  INTEGER LFFT; %LENGTH OF FAST FOURIER TRANSFORM ( >= LSEG).

  INTEGER NSEGS; %NUMBER OF DATA SEGMENTS.

  REAL DELTAT;  %TIME INTERVAL BETWEEN DATA POINTS IN SECONDS.


  COMPLEX ARRAY X[0:2047]; %DATA ARRAY FOR FFT. CONTAINS
  %DATA FROM ONE SEGMENT.

  REAL ARRAY WINDOW[0:2047]; %THE WINDOW USED TO SMOOTH THE
  %DATA POINTS.

  REAL U; %THE INCOHERENT POWER GAIN OF THE WINDOW.
```

```
   REAL ARRAY SXX[-1024 : 1023]; %ARRAY
   %OF SPECTRAL VALUES.

   REAL ARRAY FREQUENCY[-1024 : 1023];
   %ARRAY OF FREQUENCIES OF THE SPECTRAL ESTIMATES.

   REAL NORM; %NORMALIZATION FACTOR REQUIRED TO CONVERT SQUARED
   %MAGNITUDES OF FFT VALUES INTO POWER SPECTRAL DENSITY ESTIMATES.

   REAL TSEG; %TIME LENGTH OF DATA SEGMENT IN SECONDS.


   REAL RESOLUTION; %FREQUENCY RESOLUTION IN HERTZ.

   REAL FREQSTEP; %FREQUENCY STEP BETWEEN SPECTRUM/FFT POINTS IN HERTZ.

   REAL NSE; %NORMALIZED STANDARD ERROR OF SPECTRAL ESTIMATE.

   REAL COR50; %50 PERCENT OVERLAPP CORRELATION OF THE DATA WINDOW.

INTEGER ADSTEP,NBITS;

   INTEGER WINDOWTYPE; %TYPE OF DATA WINDOW:
   %              0 = RECTANGULAR
   %              1 = HAMMING
   %              2 = COOLEY,WELCH & LEWIS (CWL)
   %              3 = MINIMUM 4 TERM BLACKMAN HARRIS

   INTEGER I,J,K,MARK,STMARKER,RGNTX,NWORDS;
   REAL TWOPI;
   BOOLEAN FILEIT,PLOTIT;
   INTEGER NBLOCKS,NCHANS,NRANGES,NPBLOCK,CURRENTBLOCK,RANGENO,
   REALCHAN,IMAGCHAN;
   BOOLEAN REALDATA;        %ALLOWS THE OPTION OF PURELY REAL DATA.
   REAL CHR;
   INTEGER ARRAY DATE[0:4],RGN[1:50],RANGETABLE[1:100];
   INTEGER RINDEX,NOTOANALYSE;


$INCLUDE "PLOTA/EXTLDECLS"
   PROCEDURE FFT(X,N,INV);
   VALUE N,INV;
   INTEGER N;
   BOOLEAN INV;
   COMPLEX ARRAY X[*];
   BEGIN
      %
      %FAST FOURIER TRANSFORM PROCEDURE.
      %IF INV IS FALSE REPLACE THE COMPLEX ARRAY OF N DATA
      %POINTS, X, WITH ITS FOURIER TRANSFORM. IF INV IS
      %TRUE THE INVERSE TRANSFORM IS TAKEN.
      %
      INTEGER I,J,K,L,N2,NU1,NU;
      COMPLEX T,W;
      REAL P,TPI;


      INTEGER PROCEDURE BITREV(J,NU);
      VALUE J,NU;
      INTEGER J,NU;
      BEGIN
         INTEGER WORD,PIVOTBIT,TOPBIT,WHICHBIT;

         WORD := J;
         PIVOTBIT := (TOPBIT := NU-1) DIV 2;
```

```
      FOR WHICHBIT := 0 STEP 1 UNTIL PIVOTBIT DO
      WORD := *&WORD[WHICHBIT:TOPBIT-WHICHBIT:1]&
      WORD[TOPBIT-WHICHBIT:WHICHBIT:1];
      BITREV := WORD
   END OF BITREV;


   NU := LN(N)/LN(2);
   N2 := N DIV 2;
   NU1 := NU-1;
   K := 0;
   TPI := 8*ARCTAN(1);

   FOR L := 1 STEP 1 UNTIL NU DO
   BEGIN
      DO
      BEGIN
         FOR I := 1 STEP 1 UNTIL N2 DO
         BEGIN
            J := 2**NU1;
            P := BITREV( (K DIV J) , NU );
            W := COMPLEX( COS(TPI*P/N) , -1*SIN(TPI*P/N) );
            IF INV THEN
            W := CONJUGATE(W);

            T := X[K+N2]*W;
            X[K+N2] := X[K]-T;
            X[K] := X[K]+T;
            K := K+1
         END;
         K := K+N2
      END
      UNTIL K >= N-1;
      K := 0;
      NU1 := NU1-1;
      N2 := N2 DIV 2
   END;

   K := -1;
   DO
   BEGIN
      K := K+1;
      I := BITREV(K,NU);

      IF I > K THEN
      BEGIN
         T := X[K];
         X[K] := X[I];
         X[I] := T
      END
   END
   UNTIL K >= N-1;

   IF INV THEN
   FOR I := 0 STEP 1 UNTIL N-1 DO
   X[I] := X[I]/N
END OF FFT;


INTEGER PROCEDURE FIXSIGN(SAMP);
VALUE SAMP;
INTEGER SAMP;
BEGIN
   %
   %BIT 11 ON INDICATES A NEGATIVE NUMBER ON THE PDP8.
   %NEGATIVE NUMBERS CAN BE GENERATED BY THE FAST A-D'S.
```

```
   %
   INTEGER DUM;

   IF SAMP > 2047 THEN
   DUM := SAMP-4096
   ELSE
   DUM := SAMP;
   FIXSIGN := DUM
END OF FIXSIGN;


PROCEDURE INPUTBLOCK;
BEGIN
   INTEGER I,MRSIZE;
   %
   %READS A BLOCK FROM TSDATA FILE INTO BUFFER.
   %
   FOR I := 0 STEP 1 UNTIL 1023 DO
   BUFFER[I] := 0;

   I := 0;
   MRSIZE := 14;
   READ(TSFILE,//,NWORDS);

   DO
   BEGIN
      READ(TSFILE,MRSIZE,BUFFER[I]);
      I := I+MRSIZE
   END
   UNTIL I > NWORDS OR I >= 1023;
   CURRENTBLOCK := CURRENTBLOCK+1
END OF INPUTBLOCK;


PROCEDURE OUTPUTBLOCK;
BEGIN
   %WRITES A SPECTRUM TO THE OUTPUT FILE
   %IN COMPRESSED FORMAT.

   INTEGER I,MRSIZE;

   I := 0;
   MRSIZE := 14;

   WRITE(PLOTFILE,//,LFFT,-1*(LFFT DIV 2)*FREQSTEP,FREQSTEP);
   DO
   BEGIN
      WRITE(PLOTFILE,MRSIZE,SXX[I-(LFFT DIV 2)]);
      I := I+MRSIZE
   END
   UNTIL I > LFFT OR I > 2048
END OF OUTPUTBLOCK;


PROCEDURE SKIPTOBLOCK(BLOCK);
VALUE BLOCK;
INTEGER BLOCK;
BEGIN
   %SKIPS TO BLOCK NUMBER BLOCK IN THE INPUT FILE. THE
   %NEXT CALL OF INPUTBLOCK WILL READ BLOCK NUMBER BLOCK
   %INTO BUFFER.

   IF CURRENTBLOCK >= BLOCK THEN
   BEGIN
      REWIND(TSFILE);
      CURRENTBLOCK := 0
```

```
      END;

      WHILE CURRENTBLOCK < BLOCK-1 DO
      INPUTBLOCK
   END OF SKIPTOBLOCK;


INTEGER PROCEDURE ATOD(ADSTEP,NBITS,SAMP);
VALUE ADSTEP,NBITS;
INTEGER ADSTEP,NBITS,SAMP;
BEGIN
%THIS IS A DEMONSTRATION PROCEDURE THAT SIMULATES THE
%EFFECT OF AN A-D CONVERTOR WITH A REDUCED NUMBER OF BITS.
%IT IS NOT NECCESSARY FOR THE OPERATION OF THE PROGRAM
%AND MAY BE REMOVED IF DESIRED.
%

INTEGER X,MAX;

X := ENTIER(SAMP/ADSTEP + 0.5);
MAX := (2**NBITS - 1)/2;

IF X > MAX THEN X := MAX;
IF X < -1*MAX THEN X := -1*MAX;
ATOD := X
END OF ATOD;


   INTEGER PROCEDURE GETSAMPLE(PULSE,RANGENO,CHANNEL);
   VALUE PULSE,RANGENO,CHANNEL;
   INTEGER PULSE,RANGENO,CHANNEL;
   BEGIN
      INTEGER SAMP,BLOCKNO,PULSEINBLOCK,DATASTART,WORDNO;

      %
      %FIND OUT WHICH BLOCK THE PULSE IS IN.
      %

      BLOCKNO := (PULSE DIV NPBLOCK)+2;
      PULSEINBLOCK := PULSE MOD NPBLOCK;

      %GET THIS BLOCK INTO THE BUFFER.

      IF CURRENTBLOCK NEQ BLOCKNO THEN
      BEGIN
         SKIPTOBLOCK(BLOCKNO);
         INPUTBLOCK
      END;

      %CALCULATE WORD NUMBER OF SAMPLE.

      DATASTART := 10;
      WORDNO := DATASTART+(NRANGES*NCHANS+MARK)*PULSEINBLOCK
      +NCHANS*(RANGENO-1)+CHANNEL;

      %GET SAMPLE, CORRECT SIGN AND OUTPUT DATA.

      SAMP := WORD(WORDNO);
      SAMP := FIXSIGN(SAMP);
SAMP := ATOD(ADSTEP,NBITS,SAMP);

      GETSAMPLE := SAMP
   END OF GETSAMPLE;


   PROCEDURE BOFINFO;
```

```
   BEGIN
      %WRITES OUT THE INFORMATION CONTAINED IN A BEGINNING OF FILE
      %BLOCK;
      INTEGER I;
      REAL RANGE;

      INFORM[SPACE 10]);

      IF WORD(10) = 0 THEN
      BEGIN
         INFORM,
<X5,"RUN CONSISTS OF DIGITALY FILTERED TIMESERIES OF ECHO VOLTAGES.">);
         INFORM[SPACE 2]);
         INFORM,<X5,"TIME BETWEEN TRANSMITTED PULSES IS: ",I4,
         " ms     PRF IS: ",F10.2," Hz">,WORD(11),1000/WORD(11));
INFORM,<X5,"NUMBER OF PULSES AVERAGED PER TIMESERIES SAMPLE IS: ",
         I3>,WORD(12));
         INFORM,<X5,"DIGITAL FILTER BANDWIDTH IS: ",F10.3," Hz">,
         500/WORD(12)/WORD(11));
         INFORM[SPACE 2]);
         INFORM,<X5,"NUMBER OF SAMPLES PER BLOCK IS: ",I3>,WORD(14));
         INFORM,<X5,"NUMBER OF DATA BLOCKS IS: ",I5>,WORD(13));
         INFORM,<X5,"LENGTH OF RUN IS: ",I3," MINUTES">,
         WORD(12)*WORD(11)/1000*WORD(13)*WORD(14)/60);
         INFORM[SPACE 2]);
         INFORM,<X5,"A-D CHANNELS USED WERE: ",I2," TO ",I2>,
         WORD(16),WORD(17));
         NRANGES := WORD(20);              STMARKER := WORD(18);
         MARK := WORD(15);                 RGNTX := WORD(19);
         NCHANS := WORD(17)-WORD(16)+1;
         NBLOCKS := WORD(13);
         NPBLOCK := WORD(14);
         N := NBLOCKS*NPBLOCK;
         DELTAT := WORD(11)*WORD(12)/1000;
         FOR I := 0 STEP 1 UNTIL 4 DO
         DATE[I] := WORD(5+I);

         INFORM[SPACE 2]);
         INFORM,<X5,"THE FOLLOWING RANGES WERE SAMPLED:">);

         INFORM,<X40,"RANGE NUMBER",X6,"RANGE">);

         FOR I := 1 STEP 1 UNTIL NRANGES DO
         BEGIN
            RGN[I] := WORD(20+I);
            RANGE := 2.5*(RGN[I]+60*(STMARKER-1)-RGNTX);
            INFORM,<X46,I2,X10,F10.2," km">,I,RANGE)
         END
      END;
      INFORM[SPACE 2]);
      INFORM,<"LENGTH OF TIMESERIES IS: ",I5," POINTS",I15," SECONDS">,
      N,N*DELTAT);
      INFORM,<"SAMPLING INTERVAL: ",F7.3," S",X10,
      "SAMPLING FREQUENCY: ",F7.3," HZ">,DELTAT,1/DELTAT);
   END OF BOFINFO;


   PROCEDURE EOFINFO;
   BEGIN
      %WRITES OUT THE COMMENTS IN AN END OF FILE BLOCK.

      REAL CHAR,CHWORD;
      INTEGER I;


      REPLACE PB := POINTER(SCREENBUFF) BY CHR FOR 14 WORDS;
```

```
   CHAR := 0;
   I := 10;
   INFORM[SPACE 5]);
   INFORM,<"END OF FILE BLOCK COMMENTS:">);

   WHILE  (CHWORD NEQ 3"252") AND (I <= 4*NWORDS) DO
   BEGIN
      CHWORD := WORD(I);        CHAR.[46:7] := CHWORD.[6:7];

      IF (CHWORD = 3"212") OR (CHWORD = 3"215") THEN
      BEGIN
         PB := POINTER(SCREENBUFF);
         REPLACE PB BY PB FOR 84 WITH ASCIITOEBCDIC;
         INFORM,14,PB);
         REPLACE PB := POINTER(SCREENBUFF) BY CHR FOR 14 WORDS
      END ELSE
      REPLACE PB:PB BY CHAR FOR 1;

      I := I+1
   END;

   PB := POINTER(SCREENBUFF);
   REPLACE PB BY PB FOR 84 WITH ASCIITOEBCDIC;
   INFORM,14,PB);
   REPLACE PB := POINTER(SCREENBUFF) BY CHR FOR 14 WORDS;
END OF EOFINFO;


BOOLEAN PROCEDURE GETDATAFILE;
BEGIN
   BOOLEAN GOTFILE;
   INTEGER CRDATE,CRYEAR,CRDAY;

   %
   %GETS THE NAME OF THE DATA FILE AND ATTACHES THE INTERNAL FILE,
   %TSFILE, TO IT.
   %

   OSCR[STOP],<"ENTER DATA FILE NAME: ">);
   PB := POINTER(SCREENBUFF);
   READ(SCREEN,14,PB);
   REPLACE TSFILE.TITLE BY PB;
   GOTFILE := TSFILE.PRESENT;

   IF GOTFILE THEN
   BEGIN
      %
      %OUTPUT FILE DATA.
      %
      INFORM,<X30,"DATA FILE INFORMATION">);
      INFORM,<X30,"----------------------">);
      INFORM[SPACE 5]);

      REPLACE PB BY " " FOR 84;
      REPLACE PB:PB BY "FILENAME: ";
      REPLACE PB:PB BY TSFILE.TITLE;
      PB := POINTER(SCREENBUFF);
      INFORM,14,PB);

      CRDATE := TSFILE.CREATIONDATE;
      CRYEAR := 1900+(CRDATE DIV 1000);
      CRDAY := CRDATE MOD 1000;
      INFORM,<"CREATED ON: ",I4,"/",I3>,CRYEAR,CRDAY);
      CURRENTBLOCK := 0;
      INPUTBLOCK;
      BOFINFO;
```

```
        SKIPTOBLOCK(NBLOCKS+2);
        INPUTBLOCK;
        EOFINFO;
        INFORM[SPACE 10])
    END;
    GETDATAFILE := GOTFILE
  END OF GETDATAFILE;


  PROCEDURE GETSEGMENT(X,SEGNO);
  VALUE SEGNO;
  INTEGER SEGNO;
  COMPLEX ARRAY X[*];
  BEGIN
    %
    %GETS SEGMENT NUMBER SEGNO FROM THE DATA FILE, TSFILE, AND
    %READS IT INTO THE COMPLEX DATA ARRAY X[I].
    %
    INTEGER I,SEGSTART,PULSE;
    REAL XREAL,XIMAG;
    COMPLEX SUM,MEAN;

    %
    %CLEAR THE DATA ARRAY.
    %
    FOR I := 0 STEP 1 UNTIL LFFT-1 DO
    X[I] := 0;

    %
    %CALCULATE THE PULSE NUMBER OF THE FIRST PULSE
    %OF THE SEGMENT.
    %

    SEGSTART := SEGNO*(LSEG DIV 2);

    %LOAD SAMPLES FROM TSFILE INTO COMPLEX ARRAY.

    FOR I := 0 STEP 1 UNTIL LSEG-1 DO
    BEGIN
      PULSE := SEGSTART+I;
      XREAL := GETSAMPLE(PULSE,RANGENO,REALCHAN);
      IF REALDATA THEN
      XIMAG := 0
      ELSE
      XIMAG := GETSAMPLE(PULSE,RANGENO,IMAGCHAN);
      X[I] := COMPLEX(XREAL,XIMAG);
      SUM := SUM+X[I]
    END;

    %
    %CALCULATE THE MEAN AND SUBTRACT IT FROM THE DATA.
    %MULTIPLY THE DATA BY THE WINDOW FUNCTION.
    %

    MEAN := SUM/LSEG;

    FOR I := 0 STEP 1 UNTIL LSEG-1 DO
    BEGIN
      X[I] := X[I]-MEAN;
      X[I] := WINDOW[I]*X[I]
    END;
  END OF GETSEGMENT;

$INCLUDE "GRAPH/EXTLDEC"

%*************************************************************************
```

```
    %
    %                          MAIN PROGRAM
    %
%*************************************************************************


    %
    %INITIALIZATION SECTION.
    %
    CHR := 3"1002004010020040"; %ASCII BLANK LINE.
    TWOPI := 2*ARCCOS(-1);
    IF SCREEN.KIND=3 THEN
    BEGIN %INTERACTIVE MODE.
       SCREENOUT := TRUE;
       LPOUT := TRUE
    END
    ELSE
    BEGIN %BATCH MODE.
       SCREENOUT := FALSE;
       LPOUT := TRUE
    END;

OSCR[STOP],<"Enter step size and number of bits of A-D: ">);
READ(SCREEN,//,ADSTEP,NBITS);

INFORM,<"Data passed through a simulated A-D convertor">);
INFORM,<"with word size = ",I3," bits and step size = ",I4>,
NBITS,ADSTEP);

    OSCR[STOP],<"ENTER FILEIT & PLOTIT (TRUE OR FALSE)">);
    READ(SCREEN,//,FILEIT,PLOTIT);


    IF GETDATAFILE THEN
    BEGIN
       %
       %CALCULATE SEGMENT LENGTH FROM FREQUENCY RESOLUTION.
       %
       OSCR[STOP],<"ENTER FREQUENCY RESOLUTION IN HZ ">);
       READ(SCREEN,//,RESOLUTION);

       %READ IN THE LIST OF RANGE NUMBERS TO BE ANALYSED.

       OSCR[STOP],<"ENTER LIST OF RANGE NUMBERS: ">);
       PB := POINTER(SCREENBUFF);
       READ(SCREEN,14,PB);
       FIRSTWORD;
       RINDEX := 1;

       WHILE CHARS > 0 DO
       BEGIN
          READ(PB,//,RANGETABLE[RINDEX]);
          NEXTWORD;
          RINDEX := RINDEX+1
       END;
       NOTOANALYSE := RINDEX-1;


       OSCR[STOP],<"ENTER CHANNEL NUMBER OF REAL DATA: ">);
       READ(SCREEN,//,REALCHAN);

       OSCR[STOP],<"ENTER CHANNEL NUMBER OF IMAGINARY DATA: ">);
       READ(SCREEN,//,IMAGCHAN);
       IF IMAGCHAN = -1 THEN REALDATA := TRUE ELSE
       REALDATA := FALSE;
```

```
      TSEG := 1/RESOLUTION;
      LSEG := ENTIER(TSEG/DELTAT);
      TSEG := LSEG*DELTAT;
      RESOLUTION := 1/TSEG;
      %
      %CALCULATE THE LENGTH OF THE FFT BY EXTENDING THE SEGMENT
      %LENGTH TO THE NEXT HIGHEST POWER OF TWO.
      %
      LFFT := ENTIER(LN(LSEG)/LN(2))+1;
      LFFT := 2**LFFT;
      FREQSTEP := 1/(LFFT*DELTAT);
      %
      %CALCULATE THE NUMBER OF OVERLAPPING DATA SEGMENTS.
      %
      NSEGS := ENTIER((N-LSEG/2)/(LSEG/2));
      %
      %CALCULATE THE NEW, ROUNDED TOTAL NUMBER OF POINTS.
      %
      N := LSEG/2*(1+NSEGS);
      %GET WINDOW TYPE.
      %
      PB := POINTER(SCREENBUFF);
      OSCR[STOP],<"ENTER WINDOW TYPE ">);
      READ(SCREEN,14,PB);
      FIRSTWORD;

      IF PB = "RECTANGULAR" OR PB = "RECT" THEN
      WINDOWTYPE := 0
      ELSE
      IF PB = "HAMMING" THEN
      WINDOWTYPE := 1
      ELSE
      IF PB = "CWL" OR PB = "COOLEY, WELCH & LEWIS" THEN
      WINDOWTYPE := 2
      ELSE
      IF PB = "BH" OR PB = "BLACKMAN HARRIS" THEN
      WINDOWTYPE := 3
      ELSE
      BEGIN
INFORM,<"UNRECOGNISABLE WINDOW TYPE -- RECTANGULAR DEFAULT USED.">);
         WINDOWTYPE := 0
      END;
      %
      %OUTPUT THE SPECTRAL ANALYSIS PARAMETERS.
      %
      INFORM,<X26,"SPECTRAL ANALYSIS PARAMETERS">);
      INFORM,<X26,"---------------------------">);
      INFORM[SPACE 5]);
      IF REALDATA THEN
      INFORM,<"REAL DATA FROM A-D CHANNEL ",I2>,REALCHAN)
      ELSE
      INFORM,<"REAL CHANNEL IS A-D CHANNEL ",I2,X10,
      "IMAGINARY CHANNEL IS A-D CHANNEL ",I2>,REALCHAN,IMAGCHAN);

      INFORM,<"LENGTH OF TIMESERIES ACTUALY USED: ",I4,
      " POINTS",X10,I4," SECONDS">,N,N*DELTAT);

      INFORM,<"FREQUENCY RESOLUTION IS: ",F7.3," HZ">,RESOLUTION);

      INFORM,<"LENGTH OF DATA SEGMENT IS: ",I3," POINTS",X10,
      F6.1," SECONDS">,LSEG,TSEG);

INFORM,<"LENGTH OF FFT IS: ",I4," POINTS",X10,"FREQUENCY STEP IS: ",
      F10.6," HZ">,LFFT,FREQSTEP);
```

```
      INFORM,<"NUMBER OF OVERLAPPING DATA SEGMENTS IS: ",I3>,NSEGS);


      CASE WINDOWTYPE OF
      BEGIN
         0 : INFORM,<"RECTANGULAR DATA WINDOW WAS USED">);
         1 : INFORM,<"HAMMING DATA WINDOW WAS USED">);
         2 : INFORM,<"COOLEY, WELCH & LEWIS DATA WINDOW WAS USED">);
 3 : INFORM,<"MINIMUM 4 TERM BLACKMAN HARRIS DATA WINDOW WAS USED">)
      END OF CASE;
      INFORM[SPACE 10]);


      %
      %GENERATE THE DATA WINDOW.
      %
      CASE WINDOWTYPE OF
      BEGIN
         0 : FOR I := 0 STEP 1 UNTIL LSEG-1 DO
         WINDOW[I] := 1;
         1 : FOR I := 0 STEP 1 UNTIL LSEG-1 DO
         WINDOW[I] := 0.54-0.46*COS(TWOPI*I/LSEG);
         2 : FOR I := 0 STEP 1 UNTIL LSEG-1 DO
         WINDOW[I] := 1-((I-(LSEG-1)/2)/((LSEG+1)/2))**2;
         3 : FOR I := 0 STEP 1 UNTIL LSEG-1 DO
         WINDOW[I] := 0.35875 - 0.48829*COS(TWOPI*I/LSEG) + 0.14128*
         COS(2*TWOPI*I/LSEG) - 0.01168*COS(3*TWOPI*I/LSEG)
      END OF CASE;
      %
      %CALCULATE THE INCOHERENT POWER GAIN OF THE WINDOW.
      %
      U := 0;
      FOR I := 0 STEP 1 UNTIL LSEG-1 DO
      U := U+WINDOW[I]**2;
      U := U/LSEG;

      %CALCULATE THE 50 PERCENT OVERLAPP CORRELATION OF THE WINDOW
      %(HARRIS 1978 PROC. IEEE 66 51)

      COR50 := 0;
      FOR I := 0 STEP 1 UNTIL LSEG/2-1 DO
      COR50 := COR50 + WINDOW[I]*WINDOW[I+LSEG/2];
      COR50 := COR50/LSEG/U;

      INFORM,<"50% OVERLAPP CORRELATION OF WINDOW IS: ",F7.2>,COR50);

      %ESTIMATE THE NORMALIZED STANDARD ERROR OF THE SPECTRAL ESTIMATES.

      COR50 := COR50**2;
      NSE := (1 + 2*COR50 + 2*COR50/NSEGS)/NSEGS;
      NSE := SQRT(NSE);

      INFORM,<"ESTIMATE OF NORMALIZED STANDARD ERROR IS: ",I2,"%">,
      NSE*100);

      INFORM,<"NUMBER OF DEGREES OF FREEDOM OF CHI SQUARE PROCESS IS: ",
      I3>,2/NSE**2);

INFORM,<"GAUSSIAN APPROXIMATION TO 0.001 PROB. CONFIDENCE LIMIT IS: ",
      F10.2," dB">,10*LOG(1+3.1*NSE));

      IF FILEIT THEN
      BEGIN
         %SET UP THE OUTPUT FILE AND WRITE THE OUTPUT
         %FILENAME TO THE PRINTER AND SCREEN.
```

```
   ARRAY NAME[0:13];
   POINTER PF;
   INTEGER T,H,M;

   PF := POINTER(NAME);

   %FILENAME CONTAINS DATE AND TIME AT WHICH ANALYSIS
   %WAS PERFORMED.

   REPLACE PF BY " " FOR 84;
   REPLACE PF:PF BY "SPECTRUM/";
   REPLACE PF BY TIME(10) FOR 6;
   REPLACE PF:PF BY PF+1 FOR 5;

   T := TIME(1)/3600;
   H := T DIV 60;
   M := T MOD 60;

   REPLACE PF:PF BY "/";
   REPLACE PF:PF BY H FOR 2 DIGITS;
   REPLACE PF:PF BY M FOR 2 DIGITS;
   REPLACE PF:PF BY ".";
   PF := POINTER(NAME);

   REPLACE PLOTFILE.TITLE BY PF;

   REPLACE PF BY " " FOR 84;
   REPLACE PF:PF BY "SPECTRA SAVED AS ";
   REPLACE PF:PF BY PLOTFILE.TITLE;
   PF := POINTER(NAME);
   INFORM,14,PF)
END;


%LOOP OVER THE RANGES TO BE ANALYSED.

FOR RINDEX := 1 STEP 1 UNTIL NOTOANALYSE DO
BEGIN

   RANGENO := RANGETABLE[RINDEX];
   %
   %CLEAR THE ARRAY OF POWER SPECTRAL DENSITIES.
   %
   FOR I := -1*(LFFT DIV 2) STEP 1 UNTIL (LFFT DIV 2)-1 DO
   SXX[I] := 0;

   FOR I := 0 STEP 1 UNTIL NSEGS-1 DO
   BEGIN
      GETSEGMENT(X,I);

      FFT(X,LFFT,FALSE);

      OSCR,<"SEGMENT NUMBER ",I3," FINISHED">,I+1);
      %
   %CALCULATE SPECTRAL ESTIMATES AND FREQUENCY ARRAY FOR POSITIVE
      %FREQUENCIES.
      %
      FOR J := 0 STEP 1 UNTIL (LFFT DIV 2)-1 DO
      BEGIN
         SXX[J] := SXX[J]+REAL(X[J]*CONJUGATE(X[J]));
         FREQUENCY[J] := J*FREQSTEP
      END;

      %
   %CALCULATE SPECTRAL ESTIMATES AND FREQUENCY ARRAY FOR NEGATIVE
      %FREQUENCIES.
```

```
    %
    FOR J := LFFT DIV 2 STEP 1 UNTIL LFFT-1 DO
    BEGIN
       K := J-LFFT;
       SXX[K] := SXX[K]+REAL(X[J]*CONJUGATE(X[J]));
       FREQUENCY[K] := K*FREQSTEP
    END
END OF LOOP OVER SEGMENTS;

%
%NORMALIZE THE SUMMED SPECTRAL ESTIMATES TO GET AVERAGED,
%UNBIASED SPECTRAL ESTIMATES.
%
NORM := (LFFT/LSEG)      %CORRECTS FOR THE ADDED ZEROS.
*(1/U)    %CORRECTS FOR THE INCOHERENT POWER GAIN OF THE WINDOW.
*(1/NSEGS)           %SUM/NUMBER = AVERAGE.
*(DELTAT/LSEG);      %UNITS**2 => UNITS**2/HZ.

FOR I := -1*(LFFT DIV 2) STEP 1 UNTIL (LFFT DIV 2)-1 DO
BEGIN
    SXX[I] := NORM*SXX[I];
    %
    %CONVERT POWER SPECTRAL DENSITY TO DB.
    %
    SXX[I] := 10*LOG(SXX[I])
END;

%
%OUTPUT THE SPECTRUM.
%

INFORM[SPACE 3]);
INFORM,<"RANGE NUMBER ",I3," ANALYSED -- ",F7.1," km">,
RANGENO,2.5*(RGN[RANGENO] + 60*(STMARKER-1) - RGNTX));


IF FILEIT THEN
OUTPUTBLOCK;

IF PLOTIT THEN
BEGIN
    REAL ARRAY FREQ,SPEC[0:2047],XLABEL,YLABEL[0:13];
    BOOLEAN ARRAY XSTATUS,YSTATUS[0:2];
    POINTER PB;
    DEFINE INITPTR(X) = PB := POINTER(X);
    REPLACE PB BY " " FOR 84#;

    %
    %FORM A FORTRAN BINDABLE ARRAY OF FREQUENCIES AND
    %POWER SPECTRAL DENSITIES. I.E. ARRAYS WITH INDICES
    %RUNNING FROM 0 -> N-1.
    %

    FOR I := 0 STEP 1 UNTIL LFFT-1 DO
    BEGIN
       FREQ[I] := FREQUENCY[I-(LFFT DIV 2)];
       SPEC[I] := SXX[I-(LFFT DIV 2)]
    END;

    XSTATUS[0] := FALSE;     YSTATUS[0] := FALSE;
    XSTATUS[1] := FALSE;     YSTATUS[1] := FALSE;
    XSTATUS[2] := TRUE;      YSTATUS[2] := FALSE;

    INITPTR(XLABEL);
    REPLACE PB BY "FREQUENCY, HZ";
    INITPTR(YLABEL);
```

```
            REPLACE PB BY "POWER SPECTRAL DENSITY, DB";

            GRAPH(FREQ,SPEC,LFFT,XLABEL,YLABEL,XSTATUS,YSTATUS);

            %PLOT DATE, TIME AND RANGE INFORMATION.

            INITPTR(XLABEL);
            REPLACE PB:PB BY "DATE   ";
            WRITE(PB,<I4,"/",I2,"/",I2>,DATE[0],DATE[1],DATE[2]);
            PB := PB+10;
            REPLACE PB:PB BY "    TIME   ";
            WRITE(PB,<I2," ",I2," NZST">,DATE[3],DATE[4]);
            ALAB(400,320,XLABEL,35,1,2);

            INITPTR(XLABEL);
            REPLACE PB:PB BY "RANGE   ";
            WRITE(PB,<F7.1," KM">,2.5*(RGN[RANGENO]+60*(STMARKER-1)
            -RGNTX));

            ALAB(400,300,XLABEL,17,1,2);

            IF FILEIT THEN
            BEGIN
               INITPTR(XLABEL);
               REPLACE PB:PB BY "THIS SPECTRUM STORED ON  ",
               PLOTFILE.TITLE;
               ALAB(400,50,XLABEL,54,1,2)
            END;
            AEND
         END
      END;
      CLOSE(PLOTFILE,CRUNCH)
   END
   ELSE
   INFORM,<"FILE NOT PRESENT.">)
END.
```